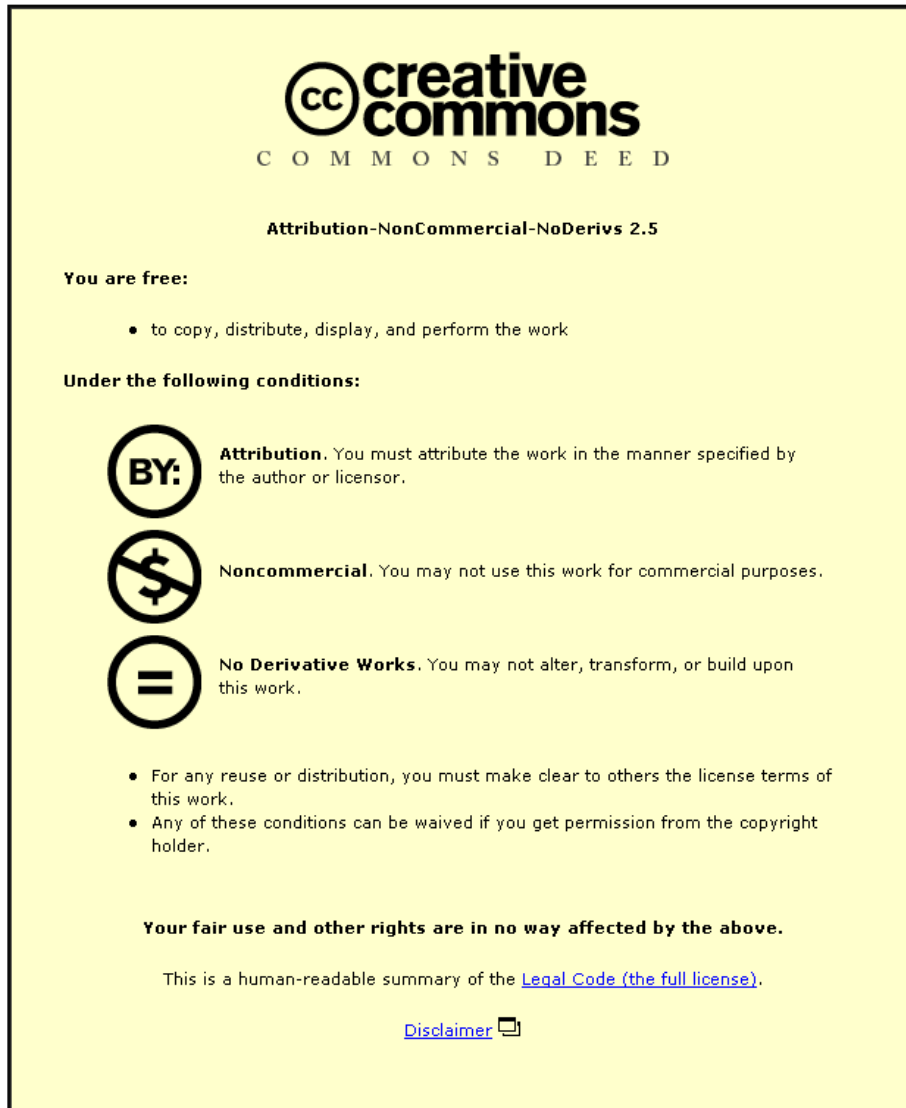


This item was submitted to Loughborough's Institutional Repository (<https://dspace.lboro.ac.uk/>) by the author and is made available under the following Creative Commons Licence conditions.



CC creative commons
COMMONS DEED

Attribution-NonCommercial-NoDerivs 2.5

You are free:

- to copy, distribute, display, and perform the work

Under the following conditions:

BY: **Attribution.** You must attribute the work in the manner specified by the author or licensor.

Noncommercial. You may not use this work for commercial purposes.

No Derivative Works. You may not alter, transform, or build upon this work.

- For any reuse or distribution, you must make clear to others the license terms of this work.
- Any of these conditions can be waived if you get permission from the copyright holder.

Your fair use and other rights are in no way affected by the above.

This is a human-readable summary of the [Legal Code \(the full license\)](#).

[Disclaimer](#) 

For the full text of this licence, please go to:
<http://creativecommons.org/licenses/by-nc-nd/2.5/>



**Experimental and Numerical Analysis of
Deformation and Damage In Thermally
Bonded Nonwoven Material**

by

FARUKH

A Doctoral Thesis

Submitted in partial fulfilment of the requirements for the award of Doctor of
Philosophy of Loughborough University

April 2013

© 2013 Farukh

ABSTRACT

Nonwovens are materials made of disordered fibres consolidated by mechanical, chemical or thermal processes. A spectrum of applications for these materials has broadened very rapidly in recent years with the advent of new technologies and incorporation of new fibres. Most of the applications of nonwovens require them to be robust enough, mechanically or structurally, to perform their intended function without damage during their working life. Thus, it is vital to understand deformation and damage behaviours of these materials to design and tailor their properties for specific applications. The research aim is to understand the deformation and damage behaviours and their relationship with underlying mechanisms of nonwoven materials employing a combination of experiments and simulations.

The type of nonwoven used as model system in this study is a low-density thermally bonded fabric with polymer-based constituent fibres. In order to understand the relationship between deformation and damage behaviours of nonwoven and its constituent fibre and to ascertain the underlying mechanisms which govern those behaviours, experiments on the fabric and single fibres extracted from it were performed. Tensile tests carried out on the rectangular coupons of fabric revealed that progressive failure of fibres led to damage initiation and propagation, ultimately resulting in failure of nonwoven fabric. Material properties of constituent fibres were measured based on single-fibre tensile, creep and relaxation tests. To obtain the criteria that control the onset and propagation of damage in the studied material, tensile tests on

single fibres, extracted from the nonwoven with bond points attached to their ends, were performed.

A novel parametric computational modelling approach based on direct introduction of fibres and other geometric entities (bond points) that form the nonwoven fabric is introduced in this study. Following the experimental observations, a scatter in material properties and a stress-based failure criterion were included into the model. The mechanical behaviour of nonwoven fabric was simulated by using this model incorporating fabric's microstructure, properties of constituent fibres including their failure criteria. The simulations demonstrated main deformation and damage mechanisms such as reorientation of fibres and their stretching, development and growth of fracture zones etc. The results obtained in simulations of the standard nonwoven were in good agreement with the experimental response at meso and macro levels. Besides, the model based on direct introduction of fibres contributed to the study of the spread of stresses and strains in each element of the fabric. Moreover, progressive failure of fibres together with the pattern of damage localization and growth in terms of fracture zones depending upon increasing level of fabric's extension were studied using the model. Finally, finite-element simulations of several nonwovens were performed using the same modelling technique and their results were compared with respective experimental data to examine the predictive capability and extendibility of the model to other types of fibrous networks.

Keywords: Nonwovens; Orientation distribution function; Anisotropy; Finite element; Viscoelastic-plastic properties; Stress distribution; Strain distribution; Deformation; Damage; Failure

ACKNOWLEDGEMENT

Given the scope of this work, I would not have accomplished it alone without support of many individuals. My appreciation goes out to them, and I would like to acknowledge some of them here.

I would like to express my gratitude to Prof. Vadim Silberschmidt for his insightful guidance and support. I would like to express my deepest gratitude to my thesis supervisor, Prof. Memis Acar, for his guidance, help and kindness. I would also like to thank Dr. Emrah Demirci for his contribution to my education throughout my PhD research. I consider myself quite fortunate to be able to work with such caring and dedicated advisors.

Support of Nonwovens Cooperative Research Center of North Carolina State University, USA is appreciated. I would like to thank my industrial advisors, Mr. Carl Wust from Fibervisions Corp., Mr. Brad Eaton and Mrs. Joe Spagnola from 3M, and Mr. Tom Godfrey from U.S. Army Natick for their support and feedbacks during the research.

PUBLICATIONS

Journals

Farukh, F., Demirci, E., Sabuncuoğlu, B., Acar, M., Pourdeyhimi, B. and Silberschmidt, V.V. (2013), “Characterisation and numerical modelling of complex deformation behaviour in thermally bonded nonwovens”, Computational Materials Science, 71, pp 165-171

<http://dx.doi.org/10.1016/j.commatsci.2013.01.007>

Farukh, F., Demirci, E., Acar, M., Pourdeyhimi, B. and Silberschmidt, V.V. (2013), “Meso-scale deformation and damage in thermally bonded nonwovens”, Journal of Materials Science, 48(6), pp 2334-2345

<http://dx.doi.org/10.1007/s10853-012-7013-y>

Farukh, F., Demirci, E., Sabuncuoğlu, B., Acar, M., Pourdeyhimi, B. and Silberschmidt, V.V. (2012), “Numerical modelling of damage initiation in low-density thermally bonded nonwovens”, Computational Materials Science, 64, pp 112-115

<http://dx.doi.org/10.1016/j.commatsci.2012.05.038>

Farukh, F., Demirci, E., Acar, M., Pourdeyhimi, B. and Silberschmidt, V.V. (2012), “Strength of fibres in lowdensity thermally bonded nonwovens: An experimental investigation”, Journal of Physics: Conference Series, 382 (012018),

<http://dx.doi.org/10.1088/1742-6596/382/1/012018>

Demirci, E., Farukh, F., Sabuncuoğlu, B., Acar, M., Pourdeyhimi, B. and Silberschmidt, V.V. (2013), “Numerical analysis of dynamic out-of-plane loading of nonwovens” submitted to Journal of Physics: Conference Series

Conference Contributions

Farukh, F., Sabuncuoğlu, B., Demirci, E., Acar, M., Pourdeyhimi, B. and Silberschmidt, V.V., “Characterisation and Numerical Modelling of Deformation and Damage in Thermally Bonded Nonwovens”, 22th International Workshop on Computational Mechanics of Materials (IWCMM22), Baltimore., Maryland, USA, 24-26 September 2012

Farukh, F., Demirci, E., Acar, M., Pourdeyhimi, B. and Silberschmidt, V.V., “Strength of fibres in low-density thermally bonded nonwovens: An experimental investigation”, Modern Practice in Stress and Vibration Analysis 2012 (MPSVA 2012), Glasgow, UNITED KINGDOM, 29-31 August 2012

Farukh, F., Demirci, E., Acar, M., Pourdeyhimi, B. and Silberschmidt, V.V., “Implementation of Damage in Finite Element Modelling of Thermally Bonded Bicomponent Fibre Nonwovens”, 21th International Workshop on Computational Mechanics of Materials (IWCMM21), Limerick, IRELAND, 22-24 August 2011

Farukh, F., Sabuncuoğlu, B., Demirci, E., Acar, M., Pourdeyhimi, B. and Silberschmidt, V.V., “Numerical Modelling of Damage Initiation in Low-Density Thermally Bonded Nonwovens”, 21th International Workshop on Computational Mechanics of Materials (IWCMM21), Limerick, IRELAND, 22-24 August 2011

Farukh, F., Demirci, E., Acar, M., Pourdeyhimi, B., Silberschmidt, V., “Experimental and numerical analysis of deformation and damage in nonwoven materials”, Semiannual International Advisory Board Meetings, Nonwovens Cooperative Research Center, NC State University, Raleigh, NC State, USA, 2007-2010.

CONTENTS

ABSTRACT.....	I
ACKNOWLEDGEMENT.....	III
PUBLICATIONS	IV
LIST OF FIGURES	X
LIST OF TABLES	XVII
1 INTRODUCTION	1
<i>1.1 Motivation.....</i>	<i>2</i>
<i>1.2 Aims and Objectives.....</i>	<i>4</i>
<i>1.3 Research Methodology</i>	<i>6</i>
<i>1.4 Outline</i>	<i>7</i>
2 NONWOVEN MATERIALS.....	10
<i>2.1 Application Areas</i>	<i>13</i>
<i>2.2 Raw Material</i>	<i>14</i>
<i>2.3 Manufacturing Stages.....</i>	<i>15</i>
2.3.1 Web Formation	15
2.3.2 Bonding.....	16
2.3.3 Finishing	16
<i>2.4 Classification.....</i>	<i>17</i>
<i>2.5 Thermally Bonded Nonwovens</i>	<i>19</i>
2.5.1 Calender Bonding	20
2.5.2 Fibre Composition and Fabric Structure.....	21
<i>2.6 Summary</i>	<i>23</i>

3	MECHANICAL BEHAVIOUR OF NONWOVENS	24
3.1	<i>Mechanical Properties of Fibres</i>	25
3.2	<i>Mechanical Anisotropy.....</i>	25
3.3	<i>Deformation and Damage Behaviour.....</i>	30
3.3.1	Nonlinearity	33
3.3.2	Time-Dependant Properties	35
3.4	<i>Factors affecting the properties of nonwovens.....</i>	36
3.4.1	Bonding Temperature	37
3.4.2	Fibre Structure and Properties	38
3.4.3	Calendering Pressure	39
3.4.4	Web Speed	40
3.4.5	Morphology and Fibres Form	41
3.4.6	Orientation Distribution of Fibres.....	41
3.4.7	Crimp in Fibres	42
3.4.8	Bond Points Geometry	43
3.5	<i>Summary</i>	44
4	MODELLING OF MECHANICAL BEHAVIOUR OF MATERIALS.....	45
4.1	<i>Modelling of Deformation</i>	46
4.1.1	Elastic Behaviour	46
4.1.2	Plastic Behaviour	50
4.1.3	Viscous Behaviour	57
4.2	<i>Modelling of Damage</i>	60
4.3	<i>Review of Finite Element Method.....</i>	62
4.3.1	General Procedure of FEM	63
4.3.2	Nonlinearity in Structural Analysis	64
4.4	<i>Existing FE models for Nonwovens</i>	68
4.5	<i>Summary</i>	75

5	CHARACTERISATION OF MECHANICAL RESPONSE OF FABRIC	77
5.1	<i>Experimental Techniques</i>	78
5.1.1	Morphological Characterisation	78
5.1.2	Mechanical Characterization	91
5.2	<i>Experimental Results</i>	95
5.2.1	Initial Microstructure Using SEM	95
5.2.2	Initial Microstructure Using X-Ray Micro Computed Tomography	98
5.2.3	Tensile Tests	100
5.2.4	Structure of Deformed Fabric	102
5.3	<i>Conclusions</i>	108
6	CHARACTERISATION OF MECHANICAL RESPONSE OF FIBRE	111
6.1	<i>Tensile Tests</i>	112
6.1.1	Experimental Techniques	112
6.1.2	Experimental Procedure.....	115
6.2	<i>Creep Tests</i>	116
6.2.1	Experimental Techniques	117
6.2.2	Experimental Procedure.....	118
6.3	<i>Relaxation Tests</i>	119
6.3.1	Experimental Techniques	120
6.3.2	Experimental Procedure.....	120
6.4	<i>Results and Discussion</i>	121
6.4.1	Tensile Tests	121
6.4.2	Creep Tests	122
6.4.3	Relaxation Tests.....	126
6.5	<i>Development of Failure Criteria</i>	127
6.5.1	Experimental Technique	128
6.5.2	Experimental Results	129
6.6	<i>Conclusions</i>	133

7	FINITE ELEMENT MODELLING OF THERMALLY BONDED NONWOVENS.....	135
7.1	<i>Modelling Objectives</i>	136
7.2	<i>Model Development</i>	137
7.2.1	Generation of Fabric Network	138
7.2.2	Geometric Properties	139
7.2.3	Boundary conditions	141
7.2.4	Material Properties.....	141
7.2.5	Fibre-Failure Criterion	141
7.3	<i>Meso-Scale Model</i>	144
7.4	<i>Macro-scale Model</i>	152
7.4.1	Material Properties and Boundary Conditions.....	155
7.4.2	Results and Experimental Verification	157
7.5	<i>Case Studies</i>	175
7.5.1	Effect of Specimen Size.....	176
7.5.2	Effect of Planar Density.....	177
7.5.3	Effect of Geometry and Pattern of Bond Points	178
7.6	<i>Conclusions</i>	184
8	CONCLUSIONS AND FUTURE WORK.....	187
8.1	<i>Conclusions</i>	187
8.2	<i>Outcomes</i>	190
8.3	<i>Future Work</i>	193
A	DETERMINATION OF OREINTATION DISTRIBUTION FUNCTION ..	195
B	IMPLEMENTATION OF SUBROUTINE	198
	REFERENCES.....	204

LIST OF FIGURES

Figure 1.1. Growth in production of nonwovens in Europe	3
Figure 1.2. SEM image of thermally bonded monocomponent fibre nonwoven.....	5
Figure 1.3. Thesis layout and research methodology	9
Figure 2.1. Felts remnants from excavation at Pazyryk (a) Carpet fragment showing male rider approaching seated figure, 5 th century B.C. (b) felt stockings, 5 th century B.C. (c) Fragment of felt covering for saddle, 5 th century B.C. ...	12
Figure 2.2. Classification of nonwovens.....	18
Figure 2.3. Typical hot calendering process	21
Figure 2.4. Typical bond point produced with hot calendering process	22
Figure 3.1. Graphical user interface of orientation distribution determination software developed by Demirci <i>et. al.</i> (2011)	27
Figure 3.2. Direction-dependant behaviour of thermally bonded nonwovens; 0° and 90° represent MD and CD, respectively (Michielsen <i>et. al.</i> , 2006).....	30
Figure 3.3. Deformation mechanisms of nonwoven fabric after 50% elongation in MD (a) and CD (b) (Kim <i>et. al.</i> , 2001).....	32
Figure 3.4. Damage micromechanisms in the nonwoven fabric during tensile (a) 0% nominal strain, (b) 20% nominal strain, (c) 40% nominal strain, and (d) 100% nominal strain (Ridruejo, 2011)	33
Figure 3.5. Images of failure of nonwovens in various loading directions (Kim, 2004a)	34
Figure 3.6. Stress - strain graph for elastoplastic material.....	35
Figure 3.7. Stress-strain curves of purely elastic (a) and viscoelastic (b) materials (The green area represents the amount of energy lost in a loading-unloading cycle)	36
Figure 3.8. Effect of bonding temperature on properties of nonwovens (Michielsen, 2006).....	38
Figure 3.9. Mechanical properties in various directions as a function of nip pressure (Michielsen <i>et. al.</i> , 2006).....	40
Figure 3.10. Photomicrograph of staple crimped fibre (Bauer-Kurz, 2000)	42

Figure 3.11. Initial portion of Load-Elongation curve of straight and crimped fibre (Brown, 1995).....	43
Figure 4.1. Mechanical behaviour of material	51
Figure 4.2. Comparison of Tresca and von Mises yield criteria in plane stress condition	56
Figure 4.3. Flow rule (Clarke and Cope, 1984)	57
Figure 4.4. (a) Perfectly elastic (b) viscoue element (E is modulus of elasticity and η is viscosity) (Ottosen and Ristinmaa, 2005).....	58
Figure 4.5. Maxwell model.....	58
Figure 4.6. Kelvin-Voigt model.....	59
Figure 4.7. Generalized Maxwell model represented by springs and dashpots.....	60
Figure 4.8. (a) Tapered bar under load P (b) model built up of four nontapered elements of equal length L (Cook <i>et. al.</i> , 1998)	63
Figure 4.9. FE model of 150g/m^2 PP/PE fibre nonwoven	69
Figure 4.10. Layered structure of fabric unit (Singh <i>et. al.</i> , 1998)	70
Figure 4.11. Unit cell with bond points connected by truss elements	71
Figure 4.12. Discontinuous FE model with square bond points	72
Figure 4.13. FE model to simulate point bonded nonwoven (Limem <i>et. al.</i> , 2005).....	73
Figure 4.14. Discontinuous FE model (a) machine direction (b) cross direction	74
Figure 5.1. Scanning electron microscopy.....	79
Figure 5.2. X-ray micro computed tomography	91
Figure 5.3. Specimen dimensions in cut-strip method.....	93
Figure 5.4. Hounsfield Benchtop Tester with pneumatic grips	94
Figure 5.5. (a) Meso-level fabric specimen showing fibres connecting between bond points; (b) Schematics of final specimen (not to scale including number of fibres).....	94
Figure 5.6. SEM images of 20 g/m^2 PP fibre nonwoven at different length scales: (a) overall microstructure; (b) bond point and surrounding fibre matrix; (c) polypropylene fibres	96
Figure 5.7. Variation in fibre diameter	97

Figure 5.8. Orientation distribution function of fibres (90° corresponds to MD whereas 0° and 180° correspond to CD).....	98
Figure 5.9. X-ray micro CT image of thermally bonded nonwoven (fibre: PP, planar density: 20 g/m^2).....	99
Figure 5.10. X-ray micro CT image showing through thickness microstructure (fibre: PP, planar density: 20 g/m^2)	99
Figure 5.11. Force vs. % extension curves for rectangular specimen in tension at a strain rate of 0.1 s^{-1} along MD (a) and CD (b)	101
Figure 5.12. Effect of fabric's planar density on its ultimate tensile strength along MD (a); CD (b)	103
Figure 5.13. Effect of fabric's planar density on its % extension at failure along MD (a); CD (b)	104
Figure 5.14. Deformation and damage mechanisms in low-density thermally bonded nonwovens during tensile tests at 0% strain (a); 25% strain (b); 50 % strain (c); 80% strain (d). Loading direction was vertical (Arrows indicate fracture zones)	106
Figure 5.15. Images of thermally bonded nonwoven deformed at 0.5 strain in: (a) MD; (b) CD (16.5 mm gauge length).....	107
Figure 5.16. Deformation and damage mechanisms in low-density thermally bonded nonwovens during tensile tests at 0% strain (a); 25% strain (b); 50 % strain (c); 75% strain (d).....	108
Figure 6.1. Preparation procedure for single-fibre specimens.....	113
Figure 6.2. Test rig Instron [®] Micro Tester 5848 (Dashed line is used to enhance contrast of image), Loughborough University, UK.....	114
Figure 6.3. Textechno Favimat fibre testing system (North Carolina State University, USA).....	115
Figure 6.4. Creep behaviour showing constant stress (a): continuous deformation (b)	117
Figure 6.5. Creep strain as function of time for viscous material (Penny and Marriot, 1995).....	119

Figure 6.6. Relaxation test with constant strain (a) resulting in continuous stress attenuation (b).....	120
Figure 6.7. Mechanical behaviour of PP fibre at various strain rates	122
Figure 6.8. Evolution of engineering stress value in creep tests.....	124
Figure 6.9. (a) Experimental creep strain (b) Creep strain after curve fitting of creep strain as a function of time	125
Figure 6.10. Relaxation behaviour of PP fibre for various strain rates.....	127
Figure 6.11. (a) Single fibre attached to bond points at each end (dashed line is used to enhance contrast of image); (b) schematics of final specimen and its fixture	130
Figure 6.12. Setup of single-fibre experiment (Instron Micro Tester 5848 and Photron Fastcam SA3)	130
Figure 6.13. Scatter in experimental results of processed PP fibres at strain rate: 0.5 (a); 0.1 (b); 0.01 (c).....	132
Figure 6.14. Mechanical behaviour of PP fibre with bond points at edges at various strain rates.....	133
Figure 7.1. Form of elements used in FE modelling of nonwovens for bond points (shell element 139) (a) and fibres (two-node truss element 9).....	140
Figure 7.2. Finite-element models: (a) with parallel fibres; (b) with randomly oriented fibres between two neighbouring bond points.....	144
Figure 7.3. Maximum orientation of fibres in relation to distance between bond points	145
Figure 7.4. Part of ODF implemented for fibres in model in Fig. 7.2b	146
Figure 7.5. FE results of model with parallel fibres showing development of fracture zone and equivalent von Mises stresses (in MPa) in thermally bonded nonwovens at various levels of global strain: (a) 0 %; (b) 25 %; (c) 50 %; (d) 75 % (Arrow indicates a fracture zone)	147
Figure 7.6. FE results of model with randomly oriented fibres showing development of fracture zones and equivalent von Mises stresses (in MPa) in thermally bonded nonwovens at various levels of global strain: (a) 0 %; (b) 25 %; (c) 50 %; (d) 75 % (Arrows indicate local fracture zones).....	148

Figure 7.7. Effect of fibre orientation on damage initiation and propagation in FE simulations of nonwoven.....	150
Figure 7.8. Effect of randomness of fibre’s material properties on damage initiation and propagation in FE simulations.....	151
Figure 7.9. Effect of state (processed and unprocessed) of fibres on damage initiation and propagation in FE simulations	151
Figure 7.10. Finite element models: (a) loading along MD; (b) loading along CD	154
Figure 7.11. Parameters of pattern of modelled fabric	155
Figure 7.12. Stochasticity in material properties implemented into FE model: (a) stress-strain curves; (b) critical values of stress and strain.....	157
Figure 7.13. FE model showing stochasticity in material properties and fibres’ orientation distribution and boundary conditions.....	158
Figure 7.14. (a) Experimental results for fabric subjected to uniaxial tension along MD to various extensions: (i) 25%; (ii) 50%; (iii) 75%; (iv) 100%; (v) 150%; (vi) 190%; (b) corresponding FE results for equivalent (von Mises) stresses in (MPa).....	161
Figure 7.15. (a) Experimental results for fabric subjected to uniaxial tension along CD to various extensions: (i) 25%; (ii) 50%; (iii) 75%; (iv) 100%; (v) 150%; (vi) 190%; (b) corresponding FE results for equivalent (von Mises) stresses in (MPa).....	162
Figure 7.16. Calculated responses to uniaxial tensile test for MD (a) and CD (b) (Shaded area represents scatter in experimental results).....	163
Figure 7.17. Flow chart on implementation of stochasticity in FE model.....	164
Figure 7.18. Distribution of normalised strains for fibres for various values of fabric strain deformed along MD (a) and CD (b)	167
Figure 7.19. Distribution of stresses for fibres for various values of fabric strain deformed along MD (a) and CD (b)	168
Figure 7.20. Distribution of stresses of fibres for various levels of fabric’s extension	169
Figure 7.21. Fibres rotation with increasing fabric’s extension for MD and CD	169
Figure 7.22. Growth in fracture zone with fabric’s strain.....	171
Figure 7.23. Evolution of damage parameter with fabric’s deformation.....	172

Figure 7.24. Minimum and maximum values of stress in fibres for various values of strain in fabric deformed along MD (a) and CD (b).....	173
Figure 7.25. Stress concentration at edges of bond points (loading direction was along MD)	175
Figure 7.26. FE models of 20 g/m ² with width (a) 5 mm; (b) 15 mm	177
Figure 7.27. FE model results showing contour plot of equivalent von Mises stresses (MPa) in fabric along MD subjected to uniaxial tension to extension: (i) 25%; (ii) 50%; (iii) 75%; (iv) 100% for 5 mm width model (a) and 15 mm width model (b)	179
Figure 7.28. FE model response to uniaxial tensile test for 5 mm width model(a) and 15 mm width model (b) (Shaded area represents scatter in experimental results)	180
Figure 7.29. FE model results showing contour plot of equivalent von Mises stresses (MPa) in fabric with 30 g/m ² planar density along MD subjected to uniaxial tension to extension: (i) 25%; (ii) 50%; (iii) 75%; (iv) 100% ...	181
Figure 7.30. FE model for 30 g/m ² nonwoven response to uniaxial tensile test (Shaded area represents scatter in experimental results)	181
Figure 7.31. (a) SEM image of 30 g/m ² nonwoven material with diamond-shaped bond points; (b) corresponding part of FE model.....	182
Figure 7.32. FE model results showing contour plot of equivalent von Mises stresses (in MPa) in fabric with diamond-shaped bond points along MD subjected to uniaxial tension to extension: (i) 25%; (ii) 50%; (iii) 75%; (iv) 100% ...	183
Figure 7.33. Response of FE model with diamond-shaped bond points to uniaxial tensile test (Shaded area represents scatter in experimental results).....	183
Figure A.1. GUI of Nonwovens Anisotropy V1 for computing ODF and mechanical anisotropy of fibrous materials	196
Figure A.2. Red lines showing fibres in image processed with Nonwoven Anisotropy V1	197
Figure A.3. Orientation distribution of modelled fabric	197
Figure B.1. Modelling bond points and planes on fabric border	200

Figure B.2. Representation of fibres; fibre A, completely inside fabric; fibre B, partially outside fabric	203
Figure B.3. Modelling of fibres	204
Figure B.4. Trimming of fibres along fabric borders.....	204
Figure B.5. Trimming of fibres within bond points.....	205
Figure B.6. Flowchart of implemented code	206

LIST OF TABLES

Table 2.1. European produced nonwovens consumption by end use (Russell, 2007) ...	13
Table 2.2. Usage of fibre material in nonwoven production.....	14
Table 3.1. Techniques used for computing ODF	29
Table 3.2. Types of bicomponent fibres.....	39
Table 6.1. Properties of polymer material used for fibre	121
Table 6.2. Mean values with standard deviation of failure stress and strain of unprocessed and processed fibres at various strain rates	129
Table 7.1. Parameters of fabric (see Fig. 7.11)	153
Table 7.2. Number of elements for MD and CD models	155
Table 7.3. Parameters of geometry and pattern of bond points	182

CHAPTER I

INTRODUCTION

Nonwovens are engineered fabrics, which are widely used in daily life. They are composed of fibrous webs bonded together by mechanical, thermal or chemical technique. Nonwovens are formally defined as “A manufactured sheet, web or batt of directionally or randomly oriented fibres, bonded by friction, and/or cohesion and/or adhesion, excluding paper and products which are woven, knitted, tufted, stitch-bonded incorporating binding yarns and filaments, or felted by wet milling, whether or not additionally needled” (ISO, 9092).

Conventional textile production operations such as roving, spinning, knitting have been partially or completely omitted in the processing of nonwovens, thus making them more economical. Nonwovens are not only the low cost replacement for more expensive textiles but also engineered for particular characteristics (e.g. fire resistant, abrasion resistant, absorbent, conductive, liquid repellent etc.) making them suitable for

many product applications such as filters, protective clothings, absorbent hygiene products (baby diaper, feminine hygiene products). With the advent of new technologies, nonwovens have become the integral part of various novel applications. For example, scaffolds for tissue engineering and fuel cell membranes, electrospun nano-fibrous mats for filtering molecular-size particles. A significant part of nonwovens consumption consists of structural and mechanical purposes, which require the appropriate knowledge of mechanical properties of these materials. Additionally, being engineered material; nonwovens have the great potential to widen the spectrum of applications which demand an insight to their mechanical behaviour. This research aims at detailed analysis of deformation as well as damage initiation and propagation in low-density thermally bonded monocomponent fibre nonwovens.

1.1 Motivation

Production of nonwovens has grown rapidly in the last few decades and is increasing continuously. It is one of the fastest growing sectors in the textile industry (EDANA, 2010) (Fig. 1.1). Application spectrum of nonwovens have expanded, because of advancement in fibre technology and manufacturing techniques in recent years, to such an extent that their usage now ranges from daily-life products, such as personal hygiene to high-tech applications, for instance in biomedical for controlled release of medicine. All of these applications require integrity of nonwoven structure during their service life. Hence, it is important to understand the deformation and damage behaviour of nonwovens so that they could be produced to perform their intended functions without being damaged when exposed to service loading conditions. Therefore, nonwoven industry requires a better understanding of the mechanical properties and behaviour of these materials.

It is indeed challenging to design and manufacture a nonwoven according to particular requirements involving numerous time-consuming and expensive optimization stages. In order to reduce the trial and error during design and optimization phase of new products and improvement of existing products, a numerical model should

be developed to predict the deformation as well as damage initiation and propagation behaviour. Thus, issues motivating this research were originated by the nonwoven industry.

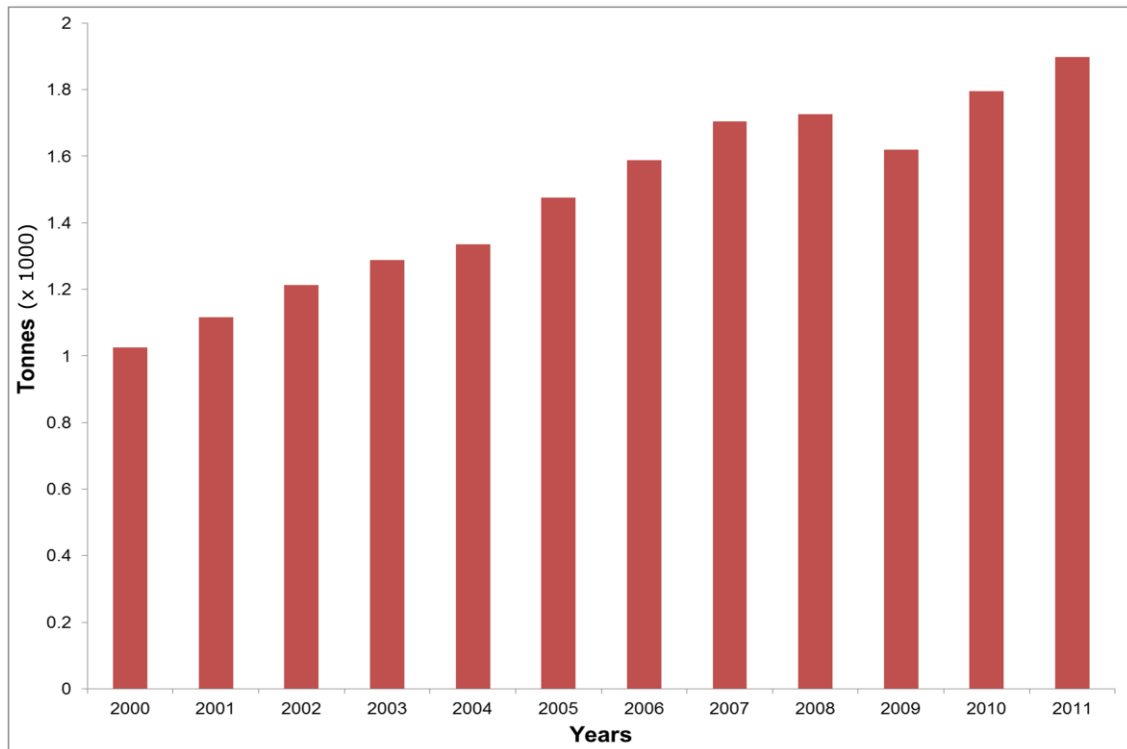


Figure 1.1. Growth in production of nonwovens in Europe (EDANA, 2011)

Designing of a product containing nonwoven parts undergoing mechanical loading during service conditions requires an understanding of the mechanical behaviour of nonwoven and the parameters defining this behaviour. Moreover, to tailor and optimise properties of these materials, an understanding of the relationship between their macroscopic behaviour and microstructure along with manufacturing-induced single-fibre properties is essential. Experimental characterization is the basic procedure to understand the mechanical behaviour of a material. Still it is not always viable and sufficient for a comprehensive understanding of complex phenomena involved in deformation and damage of nonwoven fibrous materials. These challenges are linked to the cost, time as well as to significant efforts required for experimentation, especially for nonwoven fibrous materials, in which mechanical properties are defined by their

non-trivial microstructure and constituent fibre's properties. Therefore, a numerical tool, which can adequately represent the mechanical behaviour of these materials linked to their microstructure and constituent fibre properties, is necessary for designing and optimising the properties of these materials.

Development of a numerical model for low density nonwovens, incorporating fabric's microstructure, elastic-plastic and viscous properties of constituent single-fibre and deformation as well as damage mechanisms would be a novel contribution to the academia and industry.

This research is conducted at Wolfson School of Mechanical and Manufacturing Engineering, Loughborough University, in conjunction with Nonwoven Cooperative Research Center (NCRC), North Carolina State University, Raleigh, NC, USA. NCRC is a consortium of leading companies from all over the world. The progression of the research is assessed biannually by the industrial advisors from the renowned nonwoven manufacturers such 3M, P&G, etc. The outcome of the research will help these companies to minimise costly and time consuming stages of product development and optimisation.

1.2 Aims and Objectives

This research focusses on thermally bonded monocomponent fibre nonwovens having low planar density ($< 50 \text{ g/m}^2$). In thermally bonded nonwovens, a fabric's structure is composed of continuous and discontinuous regions. The continuous regions called *bond points* are connected by a network of random fibres forming a discontinuous region with voids and gaps in it (Fig. 1.2). This combination of two micro-structurally different regions with continuous domains embedded into discontinuous medium makes it difficult to predict the deformation and damage behaviours of thermally bonded fibrous networks. Thus, overall aims of the research are:

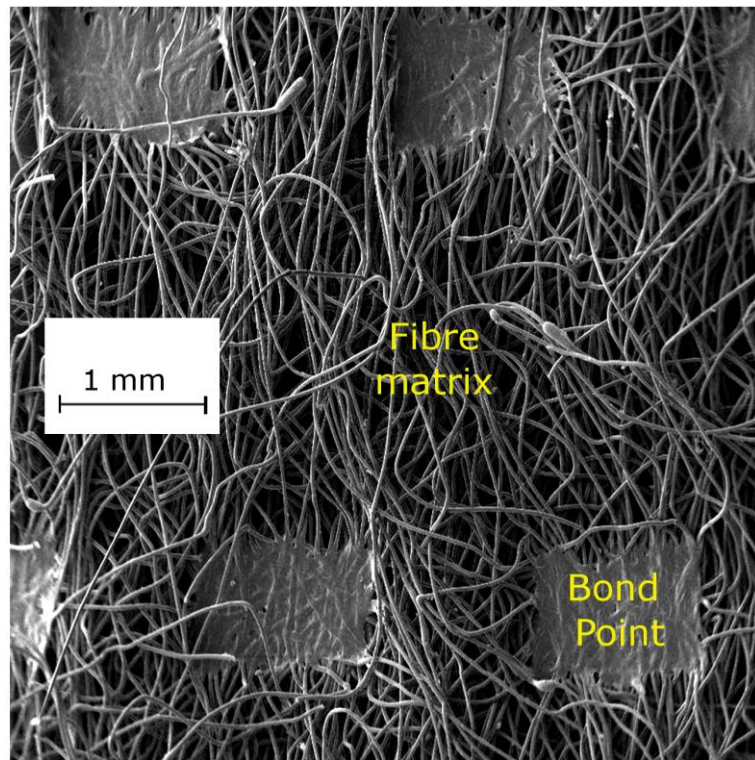


Figure 1.2. SEM image of thermally bonded monocomponent fibre nonwoven
(20 g/m²)

1. To investigate the actual sequence of deformation and damage mechanics which control the mechanical behaviour of low density nonwovens;
2. To develop a parametric computational model to reproduce the realistic deformation and damage behaviour of low-density thermally bonded nonwovens.

In order to achieve the above mentioned aims, the research framework is divided into the following objectives:

- i) To examine the fabrics behaviour under in-plane mechanical loading;
- ii) To investigate the mechanical properties of constituent fibres including viscous ones;

- iii) To analyse the failure parameters of single-fibre within fabric bonded at optimal manufacturing conditions;
- iv) To develop a finite element model incorporating fabric's microstructure, constituent fibre properties and single-fibre failure criteria to simulate the mechanical behaviour of low-density thermally bonded nonwovens;
- v) To evaluate the efficiency of the finite element model using experimental verification for several case studies.

1.3 Research Methodology

In order to accomplish the aims of the research, extensive experimentation and numerical modelling were carried out. With above mentioned aims and objectives, the most suitable approach to model the deformation and damage behaviour of nonwoven materials is direct modelling of fibres between the bond points according to realistic fibres orientation distribution function. The main advantage of this approach is the explicit inclusion of fabric's microstructure into the model and changes in network topology with damage propagation due to progressive failure of fibres. Besides, this approach has potential benefit of introducing voids and gaps into the model making it more representative of low-density nonwovens. Since model is based on realistic material's microstructure; the issue of modelling large number of fibres according to their orientation distribution, while making sure that each fibre is properly connected to the bond points to avoid convergence problem, is resolved by employing parametric modelling technique based on a subroutine. In this technique, a code written in programming language (Patran Command language) is read by the finite element software (MSC. Patran) to formulate the model. This reduces significantly the effort for reformulating the model to incorporate the changes in orientation distribution of fibres or other structural entities such as bond point geometry or dimensions.

Mechanical behaviour of nonwoven material is analysed based on the properties obtained from their fibres. At macroscopic level, the mechanical performance of fabrics

is analysed with mechanical tests. The material is simulated with the developed Finite Element (FE) model and these tests results are used to validate the simulation results.

Experimental study begins with performing the tensile tests on the fabric to study the mechanical behaviour and mechanisms involved in deformation and damage of these materials. Mechanical properties of the fibres constituting the nonwoven fabrics under the study were investigated with tensile, relaxation and creep tests. Mechanical performance of nonwovens is affected by the orientation of their fibres. In order to investigate this effect, scanning electron microscopy was used for capturing images of the material's microstructure. These images were examined by an in-house software Nonwoven Anisotropy V1, to obtain the orientation distribution function (ODF) of the fibres constituting the fabric, which was introduced to the numerical model of the nonwoven materials to define the randomness of material's microstructure.

In order to develop finite element (FE) model of nonwovens to predict their deformation and damage behaviour, a subroutine based on parametric modelling technique is used to formulate the model by direct introduction of fibres according to ODF computed with digital image processing. The fabric is treated as an assembly of two regions, namely bond points and fibrous matrix, having distinct microstructure. Bond points are treated as deformable solid bodies composed of fibre material. On the other hand, fibrous matrix is modelled as truss elements acting as load-transfer links between the bond points. Elastic-plastic and viscous properties implemented into the model are obtained from single-fibre experiments. The simulations of nonwovens are performed using this FE model and the results of these simulations are compared and validated with those obtained from the experiments. Finally, the conclusions of the entire study along with recommendations for further work are presented.

1.4 Outline

The overall flow of the thesis is summarised schematically in Fig. 1.3. Thesis overall consists of five main sections: Introduction, literature review, experimental study,

simulations and conclusions. Some of these sections are presented in more than one chapter. A brief description of each chapter is given below:

Chapter 2 provides general background information about nonwovens related to their manufacturing techniques, applications and classification. Detailed information about thermally bonded nonwovens is also presented in this chapter.

Chapter 3 presents microstructural and physical features characterizing the mechanical behaviour of nonwoven materials. Besides, parameters affecting the behaviour of thermally calendared bonded nonwovens are also discussed in this chapter.

Chapter 4 contains review of finite element method and equations used to model deformation and damage behaviour using this method. Existing numerical models developed to simulate mechanical behaviour of nonwovens are also discussed in this chapter.

Chapter 5 explains experimental studies focussing on initial as well as evolving microstructure of thermally bonded nonwovens during their deformation and damage. Besides, the mechanisms that govern these deformation and damage behaviours are also investigated in this chapter.

Chapter 6 introduces the method of assessment of mechanical properties of constituent fibres of nonwovens. This chapter also explains the experimental method to obtain failure parameters of single fibres within thermally bonded nonwovens.

Chapter 7 deals with numerical modelling to simulate the deformation and damage initiation as well as evolution behaviours of nonwovens. The simulations are compared with tests and the effects of various material parameters on structural behaviour are examined. The underlying mechanisms of stress and strain distribution in the fibres of nonwovens structure are also analysed.

Chapter 8 summarizes the outcome of the research. Some further studies are suggested based on this research.

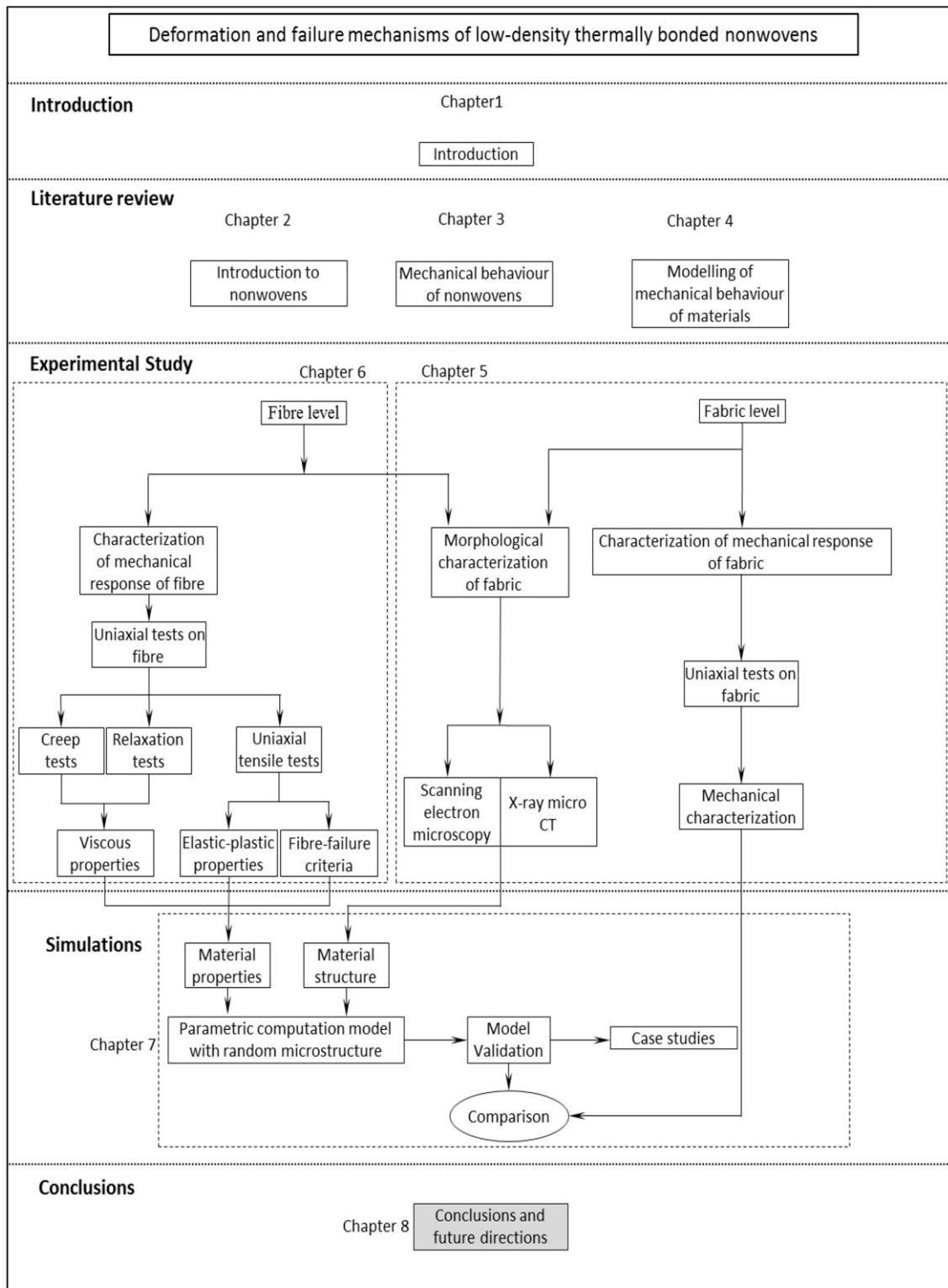


Figure 1.3. Thesis layout and research methodology

CHAPTER 2

NONWOVEN MATERIALS

Nonwovens being engineered fabrics can be designed to have particular characteristics according to their specific purpose. These characteristics are provided by the combination of various properties of nonwoven (e.g. strength, absorbency, flame-retardancy) while maintaining the profitable balance between the cost and expected product life, which can be consisted of single-use such as in disposable products to multiple use for durable products, to ensure fitness for purpose.

The term nonwoven may not be very old, but it is the oldest known textile to the man, existed long before the weaving and knitting. It has been used in times of great antiquity both in Asia and Europe in form of felts¹. The invention and perfection of felt making process can be attributed to Asiatic nomads who exploited the possibilities of its

¹ The information given in this section about history of nonwovens is taken from Burkett, (1979) and Laufer, (1930). The reader is referred there for more detail.

use to its maximum. The earliest found felt remnant was indicated during the fourth season of excavation conducted by James Mellaart in 1965 at Catal Hüyük in Turkey. The painting on the interior wall of a shrine with its pattern and edging technique was a strong reminiscent of felt applique suggested that material was known to neolithic people around 6000 B.C. This suggestion was supported by the finds of actual felt among the textiles from graves in Level VI by Mr. Harold Burnham (Burkett, 1979).

The most amazing Pazyryk felt (exhibited at Hermitage Museum in St Peterburg, Russia) remnants were found during the excavation burial chambers in Altai mountains in Siberia. These felts were preserved and found in amazingly good order by the exceptional circumstances in the regions of permafrost. The Pazyryk finds (from the period dated between 7th and 2nd century B.C.) contain items such as socks, stockings, men's shirts, decorative hangings, saddle covers, carpets etc. Some of the superbly crafted nonwoven felt Pazyryk remnants are shown in Fig. 2.1.

Asia and Europe are the two continents which were familiar with felt making in ancient times. The art of felt making was learnt by civilized nations such as Romans, Greeks, Chinese and Indians from nomads because of its usefulness. Felts have been used by nomads for religious or ceremonial purposes, whereas in civilized nations it was used for utilitarian products (Laufer, 1930). Literary references in ancient records extant in Chinese to the use of felt as shields and other clothes by the warriors go back to 2300 B.C. The use of felt in Greeks is fairly ancient and which was passed on to Roman as there are frequent references in Latin literature about its production and use. The art of felt making was brought to Europe from Central Asia.

For centuries, felt manufacturing remained manual in various parts of the world. In 19th century, the invention of steam machinery brought the industrial revolution which led to manufacturing of products on industrial scale including felt.

Returning to issue of modern nonwovens, with the advent of new technologies, nonwovens are manufactured with different techniques depending upon the types of constituent fibres, their applications and required characteristics.

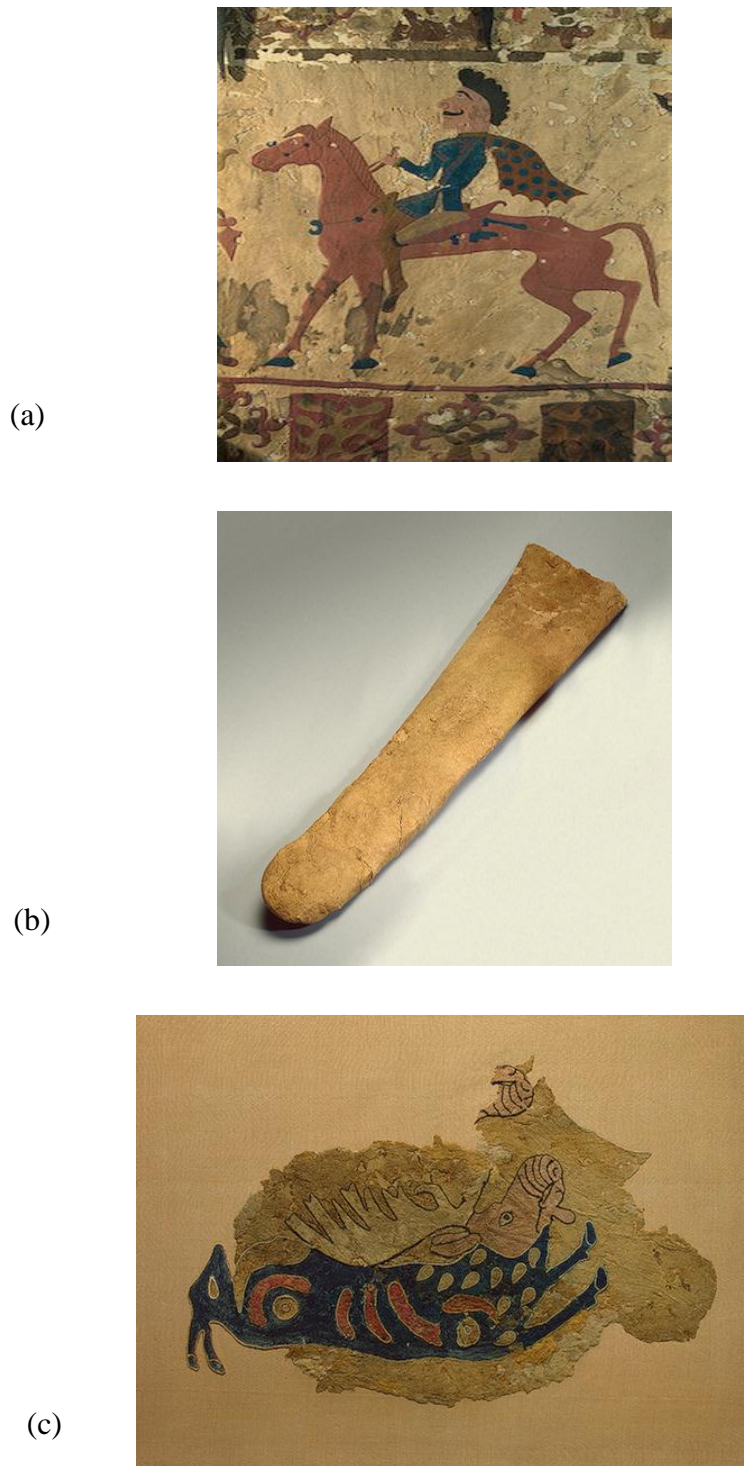


Figure 2.1. Felts remnants from excavation at Pazyryk (a) Carpet fragment showing male rider approaching seated figure, 5th century B.C. (b) felt stockings, 5th century B.C. (c) Fragment of felt covering for saddle, 5th century B.C. (Hermitage museum St. Peterberg, Russia)

Basic information about nonwovens in terms of classification, application areas and properties is provided in this chapter. Some of the basic terminologies of nonwovens, which would be used in succeeding chapters, are also introduced.

2.1 Application Areas

Over the past few decades, the use of nonwovens has augmented rapidly and now it has penetrated in almost all fields of life due to their lower manufacturing cost and flexibility in characteristics. The most popular uses of nonwovens are disposable diapers, laundry wipes, sanitary napkins, filters, carpeting, etc. to name only few end uses (Albrecht *et. al.*, 2003). The consumption of nonwovens for various end-use applications in terms of percentage of its total production is given in Table 2.1.

Table 2.1. European produced nonwovens consumption by end use (Russell, 2007)

Classification	% of Total
Hygiene	33.1
Building/roofing	12.5
Wipes, personal care	8.1
Upholstery/table linen/household	6.8
Wipes, other	6.7
Civil engineering/underground	5.4
Others/unidentified	5.3
Automotive	3.9
Liquid filtration	3.7
Medical/surgical	2.6
Air/gas filtration	2.4
Coating substrates	2.4
Floorcovering	2.3
Interlinings	2.1
Shoe leather goods	1.9
Garments	0.8

According to Table 2.1, major usage of nonwovens is for daily-life consumer products with greatest fraction of nonwoven market is for the hygiene products followed by several structural and mechanical applications such as civil engineering and automotive. Irrespective of the application area of nonwovens, a better understanding of their deformation and failure behaviour is required, so that, they could be manufactured strong enough to perform their intended functions without being disintegrated into individual fibres. Thus, understanding of the mechanical behaviour of nonwovens including their deformation and damage would help to produce the nonwovens with certain mechanical properties aiming for more reliability and durability.

2.2 Raw Material

Over 90% of the total production of nonwovens is carried out using man-made fibres; the fractions of different materials used for the production of nonwovens calculated by Tencon Ltd (Russell, 2007) are:

Table 2.2. Usage of fibre material in nonwoven production

Material	%
Polypropylene	63
Polyester	23
Viscose rayon	8
Polyamide	1.5
Others	3

The share of polypropylene in total production of nonwovens is very high due to following reasons:

- Low glass transition and melting temperatures making it ideal for thermal bonding
- Better stability against chemicals
- Low density making it suitable for light weight fabrics
- Abrasion resistance

Due to the importance of polypropylene in nonwoven industry, the nonwoven used in this research is made of polypropylene based fibres. The complete details of fibre material are given in Chapter 6.

2.3 Manufacturing Stages

Mechanical behaviour of nonwovens highly depends upon the manufacturing parameters. In order to have better understanding of the mechanical behaviour of nonwovens, knowledge of their manufacturing processes is quite important. Manufacturing process of a typical nonwoven consists of following stages:

2.3.1 Web Formation

At this manufacturing stage, fibres are arranged in a sheet or web. The fibre at this stage can be staple packed in bales or extruded filament form. Extruded filaments are produced from the molten raw material(s) and dropped freely on the conveyer belt to form the web. Four basic methods to form the web from staple fibres are:

- Drylaid
- Wetlaid
- Spunlaid

These methods are generally used standalone to form web, however, processes with the use of two or more methods in tandem are emerging.

The orientation distribution of the fibres, which defines the anisotropic properties in the material, is determined at this stage. Fibres can be randomly oriented or can be preferentially oriented along any particular direction, generally along the direction in which web is being produced, according to the requirements of the final product.

2.3.2 Bonding

The webs, with desired orientation distribution of fibres, are consolidated together in this step to obtain the required strength, since webs have very little strength in their unconsolidated form. Web bonding is carried out by the following methods (Batra, 1998):

- Mechanical
- Chemical
- Thermal

During mechanical, fibres are entangled together to give required strength exploiting inter-fibre friction. However, during chemical bonding, binders are used by various methods such as spraying or coating to join the webs together. Thermal bonding is carried out by fusing the polymer fibres together under controlled heating and pressure. Several thermal bonding systems are in use these days for the production of nonwovens such as calendaring, through-air and ultrasonic bonding.

Thermally-bonded nonwovens using calendaring technique make our case study in current research. A brief description of this technique is given in Section 2.5.

2.3.3 Finishing

Nonwovens provide an opportunity to customise their properties according to the requirements of the customer by an additional procedure called finishing. During finishing, different chemicals can be employed to provide certain characteristics to

nonwovens such as flame retardancy, water resistance, absorbency etc. to make these suitable for service conditions.

2.4 Classification

Nonwovens can be divided into many sub-groups depending on their fibre material, planar density, web forming and web bonding conditions and fibre geometric characteristics, as shown in the Fig. 2.2.

The mechanical behaviour of nonwovens depends on many factors such as manufacturing parameters, material of constituent fibres etc. Changes in any of these factors bring enormous variation in the behaviour of the fabric (Batra, 1998; Adanur and Liao 1999; Datla 2002; Lin *et. al.* 2003; Bhat *et. al.* 2004; Kim, 2004; Rawal, 2006). Therefore, different types of nonwovens possess different characteristics and exhibit distinct behaviour. Hence, in order to define a nonwoven a complete set of information including web forming and web bonding technique, fibre geometric and material properties, and planar density is required. Since, different types of nonwovens exhibit different mechanical properties; it is difficult to develop a FE model valid for all types of nonwovens. In order to set the research framework tractable, it is focused on low-density caldered bonded nonwovens manufactured with staple monocomponent polypropylene based fibres. A brief introduction of thermal bonding and the parameters involved in it affecting the mechanical properties of end product are given in next sections.

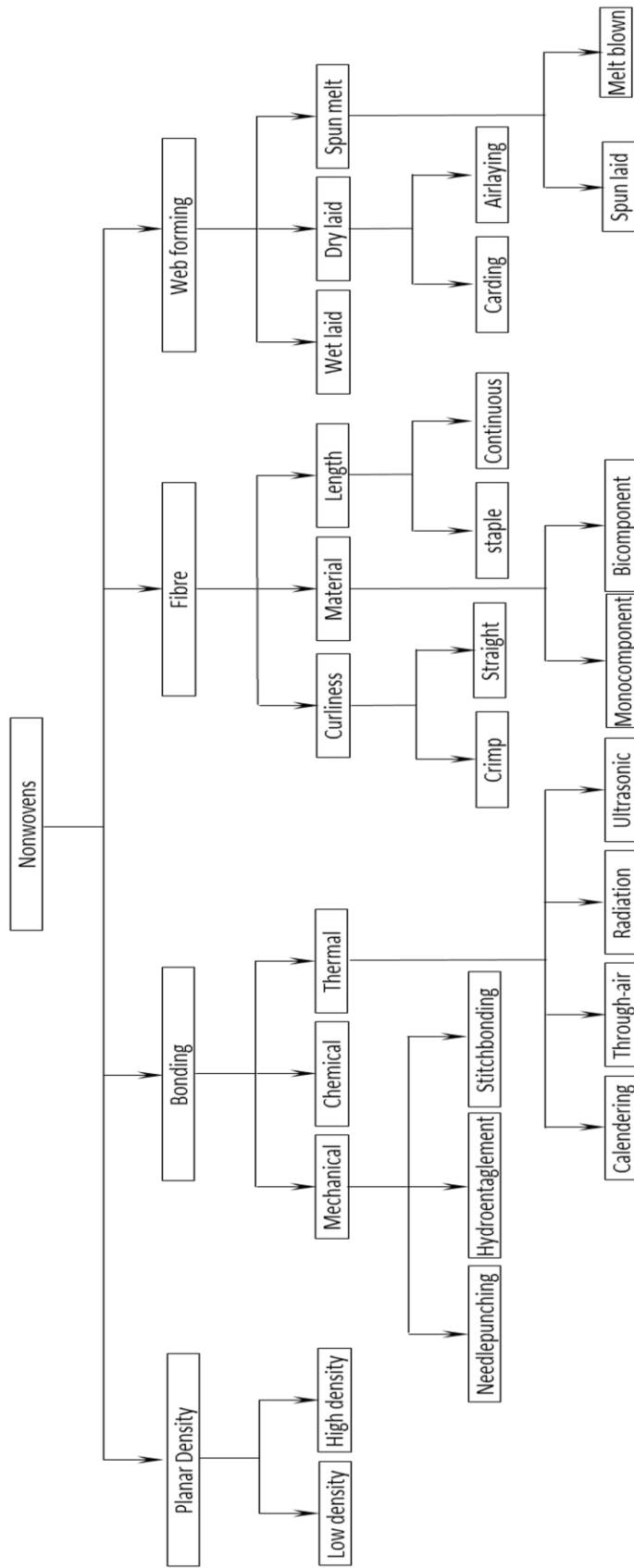


Figure 2.2. Classification of nonwovens

2.5 Thermally Bonded Nonwovens

Thermal bonding is a process in which thermoplastic properties of synthetic fibres are exploited to form the bond under controlled heating. Thus, thermoplastic component must be present in the constituent fibre or in the form of powder, film or as a sheath part of bicomponent fibre. In practice, heat is applied during thermal bonding until the thermoplastic component becomes viscous to melts. Polymer flows by surface tension and capillary action to fibre-to fibre crossover point at localized point of heating. These localized regions are fixed on subsequent cooling forming the bond points (Russell, 2007; Bhat *et. al.*, 2012; Michielsen and Wang, 2002; Michielsen *et. al.*, 2006). Thus, thermal bonding process converts a web of fibres with weak bonds between them into a tenacious fabric. Nowadays, thermal bonding is one of the most widely used technologies in manufacturing of nonwovens (Bhat *et. al.*, 2004; Mishakov *et. al.*, 2006; Michielsen *et. al.*, 2006). The viability of thermal bonding lies in the several advantages over other manufacturing processes of nonwovens. The most important of them are:

- Less capital investment (Pourdeyhimi, 2003)
- Lower manufacturing cost (Bhat *et. al.*, 2004)
- Higher production rate (Albrecht *et. al.*, 2003; Bhat *et. al.*, 2004)
- Better control on nonwoven properties (Albrecht *et. al.*, 2003)
- Less environmental impact (material can be 100% recyclable) (Russell, 2007)

There are several types of thermal bonding processes, such as hot calendaring, through air bonding, ultrasonic bonding, and radiant bonding (Gao and Huang, 2004). Following is a brief introduction to some forms of thermal bonding (Hutton, 2007):

Through air bonding: The web is thermally bonded by passing the web through hot air dryer. This type of thermal bonding result in bulkier web which is used in HVAC (heating, ventilation and air conditioning) applications.

Ultrasonic bonding: In this process, thermal energy is conveyed by a mechanical hammering action (high frequency vibration). This involves a brief contact time with a limited pressure between ultrasonic horn and the web. In this process, energy is transferred to restricted areas and thus bonding takes place along narrow lines.

Calendering or embossing: The web is squeezed between two rollers (smooth or patterned) at controlled temperature which forces the contact of molten fibres with other fibres in the web to form the bond. The fabric formed by this process can be smooth or can have bond spots in a pattern depending upon rollers.

Thermal radiation bonding: Energy transferred by radiations is used for bonding of nonwoven material in this process. The energy is transported by electromagnetic waves (or alternatively photons).

Since thermally calendered bonded nonwovens are used as representative material for fibrous network in this study, further discussion is focussed on this type of thermal bonding process.

2.5.1 Calender Bonding

During calender bonding, fibres are joined together by applying certain conditions i.e. temperature and pressure. These external conditions are provided by two hot rolls pressed against each other. The surface design of these rolls can be smooth or have an embossed pattern. When the fibres are passed through these rolls, the temperature and pressure involved cause the fibres to melt and diffuse with other fibres resulting in bonding of fabric. The process of transferring fibre web into nonwoven fabric is shown in Fig. 2.3.

Smooth rollers are designed to heat the entire surface of the web. Therefore, binder fibres produce bonding at all crossover points resulting in thin and stiff fabric. However, engraved rollers result in localised melting and diffusion of the fibres only at its raised areas resulting in bonded spots on subsequent cooling called *bond points* (see Fig. 2.4) (Hegde *et. al.*, 2008; Bhat and Malkan, 2002). Therefore, nonwovens manufactured with thermal bonding consist of two distinct regions: fibrous web and bond points (Fig.

2.3). Bond points formed by partial melting of fibres in regions under raised pattern on calendar surface are connected by fibrous matrix in calendered bonded nonwovens.

The commonly used materials for calender bonding are polymers, in which Polypropylene is most frequently used due to its chemical stability, good mechanical strength and low melting temperature (Demirci, 2010). One of the characteristics of the polymer is changing in mechanical properties with change in temperature.

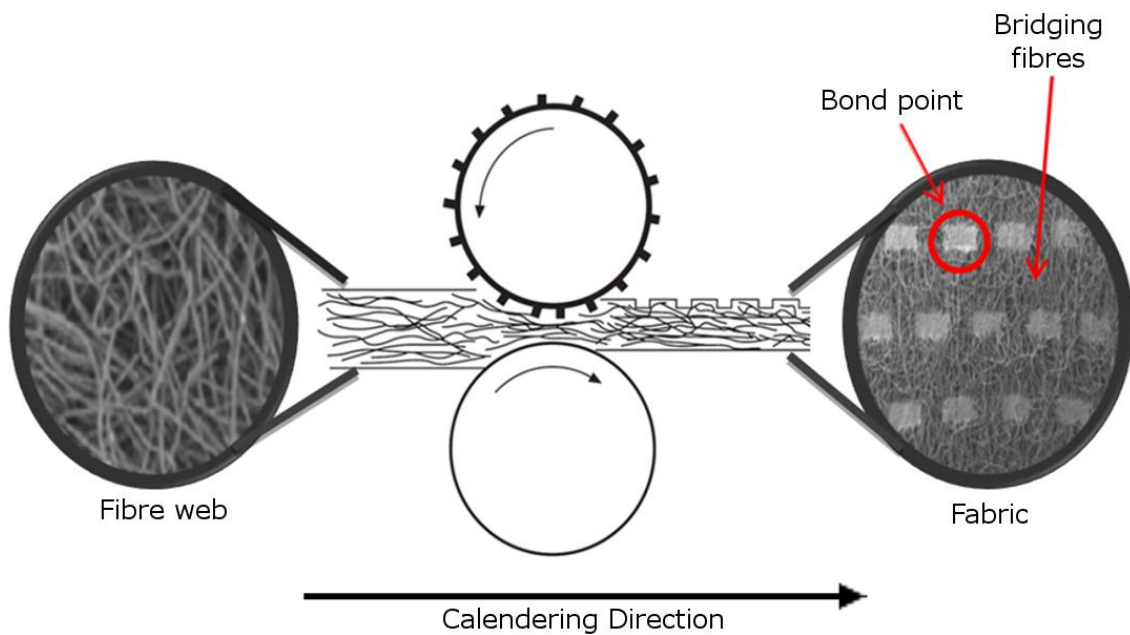


Figure 2.3. Typical hot calendering process

2.5.2 Fibre Composition and Fabric Structure

The nonwovens have unique mechanical behaviour, which is partially different from their fibres. This behaviour depends not only on the properties of constituent fibres but also on their microstructure (Ridruejo, 2011). The macroscopic properties (mechanical and physical properties) and microstructure of nonwovens are determined by the fibre composition and the fabric structure. Both of these are briefly described below:

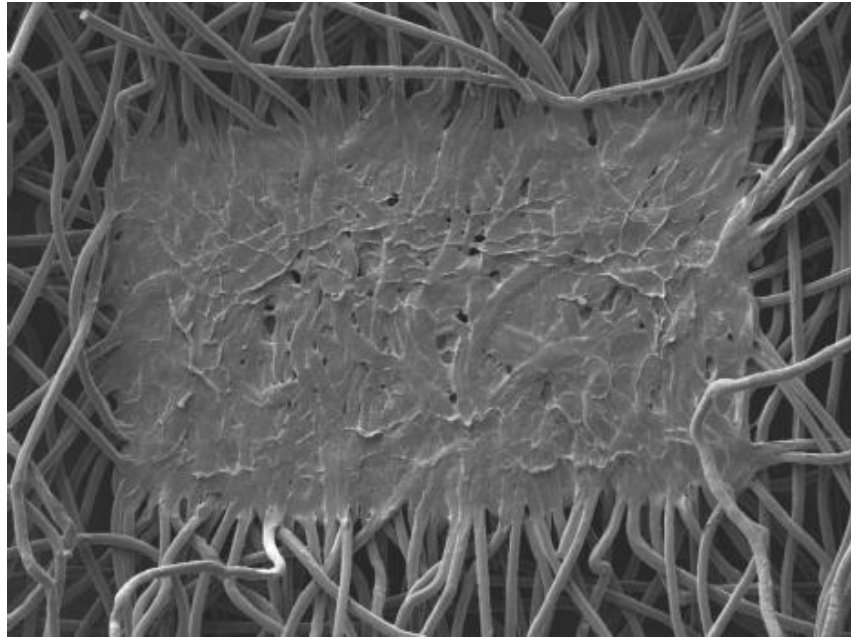


Figure 2.4. Typical bond point produced with hot calendering process

Fibre composition stands for the material, structure and mechanical behaviour of the fibre. It is an important factor in defining the properties of nonwovens. For example use of non-hazardous recyclable fibres for manufacturing of nonwoven would provide environment friendly nonwovens. Similarly, the surface area of the fabric is directly on cross-sectional area and denier of the fibres (Tascan and Edward, 2008). Furthermore, mechanical properties of constituent fibres of nonwovens determine their mechanical behaviour since fibres between bond points take load individually (Sabuncuoglu, 2012). Besides, properties of the fibres, their orientation distribution within the fabric also play role in determining nonwoven properties. Including orientation distribution of fibres, size, shape and pattern of bond points refer to fabric structure. Fabric structure of nonwovens can be optimized to tailor their characteristics for desired functionality. During thermal bonding process, some unique features are developed in the nonwovens making them distinct from other types of nonwovens. These features are as follows:

- Nonwovens are composed of two regions: bond points and a fibre matrix
- Morphological changes occur in fibres due to effect of heat during the bonding process and morphology of the fibres at bond perimeter is different from the original fibre and the bond point

2.6 Summary

Application areas, classification of nonwoven materials, manufacturing techniques and general introduction of thermally bonded nonwoven is given in this chapter. Having unique behaviour and manufacturing advantages such as cost-effectiveness and fast production rate, as compared to woven fabrics, nonwovens have a wide application spectrum. Being engineered fabrics, properties of nonwovens could be tailored depending upon the application area. Since this research focuses on mechanical behaviour of nonwoven materials for which thermally point-bonded nonwoven is used as representative material. The mechanical and physical properties of these materials must be discussed as these are closely related to the current research and are explained in the next chapter.

CHAPTER 3

MECHANICAL BEHAVIOUR OF NONWOVENS

The suitability of a nonwoven for a specific application is determined by its physical, chemical and mechanical properties. Although, these properties are very important from their manufacturing perspective, only physical and mechanical properties are discussed in this chapter as they are related to the deformation and damage behaviour of nonwovens.

The physical properties of the fabric include dimensions of its geometric entities (bond points in case of thermally bonded nonwovens), shape, size, bonding area; basis weight and orientation distribution of fibres in fabric. However, physical properties of a fibre includes its diameter, length, crimp, density (denier), cross-sectional area, structure (Russell, 2007). Physical properties of both — fabric and its constituent fibres — play an important role in defining the behaviour of nonwovens e.g. bond point size as a

percentage of fabric area influence the stiffness of the fabric and basis weight effect many parameters such as thickness, tearing strength etc. However, mechanical properties of the fabric deal with the investigation of fabric behaviour under mechanical loading. Both of these, mechanical and physical, properties are utilised to characterise the behaviour of the fabric in this study. A thermally calendered bonded nonwoven consists of two regions (bond points and fibre matrix) having distinct microstructure. Mechanical behaviour of a nonwoven fabric could only be predicted by the knowledge on the properties of these regions, which are affected by various manufacturing parameters discussed in Section 3.4.

3.1 Mechanical Properties of Fibres

The mechanical properties of the fibres forming the fabric are essential to determine the mechanical behaviour of the fabric. The mechanical properties of fibres are defined by a number of parameters such as tenacity, initial modulus, breaking force, and creep strain (Gusick *et. al.*, 1963). These properties can be determined with tensile, relaxation and creep testing on single-fibre. Due to the nature of polymer fibres and variation in temperature during bonding process affects the dimensional stability and molecular structure of fibres and thus the fibre modulus. These changes in fibre morphology eventually affect the overall mechanical properties of the nonwovens (Michielsen and Wang, 2002; Dharmadhikary *et. al.* 1999) especially related to damage and failure of the fabric. Therefore, this variation in fibres' properties caused by manufacturing parameters must be considered during characterizing the mechanical behaviour of fibres constituting nonwoven fabrics in Chapter 6.

3.2 Mechanical Anisotropy

Due to the nature of web formation and bonding processes, fibres in a nonwoven are not completely randomly oriented but predominantly oriented along the direction in which the fabric is being produced. This preferential orientation of fibres in nonwoven materials causes anisotropic mechanical properties (Michielsen *et. al.* 2006; Kim, 2004)

and it is the most prominent feature of the mechanical behaviour of nonwovens. Mechanical anisotropy of nonwovens due to preferential orientation distribution of their fibres affect the relation between neighbouring bond points connected by fibrous matrix and thus the overall behaviour of the fabric (Pourdeyhimi *et. al*, 1996). Therefore, accurate determination and implementation of the fibres orientation and bond pattern into the computational model have vital importance for successful prediction of deformation and damage initiation as well as evolution behaviours of nonwovens.

The level of anisotropy in nonwovens is much higher than those of their woven counterparts, which have different mechanical properties in two principal directions, namely, warp and weft (Price *et. al.*, 2006). In the case of nonwovens, two principle directions, machine direction (MD) and cross direction (CD), are used to make the anisotropy simple. MD is longitudinal direction corresponding to the manufacturing direction of nonwovens. CD is the perpendicular direction to MD in the plane of web.

The orientation distribution of fibres is one of the prerequisites to deal with the randomness of nonwoven materials. “Fibres distribution function” was introduced for the first time to represent the fibre orientation in the fibrous media by (Cox, 1952). After which, the orientation distribution function (ODF) became a common way to deal with the randomness of fibres. The ODF quantifies the level of randomness of fibre matrix within the nonwoven material. Since, the randomness in a fabric’s microstructure characterize its anisotropic behaviour, determination of its ODF is essential for predicting its direction-dependant mechanical behaviour of the fabric (Wood, 1990; Xu and Ting, 1996).

Many researches have been done to determine the ODF of fibrous network. Initially, the phenomenon of dichroism and birefringence was suggested to determine the ODF. Then, the development of computers and imaging devices make it possible to determine ODF directly from the images of the fibrous network. The development of different techniques has been provided in Table 3.1 in chronological order.

Currently, two main methods are used to determine ODF of textiles: Fast Fourier Transform (FFT) and Hough Transform (HT). Fast Fourier transform is one of the most

useful technique in the field of image processing (Xu and Ting, 1995). It is an indirect method which decomposes the image from its spatial domain of intensities into frequency domain. There are some drawbacks associated with this technique e.g. lighting conditions can affect the results or binarized image may give false ODF (Ghassemieh *et. al.*, 2001). Using the HT method, fibres in the fabric could be detected via straight-line segments (Xu and YU, 1997). The main advantage of HT over FFT is that the results are relatively less affected by the image noise (Ghassemieh *et. al.*, 2002).

The software used in this for the determination of ODF is developed by Demirci *et. al.*, 2012, using HT technique. It can compute the ODF of any fibrous media (e.g. fibrous metal networks, fibre-reinforced composites) from its micro-image obtained with X-ray micro CT or Scanning Electron Microscopy (SEM) technique. The graphical user interface of this software is shown in Fig. 3.1.

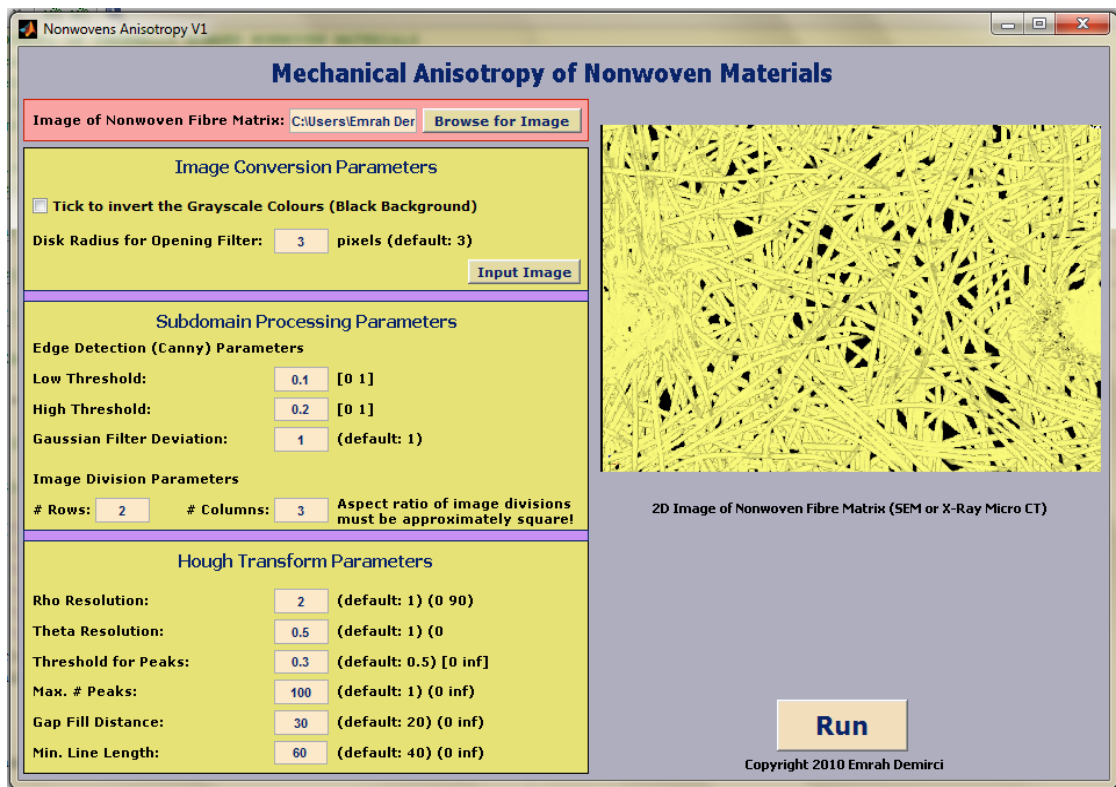


Figure 3.1. Graphical user interface of orientation distribution determination software developed by Demirci *et. al.*, 2011

This software computes the ODF and give it in the form of histogram presenting the distribution of fibres relative to the reference direction. The complete detail of obtaining the ODF using this software is given in Appendix A.

In addition to randomness of the microstructure and bond point geometry, crimp of the fibres also contributes to the anisotropic behaviour of the nonwovens. Crimp is defined as the successive waviness in the fibres induced mechanically or chemically (Brown, 1995). Unlike natural fibres, synthetic fibres such as polymer based fibres are straight when they are extruded. These fibres do not have sufficient cohesion between them to make a web. Therefore, crimp is introduced in these fibres to provide appropriate fibre to fibre cohesion and make it possible to process these fibres with the machinery originally developed for natural fibres. Fibre crimp is beneficial not only during manufacturing of fabrics but also improve desirable properties in fabrics such as wrinkle resistance, moisture absorption, wear comfort due to porosity, warmness etc. (Barach and Rainard, 1950).

Due to crimp, not all the fibres are under same loading up to a certain level of loading of fabric. Crimped fibres cause not only anisotropy but also considerable variation in mechanical behaviour with respect to their uncrimped (straight) counterparts (Shiffler, 1995). Therefore, crimp is an important factor in determining the mechanical behaviour of nonwovens during their initial deformation.

The effect of fibre crimp on the properties of fibre network was first studied by Hearle *et. al.*, 1963. A micromechanical model to predict the mechanical behaviour of nonwoven was developed by Rawal, 2006 based on the earlier work done by Adanur and Liao, 1999. In this model, fibre curl factor was introduced to develop the understanding of the effect of loading on the curled single fibre.

Table 3.1. Techniques used for computing ODF

Technique	Author(s)	Year
Visual method based on directional phenomenon of dichroism and birefringence directly from the fibrous media	Hearle and Stevenson	1963
Zero span tensile testing method	Kallmes	1969
Optical method based on the illumination of the fibres in known direction by the light microscope	Chudleigh	1984
Computer system based on the light diffraction phenomenon	Stenemur	1992
Random sampling algorithm and software to pick the random fibres and trace them to estimate the ODF	Huang and Bresee	1993
Skeletonization algorithm to extract the ODF from the images taken by CCD camera	Xu and Ting	1995
Software based on Fast Fourier Transform (FFT)	Kim and Pourdeyhimi	2001
ODF based on Hough Transform of images	Demirci <i>et. al.</i>	2011

3.3 Deformation and Damage Behaviour

Nonwoven fabrics have unique and complex deformation and damage behaviour. Many researchers have endeavoured to investigate the deformation behaviour of nonwovens which partially resembles the behaviour of other engineering materials; e.g. they present anisotropy similar to woven material and exhibit viscoelasticity similar to polymers. The two distinct regions of a celender bonded nonwoven material, bond point and fibre matrix have different microstructure and both of these region play their role in defining the overall deformation and damage initiation as well as propagation behaviour of the fabric.

Deformation characteristics of nonwoven materials vary with the direction of loading, due to their anisotropic behaviour. Normally, the MD and CD directions are used to explain these characteristics of nonwovens (Kim *et. al.*, 2000; Kim *et. al.*, 2001(b); Kim 2004(a)) but the angles between MD and CD are also used for further explanation of deformation of these materials (Michielsen *et. al.*, 2006) (Fig. 3.2).

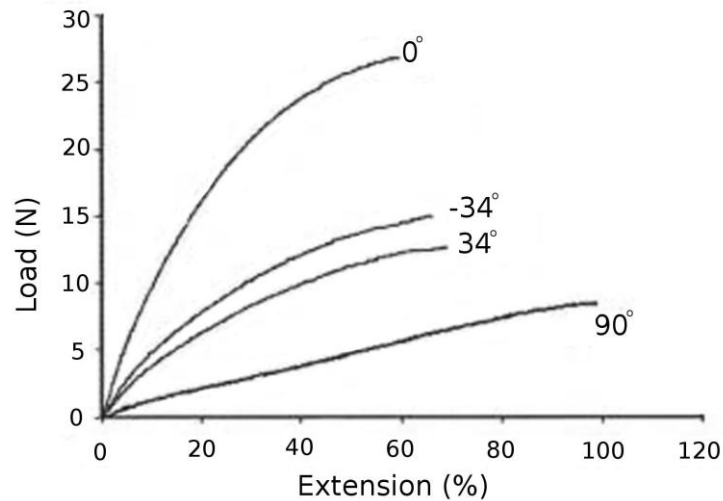


Figure 3.2. Direction-dependant behaviour of thermally bonded nonwovens; 0° and 90° represent MD and CD, respectively (Michielsen *et. al.*, 2006)

Deformation and damage initiation as well as damage evolution processes of nonwovens involve many mechanisms that affect the overall behaviour of nonwovens e.g. reorientation of fibres along loading direction, straightening of fibres to be

uncrimped, fibre sliding and stretching etc (Ridreju *et.al.*, 2010, Kim and Pourdeyhimi, 2000, Anderassen, 1995). The complexity of the deformation and damage behaviour of nonwoven materials until their failure can be referred to the fact that these mechanisms act simultaneously during their deformation and damage processes (Ridreju *et. al.*, 2011). Deformation behaviour of a nonwoven is governed by the loading direction with respect to preferred orientation of constituent fibres. The type of the load on individual fibres, during the deformation and damage processes of the fabric, depends on their orientation as compared to the direction of loading (Kim 2004(b)). Thus, random microstructure of a nonwoven gives direction dependency of its deformation and damage behaviours. Mechanical anisotropy of deformation behaviour of thermally bonded nonwovens is depicted in Fig. 3.2.

According to Fig. 3.2, the deformation of the nonwoven materials in MD is less than to that in CD at any particular loading value. Thus, nonwoven materials have higher strength along MD than CD. This is a typical behaviour of spunlaid nonwovens which are manufactured by direct conversion of polymers into endless filament and laid directly on a conveyor belt. This tend to have the filaments oriented along the conveyor belt resulting in a fabric with fibres preferentially orientation along MD. Thus, a negligible reorientation of the fibres occurs when the nonwoven materials are deformed along MD. While, the loading of material in CD results in the large number of fibres rotation along loading direction and repositioning of the bond points. These deformation mechanisms of nonwovens are illustrated in Fig. 3.3. However, in case of staple fibres, orientation distribution of fibres can be controlled in any preferred direction depending upon the requirement.

On loading, fibres start to reorient themselves along loading direction at the initial stages of deformation. This process continues upon loading and fibres start to take participation in load bearing (Fig. 3.4). On further loading, fibres start to fail leading to localized damage which ultimately leads to the rupture of the nonwovens (Ridreju *et. al.*, 2011). Due to preferential orientation of fibres in fabric results in different shapes of failure loci which are shown in Fig. 3.5. Failure loci along MD and CD are practically similar, however loading between these two principal planes result in

different failure locus. Thus, due to anisotropic behaviour, not only deformation and damage initiation but damage evolution and ultimate failure of nonwovens have directional dependency. Heterogeneity in the microstructure of nonwoven fabrics, provide anisotropic failure behaviour as shown in Fig. 3.5. The fabric failure occurs by tearing of fibres in MD and CD, while for the test angles between MD and CD, it fails by shearing at preferred fibre direction (Michielsen *et. al.*, 2006; kim *et. al.*2004a).

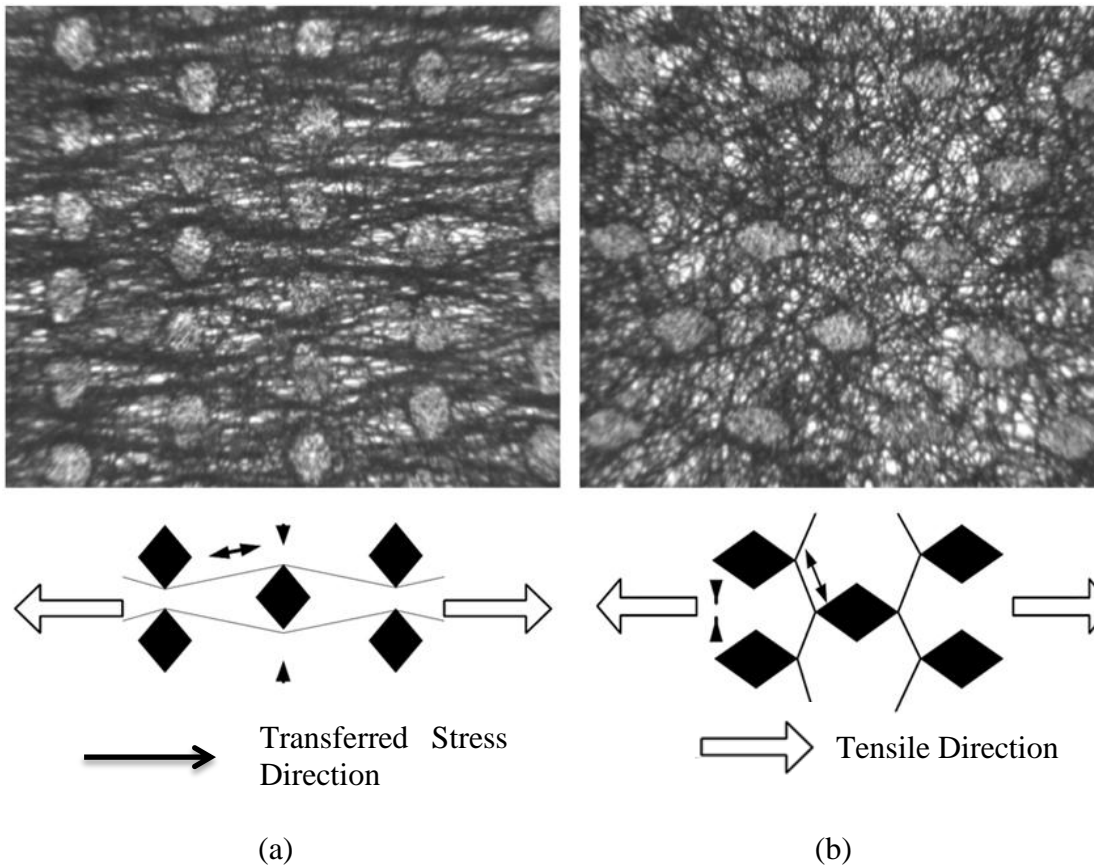


Figure 3.3. Deformation mechanisms of nonwoven fabric after 50% elongation in MD (a) and CD (b) (Kim *et. al.*, 2001)

The load-extension curve of nonwoven materials (Fig. 3.2) shows that they exhibit not only anisotropy but also nonlinear behaviour. The nonlinearity in behaviour of a nonwoven is because of two main reasons: material nonlinearity and geometric nonlinearity. In addition, nonwovens also exhibit time-dependant properties due to the viscose effects of the constituent material. The nonlinear and time-dependant properties

contribute to the complexity of deformation and damage behaviour of nonwovens. Both of them are briefly described in the following sections.

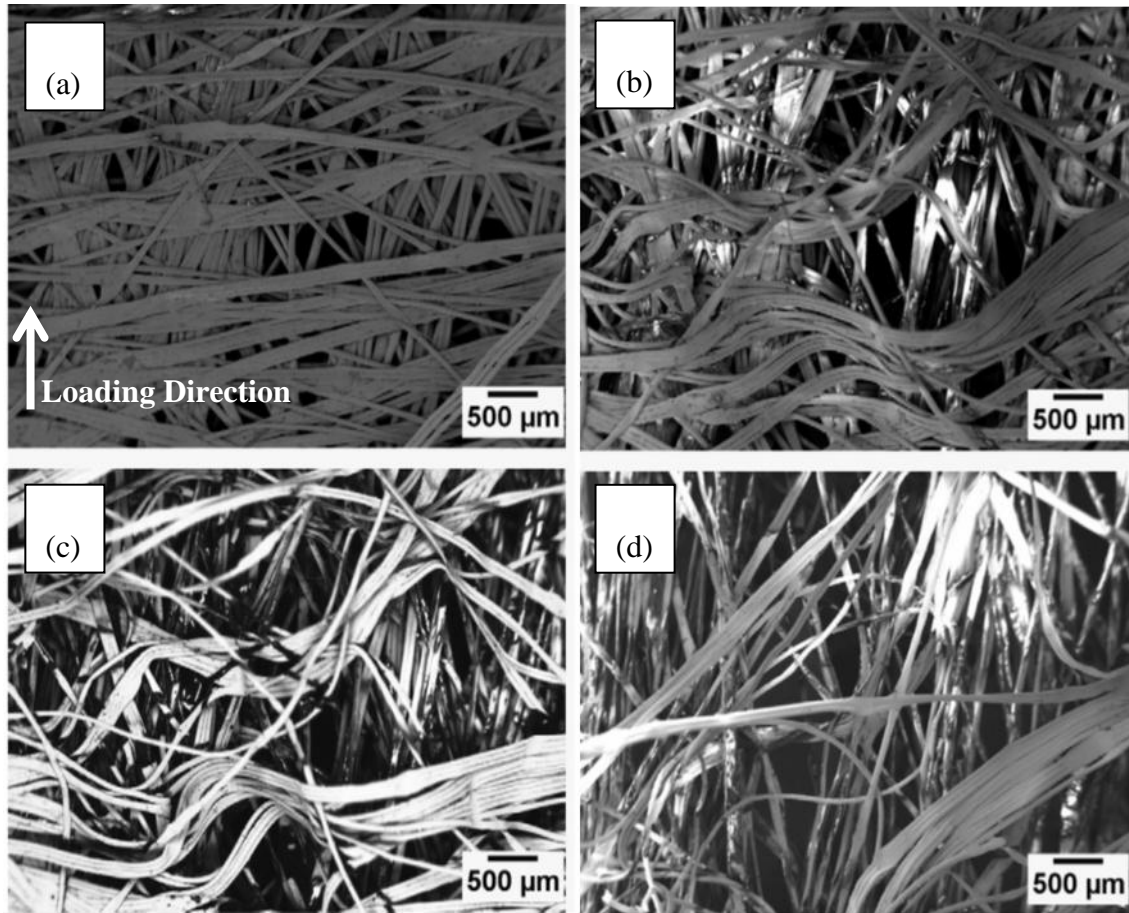


Figure 3.4. Damage micromechanisms in the nonwoven fabric during tensile (a) 0% nominal strain, (b) 20% nominal strain, (c) 40% nominal strain, and (d) 100% nominal strain (Ridruejo, 2011)

3.3.1 Nonlinearity

Nonlinear behaviour of a system can be caused by any of its several characteristics like large deformations or strains, material behaviour, and effect of contact or other boundary conditions. Thus nonlinear behaviour can be classified on the bases of origin of nonlinearity (MSC. Marc, 2011).

3.3.1.1 Material Nonlinearity

Material nonlinearity arises when the stress-strain (constitutive) response is nonlinear. This nonlinear behaviour can be observed in many cases such as in plasticity, creep, and/or damage. In some hyperelastic materials, such as rubber, nonlinear behaviour can be observed in elastic region. Material nonlinearity in plasticity is shown in Fig. 3.6.

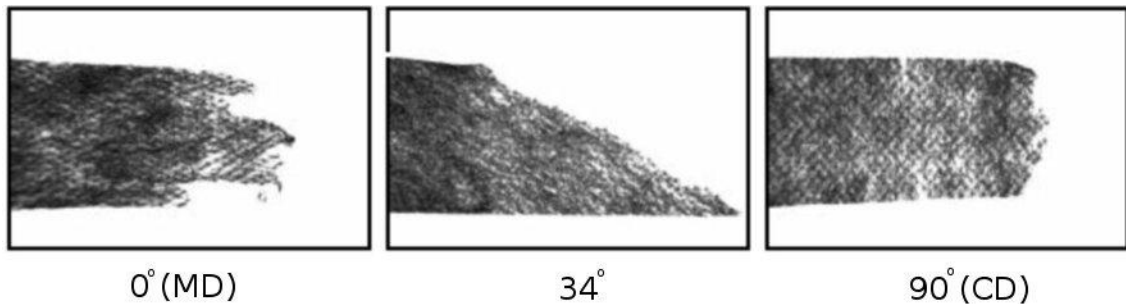


Figure 3.5. Images of failure of nonwovens in various loading directions (Kim, 2004a)

In case of nonwovens, constituent materials play an important role in defining their overall properties. Elastic and plastic properties of the constituent fibres give the nonlinear behaviour to the fabric and described as nonlinear relationship between stress and strain. During deformation of a fabric, its fibres after reorientation along loading direction remain within the elastic range up to a certain value of loading. On further loading, material enters into its plastic range and irreversible deformation starts. The elasticity and plasticity range of the nonwovens depend on the material of the constituent fibres. The higher the value of these ranges, more energy will be absorbed by the material during deformation (Ridreju *et. al.*, 2011a).

3.3.1.2 Geometric Nonlinearity

Geometric nonlinearity arises in various cases such as large strain or small strain but with large rotation and displacement. The direction, distribution and magnitude of the applied forces may also be changed as the structure deforms (Madenci and Guven, 2007).

In nonwovens geometric nonlinearity is observed because of rotation of large number of fibres even at small strain. Another, important parameter that gives rise to geometric nonlinearity of a nonwoven fabric is fibre curvature (Mittal *et. al.*, 1992). Upon loading the fabric, fibres are straightened according to the size of their curvature. At the initial deformation, only the fibres with low curvature are the main carrier of the load, while the fibres with high curvature keep their state. Thus, the number of fibres bearing the load increases with deformation which leads to nonlinear behaviour of nonwovens (Cook, 1995).

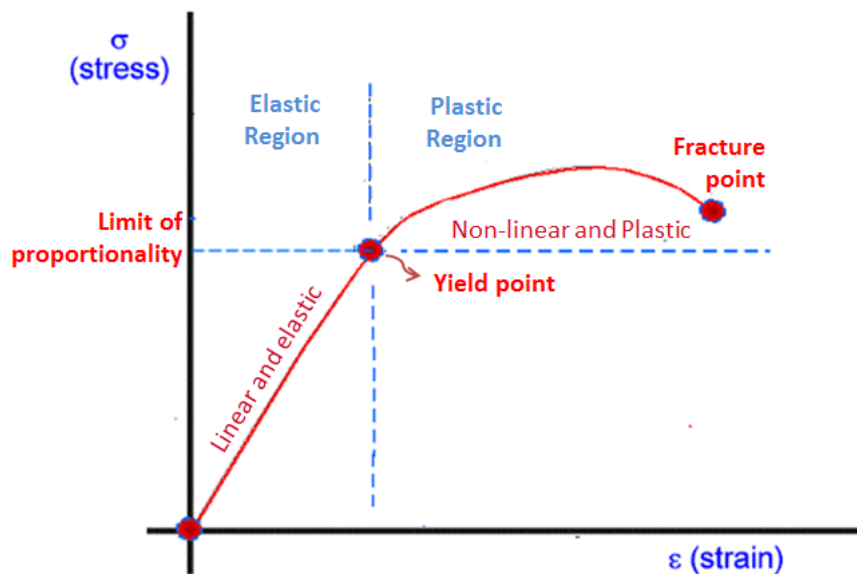


Figure 3.6. Stress - strain graph for elastoplastic material

3.3.2 Time-Dependant Properties

One of the prominent characteristics of the polymers is their time-dependency. Due to the nature of polymers, nonwoven exhibit viscous behaviour. This behaviour can be observed in many structural materials (e.g. steel, aluminium, etc.), but its effect on the overall mechanical performance of the materials could be neglected depending upon the time scale of simulation. However in polymers, its effects are prominent and cannot be neglected generally. The stress and/or strain levels in nonwovens change with time due to creep and relaxation phenomenon attributed to viscous properties of the material. Relaxation is the decrease in stresses with time when the strain is kept constant.

Conversely, increase in strain with time at constant stress level is called creep. In this class of materials, the stress-strain curve during spring back of material deviates from loading path due to energy dissipation (Fig. 3.7).

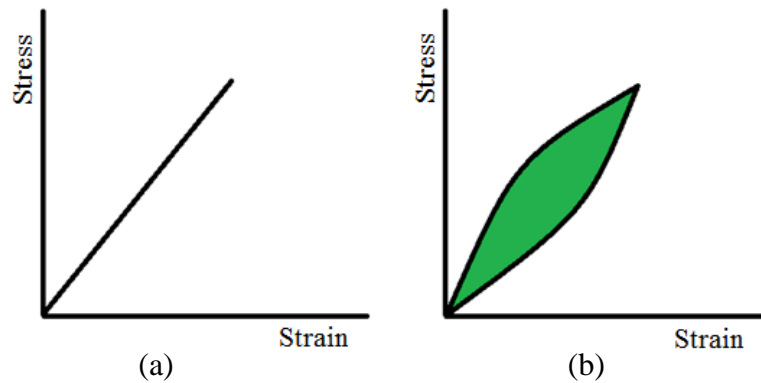


Figure 3.7. Stress-strain curves of purely elastic (a) and viscoelastic (b) materials (The green area represents the amount of energy lost in a loading-unloading cycle)

Due to the presence of viscous properties, polypropylene based nonwovens exhibit complex deformation and damage behaviour which is highly dependent on the loading rate. Viscous effects in nonwovens are very prominent and must be considered for the development of the finite element model.

3.4 Factors affecting the properties of nonwovens

A point bonded nonwoven consists of bond points and a fibrous web linking these bond points. Both of these regions, having unique properties, play their role in determining the overall behaviour of nonwovens (Chidambaram *et. al.*, 2000). The properties of both regions are affected by a number of manufacturing parameters which ultimately affect the deformation and damage behaviour of nonwovens. Besides, material properties and composition of constituent fibres are prominent in determining the mechanical behaviour of nonwovens. Some important parameters that affect the mechanical behaviour of nonwoven are briefly described in this section.

Mechanical behaviour of thermally bonded nonwovens is affected by the following parameters (Albrecht *et. al.*, 2003):

- Bonding temperature
- Fibre composition and material properties
- Calendering pressure
- Web speed
- Morphology and fibres form
- Orientation distribution of fibres
- Crimp in fibres

Detail on how these parameters affect the behaviour of nonwovens is given below.

3.4.1 Bonding Temperature

During thermal bonding, fibres are heated up to a certain temperature under pressure resulting in melting of fibres locally and produce a rigid bond on solidification. The ultimate tensile strength of fabric structure increases with increase in bonding temperature until the temperature reaches its certain maximum value after that fabric load bearing capacity decreases with further increase in temperature (Dharmadhikary *et. al.* 1999; Russell, 2007; Michielsen *et. al.*, 2006; Fedorova *et. al.* 2007). Thus, bond points of nonwovens bonded with a temperature below a certain value are immature and fabric failure starts with disintegration of bond points because of insufficient fusion of fibres so called under-bonding. Conversely, if nonwovens are bonded at temperature higher than a certain value, fabric failure starts with breaking of fibres at bond periphery leaving the bonds intact called over-bonding. The difference between these temperatures values are referred as optimum temperature window of a fabric. The optimal temperature range varies for fabrics composed of different materials (Albrecht *et. al.*, 2003). Optimal temperature window of Polypropylene based nonwovens is 150 °C – 160 °C. The fabric bonded at optimal temperature is called well-bonded fabric.

Fig. 3.8 shows the variation of properties of nonwoven with varying bonding temperature.

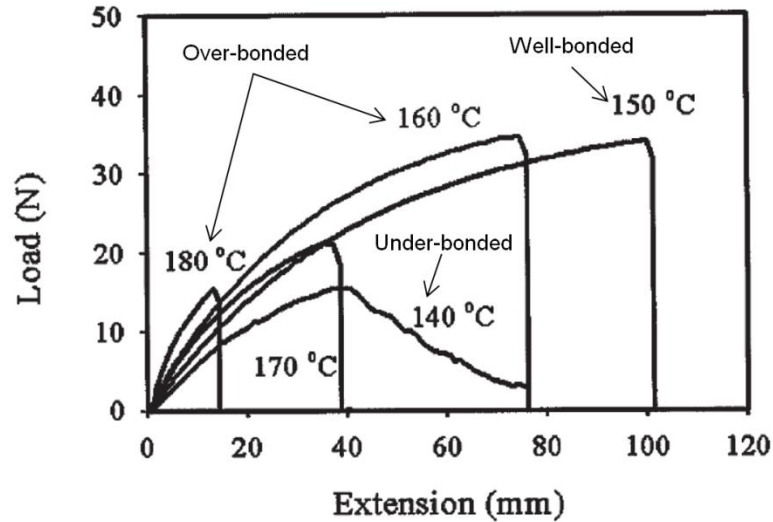


Figure 3.8. Effect of bonding temperature on properties of nonwovens (Michielsen *et al.*, 2006)

3.4.2 Fibre Structure and Properties

Thermoplastic materials and blends containing fibres can be used for manufacturing of thermal bonded fabrics. According to the composition structure, two main types of fibres are used for the thermal bonding: monocomponent and bicomponent.

In monocomponent fibres, all the structure is produced from a single type of fibre material. In other words, a single material determines the properties of both, the fibrous network and bond point. The major disadvantage encountered when using monocomponent fibre is the narrow bonding temperature window, which is difficult to achieve. Furthermore, fibre structure is discontinuous as the formation of bond points is succeeded with the melting of fibres (Datla, 2002). These problems can be rectified by using bicomponent fibres. These fibres are composed of two different polymer components, one of which has lower melting point and serves for bonding while the other has comparatively higher melting point and serves for tensile strength. When these fibres are exposed to the temperature between the melting points of two polymers,

the polymer with lower melting point melts and joins the neighbouring polymer under pressure and solidifies with cooling resulting rigid bond points. The material with the higher melting point does not melt and maintain its structure during this process. Thus, bicomponent fibres retain their continuity in the bond point and fabric can withstand higher stresses due to increased strength (Wang and Gong, 2006). Various types of cross-sections of bicomponent fibres are given in the Table 3.2.

Table 3.2. Types of bicomponent fibres

Fibre Type	Schematic diagram			
Side by side				
Sheath core				
Island in the sea				

3.4.3 Calendering Pressure

During thermal bonding, fibrous web is passed between two hot calenders, where fibres melt locally under high temperature and pressure to form the bonds on subsequent cooling. This compression has a direct relation with the melting point of fibres of nonwovens. The pressure applied during bonding process perform the following tasks (Albrecht *et. al.*, 2003):

- To augment heat transfer from rollers to the fibres through conduction
- To increase the contact area of fibres by helping in plastic flow of fibre material at bonding temperature
- To restrict the flow of material at bond spot

Therefore, appropriate compression pressure is one of the pre-requisites for the optimal bonding. Michielsen *et. al.* (2006) found that beyond the certain minimum value of compressive pressure, fabric performance is slightly or not affected as shown in Fig. 3.9. Minimum appropriate value of the pressure adequate for rigid bonding depends on the contact geometry, thermodynamic conditions and web speed during bonding process.

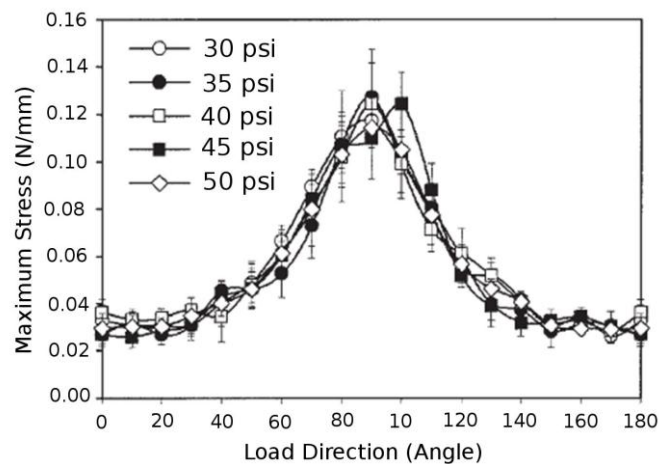


Figure 3.9. Mechanical properties in various directions as a function of nip pressure (Michielsen *et. al.*, 2006)

3.4.4 Web Speed

It is the speed at which the nonwovens are produced. In order to reduce the manufacturing cost of nonwoven, a high web speed is desired. As the web speed is increased the time available to melt the material sufficiently to form the rigid bond point on subsequent cooling is decreased. This issue can be resolved by increasing the bonding temperature. But this is only true up to a certain point, after which, increase in

speed will not give satisfactory bonding regardless to increase in calendering temperature. Thus, web processing speed is defined by the optimal temperature window of nonwovens. At higher processing speeds, the calendering temperature window gets narrower and ultimately becomes zero. That is the point after which no further processing of nonwovens with adequate bonding is possible (Michielsen *et. al.*, 2006).

3.4.5 Morphology and Fibres Form

Form and morphology of fibres have significant effect on overall properties of the nonwovens. There are many parameters defining the form and morphology of a fibre e.g. molecular weight, linearity of the molecules, length of fibres, orientation of the molecules, and presence of crystalline and amorphous zones. Length of fibres is also considered as form of the fibres. Length of the polymer molecules affects the attraction forces between the molecules during bonding which is responsible for the mechanical characteristics of the nonwovens. Longer molecules can associate closer together during bonding and produce stronger bond (Tanchis, 2008).

Ultimate tensile strength of the fibres can be associated with the molecular orientation and is determined by its birefringence (Fedorova *et. al.*, 2007). Mechanical properties of polymer-based fibres depend on the temperature history which they were exposed to during their manufacturing process. Thus, any change in temperature during manufacturing stages affects the deformation and damage behaviour. Hence, in order to predict the mechanical behaviour up to fracture, accurately, temperature variations which the fibres were exposed to during formation of web must be known. Since, fibre form and morphology significantly effects the deformation and damage behaviour of the fabric, therefore, mechanical characterization of fibres with which fabric is made of is vital for successful development of computational model to predict fabric's behaviour as discussed in Chapter 6.

3.4.6 Orientation Distribution of Fibres

Orientation distribution of the fibres plays vital role in determining the most outstanding property of nonwovens, mechanical anisotropy. Preferential orientation of the

constituting fibres along MD leads to anisotropic behaviour of the fabric. Details of how orientation distribution of fibres affects the behaviour of nonwovens are given in Section 3.2.

3.4.7 Crimp in Fibres

When dealing with anisotropy and determination of the orientation distribution function, an important factor is the crimp in fibres. It has effects on both: accurate determination of fibre distribution function and initial deformation behaviour of the fabric. Crimp which is defined as the successive waviness in the fibres induced mechanically or chemically (Brown, 1995) as shown in Fig. 3.10.

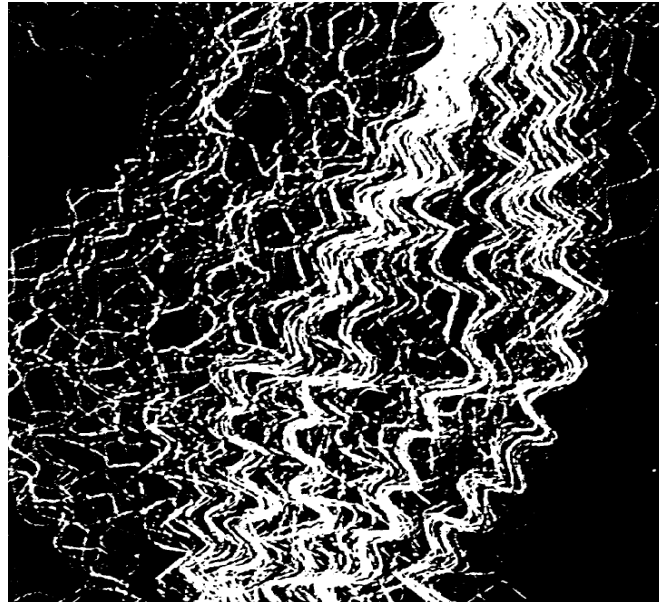


Figure 3.10. Photomicrograph of staple crimped fibre (Bauer-Kurz, 2000)

Crimp in fibres give geometrical non-linearity to the nonwovens and makes it more difficult to simulate their actual mechanical behaviour. Nevertheless, it is important for processing of fibres such as appropriate fibre-to-fibre cohesion for carding, drawing and to enhance some desirable properties in fabrics such as fabric bulk (Cook, 1984). The mechanical behaviour of a crimped fibre is different from a straight fibre as shown in Fig. 3.11. The load-elongation curve of crimped fibre consists of crimp removal part (A-B in Fig. 3.11) and tensile part (B-C in Fig. 3.11). Crimp

removal part gives less stiff initial behaviour to fibres. In order to predict the behaviour of nonwovens accurately, the crimp should be considered.

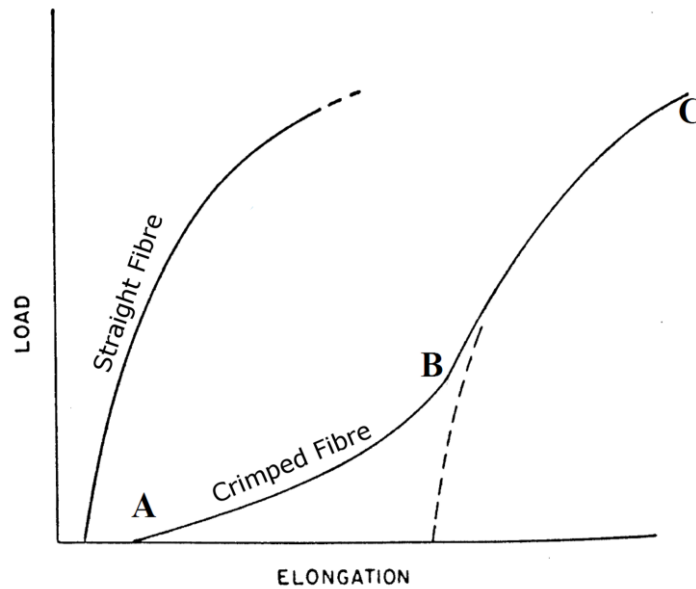


Figure 3.11. Initial portion of Load-Elongation curve of straight and crimped fibre
(Brown, 1995)

3.4.8 Bond Points Geometry

In thermally calendered bonded nonwovens, bond point shape, size and pattern affect the overall properties of nonwovens such as tensile breaking strength, drapability and softness (Gilmore *et. al.*, 1993, Fedorove *et. al.*, 2007). Due to the cost and lead time associated with engraved calendar rolls, it is very difficult to establish a relation between bond point geometry and fabric properties. Almost \$1.5M dollar and minimum 4 months' time is required to test each new bond point geometry (private communication with Mr. Carl Wust, Technical manager at Fibervisions Corp, Covington, Georgia, USA). Therefore, most of the thermally bonded fabrics available commercially are not optimally designed. Very few studies were performed to use computer model to predict the mechanical behaviour of the model as a function of bond point geometry (Gilmore *et. al.*, 1993; Xiaonan, 20011; Sabuncuoglu, 2012). However, all of these models can predict the effect of bond point geometry to only the initial

deformation behaviour of the fabric without considering damage initiation and propagation while incorporating the elastic-plastic and viscous properties of constituent fibres. Thus, there is a need for a parametric computational model that would incorporate elastic-plastic and viscous properties of the constituent fibres and their randomness to simulate the realistic deformation and damage behaviour of nonwovens. Therefore, model developed in this study is based on parametric modelling technique and incorporates material properties of constituent fibres including viscous ones as mentioned in Chapter 7. All these novel features of the model would make it a powerful design and optimisation tool.

3.5 Summary

Mechanical behaviour and basic properties of thermally bonded nonwovens are described in this chapter. Nonwovens have complex deformation performance and damage behaviour due to the presence of elastic and plastic properties of the constituent polymer based fibres affected by viscous effects and the random microstructure. Besides, the factors affecting the mechanical behaviour of thermally bonded nonwovens are described in this chapter.

In order to predict the complex deformation behaviour many models are developed in the literature. Most of the research in literature on mechanical behaviour of nonwovens is focussed to explain partial phenomenon with respect to textile engineering point of view. Since several factors affect the mechanical properties of nonwovens, a thorough investigation of mechanical behaviour from computational point of view should be implemented for successful development of finite-element model.

CHAPTER 4

MODELLING OF MECHANICAL BEHAVIOUR OF MATERIALS

Nonwovens are capable to fulfil customer demands with tailor-made characteristics and performance. This ability has made the nonwoven industry more competitive in terms of tighter product specification. However, the production of nonwovens with certain characteristics requires vast experimentation. Numerical modelling is the only antidote to reduce significantly the use of trial-and error approach in design and development of products containing nonwoven parts.

Nonwoven materials exhibit anisotropic (direction dependent) behaviour. This directional dependency of the nonwoven materials is due to preferential orientation of fibres and properties induced due to manufacturing parameters e.g. bond point pattern,

shape etc. These randomly oriented fibres present discontinuous medium rather than a continuum solid. Additionally, polymer-based fibres exhibit visco-elastoplastic behaviour, which means elements of elastic, plastic and viscous properties. All these behaviours should be considered for the development of a numerical model to simulate the realistic deformation and damage behaviour of nonwoven materials. In order to make the discussion more useful and according to the scope of this thesis, numerical modelling of nonwovens has been split up into two areas i.e. deformation behaviour and damage behaviour. Numerical modelling of these behaviours is based on their mathematical characterisations, which are briefly described in succeeding sections.

4.1 Modelling of Deformation

The deformation behaviour of a material depends upon its microstructure and properties. In case of nonwovens, complex microstructure and the properties of the constituent fibres give them unique deformation behaviour which is anisotropic in nature.

The deformation behaviour of nonwovens composed of polymer-based fibres is governed by the following three essential behaviours of the polymers:

- Elastic behaviour
- Plastic behaviour
- Viscous behaviour

The mathematical characterisation of these behaviours is briefly described below:

4.1.1 Elastic Behaviour

The forces applied on a material cause its deformation. However, provided the forces are sufficiently small, material regains its original shape and size on the removal of load and there is no dissipation of energy during loading-unloading. This is called the elastic behaviour of the material. Elastic behaviour of the material can be linear or nonlinear e.g. polymers show nonlinear elastic behaviour (Jones, 2009). This section provide

information on the stress-strain relationship and effect of the material symmetry on the numerical modelling of elastically deformed solids.

When a force is applied on a material it deforms and strain is produced; the applied stresses and the associated deformations are formulated in terms of tensors. These tensors describe the level of stresses and the deformations within the materials. The stress-tensor components of a material are related to the strain-tensor components, for elastic behaviour, by the following relation (Asaro and Lubarda, 2006)

$$\sigma_{ij} = \sum_{k=1}^3 \sum_{l=1}^3 C_{ijkl} \varepsilon_{kl} , \quad i, j \in \{1,2,3\} \quad (4.1)$$

where C_{ijkl} is known as elasticity tensor. As it relates two second-rank tensors, it must be a fourth rank tensor. Thus, it has $3^4 = 81$ components in fully populated form. Mathematical terms in Eq. 4.1 called *Hook's Law*, illustrating the behaviour of material in a specific direction, is the most basic constitutive relation. The direction-dependent behaviour normally results from particular microstructural features within the material. The mechanical properties and thus corresponding constitutive relation is affected by material symmetry such as the symmetry of the stress and strain tensors i.e. $\sigma_{ij} = \sigma_{ji}$ and $\varepsilon_{kl} = \varepsilon_{lk}$; the independent components of each of these is six. Consequently, the independent components of the elasticity tensor are thirty-six.

Elasticity of the material is based on the fact that the energy expended during deformation remains within the strained material called strain energy. Due to the presence of strain energy function, the elasticity tensor is invariant under the permutation of pairs of indices ij and kl i.e. $C_{ijkl} = C_{klij}$, which provide additional constraint on the elasticity tensor. Consequently, a fully anisotropic material has only twenty-one components of elasticity tensor. $C_{ijkl} = C_{klij}$ implies $C_{ab} = C_{ba}$ since swapping ij with kl is similar to swapping a with b . Therefore, the symmetric elasticity matrix for the anisotropic material is as follow

$$[C]_{\text{anisotropic}} = \begin{bmatrix} C_{11} & C_{12} & C_{13} & C_{14} & C_{15} & C_{16} \\ C_{21} & C_{22} & C_{23} & C_{24} & C_{25} & C_{26} \\ C_{31} & C_{32} & C_{33} & C_{34} & C_{35} & C_{36} \\ C_{41} & C_{42} & C_{43} & C_{44} & C_{45} & C_{46} \\ C_{51} & C_{52} & C_{53} & C_{54} & C_{55} & C_{56} \\ C_{61} & C_{62} & C_{63} & C_{64} & C_{65} & C_{66} \end{bmatrix}. \quad (4.2)$$

The constants of elasticity tensor are quoted in terms of Young's modulus, Poisson's ratio and shear modulus depending upon its symmetry. The relationship between the normal stress and the strain in the same direction is called the Young's modulus (E). The relationship between the axial and contraction strains is called Poisson's ration (ν). The ratio of shearing stress to shearing strain is called shear modulus (G).

Stiffness matrix in Eq. 4.2 shows most general case in which it is determined by 21 independent constants. This case corresponds to material having no symmetry property and called *triclinic material* (Berthlot, 1998). If the material has a symmetry plane, the form of stiffness matrix should be such that changing in reference system carried out about this plane should not modify the matrix e.g. if a symmetry plane is (1, 2) the exploitation of the transformation system leads to stiffness matrix of following form:

$$[C]_{\text{monoclinic}} = \begin{bmatrix} C_{11} & C_{12} & C_{13} & 0 & 0 & C_{16} \\ C_{21} & C_{22} & C_{23} & 0 & 0 & C_{26} \\ C_{31} & C_{23} & C_{33} & 0 & 0 & C_{36} \\ 0 & 0 & 0 & C_{44} & C_{45} & 0 \\ 0 & 0 & 0 & C_{54} & C_{55} & 0 \\ C_{61} & C_{62} & C_{63} & 0 & 0 & C_{66} \end{bmatrix}. \quad (4.3)$$

This type of material having one symmetry plane is called monoclinic material. The number of independent elasticity constants is reduced to thirteen. For orthotropic material, properties of material are symmetric with respect to the orthogonal planes. The form of stiffness matrix is obtained by adding one more symmetry plane orthogonal to

the preceding one, symmetric to monoclinic material. The existence of two symmetry planes implies the existence of third. The final form of stiffness matrix by adding second symmetry plane is the following:

$$[C]_{\text{orthotropic}} = \begin{bmatrix} C_{11} & C_{12} & C_{13} & 0 & 0 & 0 \\ C_{21} & C_{22} & C_{23} & 0 & 0 & 0 \\ C_{31} & C_{23} & C_{33} & 0 & 0 & 0 \\ 0 & 0 & 0 & C_{44} & 0 & 0 \\ 0 & 0 & 0 & 0 & C_{55} & 0 \\ 0 & 0 & 0 & 0 & 0 & C_{66} \end{bmatrix}. \quad (4.4)$$

Hence, only nine independent parameters are required to describe the elasticity tensor in orthotropic in the natural coordinate system. The requirement of these parameters for the elasticity tensor is further reduced if the material is assumed to be isotropic. For isotropic material all the coordinates are natural coordinates and, hence, elasticity tensor remains unchanged by the rotation of the material or the coordinate system (Singh, 2010). The application of this this type of property to unidirectional material such as fibres in case of nonwovens leads to relations:

$$C_{12} = C_{21}, C_{23} = C_{12}. \quad (4.5)$$

The number of independent constant thus reduces to two and stiffness matrix takes the form:

$$[C]_{\text{isotropic}} = \begin{bmatrix} C_{11} & C_{12} & C_{12} & 0 & 0 & 0 \\ C_{12} & C_{11} & C_{12} & 0 & 0 & 0 \\ C_{12} & C_{12} & C_{11} & 0 & 0 & 0 \\ 0 & 0 & 0 & \frac{1}{2}(C_{11} - C_{12}) & 0 & 0 \\ 0 & 0 & 0 & 0 & \frac{1}{2}(C_{11} - C_{12}) & 0 \\ 0 & 0 & 0 & 0 & 0 & \frac{1}{2}(C_{11} - C_{12}) \end{bmatrix}. \quad (4.6)$$

Thus, in order to derive the mathematical model for the elastic behaviour, the constitutive relations depending upon the material symmetry is defined first and then the number of constants required for the complete relationship between stress and strain is determined.

The initial deformation characteristics of polymer-based materials are fully dependant on their elastic behaviour. Therefore, for the modelling of the deformation behaviour of nonwovens made of polymer-based fibres, elasticity is very much important.

4.1.2 Plastic Behaviour

For the determination of the deformation behaviour of a structure until its failure, the analysis of material deformation beyond its yield point is carried out. The deformation beyond the yield point is called plastic deformation, and refers to the irreversible deformation. In polymer-based materials, a large portion of material deformation lies in the plastic range which plays an important role in the mechanical behaviour of the material. Thus, for the numerical modelling of nonwovens, this behaviour should be included. In plastically deformed solids, the relation between stress and strain is formulated using plasticity theory, the background of which is described under the following main aspects (Singh, 2010):

4.1.2.1 Decomposition of Strain

The loading on the material beyond yield point cause permanent deformation and overall strain in the material is the sum of elastic strain and plastic strain as follows:

$$\varepsilon_{\text{total}} = \varepsilon_{\text{elastic}} + \varepsilon_{\text{plastic}} \quad 4.7$$

The elastic properties of the materials do not change during the plastic deformation, which means the parameters of elastic stiffness matrix C_{ijkl} remain the same. The domain of the elastic deformation is defined by the yield function based on a yield criterion and ultimately the plastic strain of the deformed material is determined

by using equation 4.7. Thus, yield criterion is important in modelling of the material to recognise the current state of the deformed material. The information about yield criterion is given in the following section.

4.1.2.2 Yield Criterion

Yield criterion is the relation that defines the elastic limit of material under any possible combination of stresses (Hill, 1950). The material, initially, deforms elastically under stresses. Once the stresses on material become equal to the yield strength of the material, it is said to have onset of plastic deformation (Figure 4.1). The first step for the analysis of plastic deformation of the material, a yield criterion is determined which describes the limit of elastic domain for that material.

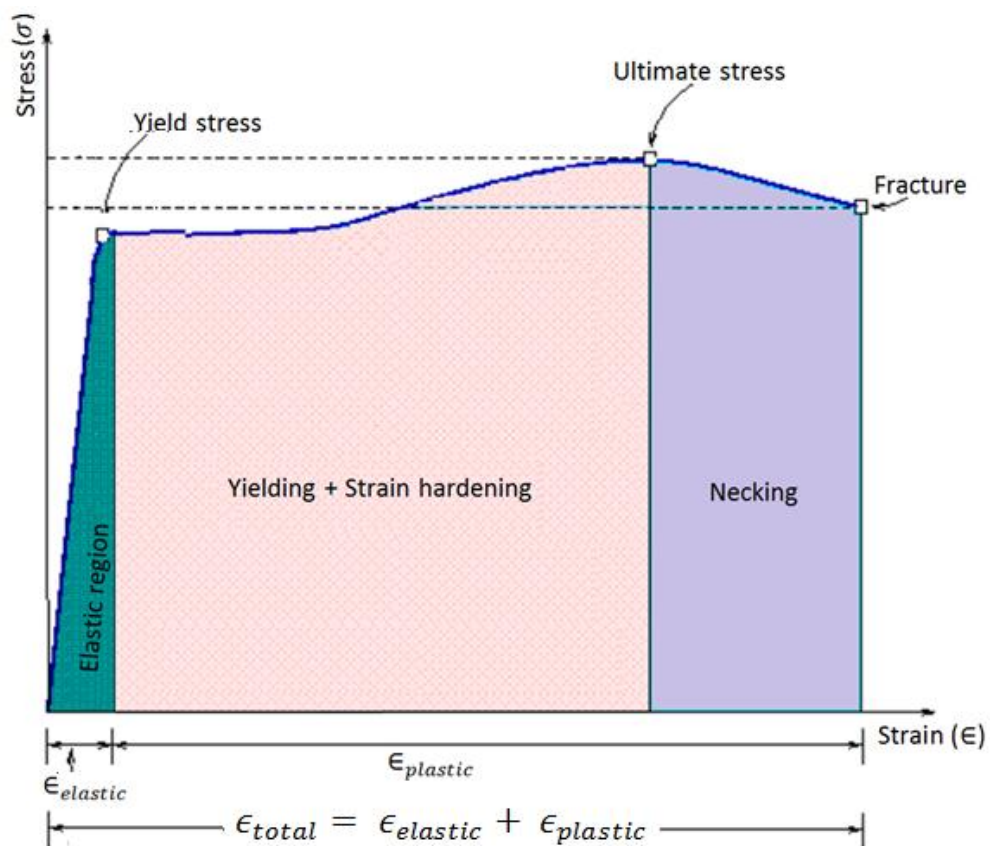


Figure 4.1. Mechanical behaviour of material

A yield criterion is described by the mathematical expression. The most general form of the yield criterion is

$$f(\sigma_{ij}) = 0,$$

or

4.8

$$f(\sigma_{xx}, \sigma_{yy}, \sigma_{zz}, \sigma_{xy}, \sigma_{yx}, \sigma_{xz}) = 0.$$

The state of stress can be determined by specifying the principle stresses (σ_i) and orientation of principle axes . Thus, Eq. 4.8 can be modified as:

$$f(\sigma_1, \sigma_2, \sigma_3, n_1, n_2, n_3) = 0. \quad 4.9$$

Eq. 4.9 shows that yielding of an anisotropic material depends not only on the magnitude of the applied stresses but also the orientation of the stress tensor. For isotropic material, yield function is independent of the orientation of principal axes and only a function of principal stresses. Thus, for isotropic materials, it can be written as

$$f(\sigma_1, \sigma_2, \sigma_3) = 0. \quad 4.10$$

By comparing Eq 4.9 and 4.10, it can be said that determination of yield criterion for anisotropic material is much more difficult than isotropic material. For a the uniaxial yield strength in one direction may differ from that in another direction in anisotropic material. Therefore, a single constant (σ_1) obtained in one direction is not sufficient to predict the uniaxial tensile yield strength of an anisotropic material.

Numerous criteria have been proposed for different materials to predict the yielding of a material such as tresca, von Mises, Hills's yield criterion. Tresca and von Mises criteria are briefly described here.

Tresca Yield Criterion

This criterion was proposed by Henri Edourad Tresca in 1864. According to this criterion, yielding occurs only when maximum shear stress reaches the critical value k (Khan and Huang, 1995). Mathematically it can be represented as:

$$\tau_{\max} = k \text{ for yielding or plastic deformation} \quad 4.11$$

$$\tau_{\max} < k \text{ for elastic deformation}$$

In terms of principal stresses, it can be given as

$$\frac{1}{2}(\sigma_{\max} - \sigma_{\min}) = \sigma_Y = 2k, \quad 4.12$$

where σ_{\max} and σ_{\min} are maximum and minimum principal stresses and σ_Y is yield stress. Thus from Eq. 4.12 becomes:

$$\sigma_Y = 2k \quad 4.13$$

By comparing Eqs. 4.11 ad 4.13, we have

$$k = \tau_Y = \frac{\sigma_Y}{2} \quad 4.14$$

According to Tresca, yield stress in pure shear is one half of the yield stress in simple tension (Mendelson, 1968)

Von Mises Yield Criterion:

It is usually believed that this criterion was suggested by von Mises in 1913. But in fact it was first published by Huber (1904). According to this criterion, plastic yielding occurs when second variant J_2 of the deviatoric stress tensor reaches critical value. Mathematically, it can be written as:

$$J_2 - k^2 = 0 \text{ for yielding or plastic deformation} \quad 4.15$$

$$J_2 < k^2 \text{ for elastic deformation}$$

Physical interpretation of von Mises is the yielding in material starts when elastic energy of distortion reaches its critical value. In terms of principal stresses, von Mises criterion can be given as:

$$\frac{1}{6} [(\sigma_1 - \sigma_2)^2 + (\sigma_2 - \sigma_3)^2 + (\sigma_3 - \sigma_1)^2] = k^2 \quad 4.16$$

To determine the value of k , a simple tension test is performed in a way that

$$\sigma_1 = \sigma_Y \text{ and } \sigma_2 = \sigma_3 = 0 \quad 4.17$$

Substituting Eq. 4.17 in Eq. 4.16 gives:

$$\frac{1}{3} \sigma_Y^2 = k^2 \quad 4.18$$

Therefore

$$k = \frac{\sigma_Y}{\sqrt{3}} \quad 4.19$$

If k is determined using the pure shear test τ_Y , we have $\sigma_1 = -\sigma_3 = \tau_Y$ and $\sigma_2 = 0$. Then Eq. 4.16 becomes:

$$\tau_Y^2 = k^2 \quad 4.20$$

By comparing Eqs. 4.19 and 4.20

$$k = \tau_Y = \frac{\sigma_Y}{\sqrt{3}} \quad 4.21$$

According to von Mises, the yield strength in uniaxial tension is $\sqrt{3}$ times the yield strength in pure shear (Khan and Huang, 1995).

Comparison of yield locus of Tresca and von Mises criteria is shown in Fig. 4.2. Von Mises is higher than Tresca yield criterion by a factor $2/\sqrt{3}$. However, under

equal biaxial loading $\sigma_1 = \sigma_2 = \sigma_Y$, yielding is presumed to occur at $\sigma_1 = \sigma_2 = \sigma_Y$ which is the same for both Tresca and von Mises criteria.

After yielding, permanent deformation occurs in the material. Stress-strain relations for modelling plastic deformation are different from elastic deformation. Next section deals with the modelling of plastic deformation.

4.1.2.3 Evolution of Plastic Strain (Flow Rule)

A relationship between evolution of plastic strain rate with the current state of loading is called flow rule (Singh, 2010). It defines the evolution of plastic strain. However, it does not provide the numerical value of the plastic strain, but merely the ratios between them or the direction of the plastic flow. A general three-dimensional relationship between increments of total strain to the stress deviation was given by Levy and Von-Mises. According to Levy-Mises, the ratio of plastic strain increments to the current deviatoric stress at any instant is constant. Mathematically, it can be expressed as:

$$\frac{d\varepsilon_1}{\sigma'_1} = \frac{d\varepsilon_2}{\sigma'_2} = \frac{d\varepsilon_3}{\sigma'_3} = d\lambda,$$

or

$$\frac{d\varepsilon_{ij}}{\sigma'_{ij}} = d\lambda,$$

4.22

where $d\varepsilon_{ij}$ is the plastic true strain increment, σ'_{ij} is the deviatoric true stress and $d\lambda$ is a non-negative real number. Since deviatoric stresses are involved here which cause yielding (change in shape at constant volume), therefore, under uniaxial tension:

$$\sigma'_1 = \sigma_1 - \sigma_m = \frac{2\sigma_1}{3}; \quad \sigma'_2 = \sigma'_3 = \frac{-\sigma_1}{3}$$

4.23

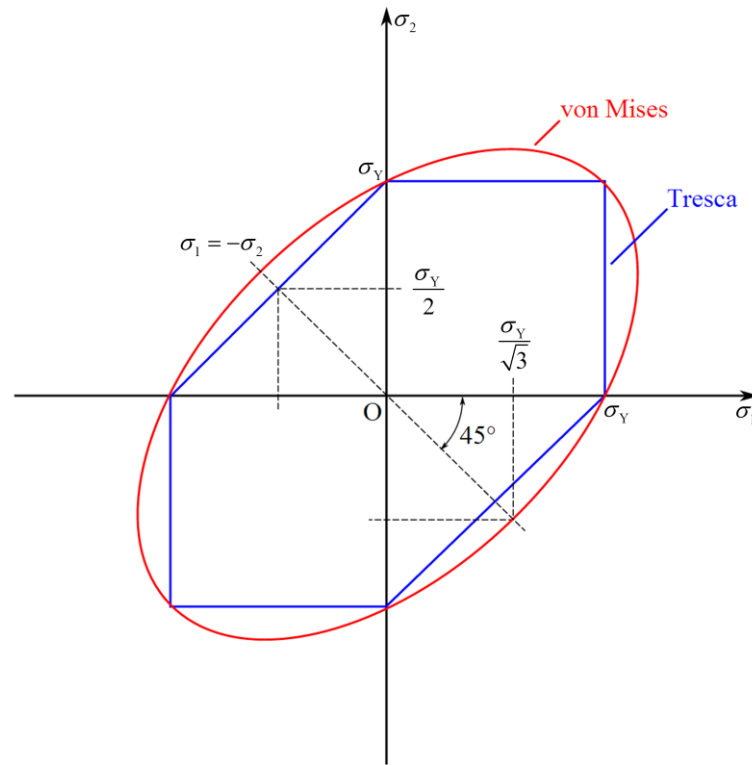


Figure 4.2. Comparison of Tresca and von Mises yield criteria in plane stress condition

In terms of actual stresses, plastic stress-strain relation can be given by an analogy with the Hook's law as:

$$d\varepsilon_1 = d\lambda \left(\sigma_1 - \frac{\sigma_2 + \sigma_3}{2} \right), \quad d\varepsilon_2 = d\lambda \left(\sigma_2 - \frac{\sigma_1 + \sigma_3}{2} \right), \quad d\varepsilon_3 = d\lambda \left(\sigma_3 - \frac{\sigma_1 + \sigma_2}{2} \right). \quad 4.24$$

The plastic strain rate is proportional to the gradient of the function of a stress, which is a flow rule and can be expressed as:

$$d\varepsilon_{ij} = d\lambda \frac{\partial F}{\partial \sigma_{ij}}, \quad (4.25)$$

where F is the plastic potential. If the yield function is taken as plastic potential, the flow rule is also called normality rule. According to this law, the plasticity straining takes place in the direction normal to the yield surface (Clarke and Cope, 1984) as shown in Figure 4.3. The direction of the strain at point P_1 on the yield surface is shown

in Fig. 4.3. The strain can be in any direction between the two normals indicated at vertex on yield surface (P_2).

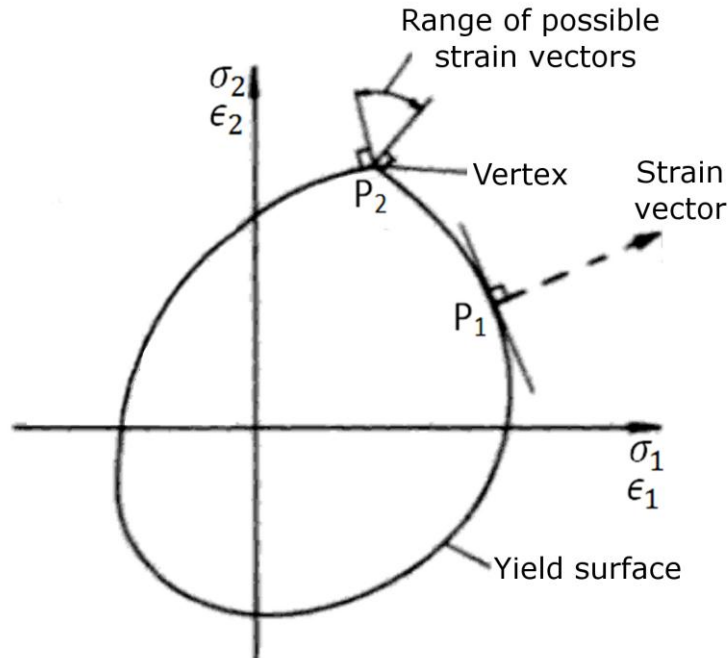


Figure 4.3. Flow rule (Clarke and Cope, 1984)

Fig. 4.3 reveals, the sharp corners on the yield surface causes instabilities while using the normality rule as shown at point P_2 . Thus, in order to obtain the stable material flow, yield surface must be convex. Since, sharp corners are involved in Tresca's yield locus as shown in Fig. 4.2, it can cause instabilities in numerical calculations of flow direction. Due to this fact, corners of Tresca's yield must be smoothed to use with normality rule.

4.1.3 Viscous Behaviour

The properties of polymer based materials are highly time-dependent, which is obvious in nonwovens made of polymer-based fibres. Nonwovens exhibit viscous behaviour as explained in Section 3.3.2, which must be considered for accurate numerical modelling of these materials.

Viscoelastic materials exhibit time-dependent behaviour in their stress-strain relationship. Two most important phenomenon related to viscoelasticity are creep and stress relaxation. Creep is increase in strain at constant stress and relaxation is decrease in stress when strain is constant. Perfectly elastic materials are modelled as springs, while the materials having time-dependent behaviour are modelled as dashpots. The viscoelastic materials exhibit elements of both viscous and elastic properties. Therefore, spring and dashpot elements, shown in Figure 4.4, are used to mimic the viscoelastic deformation.

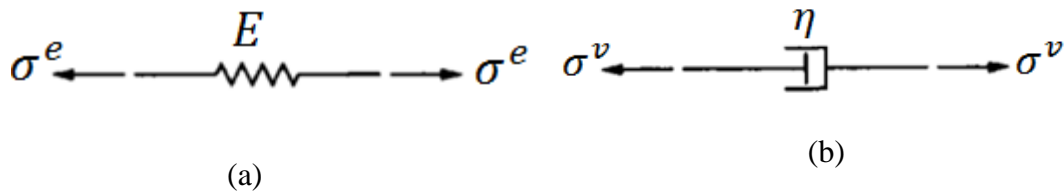


Figure 4.4. (a) Perfectly elastic (b) viscous element (E is modulus of elasticity and η is viscosity) (Ottosen and Ristinmaa, 2005)

The constitutive relationships between stress and strain for spring and dashpot, respectively, are given by the following relations:

$$\sigma^e = E\varepsilon^e \quad \text{and} \quad \sigma^v = \eta \frac{d\varepsilon^v}{dt} \quad (4.26)$$

Generally, the two models to deal with viscoelasticity of the materials are Maxwell and Kelvin-Voigt models. In Maxwell model, the viscoelasticity is modelled by introducing spring and dashpot in series as shown in Figure 4.5.

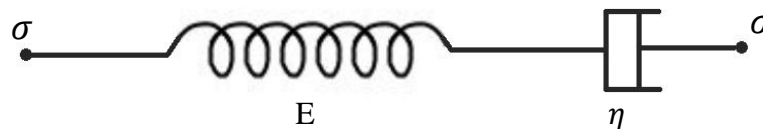


Figure 4.5. Maxwell model

The overall value of stress and strain for the spring and dashpot in series are:

$$\frac{d\varepsilon}{dt} = \frac{d\varepsilon^e}{dt} + \frac{d\varepsilon^v}{dt} \quad 4.27$$

$$\sigma = \sigma^e = \sigma^v$$

Combining equations 4.26 and 4.27 give the constitutive equation for Maxwell model as:

$$\sigma = \eta \frac{d\varepsilon}{dt} - \frac{\eta}{E} \frac{d\sigma}{dt} \quad (4.28)$$

The Kelvin-Voigt model consists of spring and dashpot in parallel (Figure 4.6). It follows:

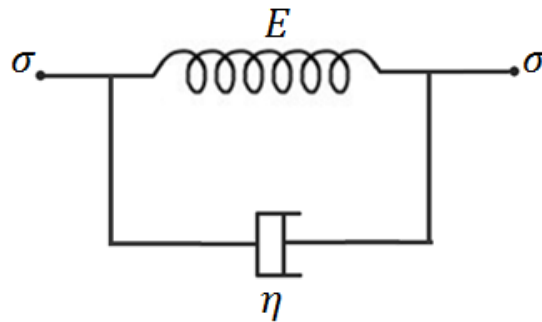


Figure 4.6. Kelvin-Voigt model

$$\varepsilon = \varepsilon^e = \varepsilon^v \quad \sigma = \sigma^e + \sigma^v \quad (4.29)$$

Insertion of 4.26 into 4.29 gives

$$\sigma = E\varepsilon + \eta \frac{d\varepsilon}{dt} \quad (4.30)$$

There are some deficiencies in both of these models e.g. Maxwell model cannot handle creep properly whereas Kelvin model cannot be used to predict stress relaxation. Many variations of spring dashpot arrangements are available in the literature to overcome the deficiencies in these models (Ottosen and Ristinmaa, 2005). These

include the Generalized Maxwell model and Generalized Kelvin-Voigt model. The Generalized Maxwell model, which combines finite number of springs and dashpots in parallel as shown in Figure 4.7, is most extensively used in analysis of viscoelastic behaviour.

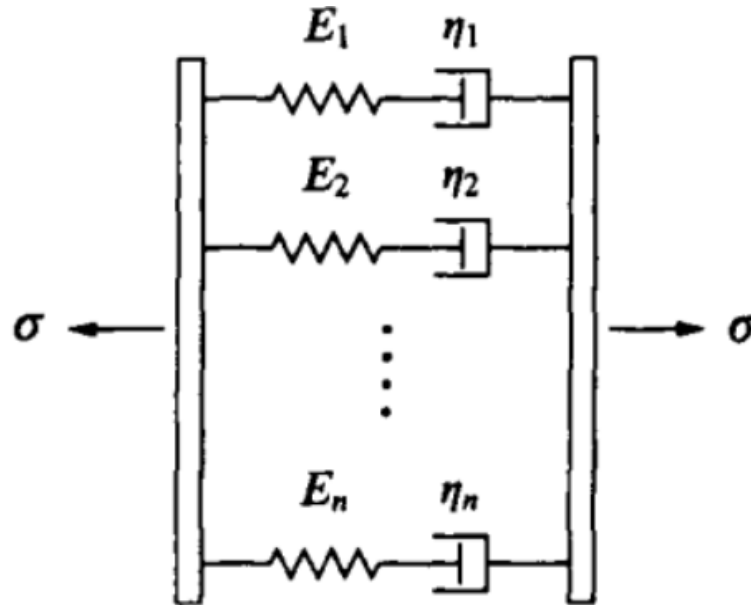


Figure 4.7. Generalized Maxwell model represented by springs and dashpots

(Ottosen and Ristinmaa, 2005)

4.2 Modelling of Damage

Failure of the material follows irreversible deterioration, which is caused by the material damage and its propagation. The existence of localized failure in material in form of cavities, voids, cracks caused by the application of load on a material is referred as damage, while the process of growth in these voids and cracks resulting in material degradation through strength reduction, is called damage propagation (Skrzypek and Ganczarski, 1999).

Damage modelling may be at atomic scale (molecular dynamics), microscale (micromechanics), and macroscale (continuum mechanics), depending upon the scale of the model (Skrzypek and Ganczarski, 1999). On atomic scale, material damage is

determined by the breaking and re-establishing of the atomic bonds. On the microscale, material damage is associated with the number of microvoids and their size. However, on macroscale modelling, material damage can be evaluated by non-destructive measuring of change of physical quantities such as elasticity modulus, thermal conductivity, acoustic wave speed, tomography etc. (Mishnaevsky, 1998). Damage of the heterogeneous and discontinuous material can be determined on macroscale by the use of Representative Volume Element (RVE). RVE is the minimal material volume, having statistically sufficient information on the microstructure yet significantly smaller than the macroscopic body. It should contain all the information about the deformation processes of material at microscale, and parameters of the evolution equation describing these processes should not change with its size (Gitman *et. al.*, 2007). Thus, RVE acts as the bridge to link the microscopic and macroscopic behaviour of the material.

Damage is localized failure and its evolution ultimately leads to total loss of load carrying capability of the material called *failure*. Based on the microscopic damage characteristics (microscale) and constitutive relationship of the materials, their damage can be classified in many ways, such as elastic-brittle damage, elastic-plastic damage, fatigue damage, creep damage, corrosion damage, creep-fatigue damage etc. Each type of the damage has its own microscopic mechanism and features (Skrzypek and Ganczarski, 1998). Currently, there is no single theory that can accurately predict failure at all levels of analysis, for all the loading conditions and for all type of materials. Generally, failure criteria are used to predict the failure in a material. Depending upon the material and mechanisms involved during damage initiation and propagation, different failure criteria are used. Two most basic failure criteria are maximum stress and maximum strain based criteria. Elementary formulations of these criteria are:

Critical stress failure criterion:

$$\text{If } \left(\frac{\sigma_1}{X_t, X_c} \right), \left(\frac{\sigma_2}{Y_t, Y_c} \right), \left(\frac{\sigma_3}{Z_t, Z_c} \right), \left(\frac{\sigma_{12}}{S_{12}} \right), \left(\frac{\sigma_{23}}{S_{23}} \right), \left(\frac{\sigma_{31}}{S_{31}} \right) = 1, \phi_{\text{stress}} = 1. \quad (4.31)$$

Critical strain failure criterion:

$$\text{If } \left(\frac{\varepsilon_1}{e_{xt}, -e_{xc}} \right), \left(\frac{\varepsilon_2}{e_{yt}, -e_{yc}} \right), \left(\frac{\varepsilon_3}{e_{zt}, -e_{zc}} \right), \left(\frac{\gamma_{12}}{g_{12}} \right), \left(\frac{\gamma_{23}}{g_{23}} \right), \left(\frac{\gamma_{31}}{g_{31}} \right) = 1, \phi_{\text{strain}} = 1. \quad (4.32)$$

Here $\sigma_1, \sigma_2, \sigma_3, \sigma_{21}, \sigma_{23}, \sigma_{31}$ and $\varepsilon_1, \varepsilon_2, \varepsilon_3, \gamma_{21}, \gamma_{23}, \gamma_{31}$ are components of the stress tensor and strain tensor at any point in the material, respectively; $X_t, Y_t, Z_t, X_c, Y_c, Z_c$ and S_{12}, S_{23}, S_{31} represent maximum allowable longitudinal tensile stress, maximum allowable compressive stress and maximum allowable shear stress in 3 directions and 3 planes, respectively; $e_{xt}, e_{yt}, e_{zt}, -e_{xc}, -e_{yc}, -e_{zc}$ and g_{12}, g_{23}, g_{31} are maximum allowable longitudinal tensile strain, maximum allowable compressive strain and maximum allowable shear strain in 3 directions and 3 planes, respectively. ϕ_{stress} is the damage variable associated with either of the failure mode of the material depending upon the stresses applied on it e.g. failure mode under tension, compressive or shear stress; ϕ_{strain} is the damage variable associated with either of the failure mode of an element depending upon the type of strain e.g. failure mode under tension, compressive or shear strain. The damage variable ϕ_{stress} and ϕ_{strain} has the values ranges from $\phi_{\text{stress}} = \phi_{\text{strain}} = 0$ for undamaged (effective) material to $\phi_{\text{stress}} = \phi_{\text{strain}} = 1$ fully damaged material.

4.3 Review of Finite Element Method

For a solution of complex engineering problem, application of the conventional analytical methods may be unfeasible or impossible. The engineering approach is to approximate the solution of the problem by dividing the continuum into appropriate number of elements having finite degree of freedom (DOF). This procedure is called finite element method (FEM). Thus, a FE model is a combination of elements having simple geometry, which is much easier to analyse than the actual geometry as shown in Fig. 4.8. The tapered bar is divided into series of finite elements, each having uniform diameter but different cross-sections. Then, the elongation of each element under the

application of axial force (P) is determined and summed up to find out the elongation (u) in the tapered bar. Accuracy of the result improves by increasing the number of elements but it takes more time to compute the solution. Thus, with FEM, there is a trade-off between the accuracy of approximation of results and processing time. FEM is used in this research to find out the behaviour of the nonwovens. The generalized procedure to carry out the FEM is described briefly in this section.

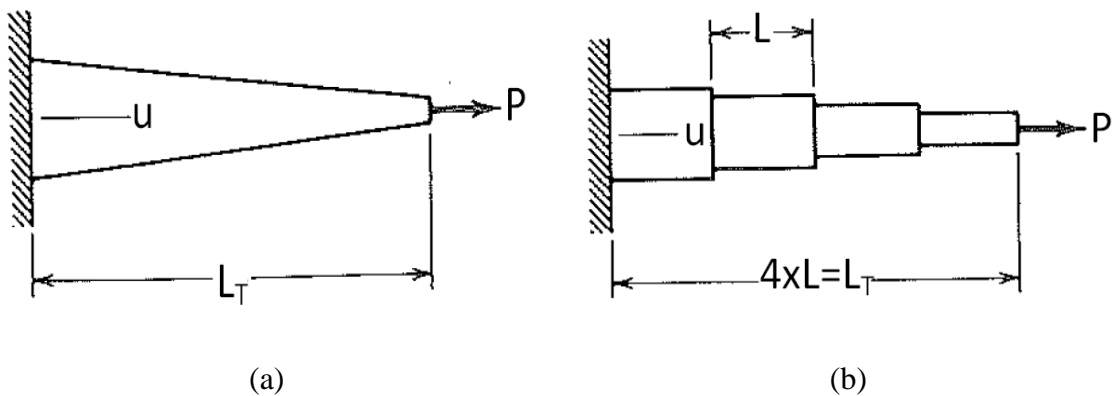


Figure 4.8. (a) Tapered bar under load P (b) model built up of four nontapered elements of equal length L (Cook *et. al.*, 1998)

4.3.1 General Procedure of FEM

FEM is method of piecewise approximation of a function formed by the combination of simple functions defined over the small regions called elements. These elements are defined in such a way that the inter-element continuity of the overall function maintains in assemblage (Cook *et. al.*, 2001). Various physical problems incorporating structure of arbitrary shape, size, load and support conditions can be solved using FEM. A typical procedure to carry out FEM is well-defined and remains the same regardless of the geometry, material, boundary conditions, and type of the engineering problem. It involves following five steps (Cook *et. al.*, 2001; Demirci, 2010):

Step 1: Divide the structure or continuum into number of simple elements in such a way that the local behaviour of the system under excitation can be reproduced by the assemblage of the elements. This is called meshing. The shape and number of the elements are directly related to the accuracy of approximation of solution.

Step 2: Formulation of properties of elements. It means the response of elements to an excitation is determined. In case of stress analysis, the nodal loads associated with the elements deformation states are determined. The relationship between the unknown deformation or displacements and the known forces is written as

$$\{f\} = [k]\{x\} \quad (4.33)$$

where $\{f\}$ is the nodal force vector, $\{x\}$ is the nodal displacement vector and $[k]$ is the characteristic matrix called stiffness matrix.

Step 3: Assemblage of the elements to obtain the finite element model of overall structure or continuum, according to the conditions of discretization. These conditions are the displacement of the nodes in contact should be equal and in equilibrium.

Step 4: Specify the known constraints on the nodes of the elements. In case of stress analysis, nodal forces, displacements and/or moments are introduced.

Step 5: Determine the unknown quantities, such as nodal displacement in case of stress analysis. Then, calculate the strain from the nodal displacement field and finally calculate stresses from strains.

The advent of modern computer has brought revolution in the field of FEM. Numerous FE software are available to compute the solution for the engineering problems. The selection of the software for solving a particular problem depends upon the capability of the software and personal choice. The software used in this research is MSC.Patran, 2010 as pre and post processor and MSC. Marc as solver.

4.3.2 Nonlinearity in Structural Analysis

Nonlinearity in finite element analysis of solid mechanics arises from dependence of characteristic matrix on the load, displacement or the nature of contact between the bodies. The types of nonlinearity are material nonlinearity and geometric nonlinearity as explained in Section 3.3.1.

Nonlinear analysis is usually more complex and takes more time as compared to the linear analysis. When dealing with this type of analysis, some considerations are required to reflect the actual behaviour of the system to an excitation. These considerations are briefly described in this section.

4.3.2.1 Large Plastic Deformation

For nonlinear analysis, two main approaches are used: elastic-plastic and perfect plastic (MSC.Marc®, 2008). In perfect plastic approach, the initial elastic deformation of the material is neglected and only the plastic deformation is considered. Numerical implementation of this approach is simple and requires less computation time as the initial elastic deformation is not included in the solution. However, the inattention to the elastic deformation leads to inaccuracy in results. Furthermore, it cannot be used for the prediction of the physical behaviour of the system based on elasticity, such as spring back behaviour. In order to avoid these limitations, another approach named elastic-plastic is used. Elastic-plastic approach includes both elastic and plastic deformation for the solution. The selection of appropriate approach for a particular application depends upon range of elastic and plastic deformations involved in that. Perfect plastic approach may be suitable for an application in which elastic deformation is small enough, as compared to plastic deformation. However, the application in which there is considerable elastic deformation that cannot be neglected to get accurate results, elastic-plastic approach should be used. In this research, elastic-plastic approach is used to deal with the nonlinearity as it gives more accurate results.

4.3.2.2 Solution Procedure

Nonlinear equations require, in general, incremental solution schemes and sometimes iterative schemes within each increment. This solution is carried out in such a way that the equilibrium is maintained in each load/time increment (MSC.Marc®, 2008). Newton-Raphson, one of the most commonly used, method to solve nonlinear equations is briefly described here.

The Newton-Raphson method is successive-approximation procedure, and each approximation is called iteration. It requires an initial estimation of solution. In stress analysis, initial estimate of displacement is required in such a way that the residual value of the force is close to zero, preferably. Then, the iteration process starts and continues until the displacement value with desired accuracy is achieved. Equilibrium is the basic requirement and must be satisfied for the structural analysis based on Newton-Raphson method (Dalziel, 1998). The equilibrium can be expressed by the following set of equation (MSC.Marc®, 2008)

$$K(u)\delta u = F - R(u), \quad (4.34)$$

where u is nodal-displacement vector, F is external nodal force vector, R is the nodal-reaction force, and K is tangent-stiffness matrix. The approximation of the displacement u gives some residual force R , which shows the out of equilibrium force. The internal nodal-reaction is given as:

$$R = \sum_{\text{elements}} \int_v \beta^T \sigma dv, \quad (4.35)$$

where β^T is the differential operator that transform displacements into strain. If i is the iteration number, then the equation 4.30 for i^{th} iteration gives:

$$K(u^{i-1})\delta u = F - R(u^{i-1}) \quad (4.36)$$

The above equation is solved for correction in incremental displacement (δu^i) and next appropriate solution is given by:

$$\Delta u^i = \Delta(u^{i-1}) + \delta u \quad (4.37)$$

Above procedure can be repeated several times until desired level of accuracy is achieved. It provides good results for most of the nonlinear problems, but computationally very expensive for three-dimensional problems (MSC.Marc®, 2008).

4.3.2.3 Convergence Control

In an accurate finite element model, iterations get closer and the difference between each successive solution reduces, called convergence. The validity and effectiveness of the finite element model is determined by convergence efficiency of its approximate solution (Dukkipati *et al.*, 2007). When the desired level of accuracy is achieved, iteration process is concluded. The accuracy level is controlled by criteria, called convergence criteria. In commercial FE software, convergence is controlled by comparison of forces (residual force and reaction force) and/or comparison of displacements (incremental displacement and correction to incremental displacement) or by the comparison of strain energies. The basic procedure for convergence controlled is described by the following equations (MSC.Marc®, 2008).

$$\text{Residual Control: } \frac{\|F_{residual}\|_{\infty}}{\|F_{reaction}\|_{\infty}} < Tolerance \quad (4.38)$$

where $\|F\|_{\infty}$ shows the component of force with highest absolute value.

$$\text{Displacement Control: } \frac{\|\delta u\|_{\infty}}{\|\Delta u\|_{\infty}} < Tolerance \quad (4.39)$$

Where $\|\Delta u\|_{\infty}$ is the incremental displacement vector and $\|\delta u\|_{\infty}$ is the correction to incremental displacement.

$$\text{Strain Energy Control: } \frac{\|\delta E\|_{\infty}}{\|\Delta E\|_{\infty}} < Tolerance \quad (4.40)$$

where $\|\Delta E\|_{\infty}$ is the strain energy increment and $\|\delta E\|_{\infty}$ is the strain incremental correction. These energies are the total energies integrated over the whole volume.

Different problems require different convergence control procedures for the accurate solution. For example, in analysis of stress-free motion of a body, only the convergence control based on displacement work is required, not the convergence based on relative energy or residual force. The value of tolerance can be decreased to achieve

more accurate solution, but it increases the computation time. Thus, there is a trade-off between the accuracy of solution and computation time.

Numerous computer software are available to carry out the finite element modelling of complex engineering problems. This makes the finite element method, a widely used numerical technique in these days. Hence, it is practical to use finite element method to model nonwovens and this research is focussed on finite element approach of numerical analysis to predict the deformation and damage behaviour of nonwovens.

4.4 Existing FE models for Nonwovens

Several attempts were made to simulate the behaviour of nonwoven materials using finite element method. These models were developed using different approaches based on method of idealization of fabric's network geometry. A brief overview of various approaches in literature to simulate the behaviour of nonwovens using finite element modelling is given in this section.

First approach models the macroscopic response of nonwovens as continuum. Demirci *et. al.* (2010, 2011a, 2011b, 2012a) idealized the geometry of nonwoven fabrics with a continuum model (Fig. 4.9) based on orthotropic symmetric planes. Randomness of the fabric in terms of orientation distribution function was introduced as orthotropic parameters calculated by using specially developed software. This model was very useful for predicting the stress—strain behaviour of high-density nonwovens accurately but damage was not introduced into the model. Since the model was based on continuum approach, it was incapable to account for mechanisms involved in deformation and damage of nonwovens. Ridruejo *et. al.* (2012) introduced a continuum model to predict the meso-level response of the fabric but fibres were not explicitly introduced into that model rather a constitutive relation concerning with fibre orientation distribution was developed. Since it was a continuum model to predict fabric's behaviour at meso-level, it was unable to mimic the actual microstructure; and

mechanisms of fabric's deformation. Besides, damage was implemented into the model in a phenomenological way.

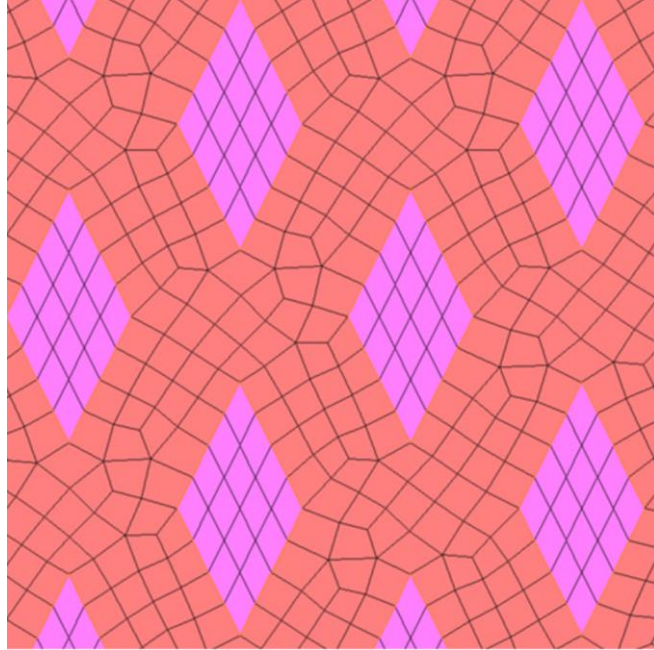


Figure 4.9. FE model of 150g/m² PP/PE fibre nonwoven

Second approach based on composite laminate model, incorporating the effect of non-uniform fibre orientation distribution, was used (Liao and Adanur, 1997; Bais *et al.*, 1998). The nonwoven, which was assumed continuum, was made of several layers of fibres. Within each layer fibres were oriented randomly or with known statistical distribution. The layers of different fibre orientation were stacked and bonded along the entire contacting interface. All the fibres in one layer were oriented in the same direction as shown in Fig. 4.10. These fibres were bound together at nodal point of mesh of finite elements. The model deals with deformation of fabric as the breaking of the individual fibres incrementally. These models were announced to produce satisfactory result agreement with the experimentation including aspects of fibre anisotropy arising from non-uniform fibre orientation distribution, particularly in small strain regime. However, the representation of the real deformation mechanisms such as non-uniform deformation and reorientation of fibres were not reflected since fibres were fixed within the layer which could not slide on top of each other.

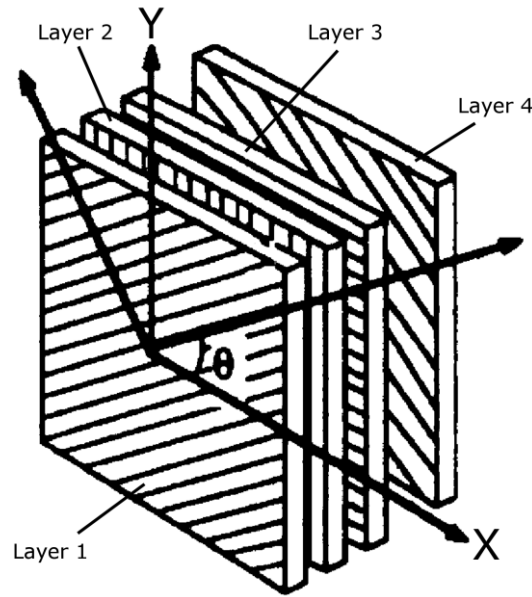


Figure 4.10. Layered structure of fabric unit (Singh *et al.*, 1998)

In an effort to incorporate the realistic effect of non-uniform microstructure of nonwovens into the model, third approach based on homogenization of the model using representative volume element (RVE) was used in literature. Petterson (1959) introduced the model to predict the macroscopic response of the fabric by homogenizing the behaviour of a unit-cell incorporating the random distribution of fibres' orientation. This model was later modified by Hearle *et al.*, 1964 and again by Kothari and Patel, 2001, to include the effects of fibre and creep response of individual fibres, respectively. Still, in that model, some inelastic deformation mechanisms such as irrecoverable textural evolution were missing. More recently, Silberstein *et al.* (2012) introduced a model based on a similar RVE-based technique to predict a macroscopic behaviour of the fabric. The model consists of a multilayer triangular network and uses a homogenization technique to predict a response to monotonic and cyclic loading. Such models based on the homogenization technique do not predict localization of damage and changes in material's microstructure caused by this damage.

Fourth approach to incorporate the randomness of nonwoven material into the model is by direct introduction of fibres to simulate realistic deformation and damage

behaviour of nonwovens. In this context, Mueller and Kochmann (2004) proposed a FE model to simulate the behaviour of thermally bonded nonwovens (Fig. 4.11).

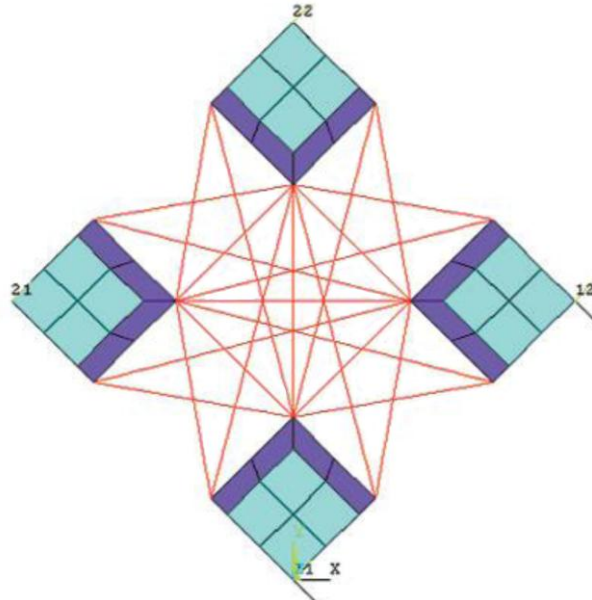


Figure 4.11. Unit cell with bond points connected by truss elements
(Mueller and Kochmann, 2004)

In that model, bond points were modelled as an element consisting of two regions: bond core and boundary zone. The boundary zone represents the deformed fibres and partly bonded fibres at the periphery of the bond points. The fibres were modelled as truss elements. Each truss element represents the fibre bundle as the behaviour of several fibres was combined and mapped onto these elements. These truss elements combined the bond points in a unit cell as shown in Figure 4.12. With this model, the effects of the geometry of bond points on the behaviour of nonwovens were also investigated. However, it was almost impossible to incorporate the randomness in the microstructure of the nonwoven into the model as the model was composed of symmetric unit cells and there was limited number of nodes on the bond point. Moreover, it failed to mimic the microstructure of nonwoven fabrics.

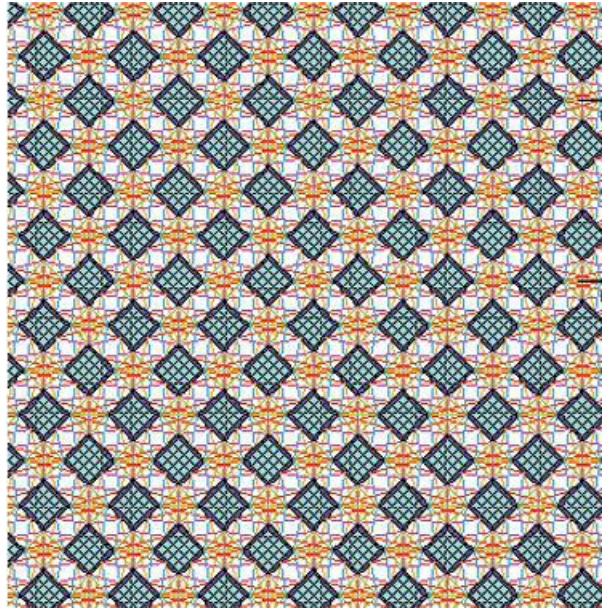


Figure 4.12. Discontinuous FE model with square bond points
(Mueller and Kochmann, 2004)

Another discontinuous model to simulate the point-bonded spun bond nonwoven was presented by Limem and warner in 2005. This model treats the fibres as truss elements connecting the bond points. The fibres were assumed as straight cylindrical elements between the bond points. All the bond points in the model were isotropic with identical square-shaped geometry (Figure 4.13).

Similar to previous models, the major limitation of this model was its periodic symmetric structure due to which it cannot represent the realistic random microstructure of nonwovens. Thus, the actual deformation mechanism cannot be understood by this model. Moreover, the fibres in that model were linear elastic, which is a very small portion of the real deformation behaviour of nonwoven materials, without any consideration of time dependency of mechanical behaviour (viscous effects).

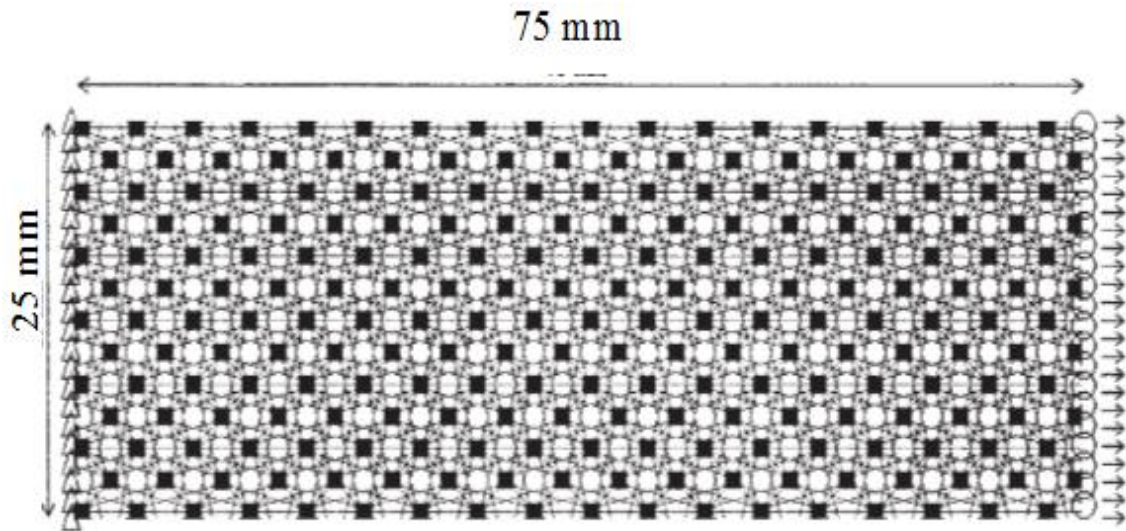


Figure 4.13. FE model to simulate point bonded nonwoven (Limem *et. al.*, 2005)

Recent development in discontinuous modelling of nonwovens was made by Hou *et. al.*, 2009. He proposed a discontinuous model incorporating realistic orientation distribution of fibres and bond point structure (Fig. 4.14). This was a good technique to imitate the geometry of the fabric network including voids and gaps in their microstructure. Since it was difficult to model all the fibres in the structure, one of the weaknesses of this model was convergence issues due to limited number of fibres modelled between bond points. Besides, it was very difficult to incorporate different realization of orientation distribution of fibres, and size, shape and pattern of bond points. Therefore, it was almost impossible to extend this model for another type of nonwoven especially with higher planar density.

A finite element model based on direct introduction of fibres into the model was developed by Sabuncuoglu *et. al.*, 2011. Being a parametric model, it had the advantage to implement the changes in the parameters such as number and orientation distribution of fibres, size, shape and pattern of bond points very easily. Fibres were modelled between the bond points according to their orientation distribution within the real fabric. The model was quite good to predict the effect of various parameters on deformation behaviour of nonwovens under monotonic loading. However, the damage initiation and evolution behaviour was not incorporated into the model. As a result, it failed to provide

insight about localization of damage and variation in network topology as a function of damage evolution along with mechanisms involved in damage evolution.

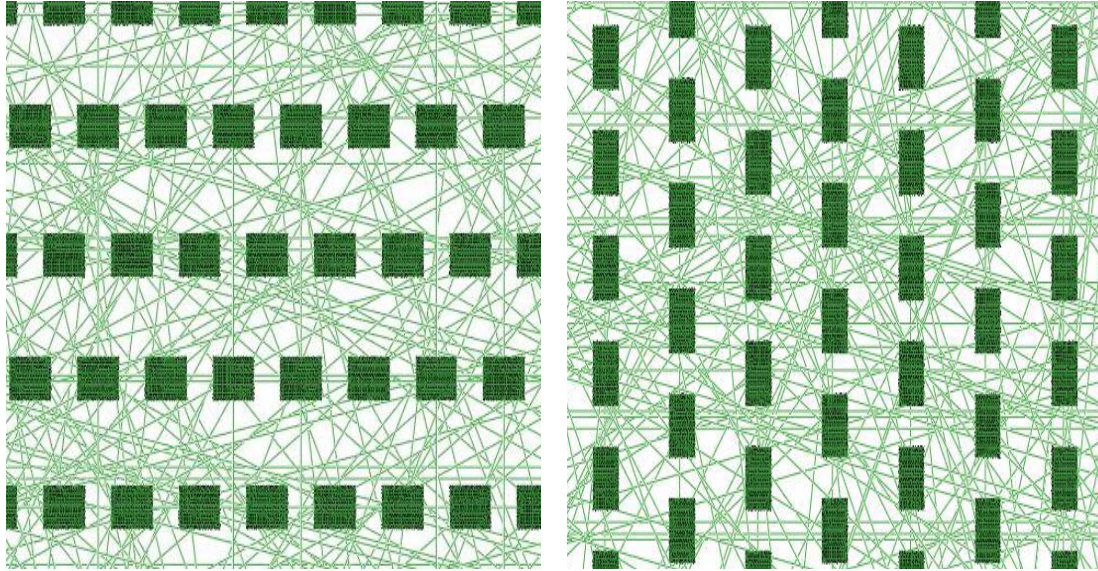


Figure 4.14. Discontinuous FE model (a) machine direction (b) cross direction

(Hou, 2010)

Most recently, a model, based on the same approach to introduction of discontinuous microstructure, was presented by Ridruejo *et. al.* (2011) who employed bundles of random fibres, without using actual orientation of fibres within the real fabric, in the model. Using this model, he studied glass-fibre nonwoven felt in which damage of the fabric occurred as failure of bonds rather than fibre bundles. Thus, this model cannot be used for other types of nonwovens in which damage is followed by fibres stretching and failure.

In summary, it can be concluded that despite the benefits of different models for analysis of various aspects, they present a partial solution for prediction of mechanical behaviour and mechanisms involved in deformation and failure of nonwoven fibrous networks. Moreover, almost all the models were developed to predict the behaviour of nonwovens under simple tensile tests. Generally, nonwovens in their service life undergo complex loading at various strain rates with or without effects of creep or stress relaxation rather than simple monotonic loading and damage occurs inevitably in the material beyond a certain level of loading. Thus, it is important to understand the

damage mechanisms that govern the material behaviour under excessive loading and to develop a finite-element model incorporating the actual orientation distribution and viscous properties of constituent fibres capable to reproduce the response of these materials including their damage.

A finite element model based on direct introduction of fibres employing parametric modelling technique developed by Sabuncuoglu (2012) is extended in this research to simulate the deformation and damage behaviour in nonwovens under real-life loading conditions. Though, this modelling technique is computationally not as efficient as a continuum one, however, it can account explicitly for all the mechanisms involved in deformation and fracture of nonwovens. Moreover, a model based on this technique naturally introduces voids and gaps into consideration that are a distinctive feature of fibrous networks especially in case of low-density nonwovens.

4.5 Summary

Background information about numerical modelling of the materials is provided in this chapter. Mathematical formulations of the elastic, plastic and viscous behaviour of the material, which plays a vital role in defining the deformation and damage behaviour of the material, are briefly described since the material under study possess these behaviours.

In order to develop better understanding of the importance of this research, a brief but critical review of existing nonlinear numerical models to simulate the behaviour of the nonwoven materials is provided. The information provided in this chapter will be used to develop the modelling approach used in this research.

In order to obtain the properties of material for FE modelling, several tests are required. These include tensile, creep/relaxation tests to obtain the elastic, plastic and viscous properties of material. Fabric tensile tests are also required to understand the deformation and damage mechanisms of nonwovens. Besides, these are used to evaluate

the efficiency of the model. The experiments performed on fabric are explained in next chapter.

CHAPTER 5

CHARACTERISATION OF MECHANICAL RESPONSE OF FABRIC

Having two discrete regions – bond points and fibrous matrix – calendered bonded nonwovens present unique mechanical behaviour which is different from their woven counter parts. Nonwoven materials focussed in this study are low-density ones ($< 50 \text{ g/m}^2$ basis weight) manufactured with carded moncomponent fibres and bonded using thermal bonding technique. Three basis weight of the fabric 20, 30, 40 g/m^2 made of Polypropylene (PP) fibres (manufactured by FiberVisions[®], USA) were selected. This study was mainly focussed on 20 g/m^2 fabric. 30 and 40 g/m^2 nonwovens were used as case studies in Section 7.5 to assess the predictive capability of the numerical model developed in Chapter 7. PP fibres were obtained by the extrusion process, resulting in approximately 18 μm mean diameter and cut to length of 38.1 mm. Crimp was incorporated into the fibres using stuffer box crimping technique. These crimped carded

fibres were then combined into a web by carding machine where most of the fibres were laid in the direction of conveyer belt called machine direction (MD). The web then point bonded by passing it through the hot calenders where the fibres melt locally under high temperature and pressure, and joined together on subsequent cooling. All the manufacturing parameters such as bonding temperature, pressure, web speed were maintained at optimized level as mentioned in manufacturer data sheet.

As mentioned in Chapter 4, information about fabric's deformation and damage initiation as well as evolution behaviour until its failure and fabric's microstructure is required for the successful development of FE model to simulate mechanical behaviour of fabric as a function of its microstructure. This chapter is focused on investigation of fabric's microstructure and its deformation and damage behaviour in two steps. First, the fabric microstructure was characterised in terms of morphological properties using image analysis technique. Then, macroscopic behaviour of the material under in-plane loading and sequence of deformation and damage processes was investigated using standard tensile tests. Knowledge obtained from these characterisations were vital for the development of finite element model of nonwovens discussed in Chapter 7. The results obtained from these experiments not only served as guidance for the development of model but also to modify and verify the numerical model developed in this study.

5.1 Experimental Techniques

The goal of this work was to study the deformation and damage behaviours and associated mechanisms of the nonwoven fabrics. To this end, the mechanical performance of the fabric together with its microstructure was analysed.

5.1.1 Morphological Characterisation

Morphological characterisation of nonwovens was obtained by means of image analysis technique. Microstructure of the fabric was obtained with scanning electron microscopy (SEM) (Carl Zeiss, Leo, 1530VP FEGSEM) (Fig. 5.1). This provided the surface

images of nonwoven fabric from which dimensional characteristics of surface entities such as bond points size and pattern were obtained.

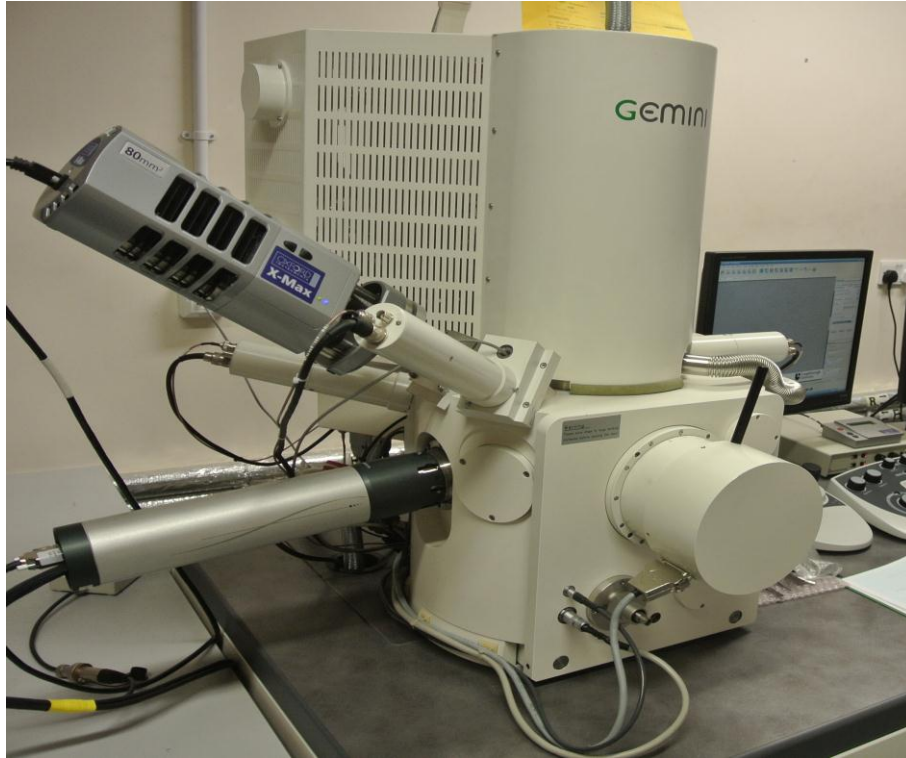


Figure 5.1. Scanning electron microscopy

The images obtained by SEM were 2D which only portrayed the surface characteristics of the fabric while leaving the information about 3D network structure of nonwoven materials. Therefore, the same fabric was scanned by X-ray Micro Computed Tomography (CT) (XTEK XT-H 160Xi) device (Fig. 5.2). This provided the information about fabric microstructure in 3D space.

In this study, morphological characterisation of the fabric was focussed on following structural entities of the fabric:

- orientation distribution of fibres (ODF)
- bond point pattern
- bond point geometry and dimensions



Figure 5.2. X-ray micro computed tomography

5.1.2 Mechanical Characterization

In order to predict the behaviour of the fabric in numerical modelling, mechanical characterisation of the fabric should be performed by mechanical testing. Tensile testing is the primary method to have an insight into deformation and damage behaviour of a material. Uniaxial tensile tests were conducted on the small coupons of the fabric. In the literature, numbers of fabric testing techniques have been established to test nonwovens under uniaxial loadings, such as, grab test of narrow width specimen (ASTM D5034-95), grab test for wide width specimen (ASTM D4595-86), and cut-strip method (ASTM D5035-95). According to ASTM, various testing standards are suitable for different type of nonwovens and loading scenarios such as (ASTM D5034-95) is applicable when total deformation in fabric is less than 11% and (ASTM D4595-86) is suitable for geotextiles. The most suitable type for testing nonwovens in this study, which were expected to undergo large uniaxial strain before failure due to polypropylene based constituent, was cut-strip method. The nonwoven specimens

extraction and mounting on the machine for testing were performed according to the guidelines for cut-strip method. According to this method, the width of the specimen cut from nonwoven should not be protruding outside the machine jaws as shown in Fig. 5.3. Since, there are different institutions which produce international standards such as American Society for Testing and Materials (ASTM), British Standards Institution (BSI), and International Organizations for Standardization (ISO), standards for uniaxial testing of nonwovens using cut-strip method from each organization are different from each other in terms of specimen size and loading rate. Moreover, big specimen sizes and high loading rates make it difficult to use these standards for characterising the mechanical response of the fabric until failure along with its microstructure. Therefore, this study is facilitated by selecting specimen size and loading rate for convenient testing while making sure that all the features involved in deformation and damage of the fabric until its failure are captured.

As mentioned in Chapter 2, nonwovens are manufactured with preferentially oriented fibres. Due to this preferential orientation, fabric was expected to show anisotropic mechanical properties. In order to understand the anisotropic mechanical characterisation of the fabric under uniaxial testing, the fabric was cut into rectangular coupons with dimensions 10 mm width and 16.5 mm length from the rolls along both MD and CD. This area of fabric chosen for tensile testing is large enough to capture all the features involved in its deformation and damage, and for convenient testing. The tensile tests were performed at a nominal strain rate of 0.1 and 0.01 s⁻¹ using Hounsfield Benchtop Tester with ±1000 N load cell and pneumatic grips with rubber inside (Fig. 5.4). The lower strain rate 0.01 s⁻¹ was chosen to ascertain the mechanisms involved in deformation and damage behaviour of fabric.

Pneumatic grips enhance handling and help to prevent slipping of specimen while making it sure that fabric is not damaged by the grips during tensile testing. A precision aligned column attached to rigid support base attached with moveable crosshead with 0.001 mm position measurement accuracy, ±0.005% of set crosshead speed accuracy and ±0.5% of applied load measurement accuracy are the main features of Benchtop Tester which results in accurate load information and displacement control. A high-

speed camera (Photron Fastcam SA3) with advanced macro capabilities was used to ascertain the evolution of deformation and damage mechanisms in thermally bonded nonwovens. Samples were loaded in tension along their planar principle directions which are MD and CD.

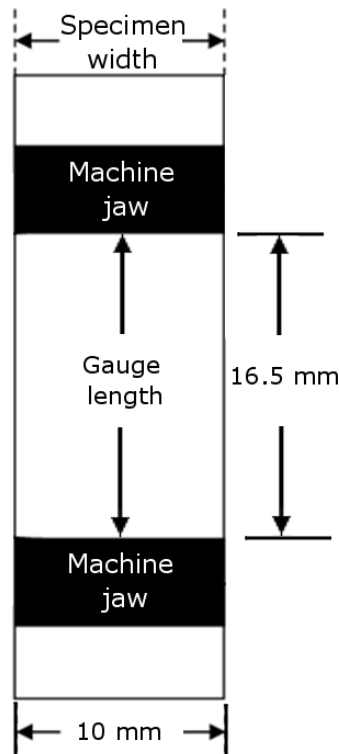


Figure 5.3. Specimen dimensions in cut-strip method

In order to study the deformation and damage behaviour of the fabric at meso level and to understand effect of bond point arrangement on fibre failure as a function of fabric extension, two bond points in front of each other along MD were cut from the fabric as shown in Fig. 5.5a. To prevent slippage and proper handling of the specimen during testing, sticky papers were attached to the bond points. The schematic configuration of the specimen and its fixture are shown in Fig. 5.5b. Those specimens were mounted on Instron[®] Micro tester 5848 using peg type grips and tensile tests were performed at a strain rate of 0.5 s^{-1} . Photron Fastcam SA3 was also used to observe the deformation and damage mechanisms in fabric at meso-level.

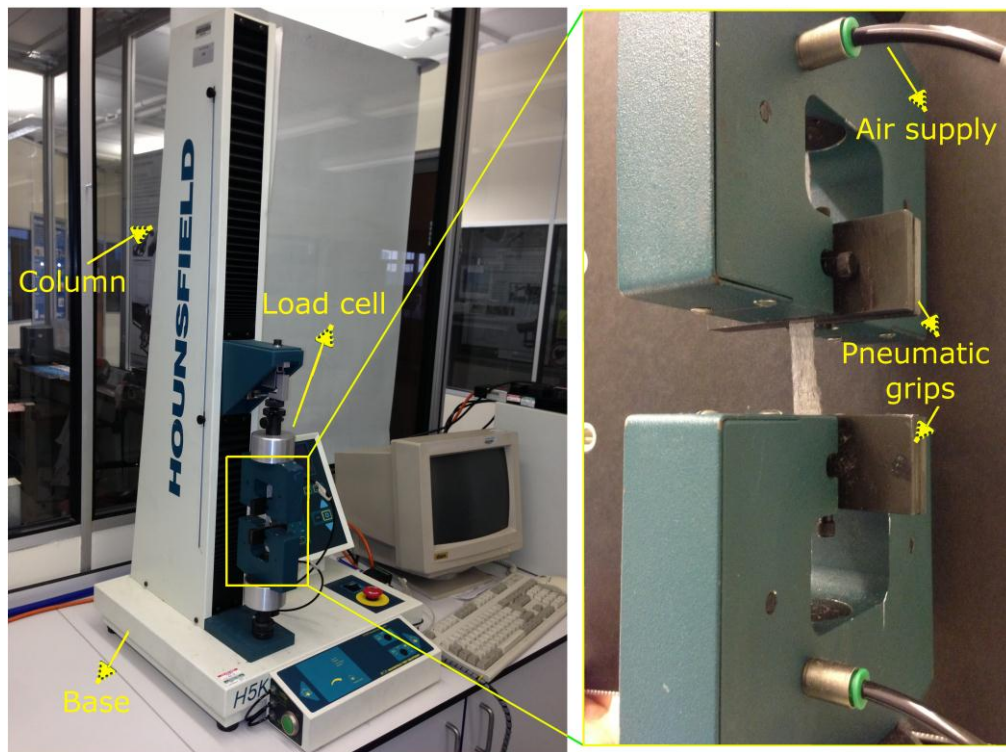


Figure 5.4. Hounsfield Benchtop Tester with pneumatic grips

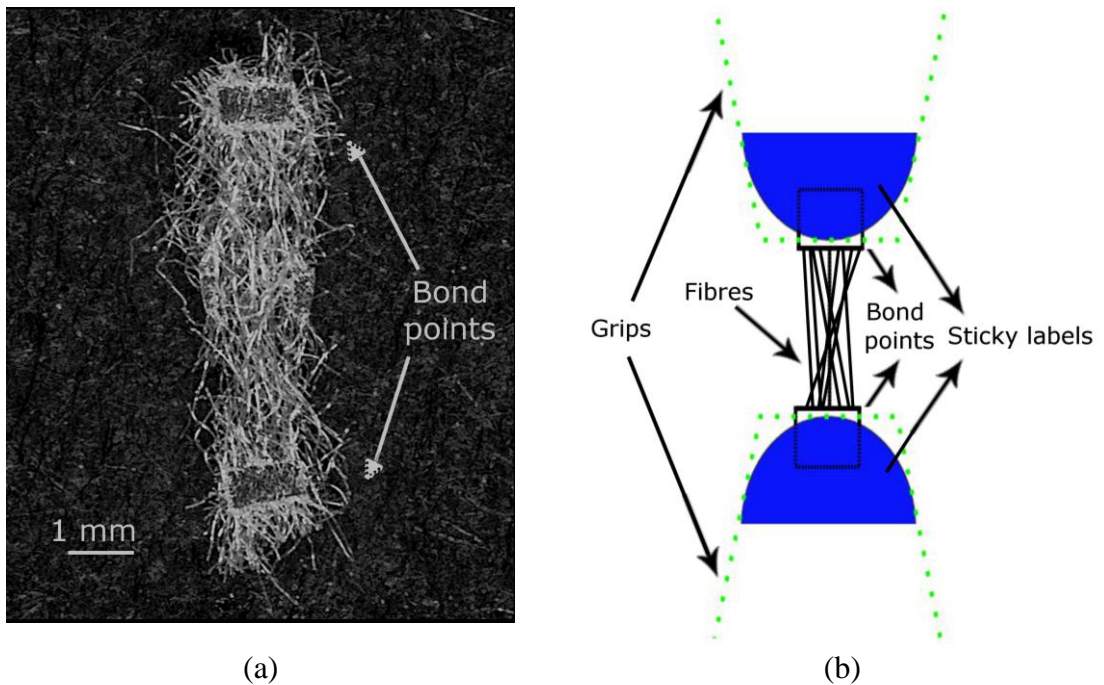


Figure 5.5. (a) Meso-level fabric specimen showing fibres connecting between bond points; (b) Schematics of final specimen (not to scale including number of fibres)

5.2 Experimental Results

The results of the experiments related to mechanical performance and morphology of the thermally calendered bonded nonwovens are given in this section. The microstructures of the nonwovens evolve during their deformation and damage. Therefore, both — initial and deformed — microstructures of thermally calendered bonded nonwoven are discussed here.

5.2.1 Initial Microstructure Using SEM

SEM images of low-density (20 g/m^2) thermally bonded nonwoven at different scales are shown in Fig. 5.6. These images show that fabric is composed of two regions, namely, bond points and fibrous matrix. Bond points were found to be composed of molten polypropylene fibres which were solidified together on cooling. Whereas, the fibrous matrix was composed of distinct fibres. Since, manufacturing parameters such as bond point geometry, pattern, dimensions etc. and web forming method for all the basis weights of fabric i.e. 20, 30 and 40 g/m^2 were the same, therefore, all of those present the same kind of microstructure having preferential orientation of fibres along MD except the difference that the number of fibres per unit area were more in fabric with higher planar density.

SEM images showed that fibres were not completely randomly oriented but most of them were aligned along machine direction which indicated the anisotropy in microstructure of nonwoven. A fibre matrix was a discontinuous medium having voids and gaps in it between fibres as shown in Fig. 5.6b. Although, the fibres used in manufacturing of nonwoven under study were produced at same manufacturing facility, but there diameters were not similar. Moreover, the diameter of a single fibre was not constant along its length as shown in Fig. 5.7. The average value of fibre diameter was very close to $18 \mu\text{m}$ (provided in datasheet by manufacturer).

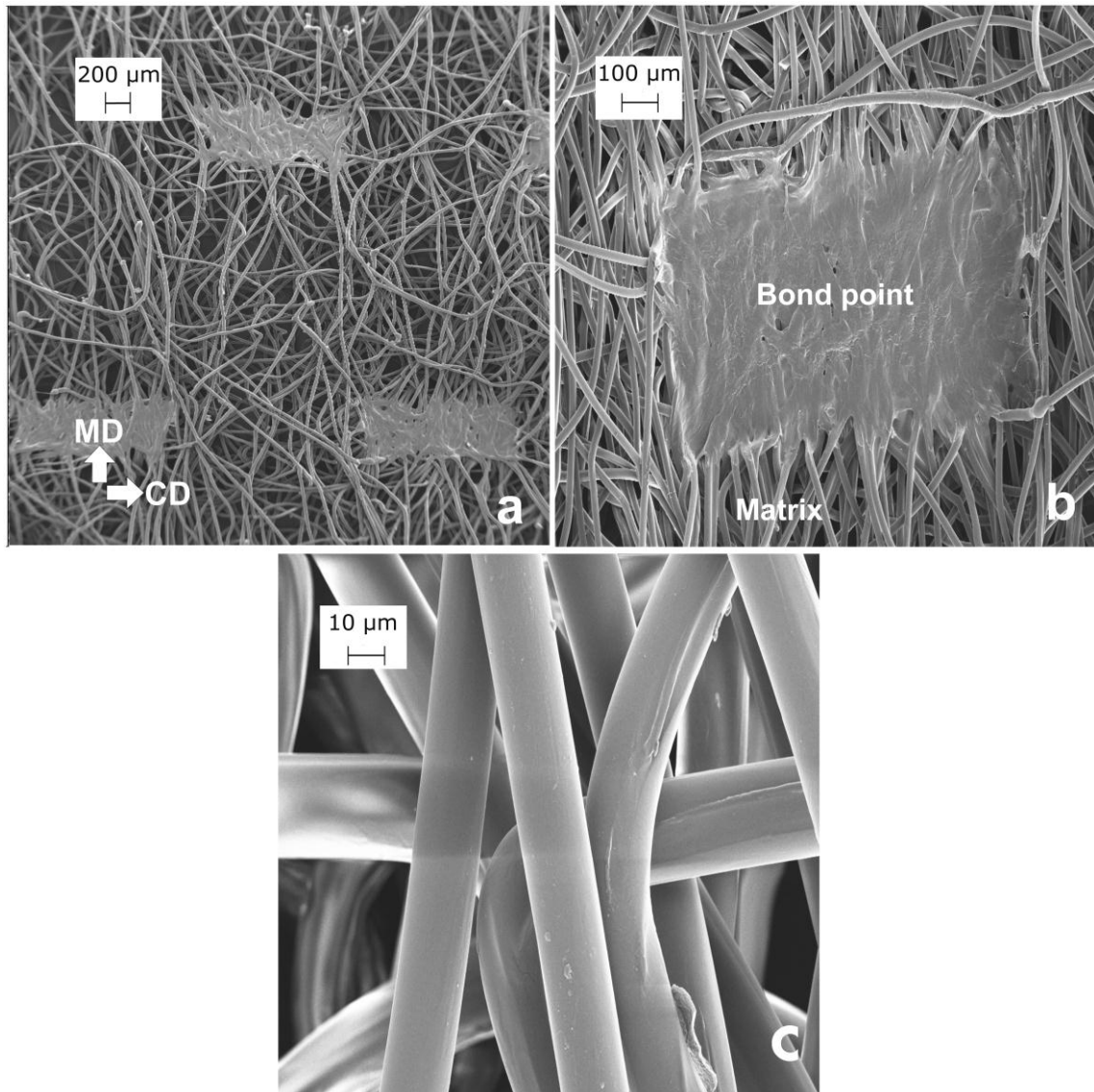


Figure 5.6. SEM images of 20 g/m² PP fibre nonwoven at different length scales: (a) overall microstructure; (b) bond point and surrounding fibre matrix; (c) polypropylene fibres

Unlike fibrous matrix, bond points had thin and continuous structure formed by melting of fibres during thermal bonding process and joining together on subsequent cooling. As mentioned in Chapter 3, nonwoven fabric has two principle directions: MD and CD, which are shown in Fig. 5.6a according to orientation of bond points in the fabric under study. Preferential orientation of fibres along MD as shown in Fig. 5.6a and b give rise to tensile strength of the fabric biased towards preferential fibre orientation which can be observed during mechanical testing of the fabric as mentioned in Section 5.2.3.

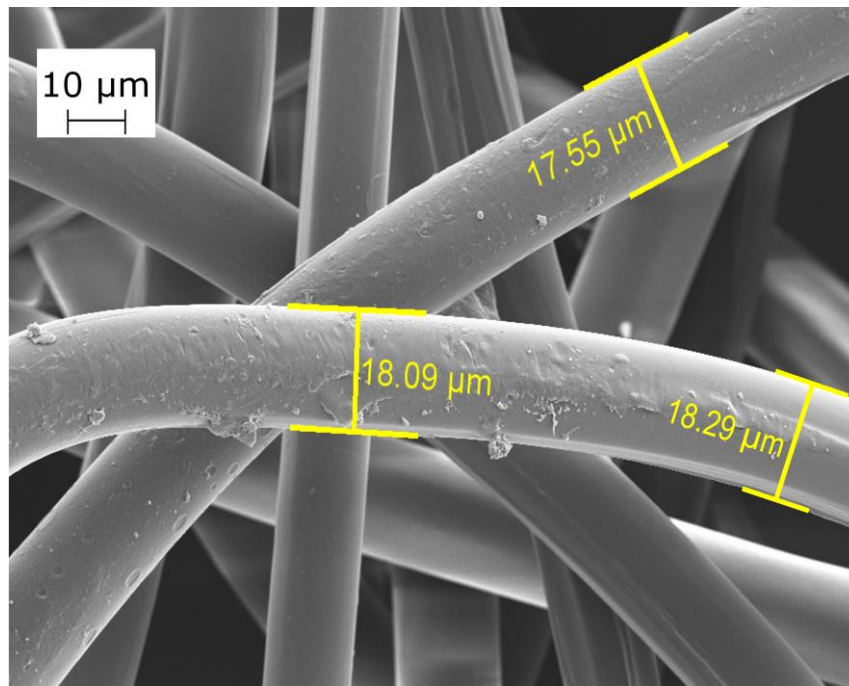


Figure 5.7. Variation in fibre diameter

Bond point dimensions and pattern required for finite-element modelling were measured directly from SEM images. Whereas, orientation distribution of fibres in the fabric was obtained with the help of in-house software Nonwoven Anisotropy V1. The SEM image with clearest view of fibres was processed with this software to obtain ODF. The software presented results in terms of orientation distribution function (ODF) of fibres as a histogram (Fig. 5.8); details of this process are given in Appendix A.

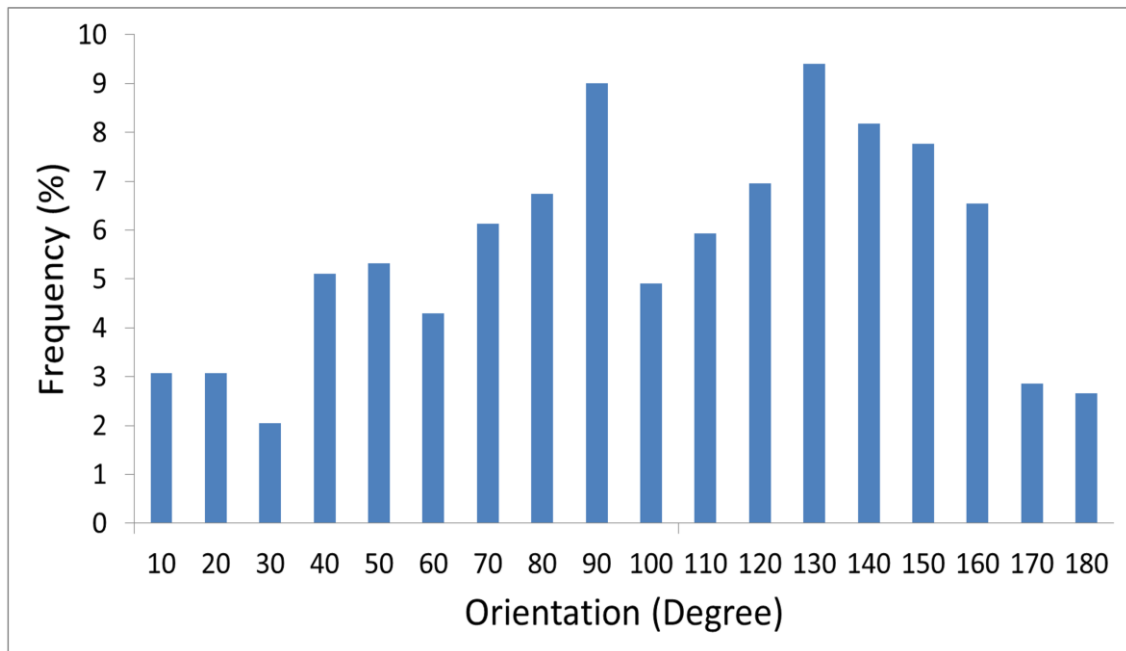


Figure 5.8. Orientation distribution function of fibres (90° corresponds to MD whereas 0° and 180° correspond to CD)

5.2.2 Initial Microstructure Using X-Ray Micro Computed Tomography

3D images of low-density thermally bonded nonwoven obtained from X-ray micro CT are shown in Fig. 5.9 and 5.10. Due to the bonding procedure, fabric was composed of hills and valleys arranged according to the bond pattern generated by engraved hot calenders. Micro CT image provided very useful information required for the numerical modelling of nonwoven. The randomness of the fibre orientation in the fibre matrix was identifiable in 3D space. Moreover, an average thickness of the bond points, which was 0.0337 mm, was measured by X-ray micro CT system. Thickness of bond points affect their deformation resistance, therefore, it was important to determine the actual thickness of the bond points experimentally and implement into FE model for realistic simulation of deformation and damage behaviour of the fabric. The difference between porosity and thickness between bond points and fibre matrix as result of pressure and temperature during bonding can be seen in Fig. 5.9 and 5.10.

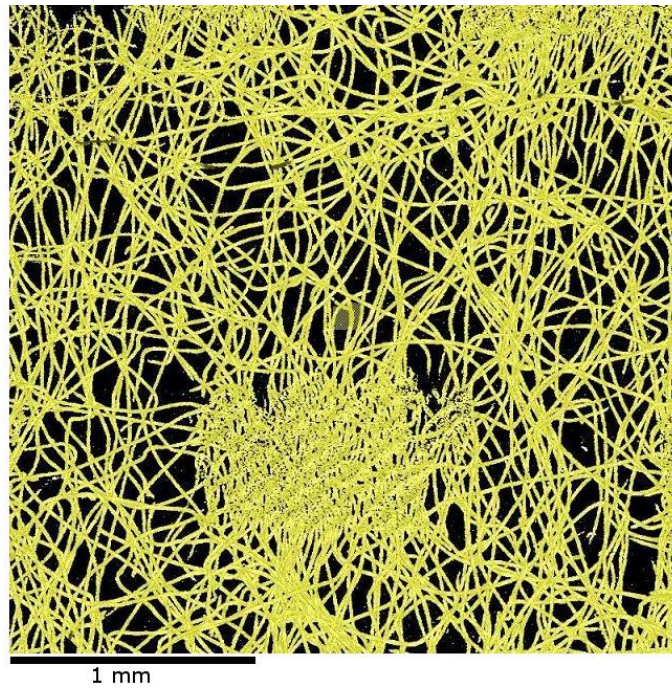


Figure 5.9. X-ray micro CT image of thermally bonded nonwoven (fibre: PP, planar density: 20 g/m²)

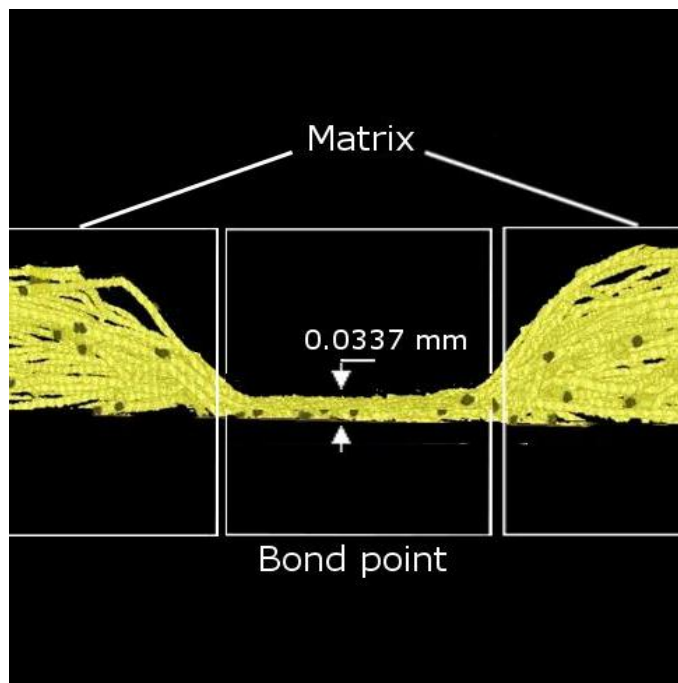
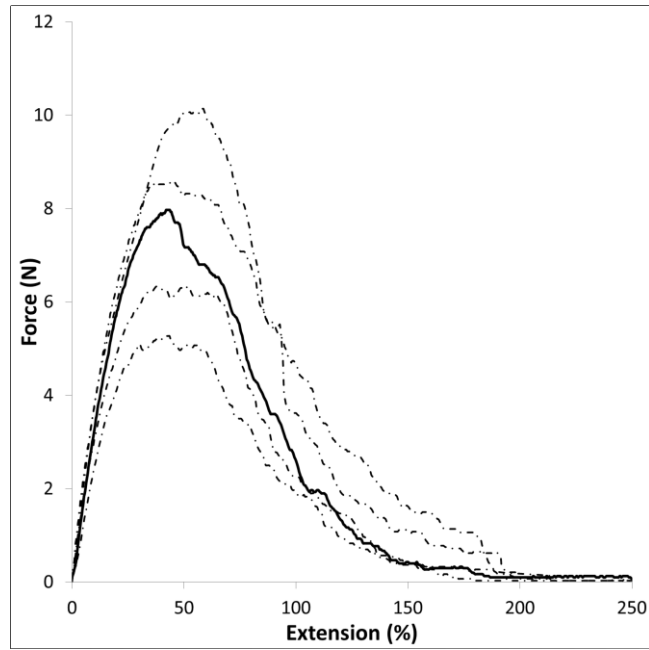


Figure 5.10. X-ray micro CT image showing through thickness microstructure (fibre: PP, planar density: 20 g/m²)

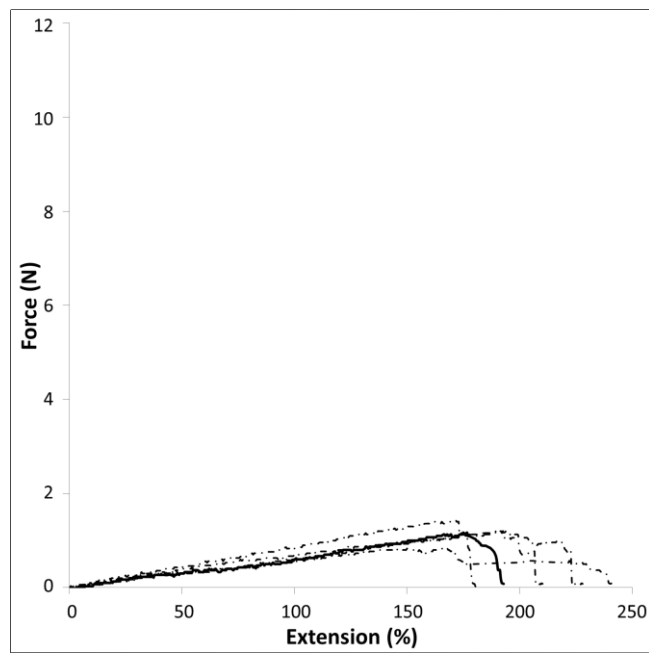
Morphological analysis of the fabric performed using SEM and X-ray micro CT shows that fabric is composed of two regions: bond point and fibre matrix. Both of these regions have distinct microstructure. Fibre matrix has discontinuous microstructure having voids and gaps in it with fibres preferentially aligned along MD. Whereas, bond points are continuous solids structure connected by the fibrous matrix. As a result of having distinct microstructures, both of these regions bond points and fibrous matrix are handled separately in FE model. The information about the bond point dimensions and pattern obtained from SEM images and orientation distribution of fibres obtained with the help of Nonwoven Anisotropy V1 was used as input for FE model in Chapter 7.

5.2.3 Tensile Tests

Response of fabric under uniaxial loading at a strain rate of 0.1 s^{-1} along MD and CD are plotted in terms of load and percentage extension in Fig. 5.11. The fabric showed a highly anisotropic behaviour under uniaxial load. Fabric's response along MD presents stiffer behaviour with smaller elongation at break as compared to CD. Moreover, fabric showed nonlinear behaviour with a gradual decrease in load carrying capacity under uniaxial loading along MD than that of CD. These experiments not only presented the difference in mechanical behaviour of the fabric along MD and CD but a significant scatter in results in both directions due to the irregularities in fabric's microstructure and constituent fibres' geometric properties as discussed in morphological characterization of the fabric (Sections 5.2.1 and 5.2.2). Along MD, the maximum load was attained at lower fabric's extension as compared to that in CD followed by a gradual process of fibre failure giving the bell-shaped form to force-extension curve. In contrast, a rapid fibre-failure process following large fabric's extension was observed in CD resulting a sudden drop on force-extension curve. The features presented by the curves for various specimens in any particular direction — MD or CD — were the same, shown by continuous lines in Fig. 5.11, even with a significant scatter among them. All the basis weights of fabric i.e. 20, 30 and 40 g/m^2 presented the same anisotropic behaviour including scatter with the difference that the fabrics with more planar density exhibited more strength in both MD and CD (Fig. 5.12). However, fabric's planar density has practically no effect on its extension at failure (see Fig. 5.13).



(a)

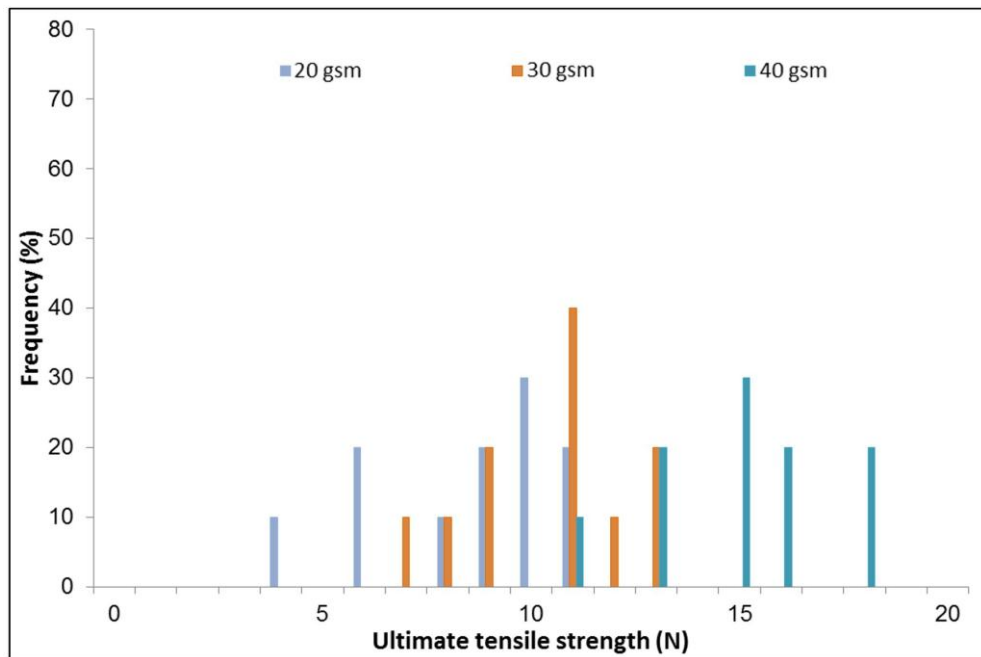


(b)

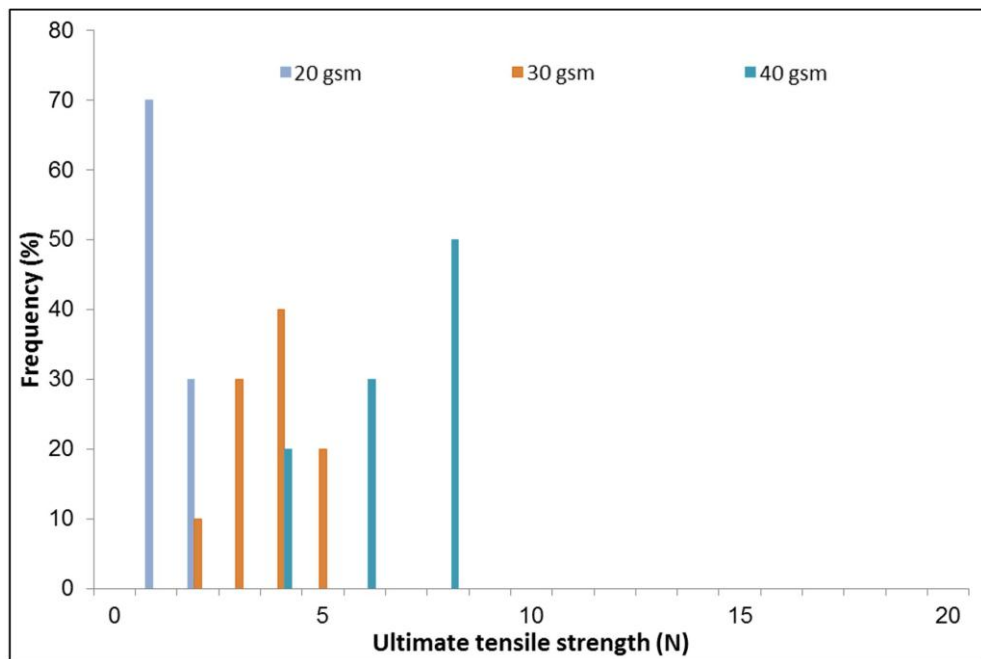
Figure 5.11. Force vs. % extension curves for rectangular specimen in tension at a strain rate of 0.1 s^{-1} along MD (a) and CD (b) (20 g/m^2)

5.2.4 Structure of Deformed Fabric

The uniaxial tensile tests on fabric revealed its deformation and damage mechanisms. Fibres within the fabric started to re-orient and straighten themselves along the loading direction immediately at the beginning of tensile deformation. As strain increased, they became aligned along the loading direction resulting in gradual transverse contraction from the grips on both sides of the fabric to the area of maximum contraction in the middle of the specimen. Once the fibres were uncurled and aligned along the loading direction, they underwent large elastic-plastic deformation and the maximum load was attained under this condition without any evidence of fibre fracture. As soon as fibres reached their stress or strain threshold, they failed resulting in localization of damage and development of fracture zones. These fracture zones were made up of the surviving straight fibres aligned along loading direction. Further fibre failures caused a growth in fracture zones followed by the ultimate failure of the fabric. A small reorientation of fibres before participating in load bearing and very gradual growth of damage was observed until failure of fabric along MD with the first and the last fibres failing at fabric extension of approximately 40–60 and 225–250%, respectively. Whereas, a large reorientation of fibres along loading direction before participating in load bearing and a rapid growth of damage until failure of the fabric was observed with the first and the last fibres failing at fabric extension of approximately 180–200 and 225–250%, respectively. Rotation of bond-points was observed during tests without significant deformation in them. Nevertheless, it should be noted that they play an important role in damage behaviour of thermally bonded nonwovens since fibres always break at the bond-point periphery. The phenomena of deformation and damage initiation as well as progression were same in both MD and CD except the only difference that rotation of fibres before participating in load bearing was very large in CD as compared to that in MD. The sequence of these phenomena is shown in Fig. 5.14, which shows images of nonwovens at increasing levels of the overall strain.



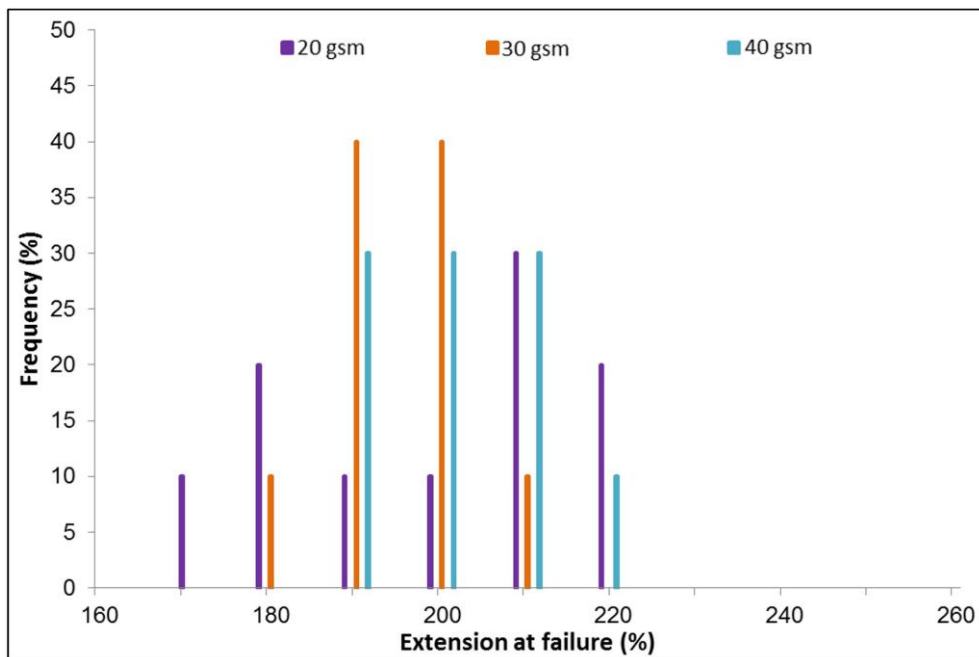
(a)



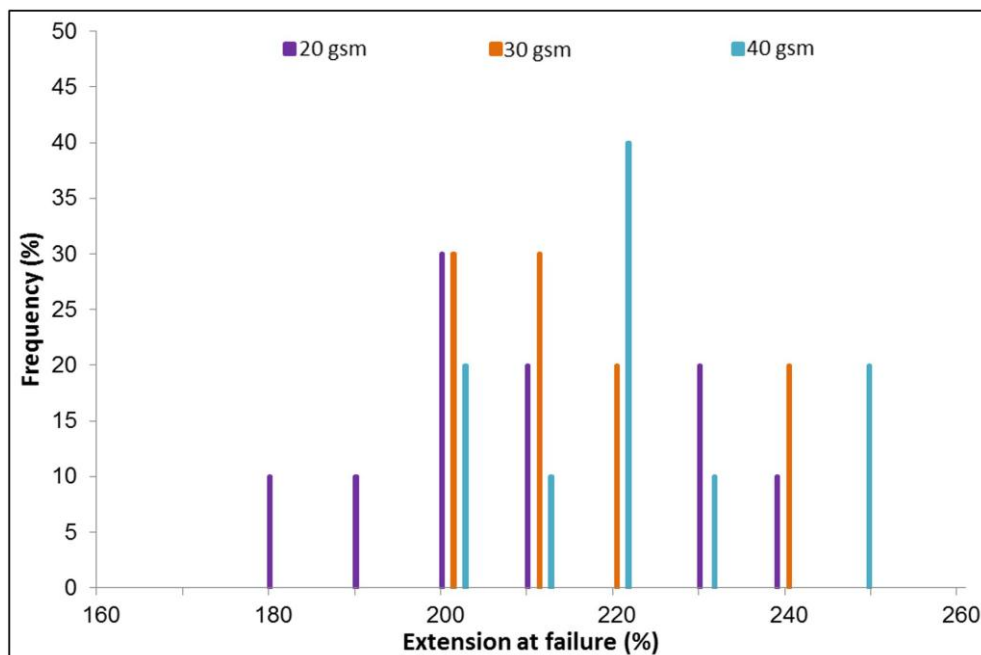
(b)

Figure 5.12. Effect of fabric's planar density on its ultimate tensile strength along MD

(a); CD (b)



(a)



(b)

Figure 5.13. Effect of fabric's planar density on its % extension at failure along MD

(a); CD (b)

When these experiments were repeated on fabrics with different basis weights, it was observed that the main mechanisms involved in deformation and damage of those materials remained the same. Furthermore, the strain rate did not cause any effect on the sequence of deformation and damage phenomena. These observations were close to those presented by Ridruejo *et. al.* (2011).

The results in Fig. 5.11 are consistent with microstructure of the fabric having crimped fibres preferentially aligned along MD as mentioned in previous section. During deformation of fabric, crimped fibres did not start participating in load bearing until they were fully uncurled. Since, resistance to straightening of fibres is way less than that of stretching of fibres, therefore, crimp in fibres gives less stiffer behaviour to the fabric. Besides, since most of the fibres were already aligned along MD, the deformation load applied along MD was mostly accommodated by elongation in fibres resulting in stiffer response of fabric along MD. Conversely, most of the fibres were aligned perpendicular to loading direction along CD; the deformation load applied along CD was mostly accommodated by realignment of fibres to diminish the angle between fibres and loading axis. Since the resistance to reorientation of fibres is significantly less than resistance to elongation in fibres, fabric response along CD was more compliant than MD. Moreover, this preferential orientation of fibres along MD was reflected in macroscopic deformation pattern of fabric. The gradual transvers contraction of the fabric from the grips at both ends of the fabric to the area of maximum contraction at the middle of the specimen at initial stages of fabric's extension was more prominent during deformation load applied along MD as compared to CD (Fig. 5.15).

Mechanical characterisation of the fabric shows that anisotropy is the most prominent feature of nonwovens caused by preferential orientation of the fibres. Therefore, determination of actual orientation distribution of fibres within the fabric is vital for the successful development of numerical model.

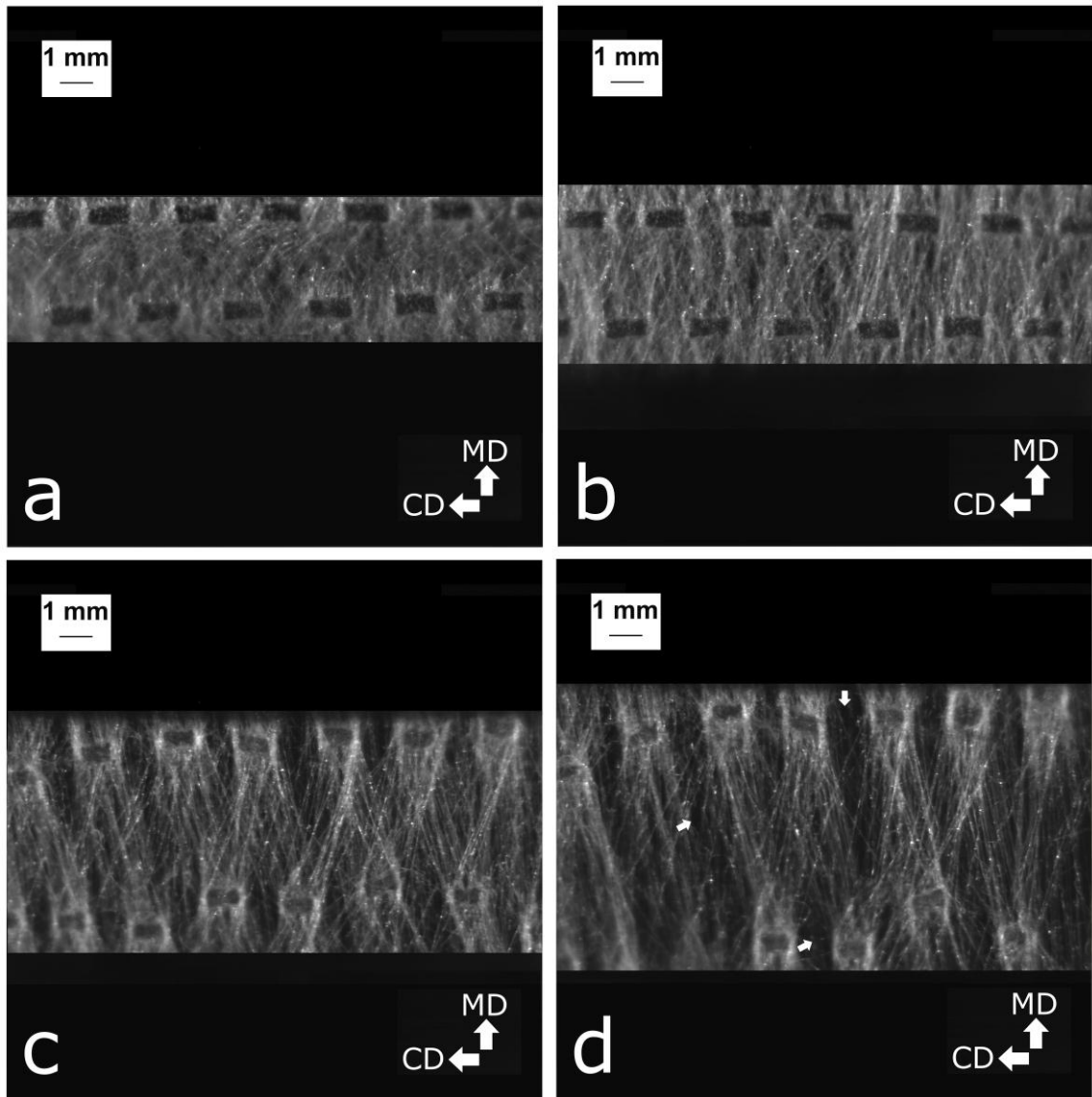


Figure 5.14. Deformation and damage mechanisms in low-density thermally bonded nonwovens during tensile tests at 0% strain (a); 25% strain (b); 50 % strain (c); 80% strain (d). Loading direction was vertical (Arrows indicate fracture zones)

An important thing to notice here is that the bond points, unlike fibrous matrix, are continuous structures without any voids and gaps in it, and they immediately start participating in load bearing on fabric's deformation giving stiffer behaviour to nonwoven, therefore, shape and size and pattern of the bond points in nonwoven is always selected according to its application requirements.

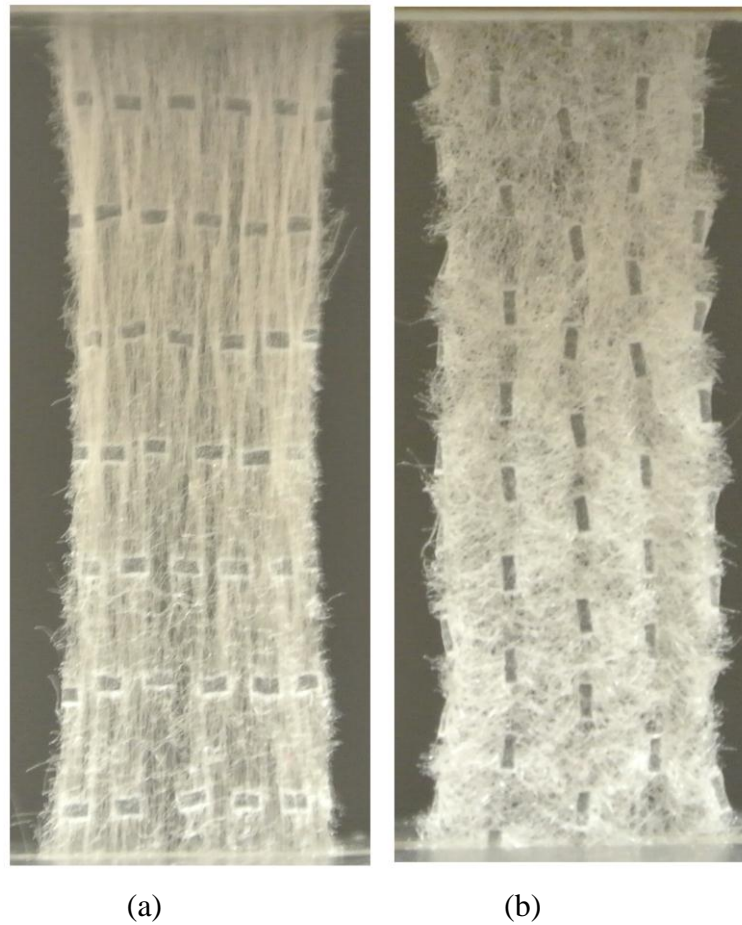


Figure 5.15. Images of thermally bonded nonwoven deformed at 0.5 strain in: (a) MD; (b) CD (16.5 mm gauge length)

It was observed during deformation and damage of the fabric that staggered bonds tend to come in front of each other along loading direction giving a large rotation to fibres before participating in load bearing as shown in Fig 5.14. During the tensile tests performed on the fabric at meso-scale, it was observed that the first and the last fibres failed at fabric extension of approximately 35-40 and 110–120 %, respectively, resulting in less gradual growth of damage as compared to that in fabric with staggered bond point arrangement. This reason for this phenomenon was that the fibres between two head-on bond points were aligned along loading direction earlier than that of fabric with staggered bond points. The sequence of deformation of damage mechanisms observed during these tests were same to that observed during tensile tests on fabric. The meso-scale images of nonwoven during tensile test at increasing level of overall

strain are given in Fig. 5.16. Tensile tests performed at meso-level of fabric consisting of two head-on bond points provide insights into not only deformation and damage behaviour of the fabric but also the effect of bond point arrangement on fibres' failure within the fabric as a function of its extension.

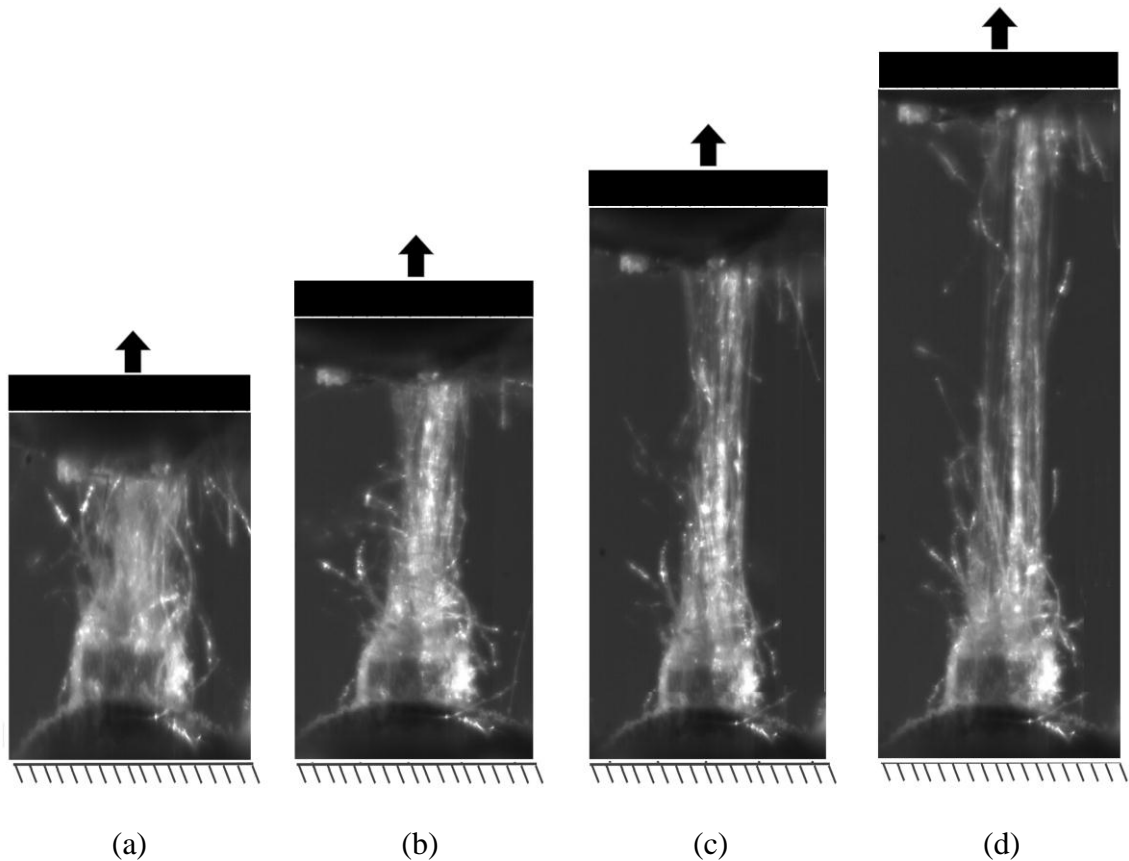


Figure 5.16. Deformation and damage mechanisms in low-density thermally bonded nonwovens during tensile tests at 0% strain (a); 25% strain (b); 50 % strain (c); 75% strain (d)

5.3 Conclusions

This chapter contains the investigation of morphological properties and mechanical characterisation under in-plane mechanical loading of thermally bonded polypropylene based nonwoven fabric. Morphological characterisation of the fabric revealed that fabric was combination of continuous and discontinuous regions with continuous regions called *bond points* were embedded into discontinuous region called *fibrous matrix*.

Fibrous matrix is a web of curly fibres preferentially aligned along MD having voids and gaps in it. Besides, bond points are continuous structures connected by fibrous web and their thickness is less than that of the fibrous web.

Mechanical characterization and mechanisms of deformation and damage in these materials was studied by performing uniaxial tensile tests on rectangular coupons of fabric. It was found that deformation and damage initiation in the fabric was triggered by the reorientation of fibres along loading direction. Fibres oriented along loading direction underwent elastic-plastic deformation upon further loading. As soon as fibres reach their stress or strain threshold, they failed resulting in damage initiation accompanied by development of fracture zone. Growth in fracture zones occurred by means of progressive failure of fibres leading to ultimate failure of the fabric. Considerable rotation without any significant deformation in bond points was observed during deformation and damage initiation as well as its evolution until failure of fabric. However, they played an important role in damage initiation and evolution as fibres always fail at their periphery. The sequence of these phenomena was same in both MD and CD except the only difference that rotation of fibres before participating load bearing was very large along CD as compared to that along MD. Moreover, fabric demonstrated anisotropic response with stiffer behaviour along MD as compared to that of CD along with significant scatter in results in both directions, consistent with observed fabric morphology.

Tensile tests at meso-scale revealed that bond point pattern had significant effect on its deformation and damage behaviour. Thus, bond point pattern of nonwovens should be included in their finite-element model for accurate prediction of their fabric's deformation and damage behaviour.

The experimental results obtained in this chapter revealed that preferential orientation of fibres is responsible for anisotropic behaviour of the fabric. Therefore, SEM and X-ray CT scan images of the fabric will be used to obtain realistic ODF which will be used to formulate the FE model in order to predict the anisotropic behaviour of the fabric. Damage initiation and propagation behaviour of the fabric until its failure is

governed by the mechanical properties of constituent fibres as it includes stretching and progressive failure of fibres. The next chapter aims to explain the procedure for determining the mechanical properties of the constituent polypropylene fibres including failure parameters which control the damage initiation and evolution in the fabric. The results obtained in this chapter were used for the validation of the numerical model developed in this study.

CHAPTER 6

CHARACTERISATION OF MECHANICAL RESPONSE OF FIBRE

As described in Chapter 5, mechanical behaviour of the fabric depends on the physical and mechanical properties of the constituent fibres. Physical properties of fibres, such as, fibre diameter, length and information about crimp in it were gained from SEM and X-ray CT images obtained in Chapter 5. In order to gain better understanding of the mechanical behaviour of nonwoven fabrics, mechanical response of their constituent fibres are investigated in this chapter.

As mentioned in Chapter 5, Polypropylene (PP) was the raw material for manufacturing of nonwoven fibres. Properties of polypropylene fibres were characterized by the temperature variation during thermal bonding of nonwovens. Moreover, during manufacturing of nonwovens, stiffness of the material is increased by drawing fibres through the nozzle. Hence, it is not appropriate to use the properties of

polypropylene available in literature for any sample size for modelling of these materials. Therefore, mechanical properties of fibres for FE modelling were measured experimentally. Mechanical testing of single-fibres provides material data input for computational model to simulate deformation and damage behaviour of the material.

6.1 Tensile Tests

Mechanical properties of the constituent fibres of a nonwoven play an important role in defining its deformation and damage performance. These constituent fibres are passed through the high temperature and pressure during manufacturing of calendered bonded nonwovens and thus adopt manufacturing induced mechanical properties such as changes in tensile strength due to sudden variation in morphology of fibres at bond point edges (Dharmadikary *et. al.*, 1999; Michielsen *et. al.*, 2001; Wang and Michielsen, 2002; Michielsen and Wang, 2002; Bhat *et. al.*, 2004; Michielsen *et. al.*, 2006; Hedge *et. al.*, 2008). Therefore, conducting tensile tests on fibres extracted from the fabric was preferred rather than unprocessed fibres. Simple tension test on single-fibre was performed as it is the basic mechanical test to characterise the material behaviour. Elastic-plastic material properties were obtained from single-fibre tensile tests.

6.1.1 Experimental Techniques

Individual fibres were extracted from a free edge of the fabric using precision-tip tweezers; such extracted fibres present accurate material properties as the extraction process does not affect them (Ridruejo, 2010). After extracting, the edges of the fibres were attached to small sticky strips of paper for firm grip during testing. The procedure of sample preparation is shown in Fig. 6.1. The specimen length was limited to approximately 15 mm as fabric was manufactured by carded fibres. Therefore, a high precision tensile testing machine capable of handling small specimens was required. The Instron[®] Micro Tester 5848, which is an electromechanical universal tester designed for miniature specimens, provided the solution to the challenge of testing the specimen at this small scale (see Fig. 6.2). A requirement of high-precision

displacement measurement together with highly sensitive load frame was inevitable for accurate testing of single-fibre. This requirement could not be fulfilled by a standard universal testing machine as it lacks the required displacement precision and repeatability. The Micro Tester 5848 system with Instron[®] 2530-439 high-precision ± 5 N capacity load cell provided sufficient sensitive loading frame with submicron displacement measurement accuracy required for testing micro-specimens such as fibres. Two precision-aligned columns fixed to a rigid support along with moveable crosshead and sensitive load cell resulted in accurate and repeatable deformation data and displacement control. It was offered with Bluehill[®] software used for simple monotonic and cyclic loading applications. The software was used to operate the machine and acquire essential data such as load, displacement etc. (Instron Microtester User Guide, 2001).

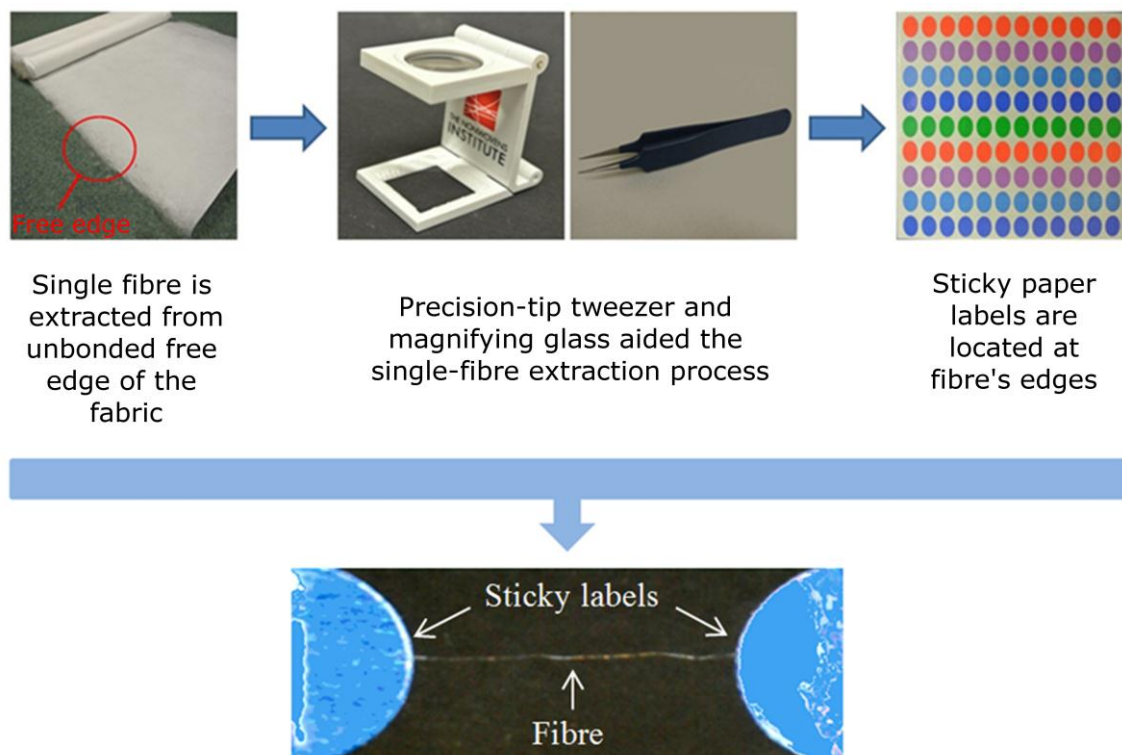


Figure 6.1. Preparation procedure for single-fibre specimens

The fibre samples with sticky labels at the ends were mounted on test rig using special grips with sticky rubber inside (Fig. 6.2). As mechanical testing of single fibres is a

challenging task due to handling issues related to the size and softness of the specimens, all the arrangements of providing sticky labels and rubber grips help to prevent damage, slippage and dislocation of fibre specimen during testing. The load carried by the fibres during the tests was measured with the high-precision load cell of ± 5 N capacity. Fibre elongation was determined by the cross-head displacement measured by the incremental encoder with a displacement resolution of $0.5 \mu\text{m}$. Single-fibre tensile tests were also performed on Textechno Favimat (Fig. 6.3) facilitated at NCRC in North Carolina State University. This machine is specially designed for polymer fibre testing and have a 2.1 N capacity load cell to measure load and $0.1 \mu\text{m}$ displacement encoder to measure displacement during testing. The results obtained with Textechno Favimat were used to verify those obtained with Micro Tester.

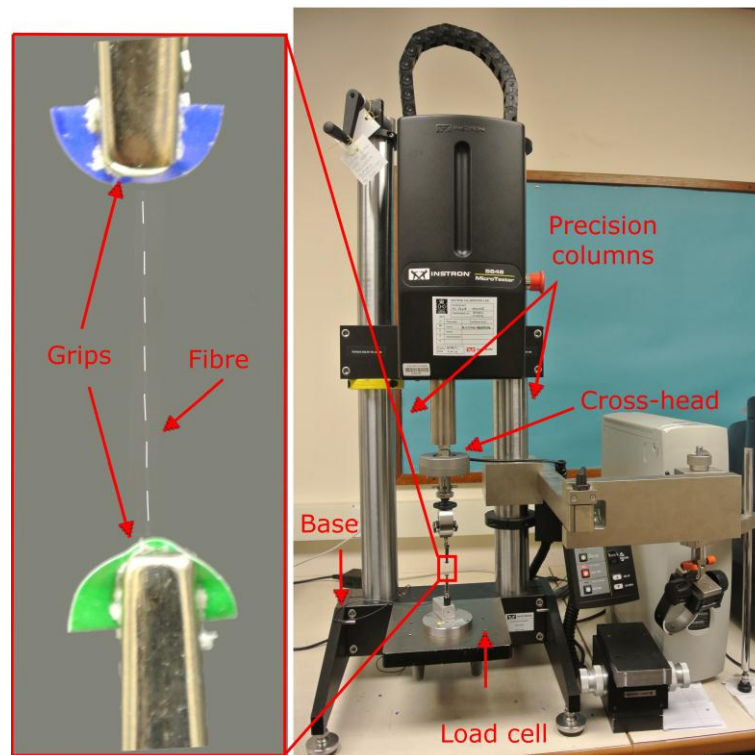


Figure 6.2. Test rig Instron[®] Micro Tester 5848 (Dashed line is used to enhance contrast of image), Loughborough University, UK



Figure 6.3. Textechno Favimat fibre testing system (North Carolina State University, USA)

6.1.2 Experimental Procedure

This part of the study is focussed on quantification of elastic-plastic material properties. Tensile tests were performed on single-fibres using Instron® Micro Tester 5848 machine that allowed the testing of miniature specimens. Monotonic loading was applied to each single-fibre specimen until failure. Sabuncuoglu (2012), in his study related to mechanical properties of polymer fibres, reported that constant true strain rate and constant engineering strain rate for single-fibre tensile tests result in similar plots. Since, achieving constant engineering strain rate is easier as compared to constant true strain rate; therefore, the tensile tests were carried out at 0.01, 0.1 and 0.5 s⁻¹ constant engineering strain rate ($\dot{\epsilon}_{\text{eng}}$). Due to difficult control of the specimen's length, a constant engineering strain rate was achieved by modifying the velocity of the cross-head with respect to length of each fibre specimen. The relationship used for this purpose is shown in Equation 6.1.

$$\frac{v}{l_o} = \dot{\varepsilon}_{\text{eng}} = \text{const} , \quad 6.1$$

where v is the cross-head velocity and l_o is the initial length of the fibre. Several tests were performed for each strain rate to measure the variability in results. Fibres were loaded until their failure during the tests.

As mentioned earlier, three different levels of strain rates – 0.01, 0.1 and 0.5 s⁻¹ – were used in the single-fibre tensile tests. In order to assess variability of the results, minimum of ten samples were tested for each strain rate. True strains ($\varepsilon_{\text{true}}$) and true stresses (σ_{true}) were recorded during the tests, which were obtained with the following relations:

$$\varepsilon_{\text{true}} = \int_{l_o}^l \frac{dl}{l} = \ln\left(\frac{l}{l_o}\right) , \quad 6.2$$

$$\sigma_{\text{true}} = \frac{F (1 + \varepsilon_{\text{eng}})}{A_o} , \quad 6.3$$

where l is the current specimen length, F is the load, A_o is the initial area of fibre's cross-section and ε_{eng} is the engineering strain. In these calculations, it was assumed that the fibre cross-section was perfectly circular and the diameter of fibre is constant along its length. True stress and true strain were computed based on hypothesis that the deformation in fibre took place at constant volume.

6.2 Creep Tests

In this section, time-dependent properties of polypropylene fibres were determined by a series of creep tests. Continued deformation under constant load is termed as creep (Fig. 6.4) (Marc User Guide, 2011).

In creep tests, application of a constant load results in material deformation, which can be made up of an instantaneous deformation followed by a continual deformation with time (viscous effect). Eventually, it can become pure viscous flow.

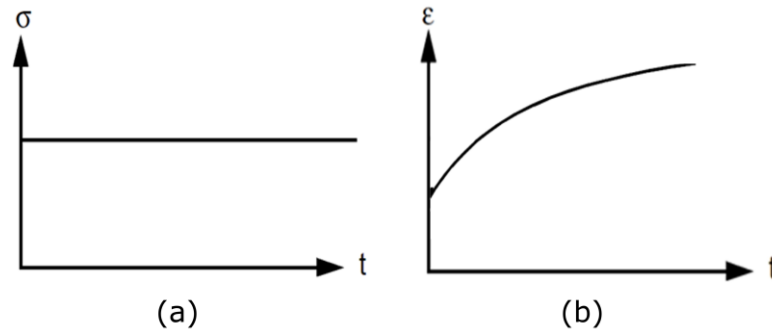


Figure 6.4. Creep behaviour showing constant stress (a): continuous deformation (b)

Creep test can be performed in two different ways: constant-stress creep and constant-strain creep. In constant-strain creep, the specimen is stretched until certain strain level is achieved. The load at this level is read and then kept constant for a specified time period. In constant-stress creep method, the material is deformed until a required stress level is achieved and then this stress is held constant. Since FE analysis software used in this study (MSC.Marc[®]) requires the creep properties as a function of stress level, constant-stress creep test method was used to obtain the viscous properties of the material.

6.2.1 Experimental Techniques

Instron[®] Micro Tester 5845, described in detail in section 6.1.1 and shown in Fig. 6.2 was used to carry out single-fibre creep tests. The method file used to control the test parameters was modified to fulfil the creep test requirements. The initial deformation rate was selected carefully as it was needed to be fast enough to reach the required stress level without any initial creep but slow enough to avoid stresses beyond the required level. Procedure of preparation and mounting of single-fibre to the machine procedure was same as that for tensile test specimens as mentioned in section 6.1.1.

6.2.2 Experimental Procedure

The method defined for the Micro Tester to carry out creep tests was prepared with stress ramping from zero to the desired level at constant engineering strain rate 1.0 s^{-1} and then held constant. In the pilot study for creep tests, it was found that the lower stress threshold at which fibre specimen started to creep was 5 MPa. Generally, creep tests are performed at stress levels below the yield point of a material and only for primary and secondary creep stages out of three stages (Fig. 6.5) are important for design and development of parts containing that material. This study is focused on deformation and damage till failure of the material, during which fibres undergo stresses much higher than their yield point before failure. Therefore, single-fibre creep tests were performed till failure of fibres at stress values much higher than their yield stress i.e. 70 MPa (will be mentioned in Section 6.4.2). After obtaining the minimum threshold of stress level for the single-fibre creep tests, six constant engineering stress levels ranging from 5 MPa to 150 MPa were achieved and then these stresses were kept constant for a certain length of time until the fibre failed. Since creep in material can cause permanent deformation leading to material damage, all three stages of creep – primary, secondary and tertiary – were investigated in this study. However, due to limitations of the test rig including its low response time, creep tests covering also a tertiary stage were performed at stresses higher than 20 MPa. At stresses below this, single-fibre creep tests were performed for max. 180000 s (50 h). As mentioned earlier, the initial deformation rate of 1.0 s^{-1} strain rate was selected so that it is fast enough to reach to the required stress without any initial creep, but slow enough to avoid stresses beyond the required level. The creep behaviour is used to assess the mechanical behaviour and performance of polypropylene fibres as a function of time. At least five samples were tested for each stress level.

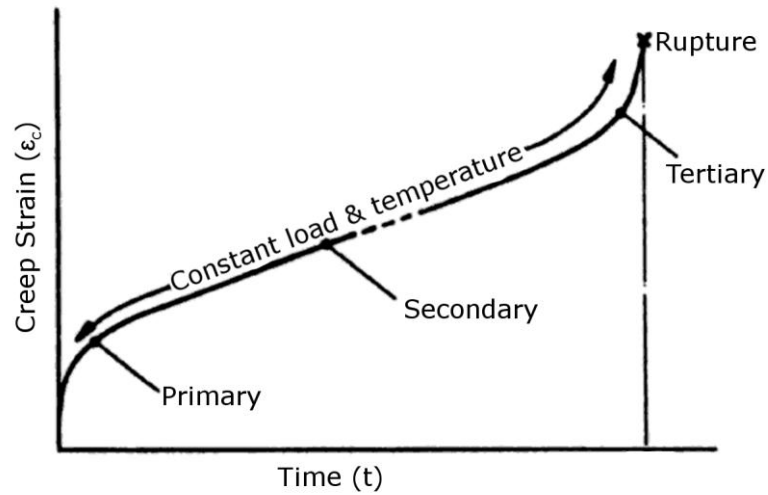


Figure 6.5. Creep strain as function of time for viscous material (Penny and Marriot, 1995)

6.3 Relaxation Tests

Stress-relaxation test is another method to obtain these viscous properties. In relaxation tests, a viscous material is subjected to sudden application of a constant deformation. This results in an instantaneous proportional load followed by a gradual reduction of the required load with time, until a limiting value of the load is attained. The decreasing of load for a constant deformation is termed relaxation (Fig. 6.6) (Marc User Guide, 2011).

Relaxation tests can be performed in two different ways: constant-stress relaxation and constant-strain relaxation. In constant-strain relaxation, load is applied until the constant strain level is reached. After that, the strain level is maintained and decrease in load with time is observed. In constant-stress relaxation, load is applied until the required constant stress level and strain is kept constant when the stress level is achieved. Constant-stress relaxation method is preferable to constant-strain relaxation as the level of initial sudden deformation is calculated regardless of the gauge length. However, it is difficult to attain a pre-determined stress level since it requires precise closed loop control. Moreover, during initial sudden deformation achieving exact required stress level is difficult. Therefore, constant-strain relaxation method is used in

this study. Typical deformation behaviour of polymers is time-dependent and should be included in numerical modelling of these materials for accurate prediction of their deformation and damage behaviour.

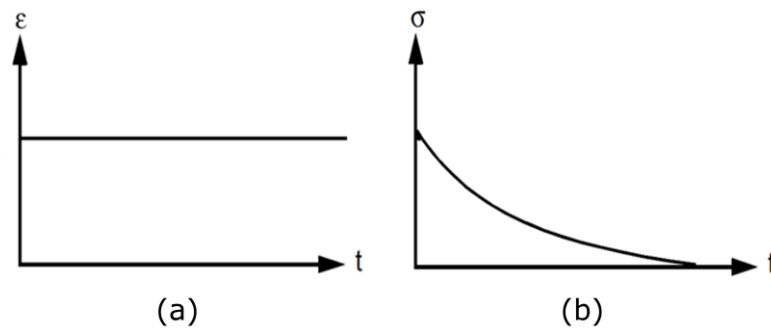


Figure 6.6. Relaxation test with constant strain (a) resulting in continuous stress attenuation (b)

6.3.1 Experimental Techniques

The sample preparation and its mounting on the test rig were the same as those for the single-fibre tensile and creep test discussed earlier in Section 6.1.1. The fibres were extracted from the free end of the fabric to obtain accurate material properties since the properties of the polymers are characterised by the temperature variation involved in manufacturing of thermally bonded nonwovens. The gauge length of the fibre specimen was not constant as it was difficult to control its length due to the issues related to its size and weakness.

6.3.2 Experimental Procedure

The relaxation tests on single-fibre were performed by modifying the method file for Instron® Micro Tester with the initial rate of fibre deformation fast enough to avoid stress attenuation in it during its extension. It was found that initial deformation rate of 1.0 s^{-1} was enough for this purpose as long as fibre length was more than 6 mm. For specimens with gauge length less than 6 mm, higher rates were used to avoid initial relaxation. The relaxation tests on single-fibre were performed at constant true strain level of 0.01, 0.1, 0.4, 0.5 and 0.8. In order to assess variability of the results, at least

ten samples were tested for each strain rate. Each test was performed for at least 18000 s (5 hours). The results obtained from relaxation tests are used to validate the mechanical properties implemented into finite element model in Chapter 7.

6.4 Results and Discussion

6.4.1 Tensile Tests

Non-linear elastic plastic behaviour with strain hardening was observed in tensile tests. The true stress-true strain curves of fibres at various strain rates show sigmoidal shape typical for polymers as shown in Fig. 6.7. These tests showed that mechanical behaviour of a fibre does scatter significantly. This phenomenon is consistent with the morphological analysis of the fabric in Section 5.2.1 exhibiting geometric variation in constituent fibres, such as, variation in diameter of various fibres and even along the length of same fibre (see Fig. 5.7). Due to significant scatter in results, average true stress-true strain curves with standard deviation at various strain rates are shown in Fig. 6.7. The median values of basic mechanical properties of the fibre are given in Table 6.1. Some of the average properties such as density and melting point were obtained from the data sheet provided by nonwoven manufacturer i.e. FiberVisions, USA.

Table 6.1. Properties of polymer material used for fibre

Young's Modulus (MPa)	Poisson's Ration	Yield Stress (MPa)
E	ν	-
350	0.42	75

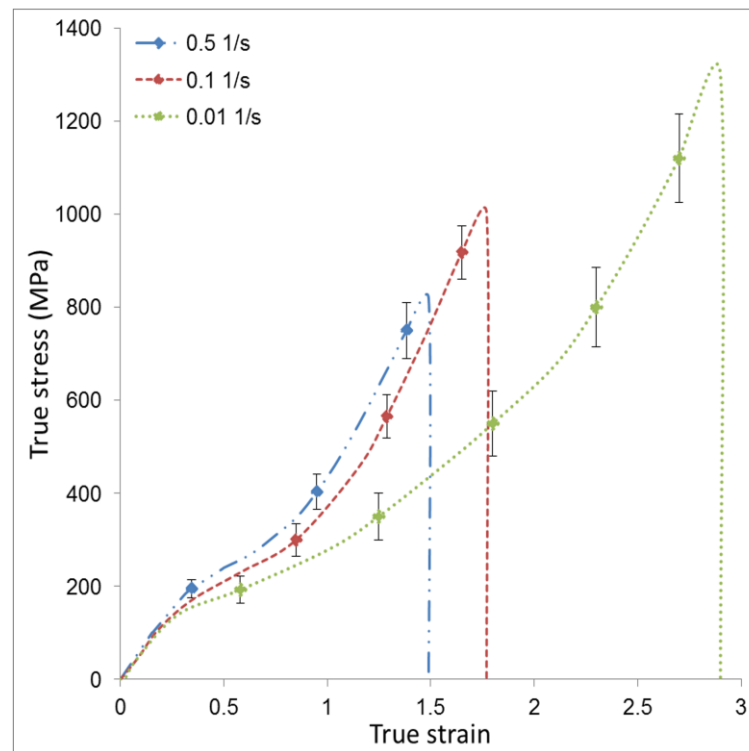


Figure 6.7. Mechanical behaviour of PP fibre at various strain rates

The difference between the curves with various strain rates in Fig. 6.7 is due to the viscous effects in the fibre material which are discussed in next section. Fibres tested at different strain rates exhibit a typical polymer behaviour characterised by a higher level of strain and nonlinearity. Moreover, the stress-strain curves indicate the hardening i.e. material's strengthening with plastic deformation occurs throughout the whole deformation range. The failure strains and corresponding stresses in fibres were changing with strain rates as shown in Fig. 6.7. At lower strain rates, fibres demonstrated larger strains and stress values than those at higher strain rates. The details of effect of strain rate on the ultimate strength and ultimate strain are discussed in Section 6.5.

6.4.2 Creep Tests

As mentioned in previous section, mechanical performance of polymer fibres is influenced by viscous effects; leading to, deformation and damage behaviour. Creep test

is a method to study the time-dependent behaviour of the material. In creep tests, the strain induced with a constant load is a function of time. As shown in Fig. 6.5, three stages can be considered in creep curve: primary creep, secondary creep and tertiary creep. During primary creep stage the creep strain rate decreases to a certain value. In secondary region it is characterized by a steady-state creep strain rate. In tertiary region, strain rate increases. At the end tertiary stage, creep rupture of the fibre occurs. Generally, tertiary creep is neglected in the analysis. Since, this study is focussed on deformation as well as on damage behaviour of nonwovens; tertiary creep is taken into account as it can lead to damage in nonwovens as mentioned in Section 6.2.

The applied stresses during tensile tests for initial few seconds are shown in Fig. 6.8 to depict the serration in applied stresses due to the displacement control feature of the machine. In order to maintain the constant desired stress level, the machine was on-off control for its cross head displacement. Because of the machine's control system, strain increased in fibres in steps. After removing initial loading strain, experimental creep strain in fibres at various levels of applied constant engineering stresses for initial few seconds are shown in Fig. 6.9a. The step-wise behaviour of the true strain curves was improved by approximating the curve with mathematical functions. The complete creep strain curves with primary, secondary and tertiary stages as a function of time at various levels of applied constant stresses are shown in Fig. 6.9b. The data was analysed after omitting the initial loading stage from the experimental results. The stepping behaviour in primary creep region was approximated by a power function:

$$FIT_n(x) = C_{1n} \ln x^{C_{2n}}, \quad 6.4$$

where n represents level of applied constant stress and C_{1n}, C_{2n} are the curve fitting coefficients which vary with stress level. The creep strain rate decreased continuously in primary region and became constant in the secondary region. The curve was approximated in secondary region according to logarithmic function:

$$FIT_n(x) = D_{1n} \ln x + D_{2n}, \quad 6.5$$

where n represents the level of constant stress applied and D_{1n}, D_{2n} are the curve fitting coefficients which vary with stress level. For approximation of tertiary region, again power function as shown in Equation 6.4 was used. The curves, obtained after fitting the power function and shifting the curves to time $t = 0$ after removing the loading stages, are shown in Fig. 6.9b.

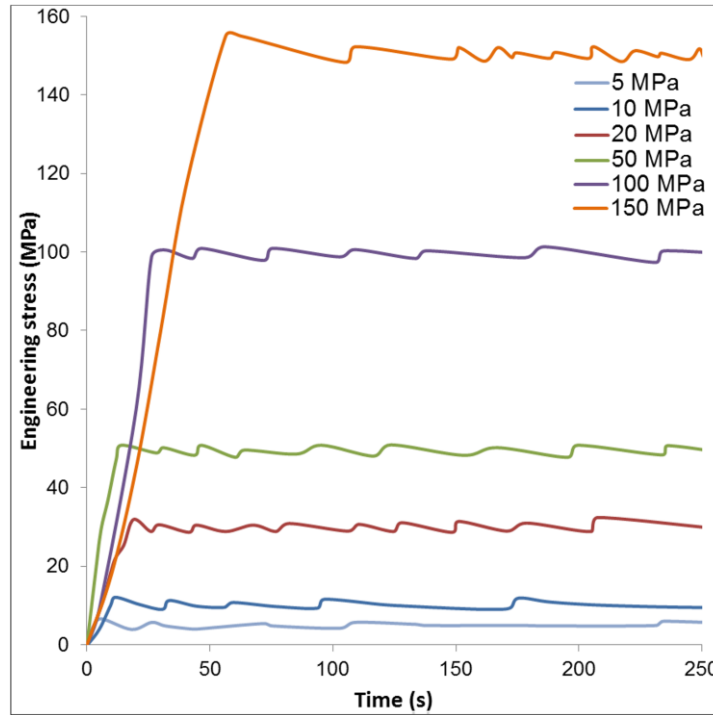
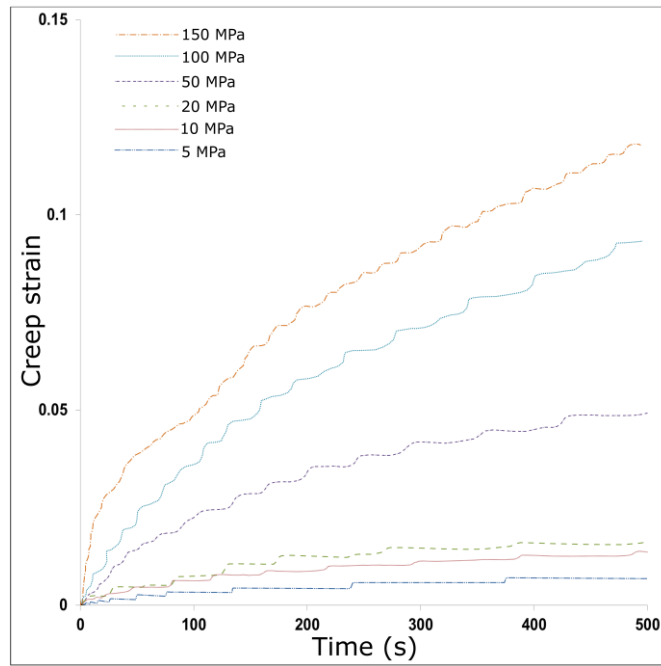


Figure 6.8. Evolution of engineering stress value in creep tests

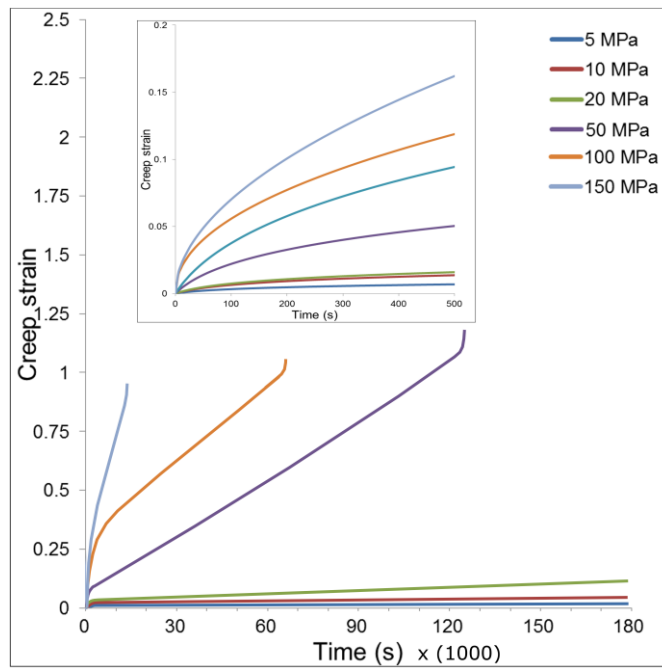
Creep strain rate required by the analysis software MSC.Marc[®] was obtained by dividing the creep strain data with the time increments.

$$\dot{\varepsilon} = \frac{d\varepsilon_{\text{creep_strain}}}{dt} \quad 6.6$$

As the creep properties of the material were obtained until its failure, these can be used to simulate the creep based damage behaviour in nonwovens.



(a)



(b)

Figure 6.9. (a) Experimental creep strain (b) Creep strain after curve fitting of creep strain as a function of time

6.4.3 Relaxation Tests

The stress relaxation curves obtained from single-fibre relaxation tests at various strain levels are plotted in Fig. 6.10 showing stress attenuation in fibres with time. According to Fig. 6.10, initial stress decay behaviour of PP fibres changed with the level of strain applied. The stress value for a non-viscous material remains the same at any level of stress regardless of the time as shown by a straight plotted line in Fig. 6.10.

Deviation of single-fibre relaxation test curves from the non-viscous value indicates that material's deformation and damage behaviour is time dependent. The stress decay rate is very high at the beginning of the relaxation test and approximately 2/3 of the stress is attenuated in the period of 200 s. This is shown in inset of Fig. 6.10. Thus, time is a vital parameter for determining the mechanical behaviour of polymer fibres. The relaxation test results were used to assess the efficiency of the developed computational model of nonwovens.

In nutshell, the complex mechanical behaviour of polypropylene fibre used for manufacturing of nonwovens can be described as nonlinear viscoelastic-plastic. Fibre deformation is mainly governed by the plastic stage as yield strain is very small in fibre. A great complexity in fibre behaviour is a significant scatter in results which is due to the manufacturing imperfections as explained in Section 5.2.1 (see Fig. 5.7).

As mentioned in Section 5.2.4, fibres always fail near the bond point periphery region in thermally bonded nonwovens; therefore, it is necessary to study this region into single-fibre experiments for better understanding of damage evolution and development of failure criteria in this kind of fabric. The consideration of this region in the development of failure criteria for individual fibre within the fabric is a challenging task which is implemented by a novel experimental technique explained in subsequent section.

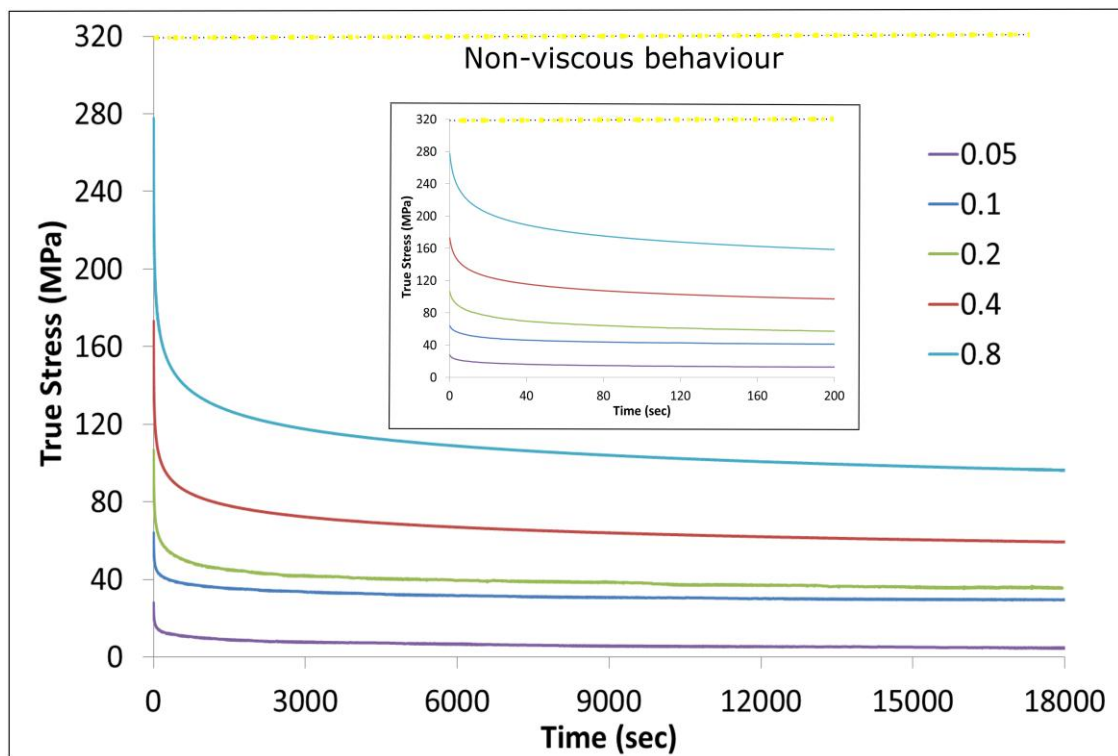


Figure 6.10. Relaxation behaviour of PP fibre for various strain rates

6.5 Development of Failure Criteria

As mentioned in Section 2.3.2, during thermal bonding fibrous web is passed through two hot calendar rolls under pressure; surface design of which can be smooth or have an embossed pattern. On embossed calendar rolls, bonding mainly occurs at raised areas resulting in bonded spots called “bond points”. As higher temperature is involved in thermal bonding, fibre properties are characterized by the temperature level (and variation) during this manufacturing stage. Therefore, a pragmatic approach is to use the individual fibres extracted from the fabric to obtain the material properties and development of failure criteria rather than unprocessed fibres. Elastic-plastic and viscous properties of fibres were obtained for processed fibres as mentioned in Section 6.4. Now, single-fibre failure criteria will be assessed by using processed fibres in this section.

As mentioned in Section 5.2.4, fibres always fail near the bond point periphery region in thermally bonded nonwovens; therefore, it is necessary to study this region

into single-fibre experiments for better understanding of damage initiation and propagation and development of failure criteria in this kind of fabric. The consideration of this region in the development of failure criteria for individual fibre within the fabric is a challenging task which is implemented by a novel experimental technique explained in subsequent section.

6.5.1 Experimental Technique

During loading of nonwovens, each fibre in the fabric takes load individually and ultimate failure in fabric occur following the progressive failure of fibres. Therefore, it is essential to develop failure criteria based on single-fibre failure characteristics within the fabric. In order to develop damage criteria based on fibre failure within thermally bonded fabric, single-fibre samples were extracted from the nonwoven fabric, thermally bonded at optimal manufacturing parameters, in a way that each fibre was attached to individual bond points at its both ends (Fig. 6.11a). Tensile tests on single fibres having single bond point at each end would provide insight of fibre deformation and damage within thermally bonded fabric and development of failure criteria. In order to prevent slippage, dislocation and damage of the single-fibre specimen during the test, sticky paper strips were attached to the bond points at the edges of the fibre in a way that only the mechanical properties of the fibre were obtained without amalgamating it with those of bonds. The schematic configuration of the specimens is shown in Fig. 6.11b. These specimens were mounted on Instron® Micro Tester 5848 (Fig.6.12) using the same load cell and grips as mentioned in Section 6.1.1. Moreover, a high-speed camera (Photron Fastcam SA3®) with advanced macro capabilities was used to make sure that fibre was not stretched during preparation and mounting of specimens. The complete arrangement of setup with the fibre mounted on tensile test rig is shown in Fig. 6.12. Tensile tests were performed by stretching the fibre samples with constant engineering strain rates corresponds to 0.01, 0.1, 0.5 s⁻¹, achieved by using the Eq. 6.1. All these tests with the same experimental parameters were also performed on unprocessed polypropylene fibres to quantify the effects of bonding on breaking strength of fibres. The tensile tests at each strain rate for processed and unprocessed fibres were repeated for at least ten times to assess the variability in results. The fibres were stretched until their failure to obtain the parameters such

as elongation at failure and ultimate tensile strength necessary for the development of failure criteria.

6.5.2 Experimental Results

The true stress-true strain curves of fibres extracted from the fabric having bond points at both ends presented sigmoidal shape (Fig. 6.14) similar to the curves obtained for fibres extracted from the fabric without bond points (Fig. 6.7). However, the damage parameters which are tensile strength σ_f and failure strain ε_f for processed fibres were much less than those of unprocessed fibres. Another interesting observation was that the critical stresses and corresponding strains obtained for unprocessed fibres were similar to those obtained for fibres extracted from nonwovens without having bonds at their edges. This finding demonstrated the importance of bond point periphery region for the development of fibre failure criteria. The experiments did not provide a certain value of failure strength and failure strain; rather there was a significant scatter in results at all strain rates as shown in Fig. 6.13, the average values with standard deviation of the failure stress σ_f and failure strain ε_f are presented in Table 6.2.

Table 6.2. Mean values with standard deviation of failure stress and strain of unprocessed and processed fibres at various strain rates

	Strain rate (s ⁻¹)	Failure stress (MPa)	Strain at failure stress
Processed fibre	0.01	481 ± 48	1.29 ± 0.67
Unprocessed fibre		1299 ± 95	2.93 ± 0.78
Processed fibre	0.1	315 ± 28	1.05 ± 0.11
Unprocessed fibre		998 ± 57	1.77 ± 0.09
Processed fibre	0.5	241 ± 53	0.79 ± 0.1
Unprocessed fibre		818 ± 60	1.49 ± 0.14

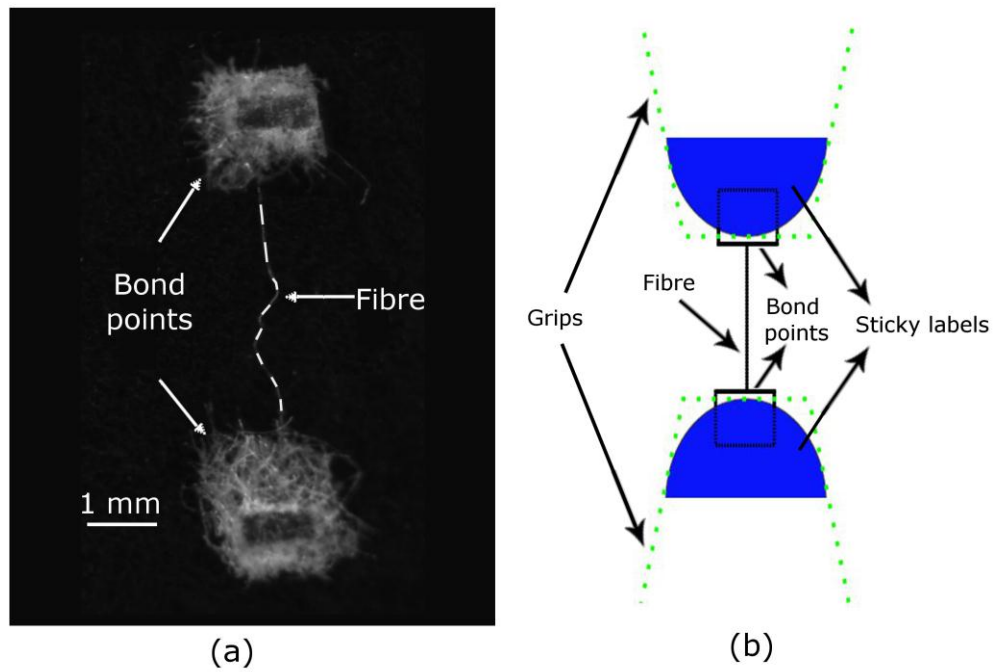


Figure 6.11. (a) Single fibre attached to bond points at each end (dashed line is used to enhance contrast of image); (b) schematics of final specimen and its fixture

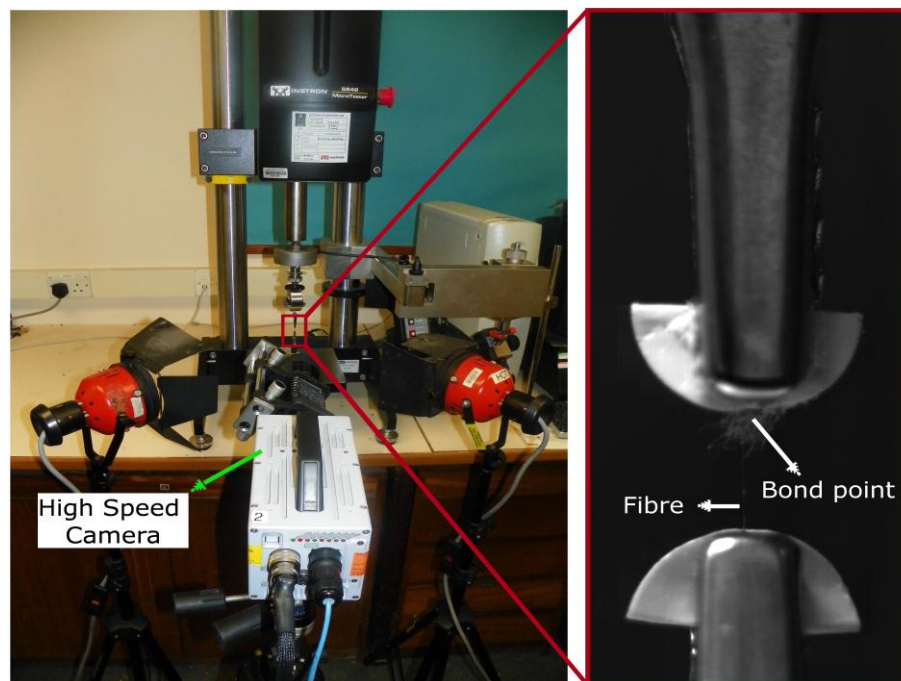
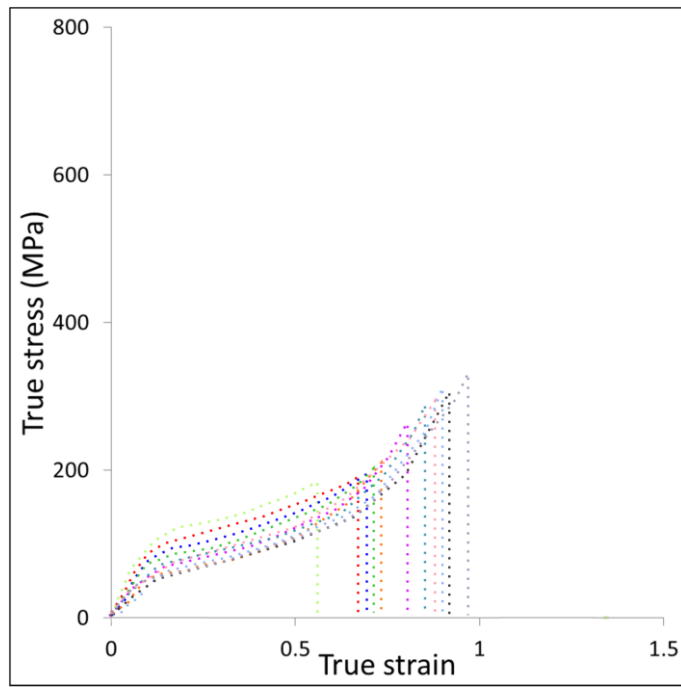
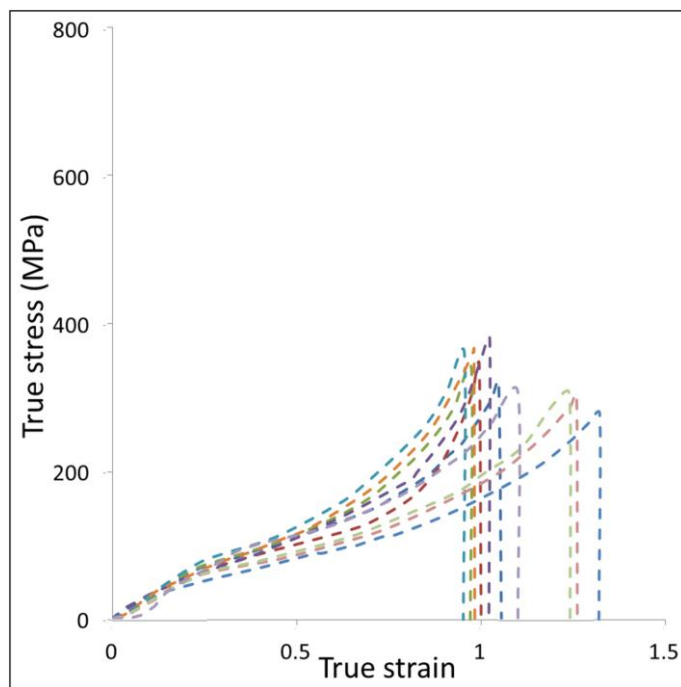


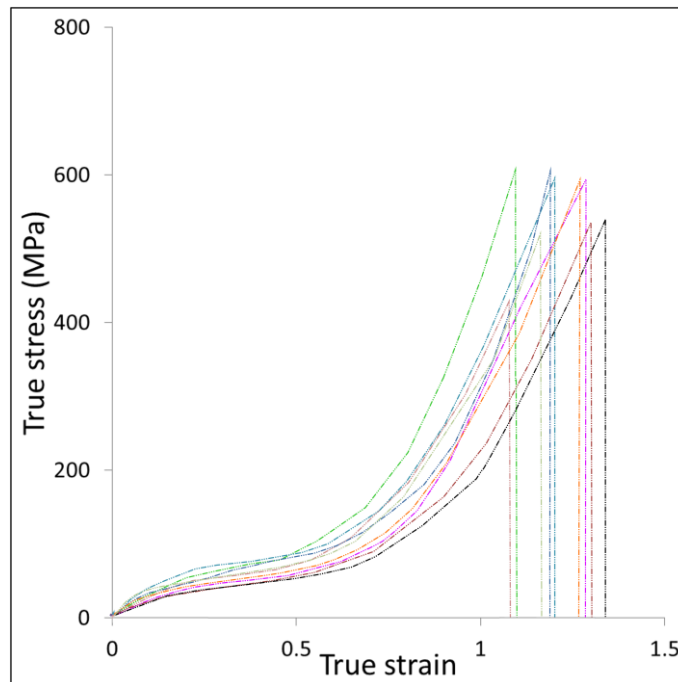
Figure 6.12. Setup of single-fibre experiment (Instron Micro Tester 5848 and Photron Fastcam SA3)



(a)



(b)



(c)

Figure 6.13. Scatter in experimental results of processed PP fibres at strain rate: 0.5 (a); 0.1 (b); 0.01 (c)

Decrease in tensile strength and strain to failure of fibres with bond points at their edges as compared to ones without bond points was due to high temperature and pressure involve in bonding process which changes molecular orientation of fibres at the bond periphery and thus failure parameters (Dharmadhikary *et. al.*, 1999; Kim *et. al.*, 2001a; Kim *et. al.*, 2001b; Wang and Michielsen, 2002; Michielsen and Wang, 2002). Hence, it is not possible to use the material properties of fibres without considering loss in tensile strength in terms of stress or strain for damage analysis of the fabric. The results obtained from these tests are used as fibre failure criteria based on ultimate tensile strength and strain to simulate the damage initiation and propagation behaviour of thermally bonded nonwovens. Since fibres in nonwoven participate in load bearing once they are aligned along the loading direction and fail one by one on reaching their critical stress or strain threshold. Therefore, the results obtained from tensile tests on processed single-fibres in terms of failure-stress and failure-strain of fibres within thermally bonded nonwovens can be used directly as criteria for fibre failure in FE model.

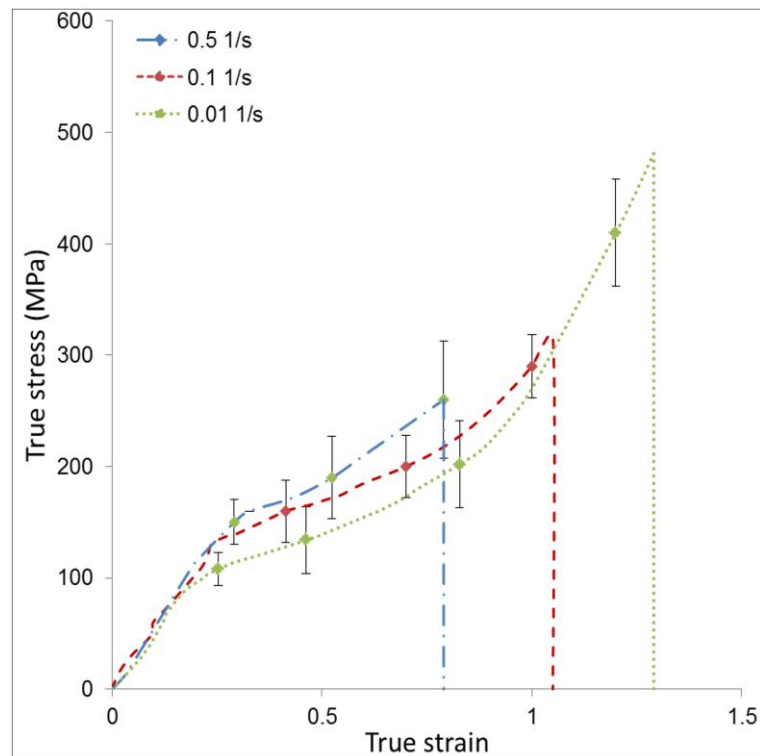


Figure 6.14. Mechanical behaviour of PP fibre with bond points at edges at various strain rates

6.6 Conclusions

The elastic-plastic and viscous properties of constituent fibres in thermally bonded nonwovens are determined in this chapter. Moreover, a practical way of determining the failure parameters, in terms of ultimate tensile stress and strain, for single-fibre within thermally bonded nonwoven is presented in this chapter.

Tensile tests on fibre exhibited variation in stress-strain behaviour with strain rate due to viscous properties. The viscous properties of fibre material were determined with single-fibre creep and stress relaxation tests. Material properties of the constituent fibres are characterised by the manufacturing parameters. Tensile tests on single-fibre extracted from the nonwoven having bond points at their edges were also performed to quantify the loss in strength of individual fibre due to bonding. Experimental mechanical characterization of single fibre, extracted from nonwoven with a bond point

attached at its each end, revealed less ultimate tensile stress and corresponding strain at failure as compared to that of unprocessed or even the processed fibres without having bond point at edges. In the next chapter, elastic-plastic properties of constituent fibre obtained from tensile test and viscous properties obtained from creep and relaxation tests will be used as material properties required for the numerical model. Besides, the critical value of stress and strain obtained with tensile tests on fibres with bond points at their edges will be used as fibre failure criterion for the model in order to predict the deformation and damage behaviour of nonwovens. The experiments performed in this chapter not only developed the understanding of single-fibre behaviour but exhibited the effect of hot calendaring on fibres' properties, quantitatively.

CHAPTER 7

FINITE ELEMENT MODELLING OF THERMALLY BONDED NONWOVENS

Experimental characterisation of a nonwoven material is not always viable and sometimes sufficient for a comprehensive understanding of complex phenomena involved in its deformation and damage as mentioned earlier. The challenges involved in experimentation may be linked to the lack of specialised experimental facilities or significant efforts required for tests, especially for nonwovens, in which mechanical properties are defined by their microstructure and constituent fibre's properties. Numerical simulations are the best alternative for predicting the behaviour of this type of materials.

As mentioned in Section 4.5, various numerical models can be found in literature with different benefits for analysis of various fabric's characteristics. They usually present only a partial solution for prediction of mechanical behaviour and mechanisms

involved in deformation and failure of nonwovens. To the author's knowledge, none of the models can predict deformation and damage of the fabric until its failure in terms of progressive failure of fibres while incorporating explicitly a realistic material's microstructure by introducing fibres into the model together with the properties of constituent fibres. Therefore, generating a numerical model that incorporates realistic randomness of microstructure and constituent fibres' properties including their failure parameters will be a novel contribution to knowledge useful for academic and industrial researchers dealing with design and development of nonwoven materials.

7.1 Modelling Objectives

Nonwoven materials exhibit complex deformation and damage behaviours including anisotropy and visco-elastoplastic properties that have a significant scatter. As mentioned in Chapters 5 and 6, anisotropy of, and scatter in, mechanical behaviour of the fabric arise from preferential orientation of fibres along MD and multiple types of the constituent fibres with different mechanical properties. Besides, application areas and technologies for manufacturing of nonwovens including those for materials of constituent fibres are increasing continuously. With the advancement of new technologies and complexity in the mechanical behaviour of nonwovens, there is a need for a fabric model that can predict their response while not only taking all the main mechanisms involved in fabric's deformation and damage behaviours into account but can easily adopting new features such as properties of constituent fibre, size and shape of bond points. Thus, the numerical model for the fabric should meet the following requirements:

- 1) It should be capable to simulate accurately the initiation of deformation and damage initiation of the fabric as well as its evolution. Moreover, it should also capture all the main mechanisms involved in deformation and damage behaviours of the fabric such as reorientation of fibres along the loading direction and progressive failure of fibres reaching their stress or strain threshold

2) It should be suitable for a use as design tool to minimise the trial-and-error stage of product design and development. In other words, it should be able to predict the response of the fabric depending upon randomness in material properties of constituent fibres and geometric properties of the network structure such as orientation distribution of fibres, dimensions and pattern of bond points

3) It should be able to predict stress distributions in all the components of fabric's structure so that the point of damage initiation could be predicted in nonwovens. Besides, stress determination in each component of the fabric would help to simulate damage evolution in the fabric as progressive failure of fibres including changes in network's topology based on damage localization.

4) It should be focussed on the practical use. Many of the models proposed in literature, although predict the deformation behaviour of certain type of nonwoven effectively, are not of practical use as they cannot be easily reformulated to incorporate the variation in geometric properties of network's structure.

With such requirements, the most suitable approach to model the nonwovens is finite element analysis based on introduction of fibres directly into the model according to their orientation distribution within the real fabric. The finite-element technique offers an opportunity to develop a numerical model based on the mechanical behaviour of constituent fibres and microstructure of the network, which could predict the deformation and damage behaviour in nonwovens at meso or macro level with ease of implementation of various loading conditions. In addition to this, if fibres are introduced directly into the model, it can predict the stresses in each component of nonwoven structure and can help to analyse localization of damage in it.

7.2 Model Development

The experimental data on nonwoven microstructure, complex nonlinear anisotropic behaviour and material properties of the constituent fibres presented in previous chapters is used to develop the FE model in this chapter. The experimental data

presented in Chapter 5 suggested that randomness in microstructure with preferential orientation distribution of fibres along MD played an important role in the deformation and damage behaviours of the fabric. Therefore, development of the FE model was started with the network-generation process, which is given in the following section.

7.2.1 Generation of Fabric Network

As mentioned in Chapter 5, in thermally bonded nonwovens, a fabric's structure is composed of continuous and discontinuous regions. These continuous regions called *bond points* are connected in a certain pattern by a network of random fibres forming a discontinuous region having voids and gaps in it. This randomness as well as voids and gaps in the microstructure of nonwovens necessitates development of the model incorporating a realistic orientation distribution of fibres within the fabric. In this study, fibres were introduced directly according to their orientation distribution within the fabric to incorporate the realistic microstructural randomness of nonwovens. However, it was challenging to model the exact number of fibres equal to that in the sample of real fabric with dimensions equal to those of the FE model and to make sure that fibres were properly connected between the bond points. These issues were resolved with the help of a subroutine, written in Patran Command Language (PCL), employing a parametric modelling technique. Finite-element software can read this subroutine and generate the fabric's network according to the given input. This reduces significantly the effort for reformulating the model to incorporate the actual orientation distribution of fibres. Parametric modelling was performed with finite element software MSC.Patran, and PCL is its own script language. The technique was adopted from (Sabuncuoglu, 2012).

A 20g/m² thermally bonded polypropylene nonwoven, shown in Fig. 5.6, was used as model system. For the development of network structure, bond points were created first according to the required pattern and size. Then fibres were introduced between the bond points according to their orientation distribution in real fabric in such a way that they were properly attached with bond points to avoid any convergence problem at later stages of analysis. The steps involved in generation of fabric's network

to ensure that the number of fibres introduced in the model be similar to the input and each fibre be properly attached to the bond point are given in Appendix B.

7.2.2 Geometric Properties

Realistic simulations of complex deformation and damage behaviours of the nonwoven fabric requires proper implementation of the element type to introduce mechanical characteristics of fibres and bond points. Bond points were modelled with the shell elements (element type 139 in MSC.Marc) sketched in Fig. 7.1a. This is a four-node, thin-shell element with global displacements and rotations as degrees of freedoms; bilinear interpolation is used for the displacements and rotations. This element thanks to its simple formulation is computationally less expensive than other higher-order shell elements which make it very attractive for nonlinear analysis. All the constitutive relations including viscoelastic-plastic one can be used with this element. Because of these attributes, element 139 seems perfect for representation of bond points. This element is used here as thin plate structures to represent bond points. It is defined geometrically by the (x, y) coordinates of its four corner nodes. Due to bilinear interpolation, the surface forms a hyperbolic paraboloid, which is allowed to degenerate to plate. The stress output is given in the local orthogonal surface directions V_1 and V_2 as shown in Fig. 7.1a. Since the shell element is used here as a flat plate structure, the direction of stress vectors at the Gauss points are identical to those at the centroid. The four nodal displacement variables are as follows:

u, v - displacement components along x and y axis, respectively, defined in global Cartesian coordinate system

ϕ_x, ϕ_y - components of rotation about global x and y axes, respectively.

The thickness of bond points obtained from X-ray micro CT images of the fabric (Fig. 5.10) was assigned to these elements in simulations.

Fibres were modelled with truss elements (element type 9 in MSC.Marc) sketched in Fig. 7.1b. The element is used for large-strain, large-displacement analysis. Here, it

has two coordinates and a degree of freedom i.e. displacement. All constitutive relations including viscoelastic-plastic properties can be used for this element. Besides, these elements approximate properly real-life fibres with only axial stiffness. These capabilities make element 9 appropriate for fibre representation. In this study, each truss element represents a single fibre (model coefficient $k = 1$ was used) and the number of truss elements introduced into the model was exactly equal to the number of fibres in the sample of the fabric with dimensions equal to those of the FE model. Thus, the cross-sectional area of a single fibre was assigned to each truss element. However, if the efficiency of the computational system is low and a higher value of the model coefficient k is used, the geometric properties related to fibre should be updated respectively. For example, if $k = 4$, the diameter of the truss element should be two times the diameter of a single fibre.

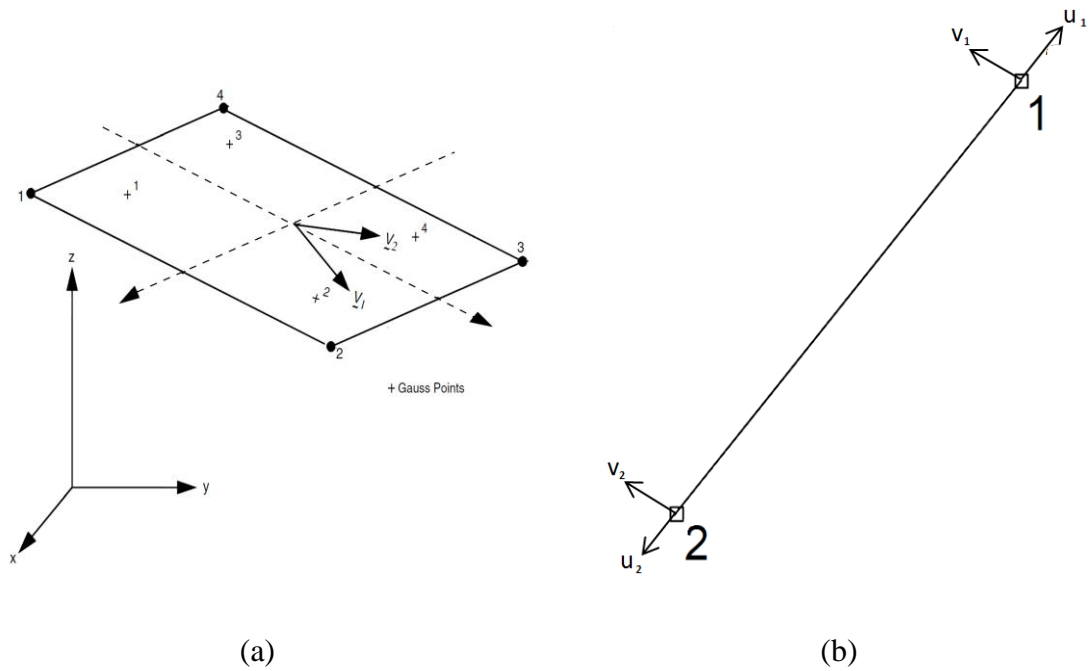


Figure 7.1. Form of elements used in FE modelling of nonwovens for bond points (shell element 139) (a) and fibres (two-node truss element 9) (b)

7.2.3 Boundary conditions

Boundary conditions in FE analysis have direct links between the simulation and the respective real-life problem as they represent the loads and constraints of the real-life case. Various types of boundary conditions were applied to the fabric in this study to simulate the mechanical behaviour of nonwovens under real-life conditions such as rate-controlled and fixed-displacements. Boundary conditions are mentioned below for each simulation for better understanding and comparison with the real-life fabric's behaviour.

7.2.4 Material Properties

For completion of the FE model, proper implementation of material properties for all the elements is required. These material properties were obtained from single-fibre experiments described in Chapter 6. Elastic-plastic properties such as the flow curve, Young's modulus obtained with single-fibre tensile tests (given in Section 6.4.1) were implemented into the models. Since FE software used in this study requires viscous properties of the material in the form of creep strain rate as a function of time, the viscous properties of the material obtained with the single-fibre creep tests (Section 6.4.2) rather than single-fibre relaxation tests were implemented into the models. Since there is a significant scatter in single-fibre material properties (Chapter 6), a case study at meso-level was performed (see Section 7.3) to establish the importance of scatter in material properties from the computational point of view. In order to simulate the deformation and damage behaviours of nonwovens, the fibre-failure criterion was also implemented into the model, which is discussed in the next section.

7.2.5 Fibre-Failure Criterion

As mentioned in Section 5.2.4, under stretching of the nonwoven its fibres started to re-orient along the loading direction, increasing their participation in a load-bearing process. The fibres failed when the applied stresses or strains reached their strength threshold causing damage initiation in nonwovens. Further failure of other fibres resulted in damage propagation followed by ultimate failure of the fabric. Since fibres were randomly oriented within the fabric and had different levels of stress and strain

threshold, they failed progressively resulting in a gradual growth of damage in nonwovens (see Figs. 5.11 and 5.14). The mechanisms involved in damage initiation and growth as well as the changes in network's topology due to fibres' failure can be explicitly accounted for in the discontinuous model like the one developed in this study.

Following the experimental observations, numerical simulations of the onset and propagation of damage as a result of progressive failure of fibres can be taken into account using critical stress-or strain-based failure criteria. The elementary formulations of these criteria are as follows:

Critical stress failure criterion:

$$\text{If } \left(\frac{\sigma_1}{X_t, X_c} \right), \left(\frac{\sigma_2}{Y_t, Y_c} \right), \left(\frac{\sigma_3}{Z_t, Z_c} \right), \left(\frac{\sigma_{12}}{S_{12}} \right), \left(\frac{\sigma_{23}}{S_{23}} \right), \left(\frac{\sigma_{31}}{S_{31}} \right) = 1, d_\sigma = 1. \quad (7.1)$$

Critical strain failure criterion:

$$\text{If } \left(\frac{\varepsilon_1}{e_{xt}, -e_{xc}} \right), \left(\frac{\varepsilon_2}{e_{yt}, -e_{yc}} \right), \left(\frac{\varepsilon_3}{e_{zt}, -e_{zc}} \right), \left(\frac{\gamma_{12}}{g_{12}} \right), \left(\frac{\gamma_{23}}{g_{23}} \right), \left(\frac{\gamma_{31}}{g_{31}} \right) = 1, d_\varepsilon = 1. \quad (7.2)$$

Here $\sigma_1, \sigma_2, \sigma_3, \sigma_{21}, \sigma_{23}, \sigma_{31}$ and $\varepsilon_1, \varepsilon_2, \varepsilon_3, \gamma_{21}, \gamma_{23}, \gamma_{31}$ are components of the stress and strain tensors at any integration point of an element, respectively; $X_t, Y_t, Z_t, X_c, Y_c, Z_c$ and S_{12}, S_{23}, S_{31} represent maximum allowable longitudinal tensile stresses, maximum allowable compressive stresses and maximum allowable shear stresses in 3 directions and 3 planes, respectively; $e_{xt}, e_{yt}, e_{zt}, -e_{xc}, -e_{yc}, -e_{zc}$ and g_{12}, g_{23}, g_{31} are maximum allowable longitudinal tensile strains, maximum allowable compressive strains and maximum allowable shear strains in 3 directions and 3 planes, respectively. d_σ and d_ε are the damage variables associated with either of the failure modes of an element depending upon the stresses and strains applied, respectively, e.g. the failure mode under tension, compression or shear stress or strain. Since it was

observed that fibres re-orient themselves in the loading direction during the tensile test of nonwovens and take only axial tensile strain and stress (Section 5.2.4); therefore, Eqs. 7.1 and 7.2 can be modified as:

$$\text{If } \left(\frac{\sigma_1}{X_t} \right), \left(\frac{\sigma_2}{Y_t} \right), \left(\frac{\sigma_3}{Z_t} \right) = 1, d_\sigma = 1, \quad (7.3)$$

$$\text{If } \left(\frac{\varepsilon_1}{e_{xt}} \right), \left(\frac{\varepsilon_2}{e_{yt}} \right), \left(\frac{\varepsilon_3}{e_{zt}} \right) = 1, d_\varepsilon = 1. \quad (7.4)$$

Here, damage variables are associated with only tensile stress or strain failure modes represented by d_σ and d_ε , respectively. Since the fibres were represented by two-dimensional truss elements in this study, which can take only uniaxial load along the direction of loading, Eqs. 7.3 and 7.4 are modified as:

$$\text{If } \left(\frac{\sigma_1}{Y_t} \right) = 1, d_\sigma = 1, \quad (7.5)$$

$$\text{If } \left(\frac{\varepsilon_1}{e_{yt}} \right) = 1, d_\varepsilon = 1. \quad (7.6)$$

As was observed in tensile tests on the fabric at various strain rates, some of the fibres sustained their participation in load bearing even at strain levels larger than the critical strain values for single fibres at corresponding strain rates (Fig. 7.14a). Following this experimental observations, it was decided to use only the maximum tensile stress for the single-fibre failure in the developed FE model. Besides, in FE simulations, an element-deletion approach was used to remove the elements from the model based on the value of damage variables as calculated with Eq. 7.5. An element (fibre in this study) was assumed to fail and removed from the model when the damage

condition (i.e. $d_\sigma = 1$) was satisfied at its integration location to avoid the convergence problem. Thus, the damage parameter was calculated for all the fibres and the elements with $d_\sigma = 1$ were removed from the model and they did not offer any resistance to subsequent deformation.

7.3 Meso-Scale Model

At the initial stages of analysis, a meso-scale model consisting of two adjacent bond points along MD was developed using the subroutine. In order to assess the effect of implementation of material's microstructure into the model, two arrangements of fibres – parallel and with random orientation – were modelled between two adjacent bond points as shown in Fig. 7.2.

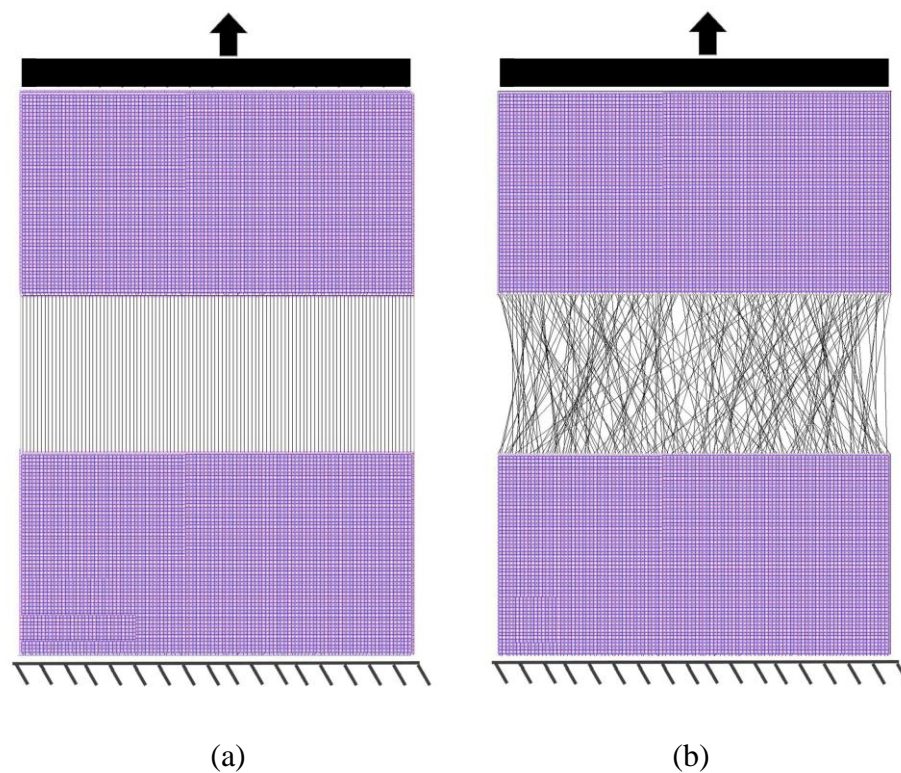


Figure 7.2. Finite-element models: (a) with parallel fibres; (b) with randomly oriented fibres between two neighbouring bond points

The randomness of fibres' orientation was implemented in the model in terms of the orientation distribution function (ODF), which was obtained in Chapter 5. Since a bond point in the real fabric was not only attached to its adjacent bond points in machine direction but rather to multiple bond points at an angle to machine direction (see Fig. 5.6), therefore, only a part of the ODF obtained from the experiments was implemented into the finite-element model. This portion of experimental ODF was dependent on the distance between two bond points as a fibre can achieve maximum angular deviation from the line connecting centres of them when it connects the corner node of one bond point and the corner node of the opposite edge of another bond point as shown in Fig. 7.3. The portion of the ODF which was implemented into the model is shown Fig. 7.4.

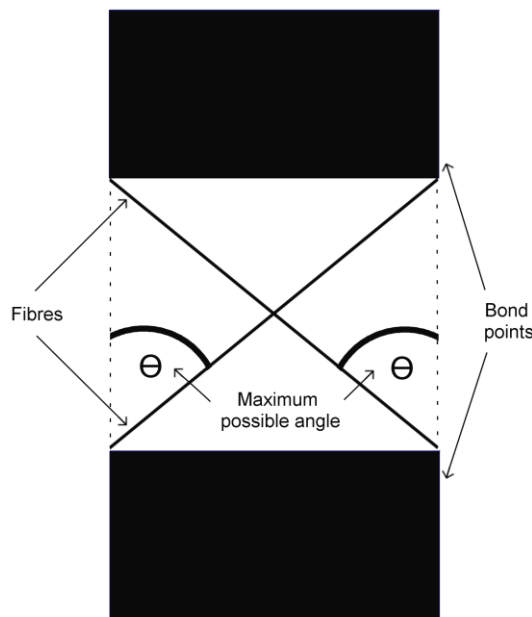


Figure 7.3. Maximum orientation of fibres in relation to distance between bond points

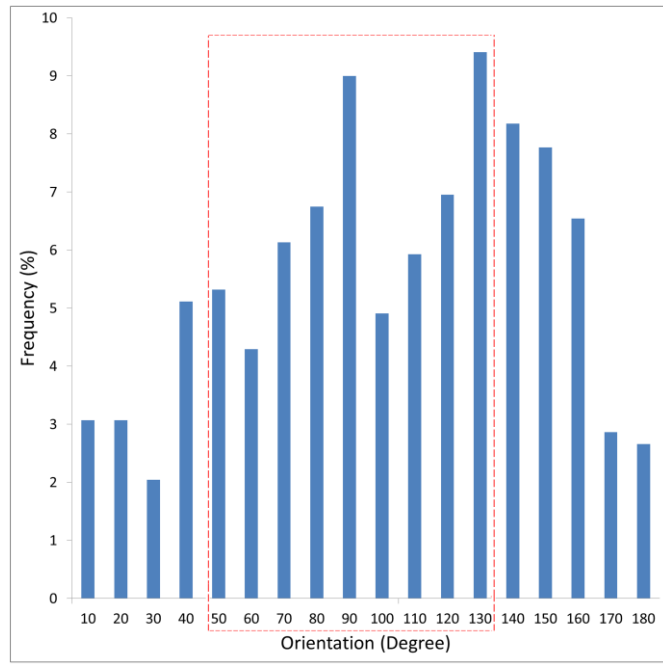


Figure 7.4. Part of ODF implemented for fibres in model in Fig. 7.2b

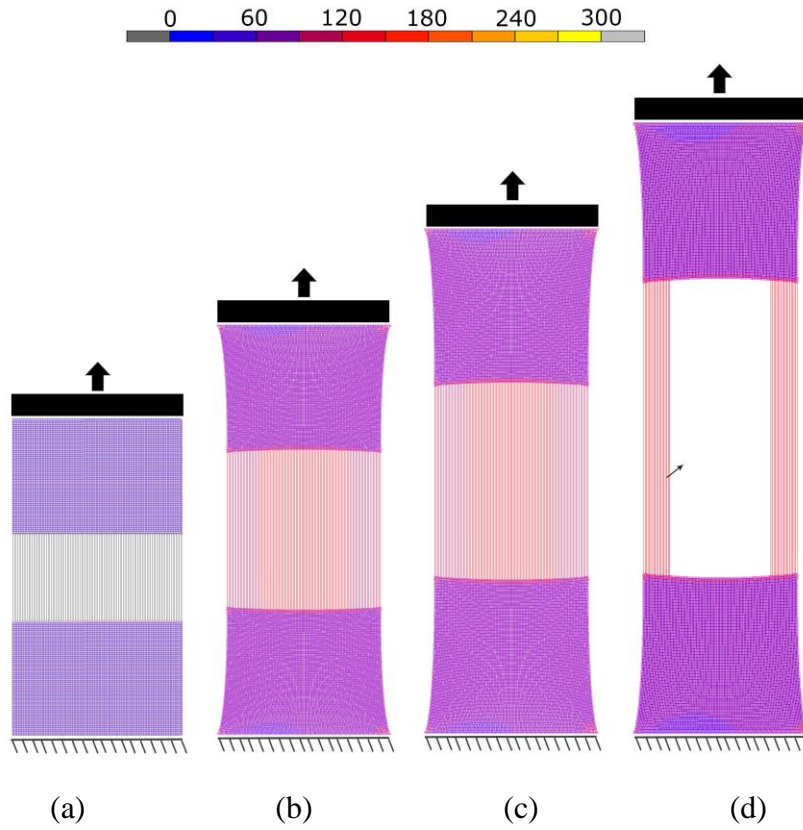


Figure 7.5. FE results of model with parallel fibres showing development of fracture zone and equivalent von Mises stresses (in MPa) in thermally bonded nonwovens at various levels of global strain: (a) 0 %; (b) 25 %; (c) 50 %; (d) 75 % (Arrow indicates a fracture zone)

The model consisting of parallel fibres between the bond points was not only lacking in representing the randomness in microstructure similar to that of the actual material but also failed to account for reorientation of fibres during initial stages of deformation, which is the key feature of deformation and fracture of nonwoven fabrics. Moreover, this model was incapable to represent the gradual increase in failure of fibres with fabric extension observed during the experiments as almost all the fibres failed nearly simultaneously at 75% fabric extension. Due to the edge effects involved, a few fibres left at that level of fabric extension (Fig. 7.5d) failed with further fabric extension. The visualization of fibre failure along with von Mises stresses in the parallel-fibres model at different levels of strain is given in Fig. 7.5. In contrast, the model consisting of randomly oriented fibres between the bond points represented the randomness in microstructure similar to that of the studied material as well as the deformation and damage behaviour observed in the tensile tests. At the initial stages of stretching, randomly oriented fibres (shown in Fig. 7.6a) were extensively reoriented to become aligned along the loading direction (see Fig. 7.6b). In this way, they started participating more in load bearing and underwent elastic-plastic deformation due to the material properties assigned.

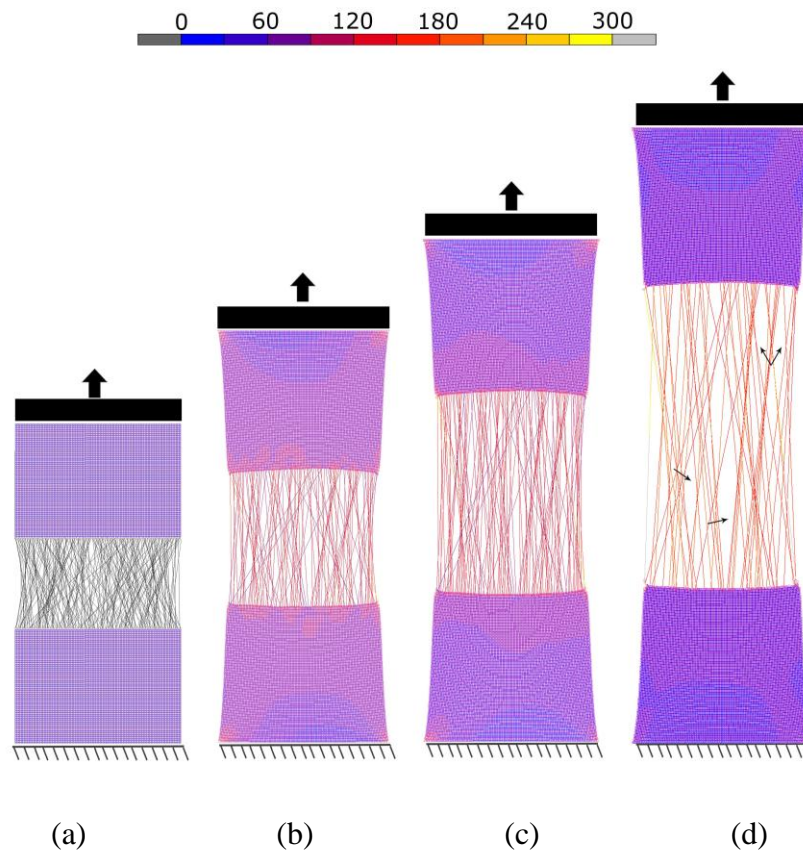


Figure 7.6. FE results of model with randomly oriented fibres showing development of fracture zones and equivalent von Mises stresses (in MPa) in thermally bonded nonwovens at various levels of global strain: (a) 0 %; (b) 25 %; (c) 50 %; (d) 75 % (Arrows indicate local fracture zones)

With continuing extension of the fabric, strains and corresponding stresses increased in fibres. The fibres with the applied stresses reaching their threshold failed triggering damage in the nonwoven. These failed fibres caused the development of local fracture zones made up by the remaining fibres aligned along the loading direction as shown in Fig. 7.6d. The complete failure of fabric did not follow immediately after the onset of macroscopic damage but occurred as a process of progressive failure of fibres. This sequence of damage was similar to the one observed during fabric's tensile deformation and failure experiments (Section 5.2.4). As mentioned earlier, the failed fibres were removed in simulations to avoid convergence problems.

The damage evolution in nonwovens can be characterised by a ratio N_f/N , where N_f is the accumulated number of fibres failed at any particular level of fabric extension and N is the total number of fibres. This damage parameter N_f/N as a function of fabric extension for both models — with parallel and random fibres— is given in Fig. 7.7. This shows that in the parallel-fibres model, ultimate failure of fabric occurred immediately at 75% extension, whereas damage grew comparatively slow with the fabric extension after the failure of the first fibres in the random-fibres model. This progressive damage caused by continuous failure of fibres in the model with randomly oriented fibres is the key feature of deformation and failure of nonwoven fabrics, which was not reflected by parallel fibres model. Hence, this study also shows the importance of introducing randomness into numerical models for nonwovens.

These simulations were carried out assuming that all the fibres had the same material properties. As there is a significant scatter in material properties obtained from the single-fibre experiments (see Chapter 6), another series of simulations including randomness of fibre material properties was also implemented with the developed FE model. The model with randomly oriented fibres was used for this purpose as it was closer to realistic microstructure of the fabric. The randomness of material properties implemented in the model was not only in terms of damage parameters but also the entire flow curve; various stress-strain curves were randomly assigned to truss elements in the FE model. The scatter in material properties obtained for processed fibres at strain rate of 0.5 s^{-1} (see Fig. 6.13a) was used for this purpose since the same strain rate was applied as boundary condition in the model. The corresponding results for evolution of the damage parameter N_f/N with fabric extension are plotted in Fig. 7.8. When these results were compared with those for the model with randomly oriented fibres, each with the same (average) material properties, a more gradual growth of damage, started at a lower strain level — approximately 34% — was observed; in the model with fibres with the same properties it was 74%. Moreover, this fibre-failure process remained continuous with increase stretching of the fabric until the final fibre failed at a strain level of 112% as shown in Fig. 7.8. This gradual growth of damage in the random-fibre material model was closer to the deformation and failure behaviours of nonwoven

observed experimentally, as mentioned in Section 5.2.4, in which fibre failure process started at 35% to 40% and gradually grew until fabric extension of 110% to 120%. Thus, a model with randomness both in fibre orientation and their material properties is more suitable to simulate the realistic deformation and failure process of nonwovens. As the scatter in material properties can be randomly assigned to various fibres in the FE model in multiple ways, simulations of numerous statistical realizations can be performed by assigning different combinations of fibre orientation and material properties, eliminating the serrated behaviour of the averaged curve of damage parameter as a function of fabric extension.

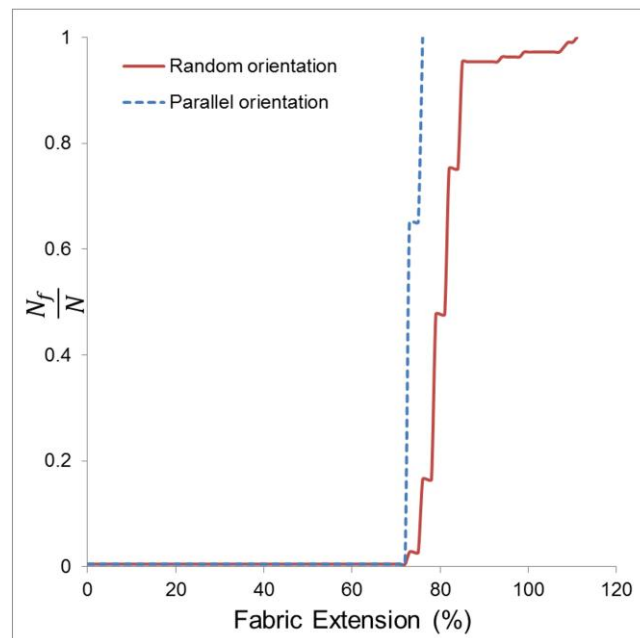


Figure 7.7. Effect of fibre orientation on damage initiation and propagation in FE simulations of nonwoven

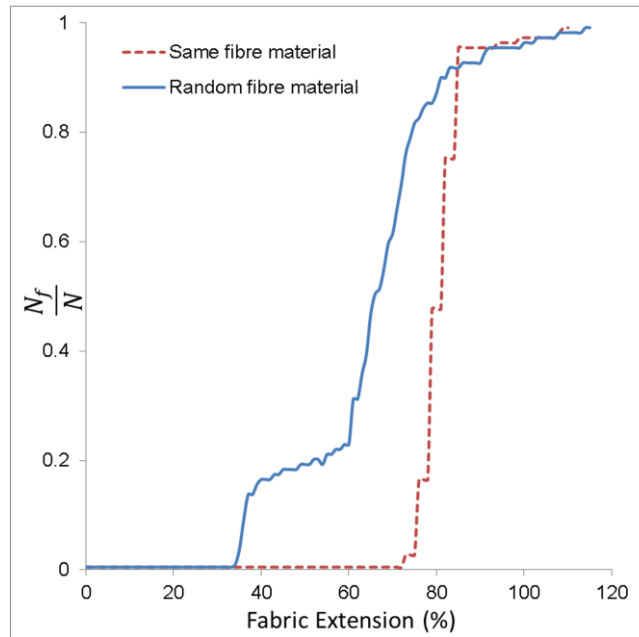


Figure 7.8. Effect of randomness of fibre's material properties on damage initiation and propagation in FE simulations

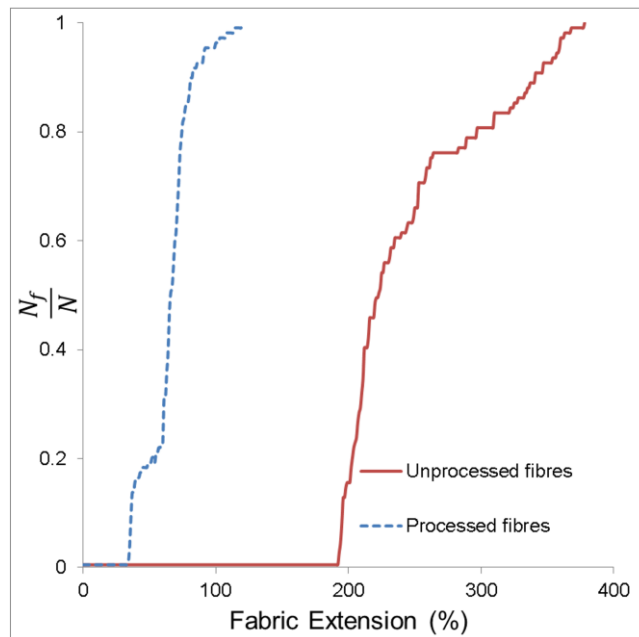


Figure 7.9. Effect of state (processed and unprocessed) of fibres on damage initiation and propagation in FE simulations

In order to assess the importance of damage criteria based on mechanical properties of processed fibres extracted from nonwoven, simulations of another tensile test were carried by implementing the damage criteria based on properties of unprocessed fibres. The material properties obtained from the single-unprocessed-fibre tensile tests at strain rate of 0.5 s^{-1} were used for this purpose. The results in terms of damage parameter as a function of fabric extension are shown in Fig. 7.9, which demonstrates that the fibre-failure process started at fabric extension of approximately 200% followed by ultimate failure of fabric at 379%. Both of these values — damage initiation and ultimate failure — are significantly higher than experimental results, which are closer to those of the model with material properties of processed fibres. Thus, it is important to use material properties, especially damage criteria, for the fibres extracted from the fabric rather than those of unprocessed fibres properties for realistic simulations of deformation and failure of nonwovens.

This study revealed that damage criteria based on processed fibres is necessary for realistic simulation of damage behaviour of nonwovens. Besides, it revealed that model with both random orientation of fibres and random material properties reproduced not only the realistic microstructure of the fabric but also the main mechanisms of mesoscopic uniaxial deformation and damage of the thermally bonded nonwoven. Thus, this model can be extended to analyse the macro level behaviour of thermally bonded nonwovens until their fracture as given in the next section. Based on the results obtained in this section, the material properties, implemented in macro-scale model, are based on those of processed fibres extracted from the fabric rather than unprocessed ones with full scatter in them.

7.4 Macro-scale Model

In this section, macro-scale models of the nonwoven are simulated and their results are compared with the experimental data. Since the studied nonwoven fabric demonstrated anisotropic properties as mentioned in Chapter 5, therefore, fibrous network along two

direction — MD and CD — were generated (Fig. 7.10) with dimensions mentioned in Table 7.2. The ODF obtained shown in Fig. 7.4 was used to develop the models.

Table 7.1. Parameters of fabric (see Fig. 7.11)

	Parameter	Magnitude
Fabric	A_{Fabric} (W x L) (mm x mm)	MD: 10 x 16.5 CD : 16.5 x 10
	ρ_{Fabric} (kg/m ²)	20 x 10 ⁻³
	Bond points	
Pattern	A (mm)	1.0668
	B (mm)	0.5588
	C (mm)	0.7
	D (mm)	1.8
	E (mm)	0.2
Fibres	a_{Fibre} (mm ²)	2.54 x 10 ⁻⁴
	L_{Fibre} (mm)	38.1
	ρ_{Fibre} (kg/m ³)	0.89 x 10 ³
Model coefficient	K	1

As mentioned before, fibres were modelled with truss elements and bond points were modelled with shell elements. The initial numbers of both types of elements in macro-scale models — along MD and CD — are given in Table 7.3.

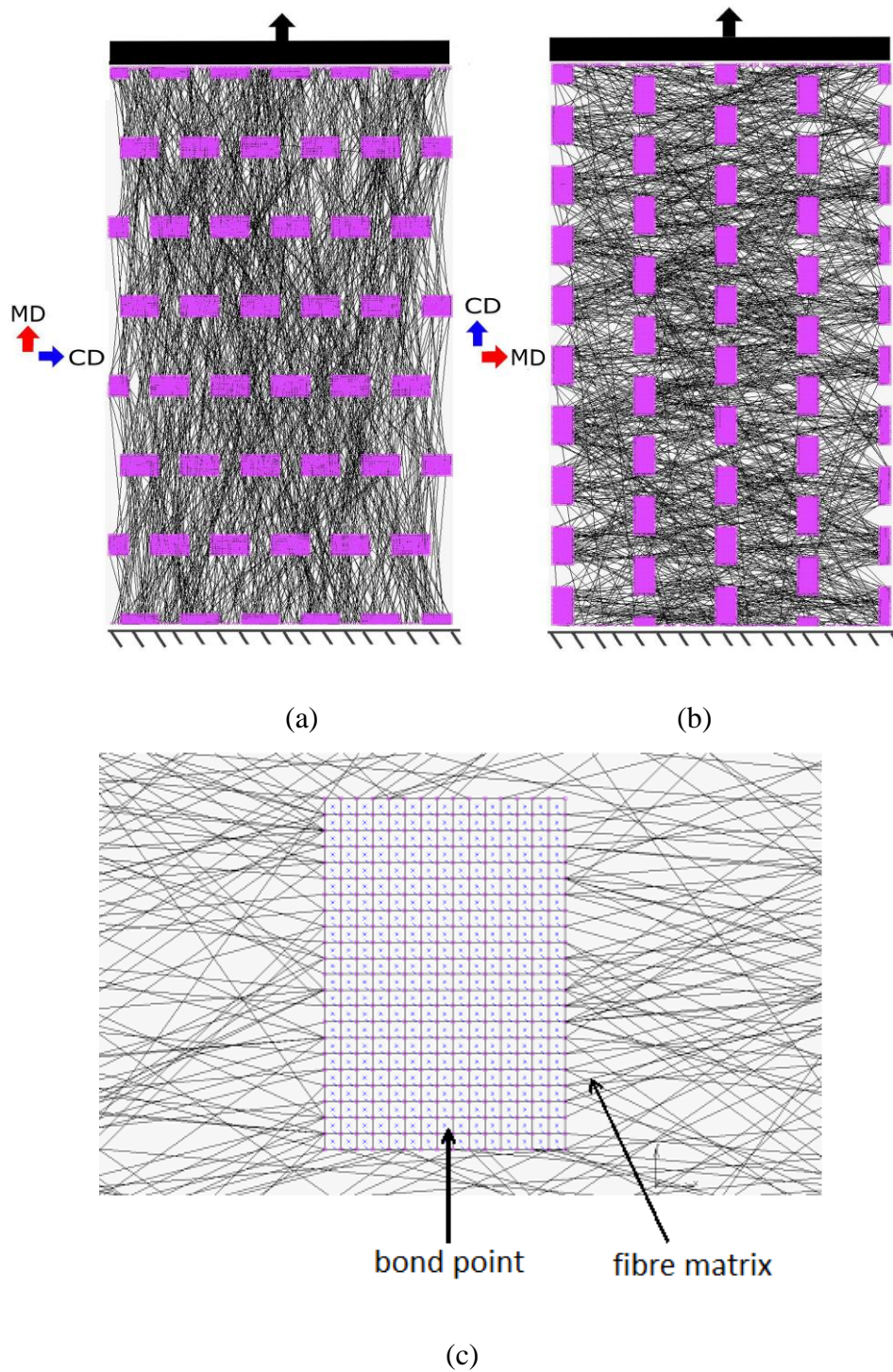


Figure 7.10. Finite element models: (a) loading along MD; (b) loading along CD; (c) zoomed view of bond point

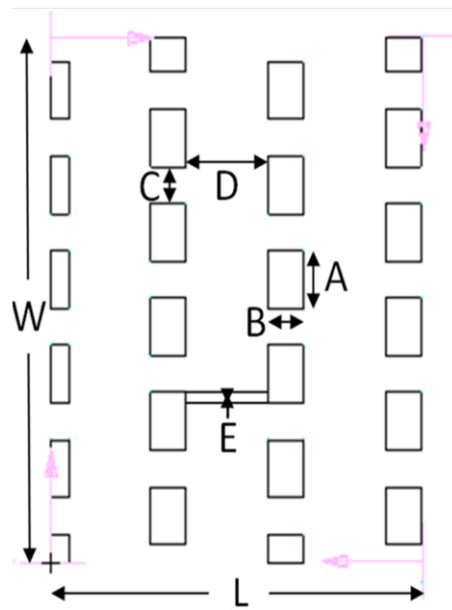


Figure 7.11. Parameters of pattern of modelled fabric

Table 7.2. Number of elements for MD and CD models

Model	Shell (Element 139)	Truss (Element 9)
MD	11417	2285
CD	9550	2019

7.4.1 Material Properties and Boundary Conditions

The material properties implemented into the model were obtained from the single-fibre tensile tests. As mentioned in Chapter 6, there is a significant scatter in results of single-fibre tests (Fig. 6.13), which show the randomness in material properties of the constituent fibres. This scatter is the result of some local shape irregularities of the tested fibres due to the effect of heat or physical contact during web-forming or hot-

calendering stages. In addition to shape irregularities, SEM images of the fabric showed that a fibre diameter is not constant along its length (see Fig. 5.7), which could be a result of slight variation in cooling conditions or shrinkage behaviour; this is another reason for a significant scatter in the results. As mentioned in the previous section, implementation of variation in fibres' material properties not only in terms of failure parameters but also the flow curve along with orientation distribution of fibres into the FE model is essential to simulate realistic deformation and damage behaviours of the fabric. Therefore, different stress-strain curves and damage parameters were assigned to truss elements in the FE model according to the data obtained from the tensile experiments at strain rate of 0.1 s^{-1} performed on ten processed single-fibre specimens. The data obtained from these specimens was used as indicator of scatter in material properties for all the fibres within the fabric. The numbers of fibres in each set as a fraction of the overall number of fibres within the fabric, obtained with the random sampling technique, with their corresponding stress and strain threshold values are given in Fig. 7.12. According to this, seven sets of fibres with different material properties in terms of their flow curve and damage parameters were implemented in the model (Fig. 7.13). Since damage was not observed in the bond points during fabric's tensile tests, therefore, damage criteria discussed below were not applied to them.

The simulations of tensile tests were carried out by applying a set of boundary conditions to the FE model, within the framework of quasi-static loading with large displacements and rotations. The nodes on the side R-S of the model (Fig. 7.13) were fully constrained whereas a uniform axial displacement condition corresponding to the

strain rate of 0.1 s^{-1} was applied to the nodes on side P-Q of the model as shown in Fig. 7.13.

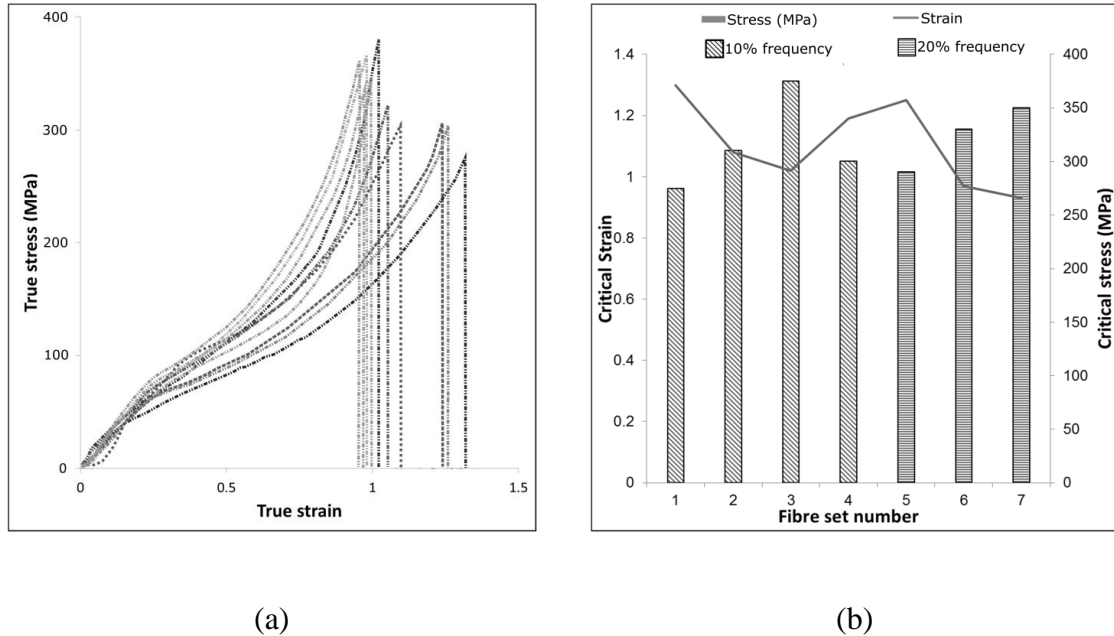


Figure 7.12. Stochasticity in material properties implemented into FE model: (a) stress-strain curves; (b) critical values of stress and strain

7.4.2 Results and Experimental Verification

The deformation and damage behaviours in the fabric, which are a result of large rotations and progressive failure of fibres, were simulated for both MD and CD, as shown in Figs. 7.14b and 7.15b. Apparently, the main features of deformation and damage process, observed in real specimens of the modelled fabric including formation and growth of localized zones (see Figs. 7.14a and 7.15a) were reproduced in simulations. In order to compare the model's predictions with the experimental results, the force-extension graphs were used as shown in Fig. 7.16. The shaded areas in Fig. 7.16 represent the bands of experimental results performed on multiple specimens for the corresponding directions. A good agreement between the simulations and

experimental results is observed, including the extent of material's anisotropy. Implementing different statistical realizations of material properties by changing them for corresponding fibre sets based on the experimentally obtained data (Fig. 7.12), led to changes in force-extension curve as shown in Fig. 7.16. Nevertheless, the extent of scatter found in experimental results was much more as compared to the numerical results. As mentioned in Section 5.2, several parameters contribute to this scatter such as variation diameter of constituent fibres, orientation distribution of fibres, single fibre parameters. Some of these parameters can easily be incorporated into the model which would give better agreement between experimental and numerical results in terms of scatter as mentioned in detail in explanation of Fig 7.17.

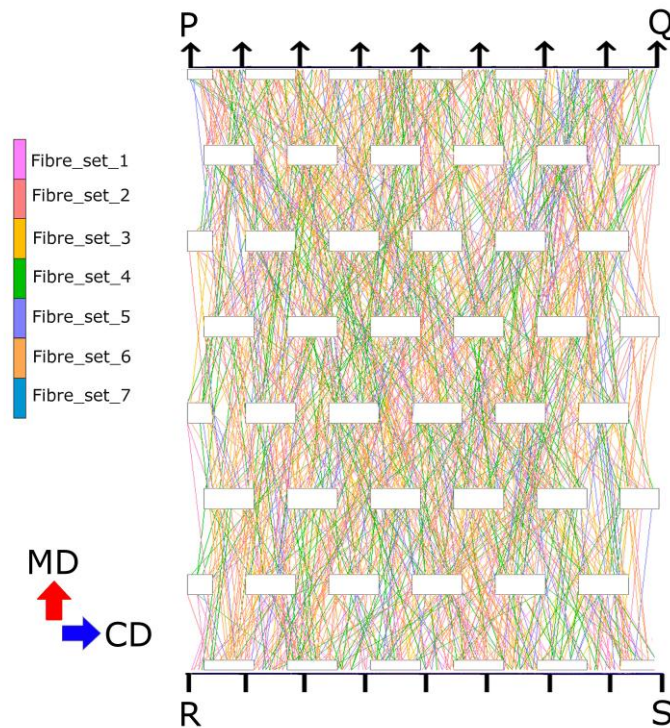


Figure 7.13. FE model showing stochasticity in material properties and fibres' orientation distribution and boundary conditions

Apparently, an initial slightly stiffer behaviour in CD as compared to experiments can be attributed to the fact that a curl of fibres was not introduced into the model. Due to the curl, fibres do not start participating in load bearing in the actual fabric until they become uncurled, resulting in a slightly softer response. Another apparent difference between the model's prediction and the experimental results is the higher scatter in the latter case. The experimental scatter can be related to the following factors: variation in material properties and strength of fibres, randomness in microstructure and variation in fibres geometry. The first source of scatter was taken into account in the simulations by providing different material properties and strength to different sets of fibres as shown in Fig. 7.17. Randomness in material's microstructure can be easily implemented into the model by using the parametric modelling technique based on the subroutine, developed in this study. In the experiments on fabric, all the testing parameters such as specimen size and boundary conditions are kept constant; the variation is linked to the orientation distribution, material properties and positions of fibres. Thus, it was obvious that using different microstructures by changing ODF for developing the model and seeding random numbers to fibre positions (Fig. 7.17) would increase the extent of variability in simulation results providing a better agreement with the experimental results. The effect of varying the material properties of individual fibres in the form of force-extension curve is given in Fig. 7.16. It should be noted that the variation in the mechanical response based on assigning different material properties to fibres in the models is identical to the scatter reported experimentally.

Explicit introduction of fibres into the model can help to predict the level of stresses and strains in each element (fibre in this case) of the model. Since fibres were

modelled randomly according to the ODF measured for the real fabric and their participation in load bearing changed as they were aligned along the loading direction, the level of strain (ε_f) and corresponding stress (σ_f) in each fibre varies from the global strain in fabric ($\bar{\varepsilon}$) depending upon its orientation with respect to loading direction and position in the network as shown in Figs. 7.18 and 7.19. The probability distribution function of normalised strains in fibres with respect to the global strain and corresponding stresses at various levels of fabric's extension are presented for each interval of strains and stresses in Figs. 7.18 and 7.19, respectively. As most of the fibres failed at less than 100% of fabric's extension along MD, therefore, the figures present the data for strains and corresponding stresses not exceeding this magnitude. Two different patterns of change in the probability distributions for MD and CD with increasing deformation of the fabric are obvious in Figs. 7.18 and 7.19.

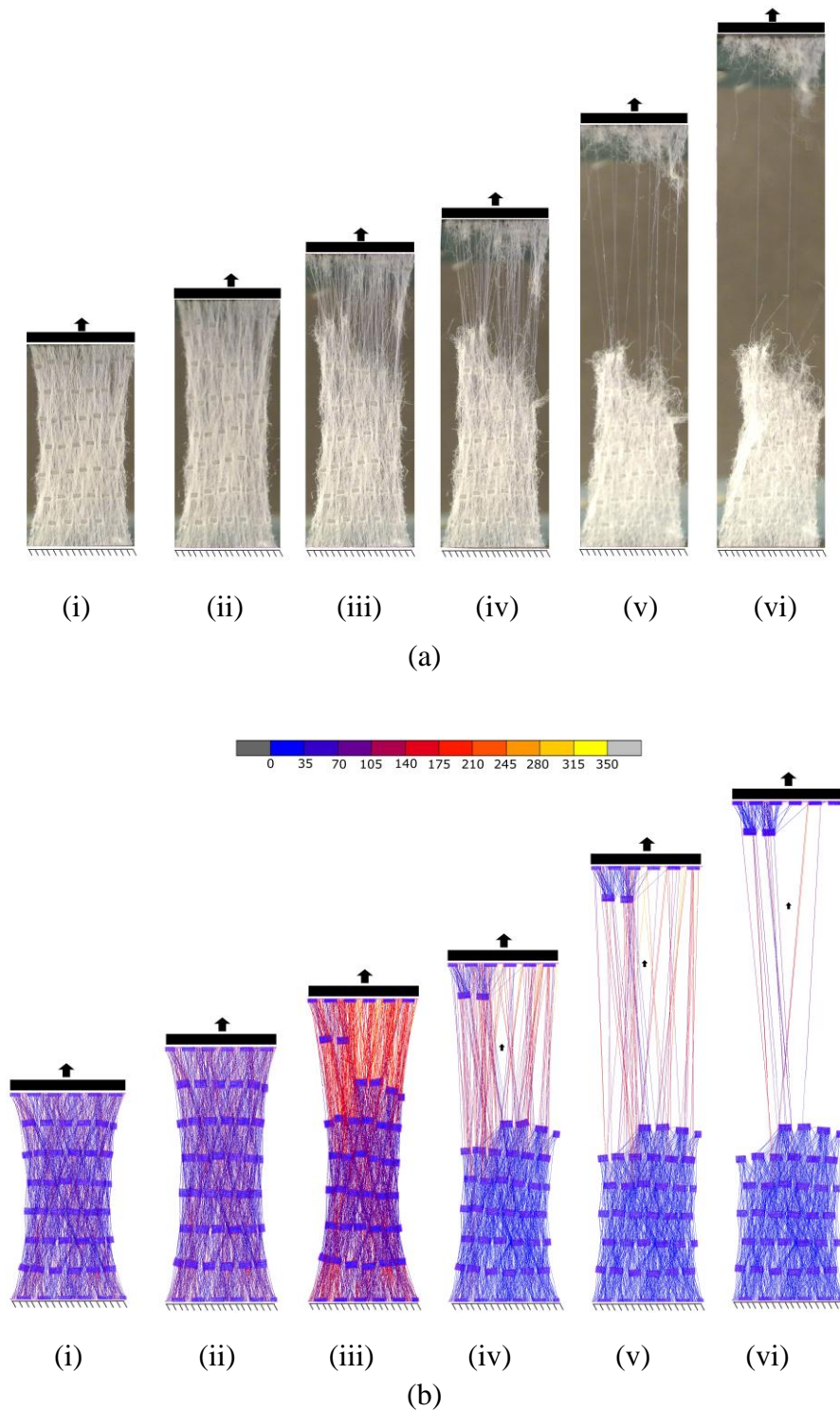


Figure 7.14. (a) Experimental results for fabric subjected to uniaxial tension along MD to various extensions: (i) 25%; (ii) 50%; (iii) 75%; (iv) 100%; (v) 150%; (vi) 190%; (b) corresponding FE results for equivalent (von Mises) stresses in (MPa)

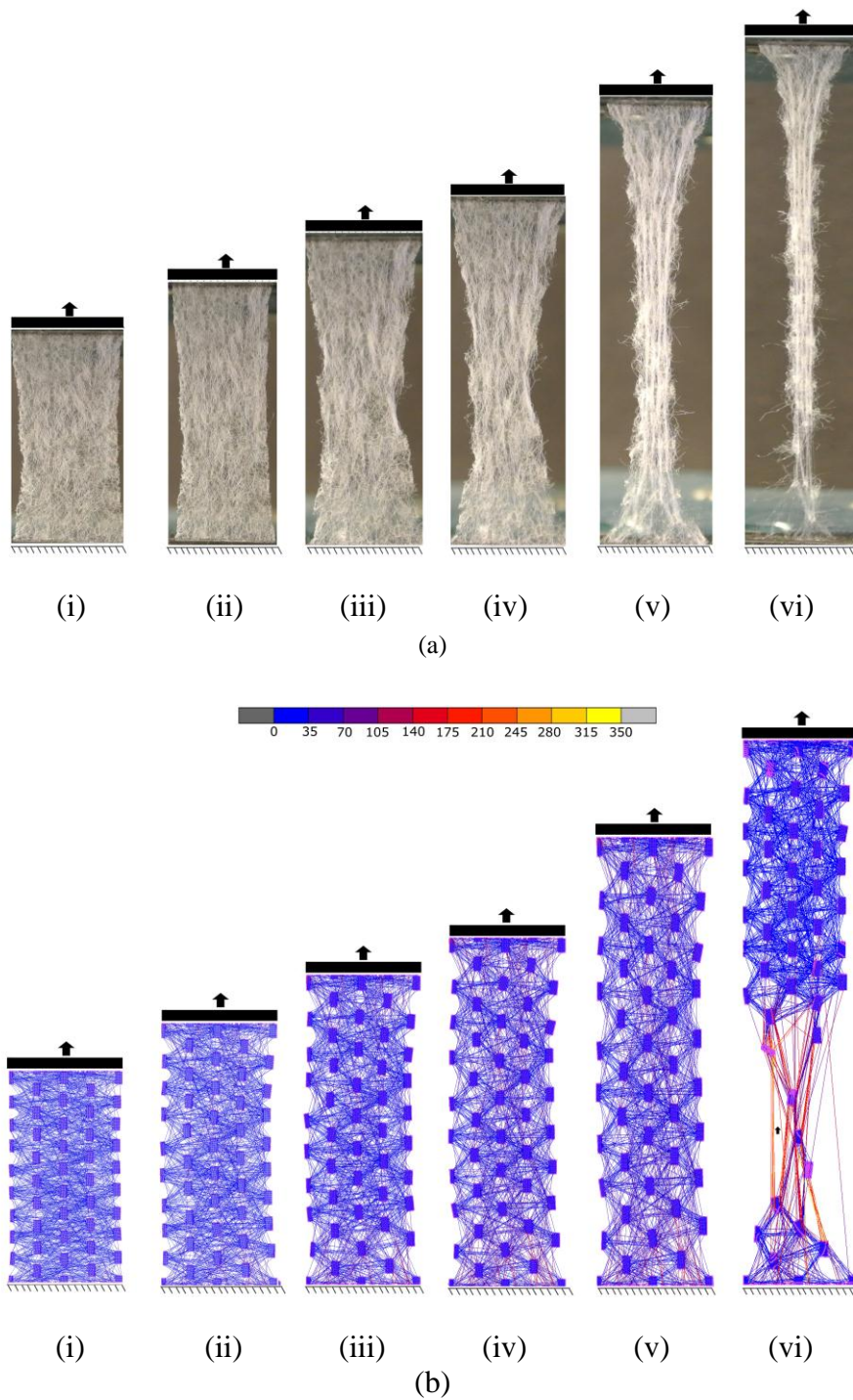


Figure 7.15. (a) Experimental results for fabric subjected to uniaxial tension along CD to various extensions: (i) 25%; (ii) 50%; (iii) 75%; (iv) 100%; (v) 150%; (vi) 190%; (b) corresponding FE results for equivalent (von Mises) stresses in (MPa)

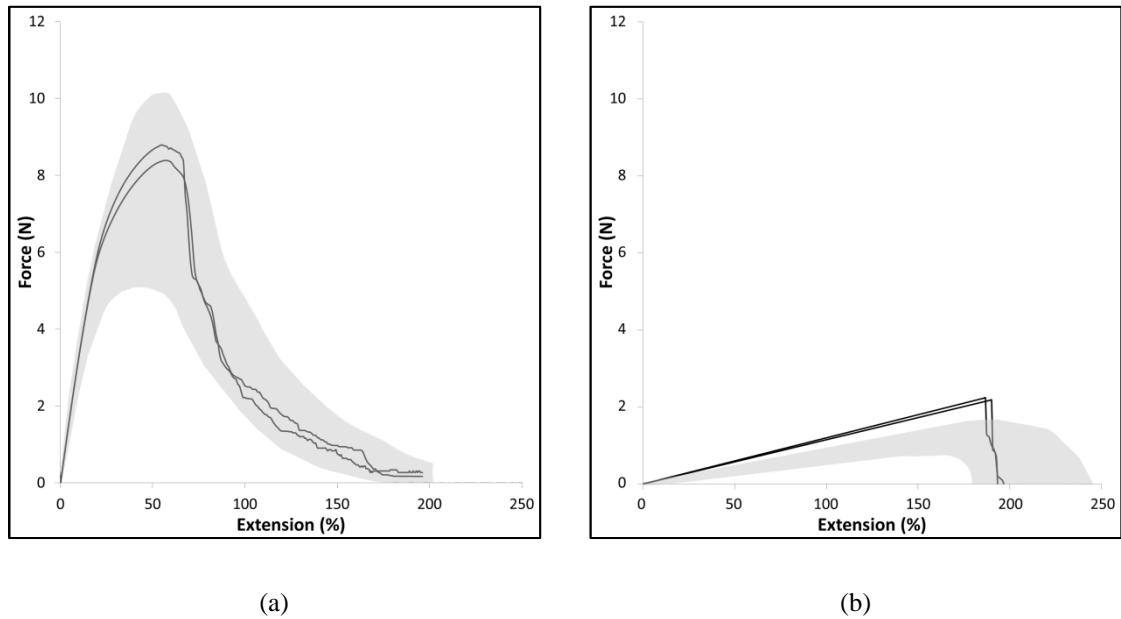


Figure 7.16. Calculated responses to uniaxial tensile test for MD (a) and CD (b)
(Shaded area represents scatter in experimental results)

For CD (Fig. 7.18b) the distribution effectively retains its shape with only minor changes to the bands. For MD (Fig. 18a), in contrast, significant shifts of the distribution's median are observed. The peak for normalised fibre strains shifts to lower values with increasing fabric strain. The reason for this kind of behaviour of the fabric lies in its microstructure. Since fibres were preferentially aligned along MD, large reorientation of fibres occurred for loading along CD resulting in negligible increase in strain in fibres. However, for MD, fibres started participating in load bearing at comparatively smaller fabric's extension and failed progressively resulting in relaxation of fabric (see Fig. 7.14), which caused the peak for normalised fibre strains to shift to lower values. The difference in patterns for stress distributions for MD and CD (Fig. 7.19) is also similar to that for normalised strains. Still, if for CD the character of changes is practically the same, the case of MD (Fig. 7.19a) has its specific

development. Here, at the initial stage (up to fabric strain of 50%) the shift is to higher levels of stress of fibres, reflecting their increasing participation in the load-bearing process as a result of reorientation towards the loading direction. However, this trend reversed between 75% and 100% of fabric's extension when many fibres reached their stress threshold and failed resulting in the unstretched state of fibres outside the localised failure zones due to elasticity (Fig. 7.18a).

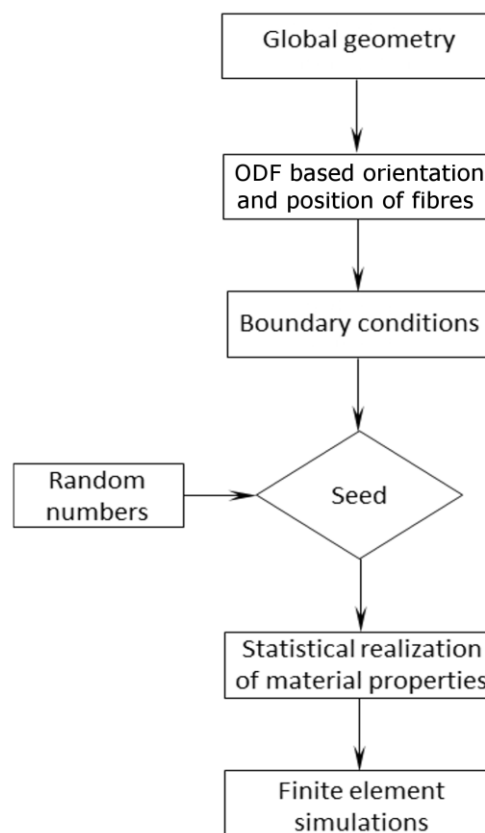


Figure 7.17. Flow chart on implementation of stochasticity in FE model

Thus, the developed model can be used to predict stress distributions at any level of fabric's extension. Besides, explicit introduction of fibres into the model helped to understand the evolution in stresses of fibres and arrangement of the neighbouring elements caused by progressive failure of fibres. Since most of the fibres regained their

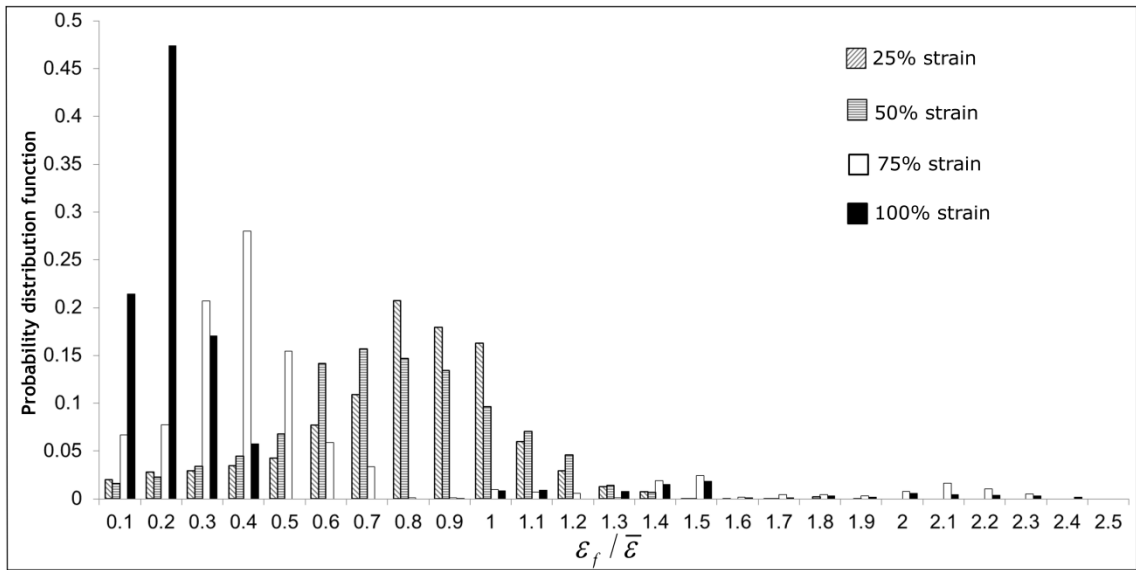
unstressed or negligible stress state at 100% of fabric's extension along MD (Fig. 7.19a), therefore the stretch back in the fabric after 100% fabric extension is negligible as shown in Fig. 7.14a (v) and (vi).

The stress distribution in fibres for MD and CD with respect to fabric's extension is shown in Fig. 7.20 in the form of percentile bands. Each band presents ten percentile ranks of fibres. For MD (Fig. 7.20a), stresses in all the fibres increased till 50% of fabric's extension. On further extension, 80 percentile of fibres stretch back due to progressive failure of fibres with increasing extension in fabric result in the decrease in stress in them. Thus, after 50% of fabric's extension only 20% of fibres took load while the rest of the fibres tried to regain their original shape due to stretch back. Since progressive failure of fibres resulted in continuous transfer of stresses to the neighbouring elements, a sudden increase in stresses in remaining 20% of fibres bearing load after 50% of fabric's extension for MD was observed (Fig. 7.20a). For CD (Fig. 7.20b), continuous increase in stresses in fibres shows a growing extent of participation in load bearing. It is obvious here that the increase in stresses in fibres was gradual for CD as compared to that of for MD, showing large reorientation of fibres takes place before participation in load bearing for CD than MD which is consistent with fabric's microstructure. Since this model provides information on fibres participating in load bearing at any level of fabric's extension, it can be used to optimise the ODF of the fabric for its better strength and robustness. The average reorientation of fibres for loading along both directions — MD and CD — against increasing levels of fabric's extension is given in Fig. 7.21 in terms of average reorientation $\langle \Delta\theta \rangle$ at any level of fabric's extension. It was calculated by subtracting the average of absolute values of

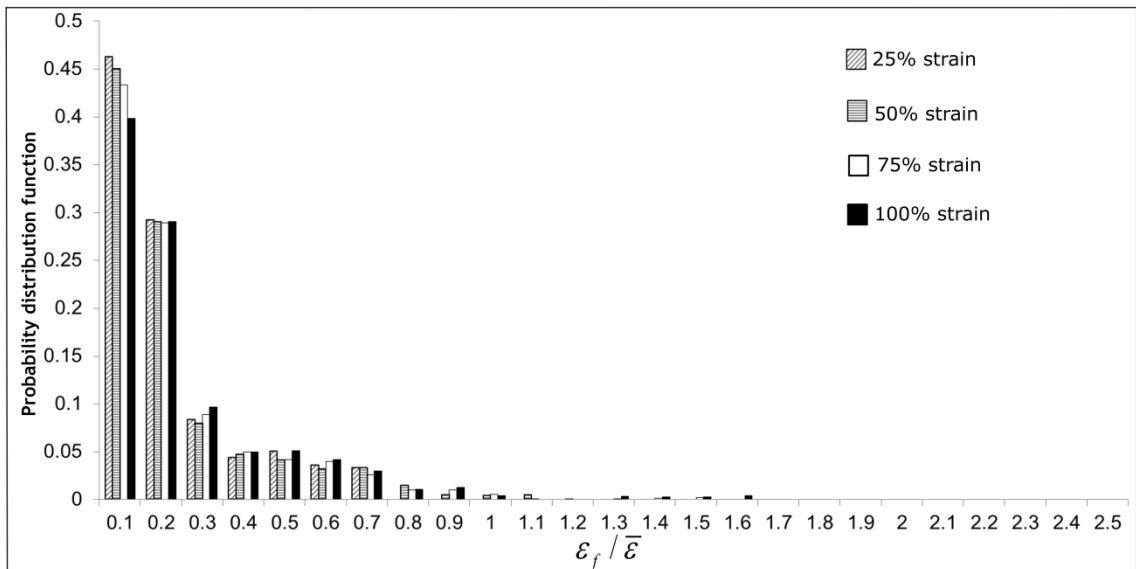
initial fibres' angles with the loading axes from the average of absolute values of fibres' angles with the loading axes at that level of extension:

$$\langle \Delta\theta \rangle = \left| \theta_f \right|_{\text{avg}} - \left| \theta_i \right|_{\text{avg}} . \quad 7.7$$

The reason behind using the absolute values of angles is to get the net fibres reorientation whether it is in clockwise or anti-clockwise direction. Besides, the difference with the initial orientation of fibres provides the information about evolution of the fabric's microstructure with its extension. For CD (Fig. 7.21), the continuous increase in the difference of average fibre's angle with initial fibre's orientation was observed showing constant evolution of the fabric's network structure with the increasing level of its extension. For MD (Fig. 7.21), in contrast, reorientation of fibres was observed until 50% of fabric's extension. After this level of extension, due to progressive failure of fibres reaching their stress threshold, stretch back in fabric was observed. This caused the remaining fibres to reorient towards their initial orientation, i.e. the state when no load was applied. However, fibres did not regain their initial orientation, demonstrating permanent deformation of the fabric similar to that observed experimentally (Fig. 7.14 and 7.15). Thus, the model is capable to predict the changes in network's topology with its extension, which will help a designer and a manufacturer of nonwovens to determine the life and safety factor of products containing nonwoven parts.

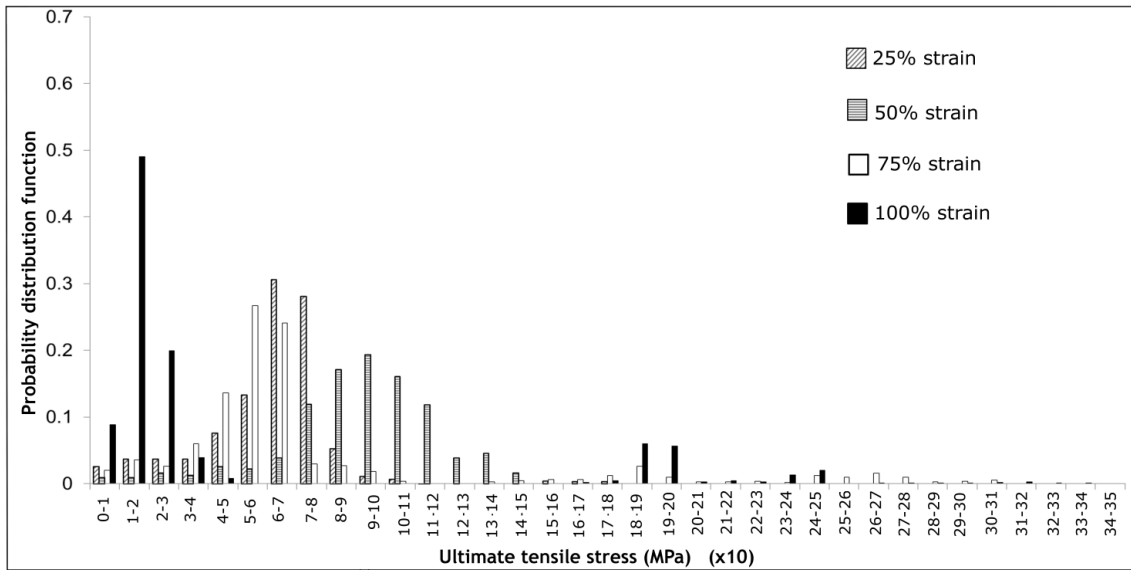


(a)

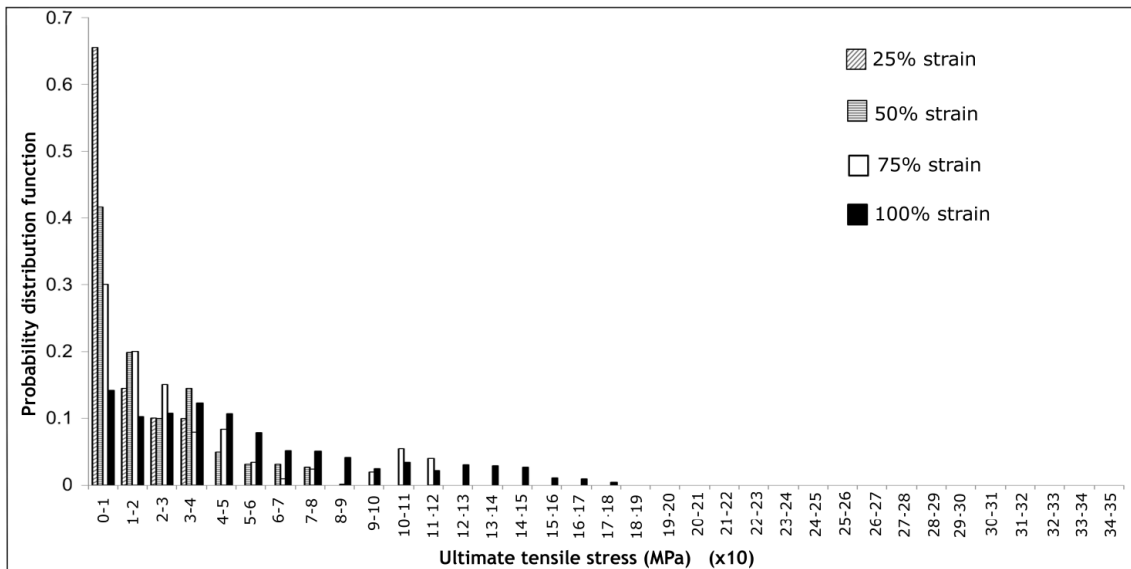


(b)

Figure 7.18. Distribution of normalised strains for fibres for various values of fabric strain deformed along MD (a) and CD (b)



(a)



(b)

Figure 7.19. Distribution of stresses for fibres for various values of fabric strain deformed along MD (a) and CD (b)

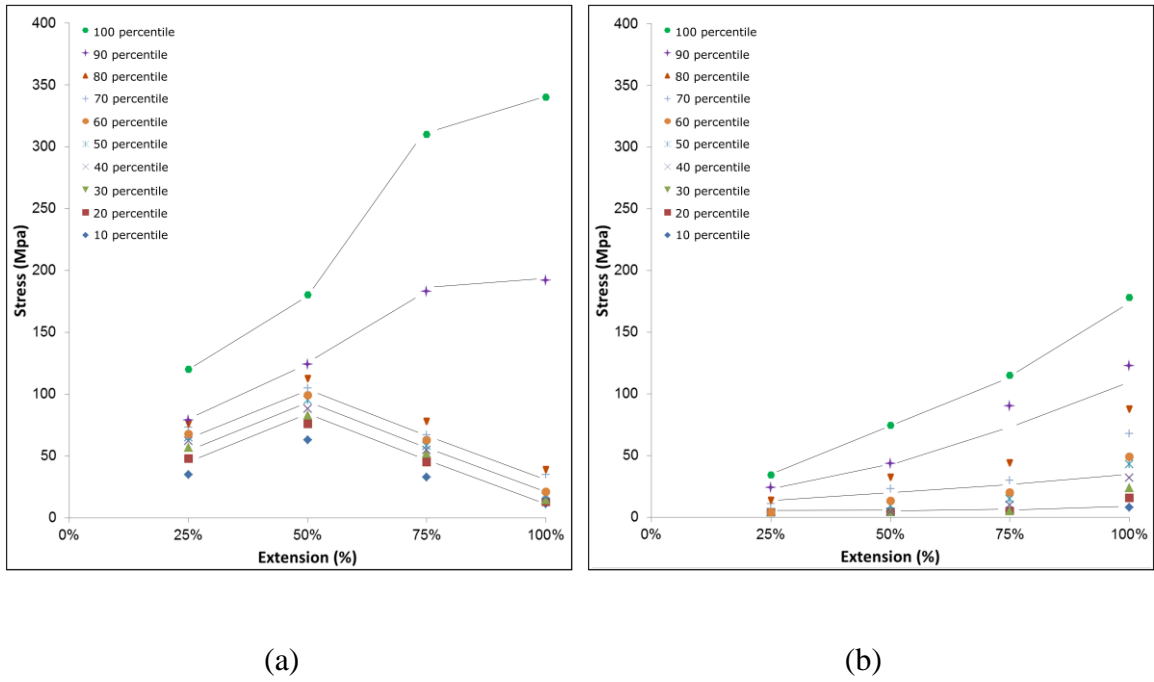


Figure 7.20. Distribution of stresses of fibres for various levels of fabric's extension for MD (a); CD (b)

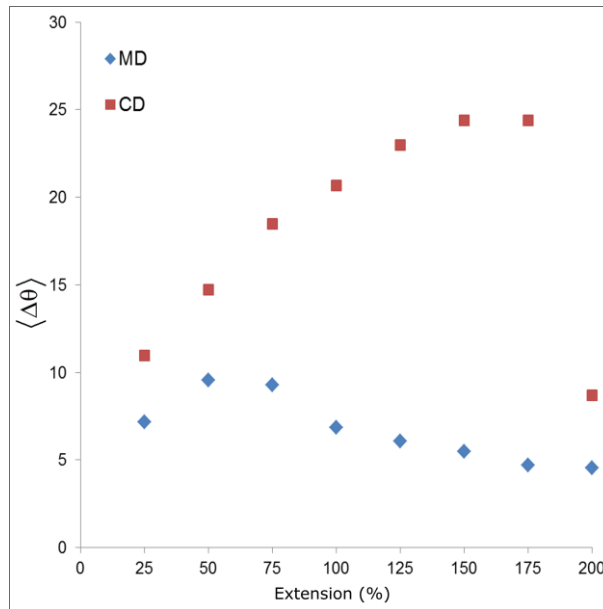


Figure 7.21. Fibres rotation with increasing fabric's extension for MD and CD

The process of reorientation of fibres towards the loading direction followed by their failure upon reaching the critical stress led to localisation of damage in the form of fracture zones as shown in Figs. 7.14 and 7.15, which appearance was similar to that observed in experiments. These fracture zones were formed by the remaining fibres oriented along the loading direction. The development of localised fracture zones was caused by an avalanche of failures due to load redistribution (i.e. increase in the load of neighbouring fibres from the ruptured ones). Subsequent loading caused more fibres to fail, resulting in the growth of fracture zones. These phenomena of initiation and growth of fracture zones with fabric's extension are shown in Fig. 7.14 and 7.15. The growth in fracture zones for loading along MD was slower as compared to that along CD. Since multiple fracture zones are developed in the fabric during its extension, the ones shown by the arrows in Figs. 7.14 and 7.15 are presented in Fig. 7.22 in terms of the ratio of length of fracture zone (l_{fz}) to the total length of fabric (L) for all stages of its extension. The fracture zone developed along MD after 50% of fabrics' extension and reached approximately one half of the fabric's length at 200% extension. In contrast, for CD it started after 180% extension, and the fabric failed at that fracture zone at fabric's extension of 200%. This shows that the development of fracture zone by the progressive failure of fibres was rapid along CD and more continuous for MD. This phenomenon can be attributed to the preferential orientation of fibres along MD, i.e. in this case fibres already more aligned along the loading direction (coinciding with MD) started participating in a load transfer while other fibres were still re-orienting, resulting in more gradual damage evolution. Whereas, during loading in CD, most of the fibres were reoriented along the loading direction and started participating in the load-bearing

process practically at the same stage of deformation. Since the process of individual fibre failures responsible for progressive damage evolution in the fabric was more gradual along MD than CD, a longer tail in force-extension curves was observed in the former case as shown in Fig. 7.16.

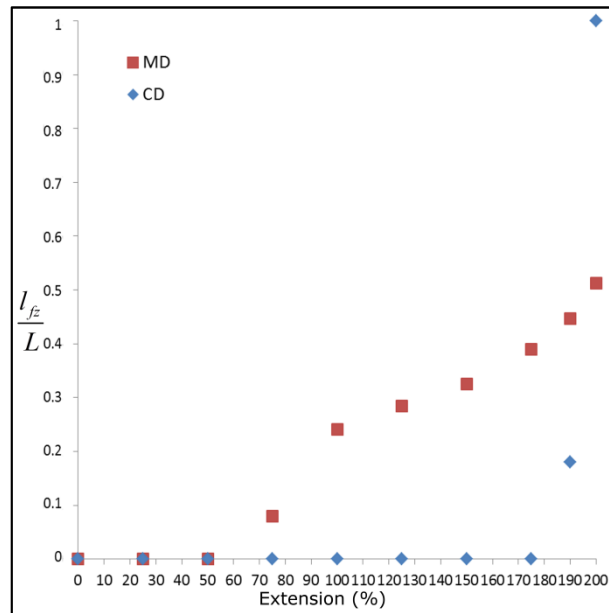


Figure 7.22. Growth in fracture zone with fabric's strain

The damage evolution in fibrous networks can be characterised by a ratio N_f / \bar{N} , where N_f is the accumulated number of fibres failed at any particular level of fabric's extension and \bar{N} is the total number of fibres failed during deformation and damage of the fabric up to its rupture. Since the number of failed fibres depends upon the failure locus, it can vary with variation in ODF and position of fibres within the fabric. Therefore, the total number of fibres within the fabric specimen was not used as denominator in the fibre ratio. Evolution of the damage parameter N_f / \bar{N} with fabric's extension for both studied cases — MD and CD — is given in Fig. 7.23. It shows that

the growth of damage caused by progressive fibre failure, a key feature of deformation and damage of fibrous networks, was more gradual along MD than CD because of the reasons discussed above.

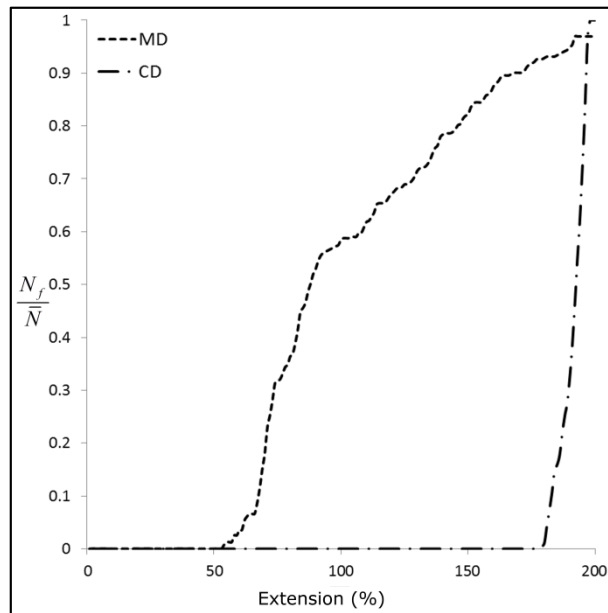


Figure 7.23. Evolution of damage parameter with fabric's deformation

The discussed change in distributions of fibres' parameters with increasing deformation of the fabric and development of fracture zones is also reflected in changes of the maximum and minimum values of stresses shown in Fig. 7.24. Apparently, the maximum stress in fibres along MD and CD increased continuously until it reached its maximum value. However, this increase for MD was rapid as compared to that for CD; fibres in the former case started to participate in load transfer earlier than in the latter; this was also consistent with the fabric's structure having preferential orientation of fibres along MD. The minimum value of stress in fibres for CD was negative as a result of lateral shrinking. Such fibres under compressive load offered resistance to reorientation of other fibres along the loading direction during the fabric's extension

process; therefore, the model predicted a slightly stiffer behaviour compared to that observed in experiments as shown in Fig. 7.16b. An interesting point can be noted here: the variation in the minimum value of stresses for both MD and CD is negligible for all the levels of fabric's extension as a result of a continuous transfer of stresses to the neighbouring elements caused by progressive failure of fibres. Due to this stress shift, some fibres started to take load during fabric's extension while some fibres returned back to the unstressed state due to failure of neighbours.

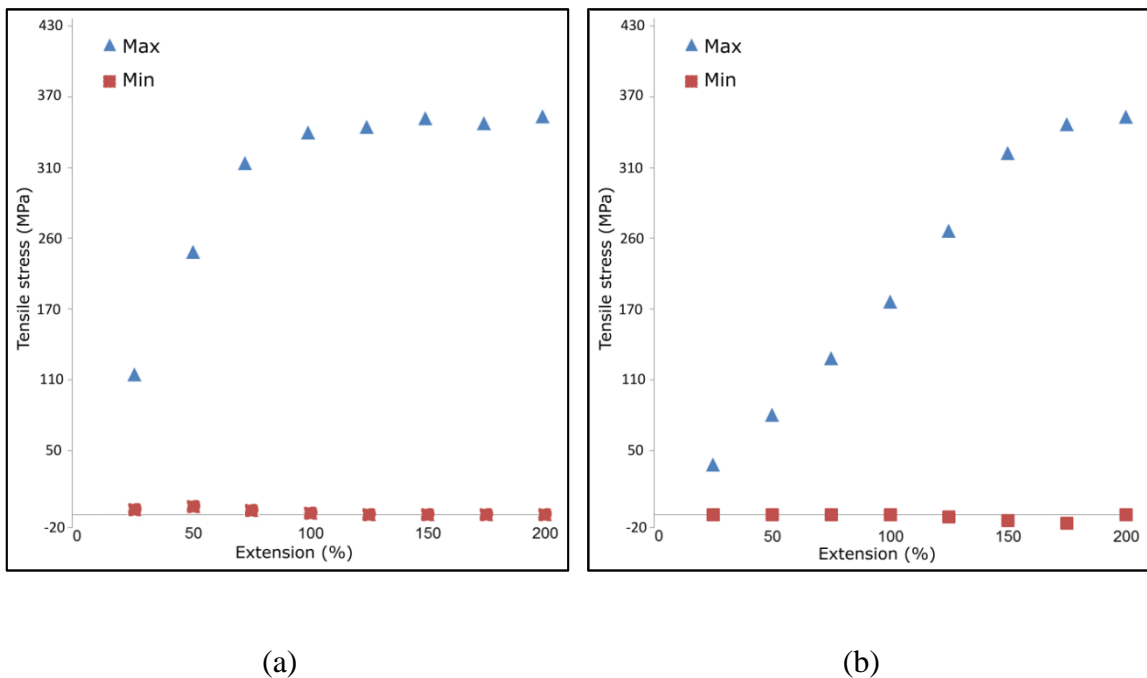


Figure 7.24. Minimum and maximum values of stress in fibres for various values of strain in fabric deformed along MD (a) and CD (b)

The model developed in this study is not only capable to predict the deformation and damage behaviours accurately in terms of anisotropy, nominal strength, force-extension behaviour and changes in network's topology as a result of damage evolution but it also properly reflects the effect of grip constraints on the deformation behaviour

of the fabric (Figs. 7.14b and 7.15b). The transverse strain in the fabric gradually increased from the grip on each end of the fabric to the region of maximum transverse strains in the middle. Such transverse strains in the fabric were significantly higher for MD producing a visible necking effect in this case as compared to that in CD with negligibly small transverse strains at initial stages of fabric's extension as shown in Fig. 7.14 and 7.15. However, after a certain level of fabric's extension along CD, significant transverse strains and, thus, necking was observed there (Fig. 7.15a). The reason for this different behaviour was the preferential orientation of fibres along MD in the fabric. In the model, for MD, visible necking in the fabric was observed similar to the experimental observations. Due to preferential orientation of fibres along MD, a large number of fibres started reoriented along loading direction in CD. Some of the fibres started participating in load bearing while some of them were practically still in their actual orientation and took the compressive load during fabric's extension along CD (shown in Fig. 7.24b). In the model, fibres taking compressive load braced the fabric's structure against deformation. Since number of fibres participating in compressive load bearing in CD was very high as compared to MD, therefore, almost negligible transverse strain (necking) was observed in the model along CD even at higher levels of strains along this direction.

Another interesting observation is that the concentration of stresses at the edges of the bond points perpendicular to the direction of loading is very pronounced as compared to the rest as shown in Fig. 7.25. Since fibres in thermally bonded nonwovens always fail at bond point's edges, sharp stress concentrations at bond point edges is consistent with the experimental observations as well as various studies in the literature

(Dharmadhikary *et. al.*, 1999; Wang and Michielsen, 2001; Wang and Michielsen, 2002; Michchielsen and Wang, 2002). However, the stress concentration at the edges of bond points parallel to the loading direction was limited because these edges undergo compressive loading due to lateral contraction of the fabric as mentioned before (Fig. 7.14 and 7.15). Thus, the model developed in this study is also capable to simulate the stress distribution within bond points along with pronounced stress-concentration areas along their edges.

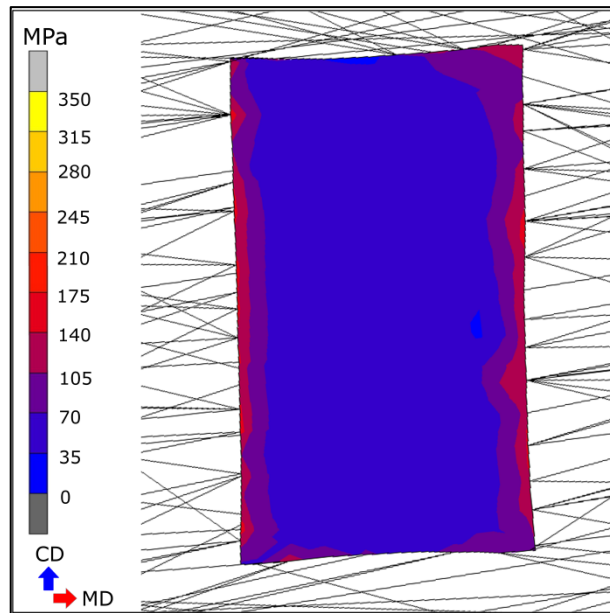


Figure 7.25. Stress concentration at edges of bond points (loading direction was along MD)

7.5 Case Studies

To investigate the predictive capability of the model in a more detailed way, various analyses were performed with changes in the model parameters such as planar density, shape and pattern of bond points etc. In this section, effects of some of the parameters are studied using the developed finite-element model. These parameters were selected

in a way that they not only helped to understand the predictive capability and usability of the model for certain types of nonwoven fabrics but also demonstrated that the model was extendable to almost all types of fibrous networks. The simulation results were compared with that of uniaxial experiments on the fabric with corresponding parameters.

7.5.1 Effect of Specimen Size

First of the various parameters to study is the size of the fabric specimen, as the behaviour of the fabric depends upon its size (Hou, 2009). In order to investigate the model's capability to predict the effects of varying specimen size, two models of different sizes for 20 g/m² nonwoven were developed (Fig. 7.26). The gauge length of specimens was 16.5 mm. Geometric properties such as bond point size and shape and ODF were similar to those used in Section 7.4. The nodes on the bottom side of the model were fully constrained whereas the uniform axial displacement corresponding to the strain rate of 0.1 s⁻¹ was applied to the nodes on the top side of the models. Critical stress of processed fibres obtained at strain rate of 0.1 s⁻¹ was used as fibre failure criteria.

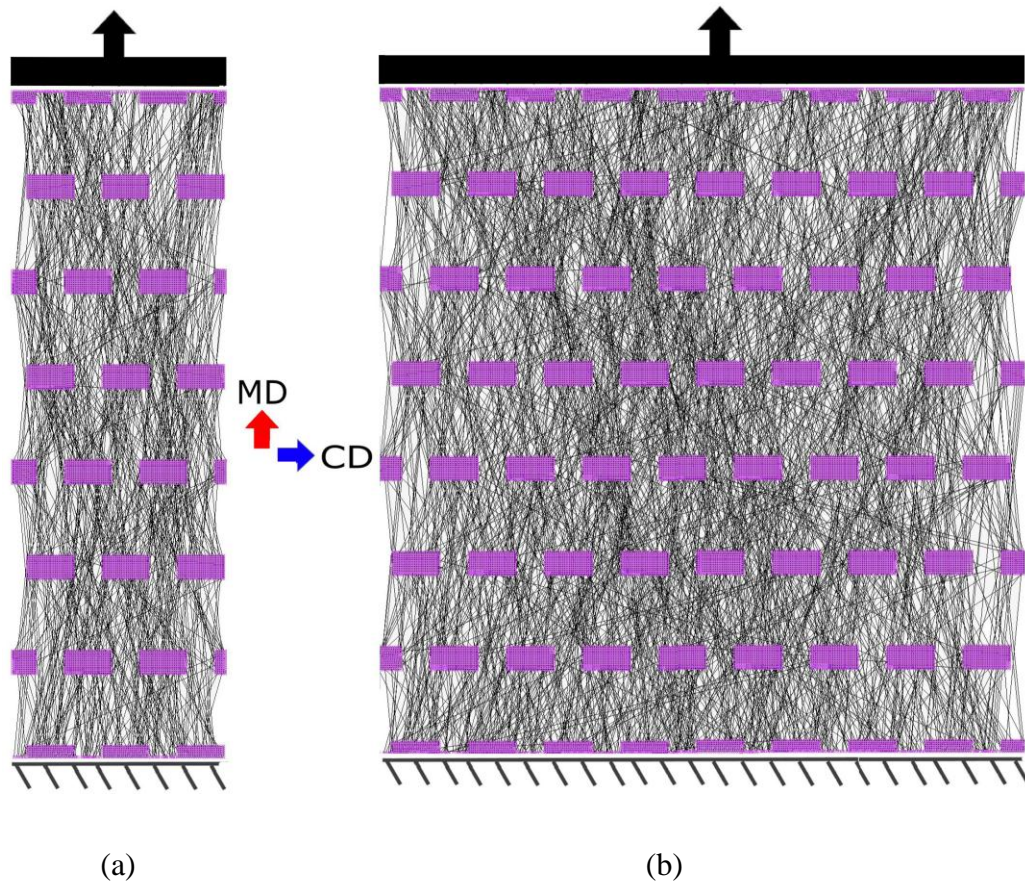


Figure 7.26. FE models of 20 g/m² with width (a) 5 mm; (b) 15 mm

The deformation behaviours of the models with increasing fabric's extension are shown in Fig. 7.27. The variation in material behaviour with specimen size in terms of force-extension curve is shown in Fig. 7.28. Note that the change in specimen's size was reflected by the model. The model showed that the increase in the specimen's width resulted in the increase in axial stiffness (Fig. 7.28) which is similar to that of experimental observations. This demonstrates the capability of the model to predict the size-dependent material's behaviour which is very important from the design point of view for products containing nonwoven parts as various sizes of fabrics are used in different products.

7.5.2 Effect of Planar Density

Another parameter under the examination was the fabric's planar density. In order to study its effect, a nonwoven with rectangular-shaped bond points with 30 g/m² planar

density was used as model system. The shape, size and pattern of bond points were similar to that of the fabric mentioned in Section 7.5.2. Besides, boundary conditions and material properties were also the same as in the previous sub-section. The simulation results in form of deformed fabric at various level of fabric's extension are shown in Fig. 7.29. In order to compare the results with those of experimental observations, the force-extension graph was used (see Fig.7.30).

As obvious from Fig. 7.30, the results of FE simulations and the experimental data are in good agreement. Similar to the results mentioned in Section 7.4.2, the model predicted a slightly stiffer behaviour as compared to that in the experiments at the beginning of deformation, which can be attributed to exclusion of curliness of fibres. Despite this possible source of deviation, the model successfully predicted the response of the nonwoven specimen to uniaxial tension. It shows that predictive capability of the model is not limited to nonwovens with a certain planar density.

7.5.3 Effect of Geometry and Pattern of Bond Points

In order to examine the capability of the model to predict the effect of changes in geometry and pattern of bond points, another fabric was chosen-with diamond-shaped bond points as shown in Fig. 7.30a. The planar density of this material was 30 g/m². The finite-element model was developed using the subroutine for this fabric with the exact shape, size, pattern of bond points and the planar density (Fig. 7.27b). The fibres were modelled according to the ODF obtained for this fabric using the subroutine as it is based on parametric technique, which can handle the variation in geometric entities of the nonwoven network structure. Uniform axial displacement at the strain rate of 0.1 s⁻¹ was applied to nodes on one side of the model whereas another side of the model was fully constrained to simulate the uniaxial tensile test. The failure stress parameter corresponding to 0.1 s⁻¹ strain rate was applied in the model as the same extension rate was employed as boundary conditions. Dimensions of the model for MD were 16.5 mm along MD and 10 mm along CD; parameters of the pattern of bond points are given in Table 7.3.

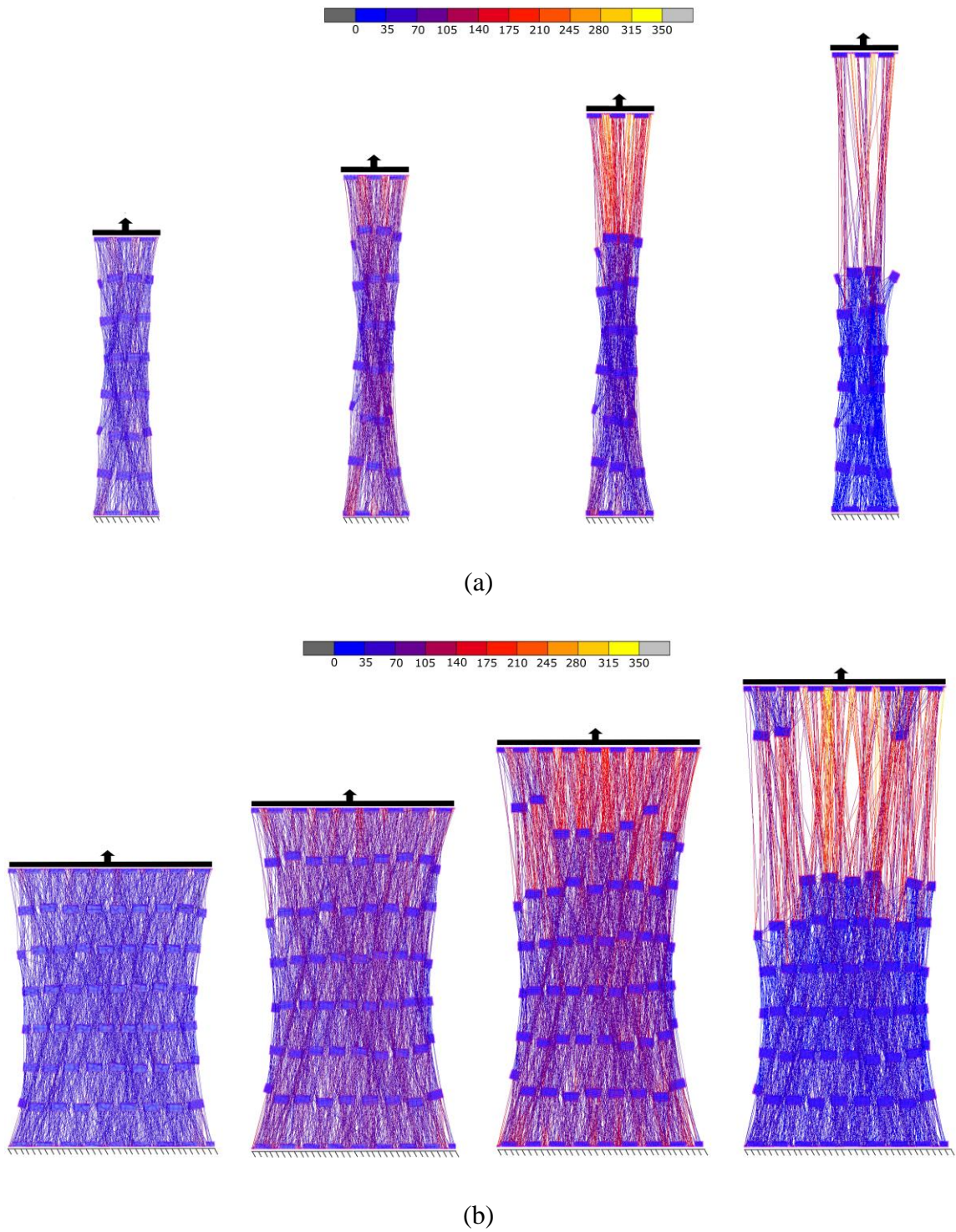
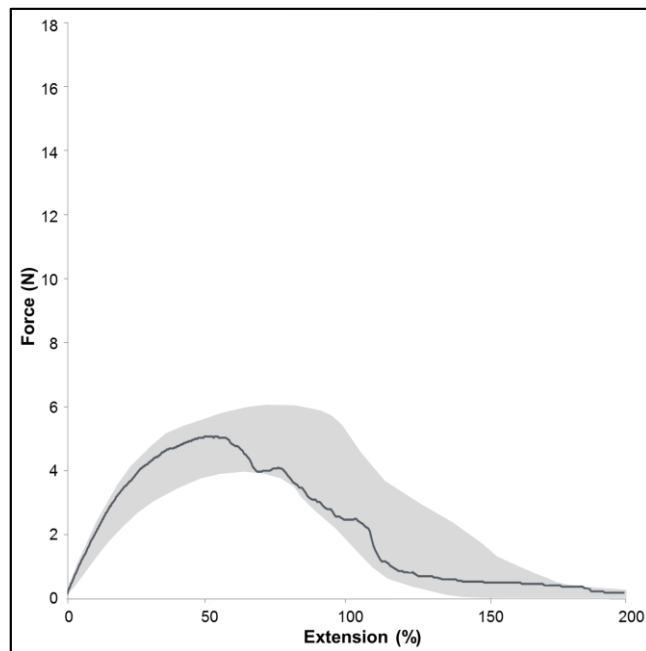
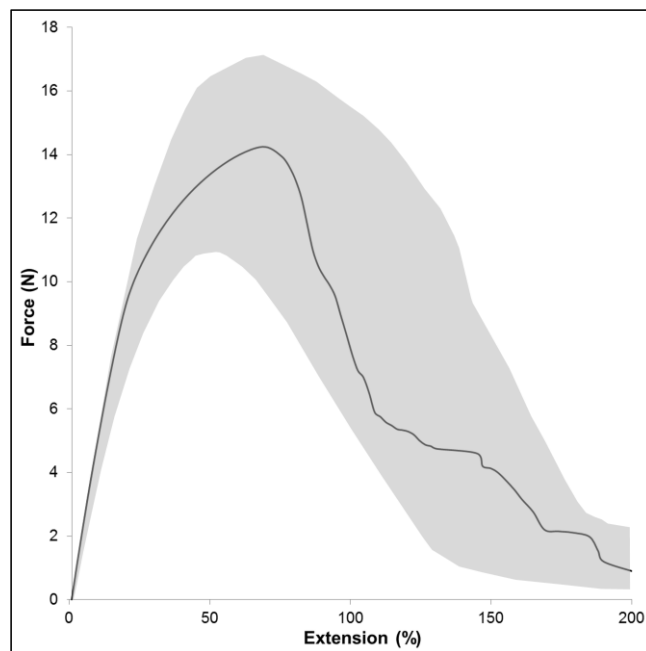


Figure 7.27. FE model results showing contour plot of equivalent von Mises stresses (MPa) in fabric along MD subjected to uniaxial tension to extension: (i) 25%; (ii) 50%; (iii) 75%; (iv) 100% for 5 mm width model (a) and 15 mm width model (b)



(a)



(b)

Figure 7.28. FE model response to uniaxial tensile test for 5 mm width model (a) and 15 mm width model (b) (Shaded area represents scatter in experimental results)

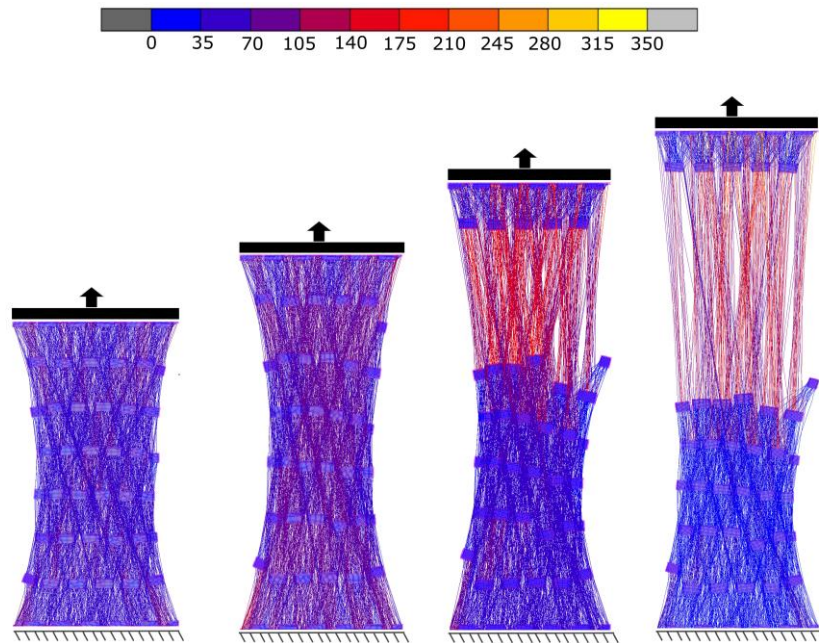


Figure 7.29. FE model results showing contour plot of equivalent von Mises stresses (MPa) in fabric with 30 g/m^2 planar density along MD subjected to uniaxial tension to extension: (i) 25%; (ii) 50%; (iii) 75%; (iv) 100%

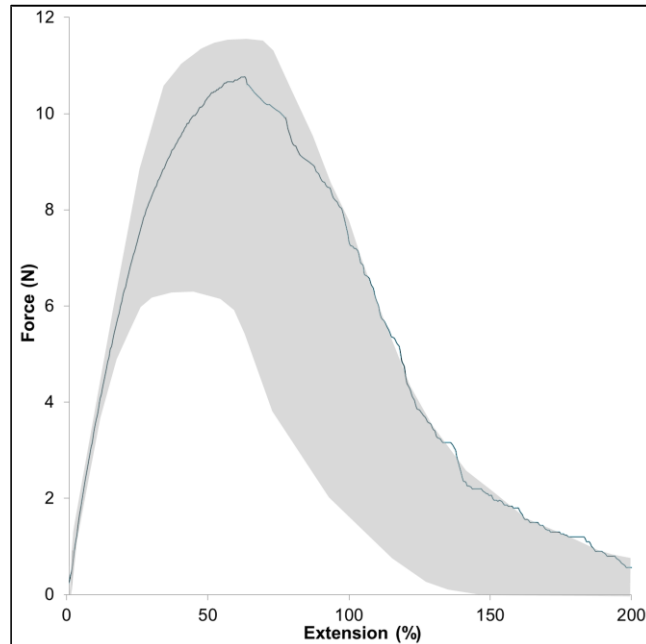


Figure 7.30. FE model for 30 g/m^2 nonwoven response to uniaxial tensile test (Shaded area represents scatter in experimental results)

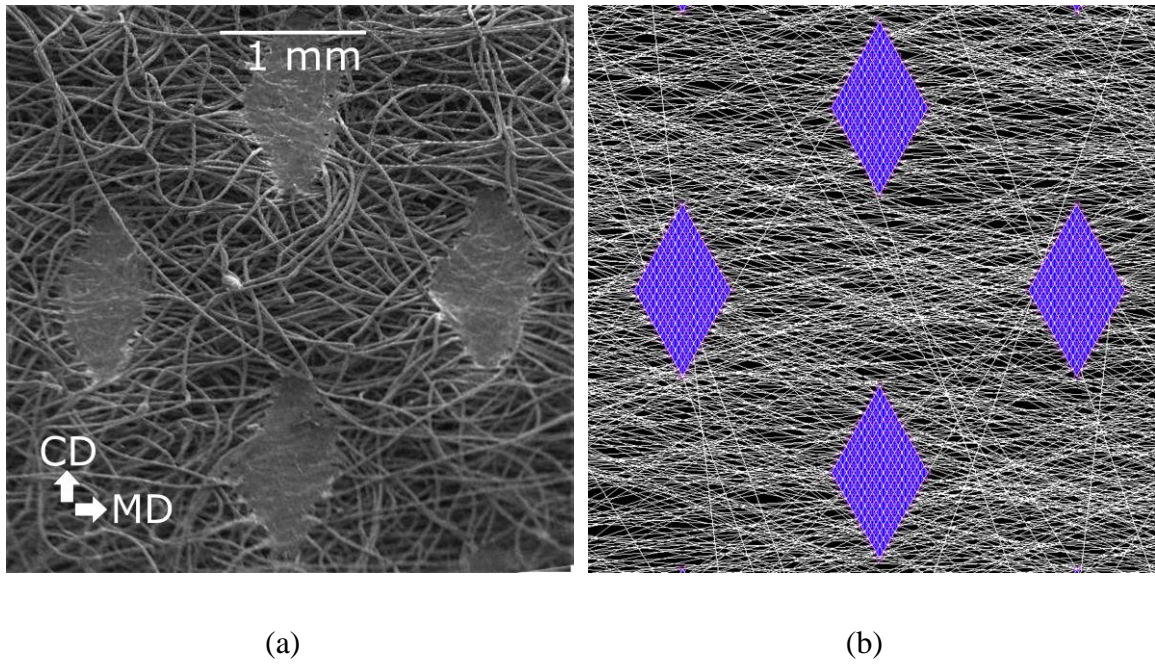


Figure 7.31. (a) SEM image of 30 g/m² nonwoven material with diamond-shaped bond points; (b) corresponding part of FE model

Table 7.3. Parameters of geometry and pattern of bond points

Fabric's orientation with reference to BP	BP pattern	A	B	C	D
		(mm)			
		1.0668	0.5588	0.7	1.8

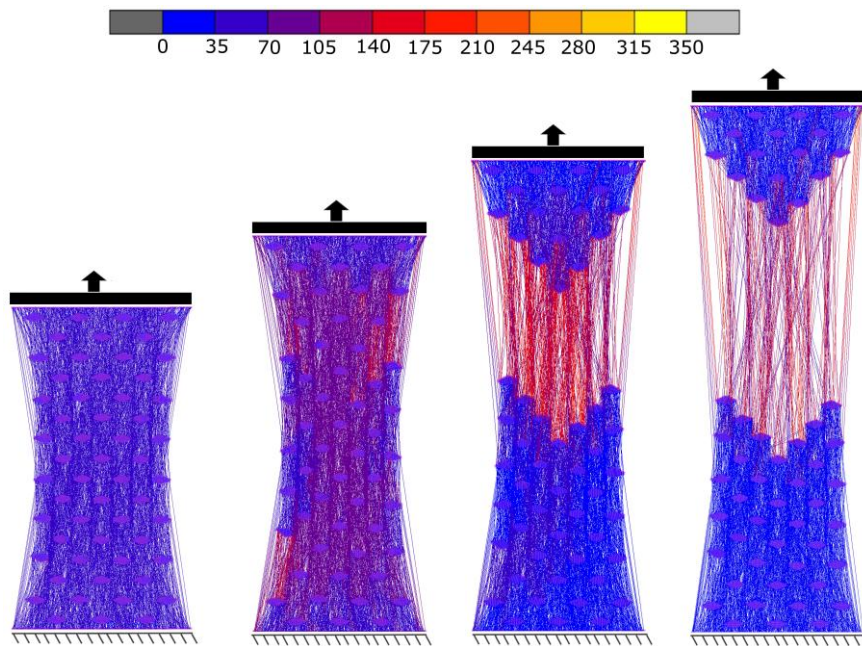


Figure 7.32. FE model results showing contour plot of equivalent von Mises stresses (in MPa) in fabric with diamond-shaped bond points along MD subjected to uniaxial tension to extension: (i) 25%; (ii) 50%; (iii) 75%; (iv) 100%

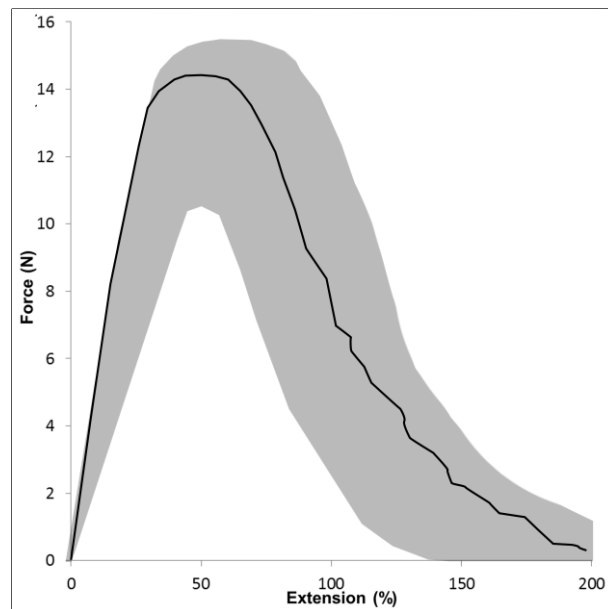


Figure 7.33. Response of FE model with diamond-shaped bond points to uniaxial tensile test (Shaded area represents scatter in experimental results)

The deformation behaviours of the models with increasing fabric's extension are shown in Fig. 7.32. Force-extension curves were used to compare the model's predictions with experimental results (Fig. 7.33). A good agreement, obvious from Fig. 7.33, between the model and experimental results shows that the model is capable to predict the effect of variation in nonwoven's behaviour caused by the shape and pattern of bond points.

The above discussion shows that model can predict variations in the behaviour of nonwoven materials with different planar densities, sizes and geometric entities of their network structure. Recall that the model is based on direct introduction of fibres with the accurate number of fibres, size and shape of network's geometric entities (bond points) and material properties of its constituent fibres. Since the model is based on the parametric modelling technique, the effect of various dimensions of network entities and the length of fibres can easily be studied. Besides, the model is based on direct introduction of fibres which means that various lengths of individual fibres can also be implemented with low effort. This direct introduction of fibres into the model makes it possible to implement variation in material properties. Thus, the material properties of various types of constituent fibres can be implemented easily into the model to investigate the behaviour of other types of fabrics with different constituent fibres. To sum up, the model can account for variations in dimensions and pattern of bond points, length, diameter, orientation and material properties of constituent fibres and specimen size. Generally, not only nonwoven fabrics but all types of fibrous networks including biomaterials such as collagen in tissues and scaffolds differs from each other in terms of these parameters. Since the model can be reformulated to incorporate the variations in these parameters and can predict the changes in material's behaviour caused by them, it is expected that the model is extendable to other types of fibrous networks.

7.6 Conclusions

This chapter presents a continuous-discontinuous finite-element model used to simulate the mechanical behaviour of nonwoven fabrics based on their microstructure,

constituent fibres' properties and underlying deformation and damage mechanisms. This model provides the response of the material at meso and macro level within the framework of the finite-element environment. For nonwoven materials, in which orientation distribution of fibres is directly related to their anisotropic mechanical properties, a new method based on direct introduction of fibres, according to their ODF in the actual fabric, into the model is proposed in this chapter. Due to a large number of fibres to be modelled, the parametric modelling technique based on a subroutine is used. This subroutine written in Patran Command Language (PCL) is read by the finite-element software that generates the fibrous network according to the given input. This reduces significantly the effort for reformulating the model to incorporate the actual orientation distribution of fibres as well as the size and shape of bond points. Besides, the model based on direct introduction of fibres mimic realistic fabric's microstructure with voids and gaps in it.

The proposed model was implemented in MSC. Marc as solver incorporating carefully measured nonlinear elasto-viscoplastic material properties and single-fibre failure parameters. The model simulations reproduced very accurately the main deformation and damage mechanisms including:

- anisotropic behaviour;
- fibre re-orientation towards the loading direction that was more pronounced for CD than MD;
- failure of fibres on reaching their stress or strain thresholds leading to development of fracture zones;
- growth in fracture zones due to progressive failure of fibres; the growth rate in fracture zone was higher for CD than MD;
- character of transverse strain including the grip effect;
- stress concentration at edges of the bond points.

Besides, the model can predict the spread in stresses and strains in the members of network structure. Such capabilities of the model to capture all the main mechanisms and features of the fabric's response would underpin understanding of the behaviour of nonwoven fabrics and their structure-properties relationships. Since the model is based on direct introduction of fibres by employing the parametric modelling technique it allows easy reformulation of the model to incorporate various microstructures, sizes and shapes of bond points and material properties of constituent fibres. The model can predict the variation in the material's behaviour with the change in all of these parameters. However, this prediction of variation in material's behaviour is effectively only for a small perturbation in these parameters such as model can predict the effect of planar density on mechanical behaviour of the fabric but it is limited to only low density fabrics. After certain level of planar density, the effect of non-uniformity of deformation and damage mechanisms through thickness become so important that the exclusion of these would lead to inaccurate solutions. As variation in any or combination of these parameters, especially the size and pattern of bond points, planar density and constituent fibre's material properties lead to different types of fibrous networks, the model has the potential to be extended to understand the behaviour of other types of nonwoven fibrous networks and their structure-properties relationships. Still, the model was developed to assess a mechanical performance of, mostly of, thermally calendered bonded nonwovens. The behaviour of other types of nonwovens, especially mechanically bonded ones, in which fibres are entangled to form the bond, cannot be predicted efficiently using this model.

CHAPTER 8

CONCLUSIONS AND FUTURE WORK

8.1 Conclusions

A novel parametric computational model was introduced in this study for predicting the mechanical behaviour of nonwoven materials. Development of the model started with a thorough literature review of respective manufacturing techniques, their application areas and various numerical models based on different approaches including their limitations and shortcomings. A systematic approach for characterization of the mechanical response of nonwoven materials and development of a continuous-discontinuous finite-element model used to simulate the behaviour of thermally calendered bonded nonwovens based on the experimental observation was presented in this study. Low-density thermally bonded nonwovens with polymer constituents were employed as representative materials in this study.

A number of experimental characterization techniques were employed to investigate the morphology of fabric's structure and to analyse the deformation and damage behaviour together with underlying mechanisms which govern those behaviours. Fabric's structure was characterised with SEM and X-ray Micro CT, and orientation distributions of fibres were obtained with the use of the in-house software — Nonwoven Anisotropy V1 — based on the image-analysis technique. Uniaxial tensile testing on the fabric revealed its anisotropic behaviour biased towards MD (preferential orientation of fibres). The mechanisms governing the deformation and damage behaviours of the fabric include reorientation of fibres towards the loading direction, their stretching and ultimately failure, on reaching their stress or strain threshold. Stretching of fibres consisted of recoverable and irrecoverable parts. The latter resulted in permanent deformation observed in fabric. Experimental observations indicated that the material properties of constituent fibres dominated the deformation and damage behaviours of the fabric. Therefore, the mechanical properties of the fibres were obtained from the tensile tests. Those tests revealed the presence of viscous behaviour in fibres, which was assessed with single-fibre relaxation and creep tests.

Motivated by morphological evolution of fabric's microstructure and underlying mechanisms, a continuous-discontinuous finite-element model was developed using direct introduction of fibres by employing the parametric modelling technique. The proposed model consists of directly introduced fibres according to their orientation distribution representing the actual fabric's microstructure with voids and gaps in it. The fibres were modelled as truss elements forming a discontinuous part of the model whereas shell elements were used for continuous parts representing the bond points. An appropriate failure criterion and visco-elasticplastic properties were assigned to the corresponding elements and a series of simulations was performed. The results obtained from the simulations were compared with the experimental data to evaluate the efficiency of the proposed numerical model.

As a result of the experimental and numerical studies performed in this research, it can be concluded that:

- Microstructure of the low-density nonwoven fabric evolves continuously with the rearrangement of its fibres tending to align along the loading direction.
- Fibres start to participate in load bearing practically when they are fully aligned along the loading direction. Extensive reorientation of fibres before their participation in load bearing was observed during loading along CD as compared to MD due to preferential orientation of fibres along MD.
- Fibres undergo visco-elastoplastic deformation depending upon their material properties before failing.
- Damage initiates and propagates in the fabric caused by progressive failure of fibres reaching their stress or strain threshold during the loading. This progressive failure of fibres is more gradual along MD as compared to CD, consistent with the fabric's microstructure.
- Progressive failure of fibres is accompanied by initiation and growth of fracture zones. A growth rate of fracture zones in the fabric during its loading along the direction parallel to the preferential orientation of fibres is gradual as compared to the transverse direction. The reason for this behaviour lies again in microstructure of the fabric.
- The proposed numerical modelling approach for simulating the deformation and damage behaviours of calendered bonded nonwovens is promising since a direct comparison between model simulations and the corresponding data from experiments shows that the model can capture the complex nonlinear anisotropic response of the material. Specifically, the model is shown to capture the load-extension behaviour of the fabric.
- Truss elements are effective in representing fibres as they have only axial stiffness.
- The numerical model based on direct introduction of fibres according to their orientation distribution is effective not only to understand the deformation and

damage mechanisms but it can also predict the nonhomogeneous deformation, anisotropic behaviour and localization of damage.

- A spread in stresses and strains in members of the fibrous networks can be predicted by the model. Besides, it can predict the fraction of fibres bearing load at any level of fabric's extension. Thus, it can help to modify the structure of the fabric's network in terms of orientation distribution and location of fibres in the nonwoven network with an aim to achieve higher reliability and durability by keeping the stress and strain distribution uniform.
- Textural evolution by reorientation of fibres towards the loading direction and permanent deformation at any level of fabric's extension can be obtained with the model. Thus, it can be used to predict the safety factor for nonwoven materials in terms of force or extension.
- A character of stress distribution in bond points can also be studied using this model; this can be helpful to optimise the size, shape and pattern of bond points.
- The model successfully reproduces the observed size effects, variation in planar density of nonwoven network and the effects of size, shape and pattern of bond points. Besides, it can easily handle variations in orientation distribution and material properties of constituent fibres thanks to the use of parametric modelling technique based on direct introduction of fibres. Since variations in these parameters lead to different types of nonwovens, the model proposed in this study may be extended to almost all types of fibrous networks including biological materials such as collagen and tissue-engineering scaffolds.

8.2 Outcomes

- A better understanding of deformation and damage behaviours of nonwovens and a relationship between their macroscopic mechanical behaviour and

properties of constituent fibres, required to design nonwoven materials, are gained in this study.

- A numerical model incorporating fabric's microstructure, deformation and damage mechanisms and constituent fibre's properties is introduced in this study which can provide insights and underpin quantitative exploration of design space of nonwoven products.
- A parametric numerical tool based on direct introduction of fibres and other geometric entities (bond points) makes it easy to reformulate the model to study the effect of various aspects of geometry on material's deformation and damage behaviour. Such a tool can be used by designers for tailoring the properties of nonwovens for particular applications. Besides, it can be used to study structure-properties relationships for almost all types of fibrous networks.
- It is a potential tool for product development and optimisation. Since it can facilitate the design and optimisation of products containing nonwoven parts by reducing trial-and-error stages, it can help manufacturers to reduce the cost and time of bringing new products containing nonwovens to the market. Besides, product design can be improved aimed at higher reliability and durability, which can provide a competitive advantage to a manufacturer.
- The effect on mechanical properties of nonwoven networks due to localization of damage is one of the main concerns in biodegradable fibrous materials, for instance, for polymer scaffolds, which are required to provide sufficient structural integrity to maintain their dimensions during a wound-healing process even after degradation of some of their constituents. Since the model in this study is based on explicit introduction of fibres, it is possible to predict the changes in network's topology and its load-bearing capacity as a result of localization of damage due to progressive failure of fibres. It can be extended to predict the behaviour of biodegradable fibrous networks.

- A comprehensive modelling technique based on the subroutine is developed in this research to simulate real-life deformation and damage behaviours of nonwovens. Unlike the existing models in the literature (see Section 4.4), the model developed in this study can predict evolution of deformation and damage of the fabric up to its failure in terms of progressive failure of fibres while incorporating explicitly the realistic material's microstructure by introducing their properties into the model. It can provide information such as spread in levels of stresses and strains in each element of the fabric, reorientation of the fibres, fraction of fibres taking the load, number of fibres failed etc. for any level of fabric's extension, which cannot be obtained easily with the existing models or from the experiments.

8.3 Limitations

Although the finite-element model developed in this study captures main deformation and damage mechanisms of nonwoven networks, still, like other models, it has some limitations, which are given below:

- The model is developed predominantly for low-density thermally calendared bonded nonwoven networks in which fibres fail at bond point periphery. This is the main cause of damage initiation and growth in nonwoven network. The damage behaviour of other types of thermally bonded nonwovens such as hot-air bonding, in which inter-fibre bond failure is the major cause of fabric failure cannot be predicted using this model.
- Due to a single-fibre failure criteria and modelling technique adopted in this study, models with continuous and staple fibre will result in the same behaviour. Thus, the model cannot be used to predict the variation in behaviour of nonwoven's network due to the changes in the length.

- The developed model is based on assumption that most of the main deformation and damage mechanisms occur in plane of the fabric and neglects its through-thickness behaviour. Since thickness of the fabric increases with its increasing planar density, the through thickness behaviour for high-density nonwovens is important and cannot be neglected. Hence, the model proposed in this study cannot accurately predict the behaviour of nonwovens for high-density fabrics.

8.4 Future Work

In order to continue the present study, the following research lines can be mentioned:

- Incorporation of fibre-curl distributions into the model is an important step. The fibre curl affects significantly the deformation behaviour of nonwovens. Quantification of this distribution is a challenging task. An image-processing method can be developed to determine the curl distribution for the structure. Besides, incorporation of fibre curl into the model would predict a more realistic response of the fabric.
- Nonwovens in their life in service undergo complex loading, rather than a monotonic one, at various strain rates with or without the effect of creep or stress relaxation. Thus, quantifying this behaviour of the material experimentally and numerically for complex loading histories would be of great interest.
- Apart of uniaxial loading, nonwovens are often used under biaxial loading conditions. Furthermore, out-of-plane loading regimes are also important for some applications such as filters. The experimental and numerical analysis of deformation and damage behaviours of nonwovens under biaxial and out-of-plane loading would be relevant.
- Bond points are considered as continuous structures with uniform material properties in this study. However, in reality the strength of bond points in nonwovens depends upon temperature, pressure and other parameters of the

bonding process. By incorporating these variables a more realistic model to define the properties of bond points can be achieved.

- Constituent fibres of nonwovens are not always mono-component. For nonwovens with bicomponent constituent fibres, bond points act as a composite with a sheath material working as matrix and a core material as fibre reinforcement. The model of this type of fabric would consist of composite areas in fibrous network. The analysis of bicomponent-fibre nonwoven would be particularly relevant, for such materials.

Appendix A

DETERMINATION OF ORIENTATION DISTRIBUTION FUNCTION

As discussed in the thesis, the orientation distribution of fibres is one of the major issues regarding the determination of material behaviour of nonwoven fibrous networks. Microstructural images of nonwoven network were required to determine the orientation distribution. Images obtained from Scanning Electron Microscopy (SEM) (see Fig. 5.6) were used for this purpose. These images were analysed with the use of in-house software — Nonwoven Anisotropy V1— based on image analysis technique (Fig. A.1).

Nonwoven Anisotropy V1 computes the ODF from micro-scale images of fibrous networks and presents it in the form of histogram (Fig. A.3). Since microstructural images can be affected significantly by the brightness and noise conditions which make it difficult to distinguish individual fibres. Therefore, in order to

achieve better fibre detection, software divides each image into sub-images. The ODF of each sub-domain is then computed separately by the code. Detected fibres in each subdomain are designated with lines drawn on top of them (Fig. A.2). These lines indicating orientation of fibres help a user to optimize the outcome with respect to microstructure and imaging conditions. The resultant ODF is based on ODFs from each subdomain. Based on number and orientations of fibres computed in each sub-domain resultant ODF is generated by the code².

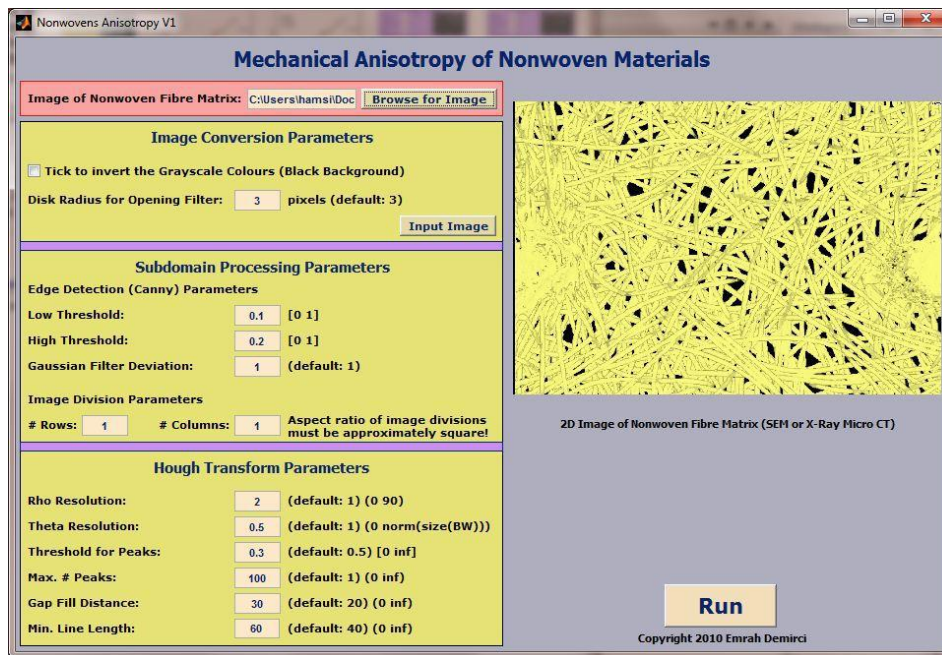


Figure A.1. GUI of Nonwovens Anisotropy V1 for computing ODF and mechanical anisotropy of fibrous materials

Computation efficiency of the code of the software can be improved by increasing the resolution and sharpness of the image with the help of various image processing parameters available of the GUI of the code as illustrated in Fig. A.1. Besides, the subdomain processing features with larger number of image division gives improved ODF results. The ODF obtained from the software for 20 g/m² PP nonwoven fabric used as reference material in the thesis is given in Fig. A.3.

² The reader is referred to Demirci, 2010 for further details on Nonwoven Anisotropy V1.

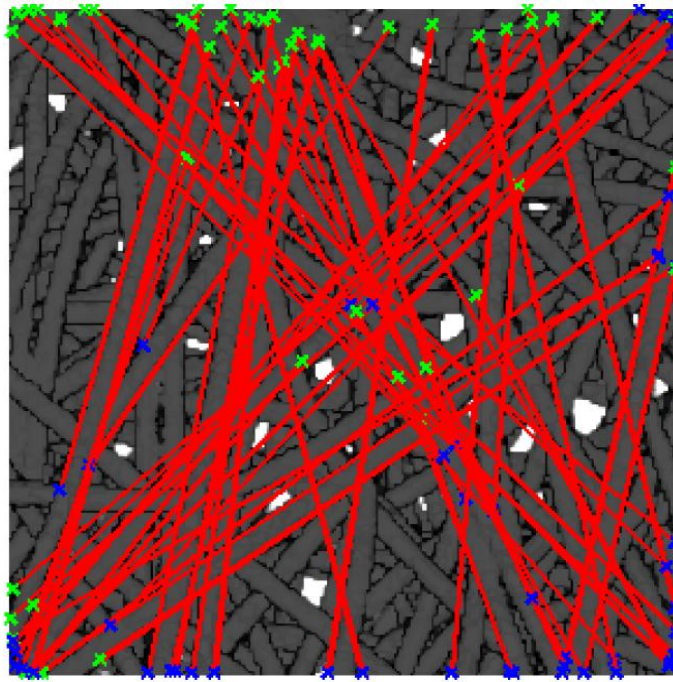


Figure A.2. Red lines showing fibres in image processed with Nonwoven Anisotropy V1

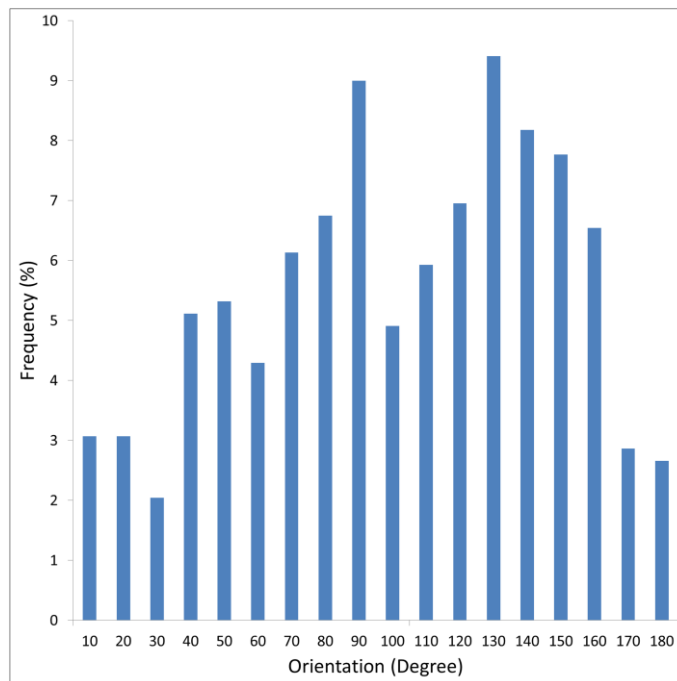


Figure A.3. Orientation distribution of modelled fabric

Appendix B

IMPLEMENTATION OF SUBROUTINE

The parametric model developed in this study to simulate the deformation and damage behaviour of nonwovens is based on subroutine, written in Patran Command Language (PCL). Finite-element software could read this subroutine and generate the fabric's network according to the given input. A 20g/m² thermally bonded polypropylene nonwoven, shown in Fig. 5.6, is used as model system to describe the steps involved in implementation of subroutine, which are given below:

B.1 Generation of Fabric's Network

Development of FE model started with the generation of network structure. Two regions — bond points and fibre matrix — forming a nonwoven fabric were introduced one by one. The process of fabric's network generation is as follows:

B.2 Modelling of Bond Points

The process of generating the fabric network was started with the generation of bond points corresponding to the required dimensions of the fabric to be modelled. These bond points were generated according to dimensions and pattern obtained from SEM images of the fabric in Section 5.2.1. The bond point size and pattern as well as dimensions of the fabric to be modelled were read from the code and generated using surfaces. In addition to bond points, four planes were created at the corner of the fabric's limits which would be used to trim the fibres generated in next step. The generation of bond points and planes is shown in Fig. B.1.

B.3 Modelling of Fibres

Fibres were modelled directly according to their orientation distribution obtained from in-house software Anisotropy VI as mentioned in Section 5.1.1. Software provided numbers of fibres in form of 10° angle bands ranges from 0° to 180° . This means, for example, if a fibre is at an angle of 35° it will belongs to fourth band ranges from 30° to 40° . This ODF was used as one of the input to subroutine.

In order to calculate the number of fibres for each orientation band, first total number of fibres in the model were calculated by using an assumption that total fibre mass in the model was equal to that of fabric with dimensions equal to those of the model. Fibre mass was calculated by subtracting the mass of the bond points from the fabric mass. Fabric mass was calculated by the following relation:

$$M_{\text{Fabric}} = \rho_{\text{Fabric}} A_{\text{Fabric}}, \quad \text{B.1}$$

where M_{Fabric} is fabric mass, ρ_{Fabric} is fabric's planar density (20g/m^2 in this study) and A_{Fabric} is the area of the fabric to be modelled, calculated by multiplying fabric length and width. Bond point mass (m_{bonds}) was calculated by the following relation:

$$m_{\text{bonds}} = \rho_{\text{pp}} A_{\text{bond}} t_{\text{bond}},$$

where ρ_{pp} is the density of constituent fibre material (0.89 g/cm³ in this study), A_{bond} is the total area covered by bond points within the fabric and t_{bond} is the thickness of bond points. Area covered by bond points (A_{bond}) was calculated by multiplying the fabric's area to be modelled with bond points per unit area of fabric. Mass of bond points was calculated by considering them as continuous regions following the experimental observations. Total fibre mass was calculated by the relation:

$$m_{Fibre} = M_{Fabric} - m_{bonds}, \quad B.2$$

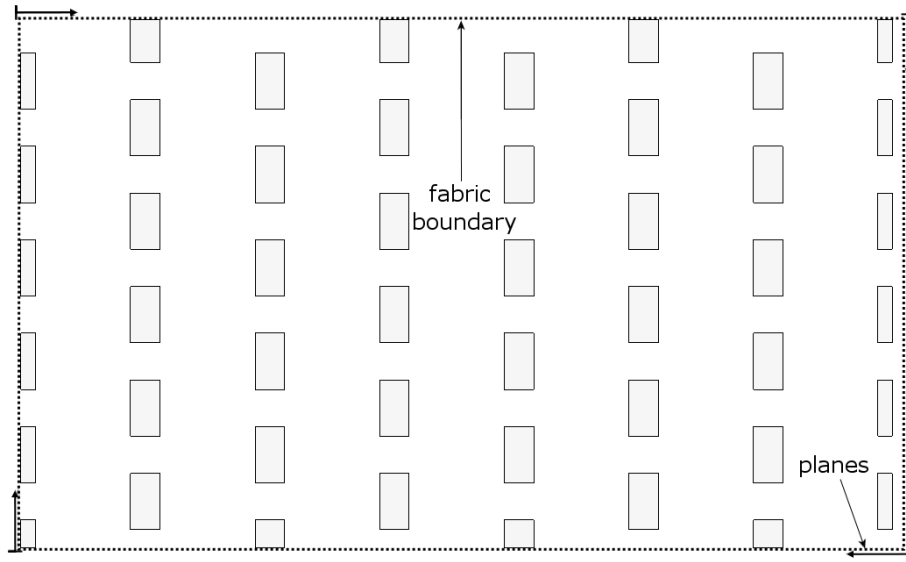


Figure B.1. Modelling bond points and planes on fabric border

Number of fibres to be modelled was calculated by using the relation:

$$N_{Fibre} = \frac{m_{Fibre}}{\rho_{pp} a_{Fibre} L_{single_Fibre}}, \quad B.3$$

where a_{Fibre} is cross-sectional area of fibres and L_{single_fibre} is the length of individual fibre. Eq. B.1 gives the total number of fibres to be modelled. This calculation was based on assumption that fibres lie completely inside the specified fabric region. Since fibres were modelled randomly in the microstructure, characterized by orientation distribution function, some of the fibres could be located at the edge of the fabric and part of them

could be outside the fabric region (Fig. B.2). For example, some part of fibre B in Fig. B.2. is outside the fabric limit and would be trimmed at later stages of modelling. In order to make the total mass of fibres in FE model equal to fabric sample with dimensions equal to those of the model, additional fibres were added one by one until both the masses became equal. Therefore, before actual starting of fibre modelling process, it was performed virtually to reduce the computation time as shown in Fig. B.6.

The total length of the fibres, which was achieved by virtual modelling process, was compared with the total length of fibres that should be present in the model. The number of fibres to be modelled increased one by one until the former one became equal or greater than latter one. One thing should be noted that initially number of fibres in the model cannot exceed the real number of fibres as the former one was based on assumption that fibre lie completely inside the fabric. After calculating the number of fibres to be modelled by virtual modelling process, real modelling process of fibres using lines was started as shown in Fig. B.6.

In order to calculate the number of fibres for each angle band, frequency of fibres in each fibre orientation band should be multiplied by total number of fibres. As fibres are modelled using lines, the number of lines showing fibres for each orientation distribution band are calculated by using the following relation:

$$NL(j) = \frac{N_{\text{Fibre}}(j)}{K}, \quad \text{B.4}$$

where $NL(j)$ is the number of lines having same orientation as fibres in any particular fibre orientation band. K is the model coefficient which is equal to the number of fibres represented by each fibre line. The value of can be ranges from 1 to a certain higher value depending upon the computational efficiency of the system. All these calculations of number of fibres in any particular fibre orientation band were performed by the subroutine based on input parameters before actually modelling the fibres as shown in Fig. B.6. It reduces the time to generate the model with large number of fibres.

Once numbers of fibre for each orientation band were determined, they were modelled by lines as shown in Fig. B.3. Fibres in the model were drawn according the results obtained from above calculations by considering the criteria, mentioned below, following the experimental observations:

- Fibres should not be connected to same bond point
- Fibres should not pass through the bond points
- Fibres should not connect very far bond points without intersecting other bond points

Starting point of the fibre lines were picked randomly within the modelling area and then drawn according to their orientation distribution function.

B.4 Editing Of Fibres

Fibre lines were trimmed at the boundary of the model by the planes created in the beginning and within the bond points as shown in Fig. B.4 and B.5, respectively. After this, the fibres in at the boundary of the modelled fabric were analysed. If no boundary conditions were applied on these fibres, they will not play any role in the structural behaviour of the fabric. Rather, their presence in the model would increase the computational time and cause converging issues. These fibres were deleted from the model according to the boundary conditions.

Fibres were also edited to coincide their nodes with the nodes of the bond point for element-connectivity requirement. Since fibres were model randomly in the structure, they could result in distorted elements in bond point during meshing. This problem was avoided by shifting the nearest tip of the fibres to the nearest nodes on bond points. Element size of the bond point should be in such a way that the maximum angle change of the fibre is less than 5° . As the orientation distribution was given for an interval of 10° , and fibres were model at an angle equal to average of mid-point of respective band such as for third band 30° - 40° :

$$\text{Fibre angle} = \frac{30^\circ + 40^\circ}{2} = 35^\circ$$

B.5

Thus, this amount of angle change in fibres did not cause the fibres to change their orientation band. Before this angle shift of fibre, meshing of the model was performed by running a loop for fibre and bond points.

All these calculations about fibre numbers, their generation and association with bond points were performed by the subroutine. Thus, subroutine reduces significantly the effort required to reformulate the model to incorporate the different realizations of orientation distribution of fibres, size, shape and pattern of bond points as well as fabric dimensions and areal densities.

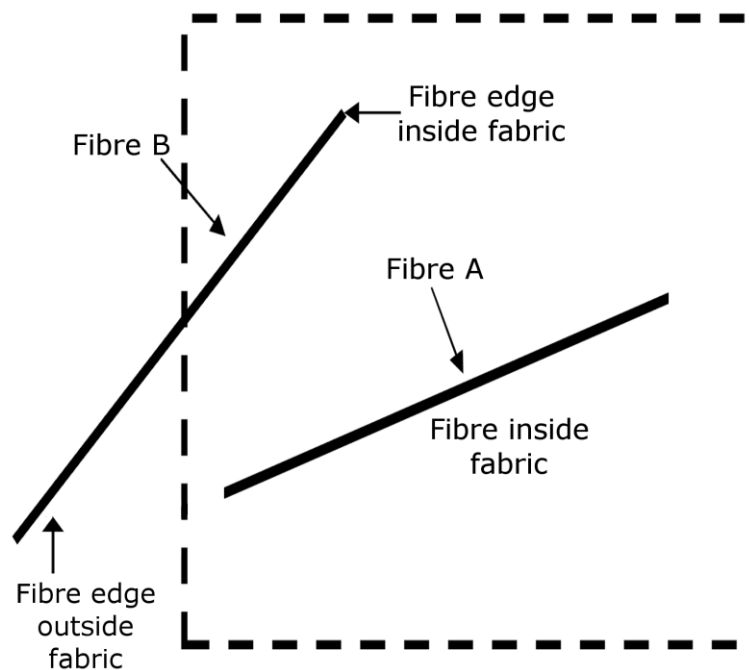


Figure B.2. Representation of fibres; fibre A, completely inside fabric; fibre B, partially outside fabric

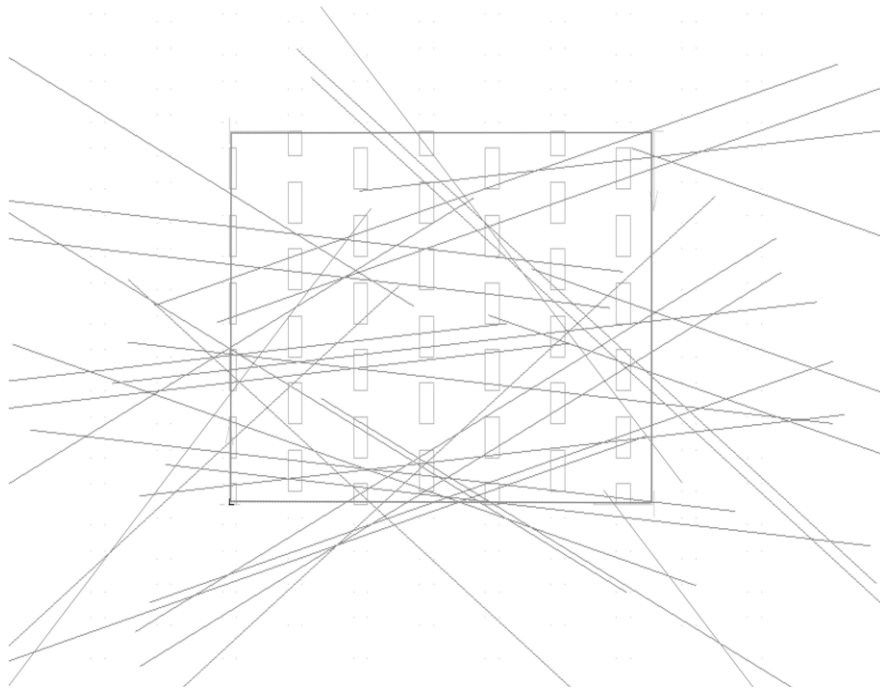


Figure B.3. Modelling of fibres

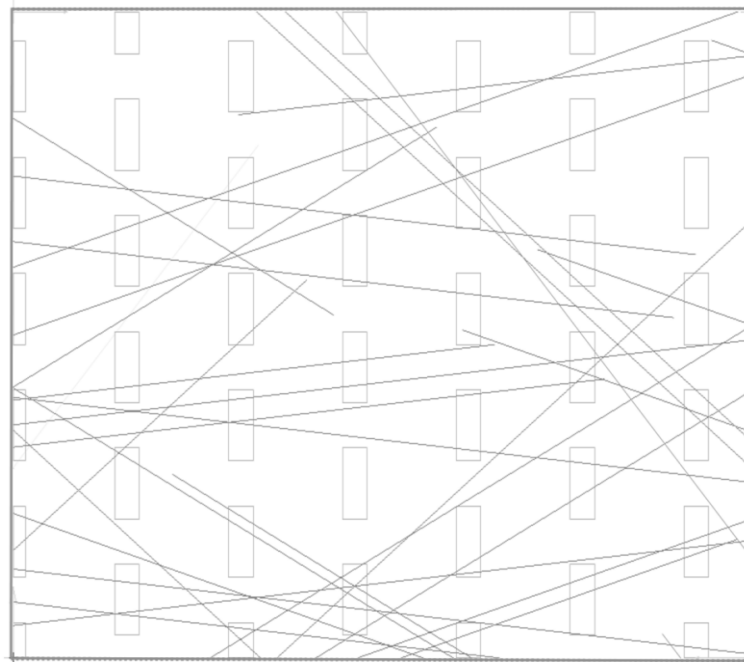


Figure B.4. Trimming of fibres along fabric borders

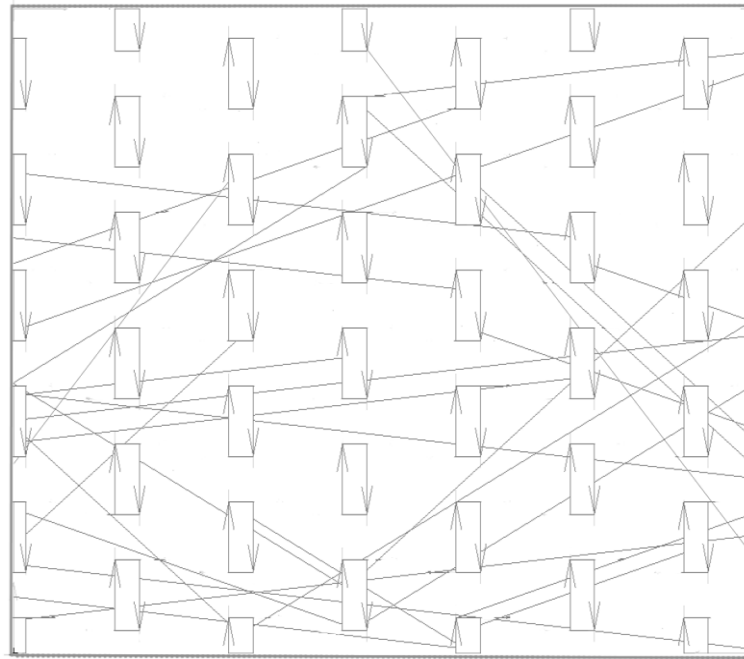


Figure B.5. Trimming of fibres within bond points

After generation of fabric network, meshing was performed. Then, geometric and material properties, obtained in Chapter 5 and 6, respectively, were assigned to the respective elements. After implementing proper boundary conditions, finite-element analyses were performed. The flow chart for the generation of fabric network using subroutine is given in Fig. B.6.

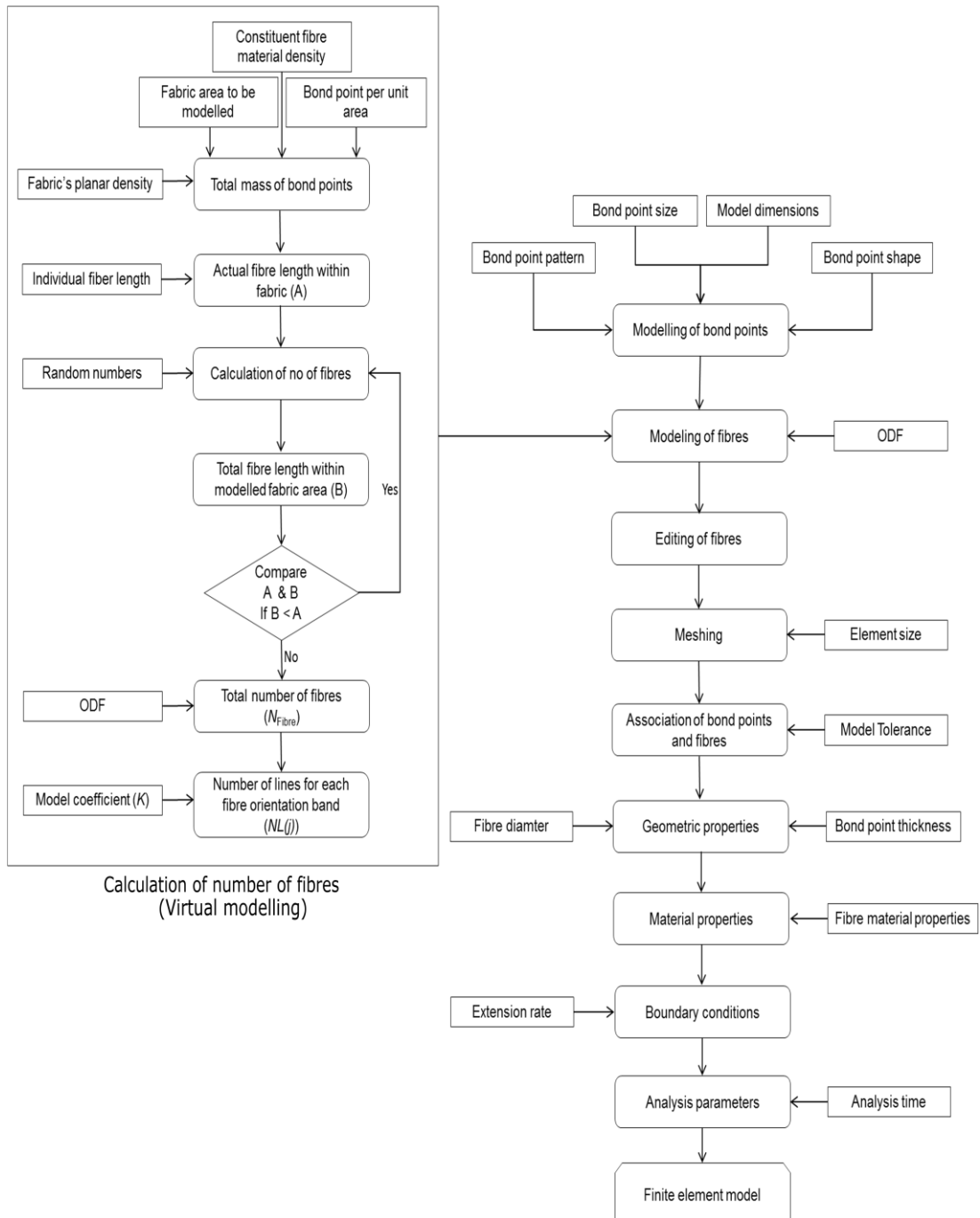


Figure B.6. Flowchart of implemented code

REFERENCES

Albrecht, W., Fuchs, H. & Kittelmann, W. 2003, *Nonwoven Fabrics: Raw Materials, Manufacture, Applications, Characteristics, Testing Processes*, Wiley-VCH.

Adanur, S. & Liao, T. 1999, "Fiber Arrangement Characteristics and Their Effects on Nonwoven Tensile Behavior", *Textile Research Journal*, vol. 69, no. 11, pp. 816-824.

Andreassen, E., Myhre, O.J., Hinrichsen, E.L., Braathen, M.D. & Grøstad, K. 1995, "Relationships between the properties of fibers and thermally bonded nonwoven fabrics made of polypropylene", *Journal of Applied Polymer Science*, vol. 58, no. 9, pp. 1633-1645.

Asaro, R. J. and Lubarda, V. A. (2006), *Mechanics of Solids and Materials*, Cambridge University Press, Cambridge, UK.

-
- Barach, J.L. & Rainard, L.W. 1950, "Effect of Crimp on Fiber Behavior Part II: Addition of Crimp to Wool Fibers and Its Effect on Fiber Properties", *Textile Research Journal*, vol. 20, pp 308-316.
- Bauer-Kurz, I. 2000, *Fiber crimp and crimp stability in nonwoven fabric processes*, North Carolina State University.
- Berthlot, J. M.1998, *Composite Materials: Mechanical Behavior and Structural Analysis*, Springer.
- Batra, S.K. 1998, *Basics of Nonwoven Fabrics and Technology*, NCRC, NC State University, Raleigh, USA.
- Batra, S. K., Pourdeyhimi, B. 2012, *Introduction to Nonwovens Technology*, DEStech Publications, Inc.
- Bhat, G.S., Jangala, P.K. & Spruiell, J.E. 2004, "Thermal bonding of polypropylene nonwovens: Effect of bonding variables on the structure and properties of the fabrics", *Journal of Applied Polymer Science*, vol. 92, no. 6, pp. 3593-3600.
- Bhat, G.S. & Malkan, S.R. 2002, "Extruded continuous filament nonwovens: Advances in scientific aspects", *Journal of Applied Polymer Science*, vol. 83, no. 3, pp. 572-585.
- Brown, A. 1955, "Measurement of Crimp in Single Fibers¹", *Textile Research Journal*, vol. 25, no. 12, pp. 969-976.
- Burkett, M. E. 1979, *The art of felt maker*, Abbot Hall Art Gallery.
- Chuleigh, P.W. 1984, "Image Formation of Fibers and Fibers Assemblies", *Textile Research Journal*, vol. 54, pp. 813.
- Chidambaram, A., Davis, H. and Batra, S. K., ed., (2000), *Strength Loss In Thermally Bonded Polypropylene Fibers*, INTC 2000 Conference, Dallas, USA.
- Clarke, L.A. & Cope, R.J. 1984, *Concrete Slabs: Analysis and Design* 1st edn, Taylor & Francis, USA.

-
- Cook, R.D. 1995, *Finite Element Modeling for Stress Analysis*, John Wiley and Sons, New York, USA.
- Cook, R. D. (1995), *Finite Element Modelling for Stress Analysis*, John Wiley and Sons, New York, USA.
- Cook, R. D., Malkus, D. S., Plesha, M. E. 1998, *Concepts and Applications of Finite Element Analysis*, John Wiley & Sons.
- Cox, H.L. 1952, "The Elasticity and Strength of Paper and Other Fibrous Materials", *British Journal of Applied Physics*, vol. 3, pp. 72-79.
- Datla, V.M. 2002, *The Influence of Fiber Properties and Processing Conditions on the Characteristics of Needled Fabrics*, Master's thesis edn, North Carolina State University, USA.
- Demirci, E., Acar, M., Pourdeyhimi, B., Silberschmidt, V. V. 2010a, "Anisotropic Elastic-Plastic Mechanical Properties of Thermally Bonded Bicomponent Fibre Nonwovens", *Computational Mechanics* ASME, Istanbul, Turkey, July, 2010, pp. 117-122.
- Demirci, E. 2010b, *Mechanical Behaviour of Thermally Bonded Bicomponent fibre Nonwovens Experimental Analysis and Numerical Modelling*, PhD Thesis, Loughborough University.
- Demirci, E., Acar, M., Pourdeyhimi, B. & Silberschmidt, V.V. 2011a, "Computation of mechanical anisotropy in thermally bonded bicomponent fibre nonwovens", *Computational Materials Science*, vol. In Press, Corrected Proof.
- Demirci, E., Acar, M., Pourdeyhimi, B. & Silberschmidt, V.V. 2011b, "Finite element modelling of thermally bonded bicomponent fibre nonwovens: Tensile behaviour", *Computational Materials Science*, vol. 50, no. 4, pp. 1286-1291.
- Dharmadhikary, R.K., Gilmore, T.F., Davis, H.A. & Batra, S.K. 1999a, "Thermal Bonding Of Nonwoven Fabrics", *Textile Progress*, vol. 26, no. 2, pp. 1-37.

- Dharmadhikary, R.K., Davis, H., Gilmore, T.F. & Batra, S.K. 1999b, "Influence of Fiber Structure on Properties of Thermally Point Bonded Polypropylene Nonwovens", *Textile Research Journal*, vol. 69, no. 10, pp. 725-734.
- Dukkipati, R.V., Ananda, M.R. & Bhat, R. 2007, *Computer Aided Analysis and Design of Machine Elements* to New Age International Pvt Ltd Publishers, New Delhi, INDIA.
- EDANA (2012), 'The European Nonwovens Industry in a Global Context', [Online] <http://www.edana.org/discover-nonwovens/facts-and-figures> [03/09/2012].
- Fedorova, N., Verenich, S. & Pourdeyhimi, B. 2007, "Strength Optimization of Thermally Bonded Spunbond Nonwovens", *Jouranal of Engineered Fibers and Fabrics*, vol. 2, no. 1, pp. 38-48; 38-48.
- Gao, X. and Huang, H. Y. 2004, *Thermal Bonding of Nonwoven Fabrics*. Available: <http://www.engr.utk.edu/mse/pages/Textiles/Thermal> Bonding.htm [2011, 08/29].
- Ghassemieh, E., Acar, M. & Versteeg, H. 2002, "Microstructural analysis of non-woven fabrics using scanning electron microscopy and image processing. Part 1: Development and verification of the methods", *Proceedings of the Institution of Mechanical Engineers, Part L: Journal of Materials Design and Applications*, vol. 216, no. 3, pp. 199-207.
- Gilmore, T.F., Mi, Z.X., Batra, S.K. 1993. "Effect of Bond Point Design and Bond Strength on the Load-Deformation of Point Bonded Nonwovens: A Computer-Based Study, *Nonwovens Conference Proceedings*, NCRC, North Carolina, USA.
- Gitman, I.M., Askes, H. & Sluys, L.J. 2007, "Representative volume: Existence and size determination", *Engineering Fracture Mechanics*, vol. 74, no. 16, pp. 2518-2534.
- Gusick, G. E., Hearle, J. W. S., Michie, R. I. C. and Peters, R. H. 1963, "The Physical Properties of Nonwoven Fabrics", *Journal of the Textile Institute*, vol. 54, pp. 52-74.

-
- Hegde, R.R., Bhat, G.S. & Campbell, R.A. 2008, "Thermal bonding of polypropylene films and fibers", *Journal of Applied Polymer Science*, vol. 110, no. 5, pp. 3047-3058.
- Hearle, J.W.S., and Stevenson, P.J., "Studies in Nonwoven Fabrics, Part IV: Prediction of Tensile Properties", *Textile Research Journal*, 34(3): 181-191 (1964).
- Hietel, D. & Marheineke, N. 2005, "Modeling and Numerical Simulation of Fiber Dynamics", *PAMM*, vol. 5, no. 1, pp. 667-670.
- Hill, R. (ed) 1950, *The Mathematical Theory of Plasticity*, Oxford University Press, New York, USA.
- Hill, R. 1948, "A Theory of the Yielding and Plastic Flow of Anisotropic Metals", *Proceedings of the Royal Society of London. Series A, Mathematical and Physical Sciences*, vol. 193, no. 1033, pp. pp. 281-297.
- Hou, X. 2010, *Experimental and Numerical Analysis of Deformation Of Low-Density Thermally Bonded Nonwovens*, PhD Thesis, Loughborough University.
- Hou, X., Acar, M. & Silberschmidt, V.V. 2009, "2D finite element analysis of thermally bonded nonwoven materials: Continuous and discontinuous models", *Computational Materials Science*, vol. 46, no. 3, pp. 700-707.
- Huang, X. C., Bresee , R. R., 1993, "Characterizing non-woven web structure using image analysis techniques, Part II: Fibre orientation analysis in thin webs, *INDA Journal of Nonwoven Research*, 2, 14-21
- Hutton, I. M., 2007, *Handbook of Nonwoven Filter Media*, Elsevier Science.
- ISO 9092:2011, Textiles – Nonwovens – Definitions, 2011.
- Jones, R.M. (ed) 2009, *Deformation Theory of Plasticity*, 2nd edn, Bull Ridge Publishing, Virginia, USA.
- Kallmes, O.J. "Technique for determining the fibre orientation distribution function throughout the thickness of sheet", *Tappi Journal*, 52(4), 482-485.

-
- Khan, A. S., Huang, S. 1995. *Continuum theory of plasticity*, John Wiley & sons.
- Kim, H.S. 2004(a), "Orthotropic theory for the prediction of mechanical performance in thermally point-bonded nonwovens", *Fibers and Polymers*, vol. 5, no. 2, pp. 139-144.
- Kim, H.S., Pourdeyhimi, B. & Abhiraman, A. and Desai, P. 2000, "Characterizing Structural Changes in Nonwoven Fabrics During Load-Deformation Experiments", *Journal of Textile and Apparel*, vol. 1, no. 1, pp. 1-6.
- Kim, H.S. 2004(b), "Relationship between fiber orientation distribution function and mechanical anisotropy of thermally point-bonded nonwovens", *Fibers and Polymers*, vol. 5, no. 3, pp. 177-181; 177-181.
- Kim, H.S.a.P., B. 2001, "Computational Modeling of Mechanical Performance in Thermally Point Bonded Nonwovens", *Journal of Textile and Apparel, Technology and Management*, vol. 1, no. 4, pp. 1-7; 1-7.
- Kim, H.S., Deshpande, A., Pourdeyhimi, B., Abhiraman, A.S. & Desai, P. 2001(b), "Characterizing Structural Changes in Point-Bonded Nonwoven Fabrics During Load-Deformation Experiments", *Textile Research Journal*, vol. 71, no. 2, pp. 157-164.
- Kim, H.S., Pourdeyhimi, B., Desai, P. & Abhiraman, A.S. 2001, "Anisotropy in the Mechanical Properties of Thermally Spot-Bonded Nonwovens: Experimental Observations", *Textile Research Journal*, vol. 71, no. 11, pp. 965-976.
- Kothari, V.K., and Patel, P.C., "Theoretical Model for Predicting Creep Behaviour of Nonwoven Fabrics", *Indian Journal of Fibre & Textile Research*, 26: 273-279 (2001).
- Laufer, B. 1930, "The early history of felt making", *American Anthropologist*, vol. 32, no. 1, pp. 1-18.
- Liao, T.Y. & Adanur, S. 1997, "Predicting the Mechanical Properties of Nonwoven Geotextiles with the Finite Element Method", *Textile Research Journal*, vol. 67, no. 10, pp. 753-760.

-
- Limem, S. and Warner, S. B. 2005, "Adhesive Point-Bonded Spunbond Fabrics", *Textile Research Journal*, vol. 75, no. 1, pp. 63-72.
- Lin, J., Xu, Z., Lei, C. & Lou, C. 2003, "Effect of Fiber Arrangement on the Mechanical Properties of Thermally Bonded Nonwoven Fabrics", *Textile Research Journal*, vol. 73, no. 10, pp. 917-920.
- Madenci, E. & Guven, I. 2007, *The Finite Element Method and Applications in Engineering Using ANSYS*, 1st edn, Springer, USA.
- Marc 2008, *User Guide A: Theory and User Information*, MSC Software.
- Michielsen, S. and Wang, X. 2002, "Rapid Morphology (Property) Changes at the Bond Periphery In Thermal Point-bonded Nonwovens", *International Nonwovens Journal*, vol. 11, no. 2, pp. 35-38.
- Michielsen, S., Pourdeyhimi, B. & Desai, P. 2006, "Review of thermally point-bonded nonwovens: Materials, processes, and properties", *Journal of Applied Polymer Science*, vol. 99, no. 5, pp. 2489-2496.
- Mishakov, V., Slutsker, G., Stalevich, A. 2006, "Modeling the viscoelasticity of nonwoven material with consideration of the irreversible strain component", *Fibre Chemistry*, vol. 38, no. 1, pp. 50-54.
- Mishnaevsky, L.L. 1998, *Damage and Fracture in Heterogeneous Materials*, 1st edn, Taylor & Francis, Netherland.
- Mittal, J.P., Kaur, I. & Sharma, R.C. 1992, "Fibres and Textiles" in *Encyclopedia of Technical Education*, 25th edn, Mittal Publications, New Delhi, India, pp. 278-293.
- Mueller, D.H. & Kochmann, M. 2004, "Numerical Modeling of Thermobonded Nonwovens", *International Nonwovens Journal*, vol. 13, no. 1, pp. 56-62; 56-62.
- Ottosen, N.S. & Ristinmaa, M. 2005, *The Mechanics of Constitutive Modeling* 1st edn, Elsevier Science, Great Britain.

-
- Pourdeyhimi, B., Ramanathan, R. & Dent, R. 1996, "Measuring Fiber Orientation in Nonwovens", *Textile Research Journal*, vol. 66, no. 11, pp. 713-722.
- Pourdeyhimi, B. 2003, "Mechanical performance of thermally bonded nonwovens", *Notes*, NC State University, NCRC, USA.
- Price, D.S., Jones, R. & Harland, A.R. 2006, "Soccer ball anisotropy modelling", *Materials Science and Engineering: A*, vol. 420, no. 1-2, pp. 100-108.
- Rawal, A. 2006, "A Modified Micromechanical Model for the Prediction of Tensile Behavior of Nonwoven Structures", *Journal of Industrial Textiles*, vol. 36, no. 2, pp. 133-149.
- Ridruejo, A., González, C. & LLorca, J. 2011, "Micromechanisms of deformation and fracture of polypropylene nonwoven fabrics", *International Journal of Solids and Structures*, vol. 48, no. 1, pp. 153-162.
- Ridruejo, A., González, C. & LLorca, J. 2010, "Damage micromechanisms and notch sensitivity of glass-fiber non-woven felts: An experimental and numerical study", *Journal of the Mechanics and Physics of Solids*, vol. 58, no. 10, pp. 1628-1645.
- Russell, S.J. 2007, *Handbook of Nonwovens*, Woodhead Publishing Ltd, Cambridge, UK.
- Sabuncuoglu, B., Acar, M. & Silberschmidt, V.V. "A parametric finite element analysis method for low-density thermally bonded nonwovens", *Computational Materials Science*, vol. 52, no. 1, pp. 164-170.
- Sabuncuoglu, B., 2012, *Development of Parametric Finite Element Modelling Methods for Nonwoven Materials Including Rate Dependent Material Behaviour*, PhD Thesis, Loughborough University.
- Shiffler, D.A. 1995, "An Examination of the Stress-strain Curve of Crimped Polyethylene Terephthalate Staple Fibers", *Journal of the Textile Institute*, vol. 86, no. 1, pp. 1-9.

Silberstein, M. N.; Lhai-Ling, P.; Boyce, M.C. “ Elastic-plastic behaviour of nonwoven fibrous mats”. *Journal of Mechanics and Physics of Solids*, 2012, 60(2), 295-318.

Singh, A.K. 2010, *Mechanics of Solids*, Prentice-Hall of India, New Delhi, India.

Skrzypek, J. & Ganczarski, A. 1999, *Modeling of Material Damage and Failure of Structures: Theory and Applications*, Springer, Germany.

Stenemur, B., 1992, Method and device for monitoring fibre orientation distribution and web uniformity on running webs of paper and nonwoven based light diffraction phenomenon, *INDA Journal of Nonwoven Resesarch*, 4, 42-45

Tanchis, G. (ed) 2008, *The Nonwovens*, 1st edn, Fondazione Acimit, Italy.

Tascan, M., Vaughn, E. A., 2008, “Effects of Fiber Denier, Fiber Cross-Sectional Shape and Fabric Density on Acoustical Behavior of Vertically Lapped Nonwoven Fabrics”, *Journal of Engineered Fibers and Fabrics*, vol. 3, issue 2, pp. 32-38.

User manual guide, “Instron Microtester (5848), User’s Guide, Instron Corporation, 2001.

Wang, X.Y. & Gong, R.H. 2006, "Thermally bonded nonwoven filters composed of bi-component polypropylene/polyester fiber. II. Relationships between fabric area density, air permeability, and pore size distribution", *Journal of Applied Polymer Science*, vol. 102, no. 3, pp. 2264-2275.

Wang, X. & Michielsen, S. 2001, "Morphology Gradients in Thermally Point-Bonded Polypropylene Nonwovens", *Textile Research Journal*, vol. 71, no. 6, pp. 475-480.

Wang, X. & Michielsen, S. 2002, "Morphology Gradients in Thermally Point-Bonded Poly(ethylene Terephthalate) Nonwovens", *Textile Research Journal*, vol. 72, no. 5, pp. 394-398.

Wood, E. J. (1990), 'Applying Fourier and Associated Transforms to Pattern Characterization in Textiles', *Textile Research Journal*, vol. 60, no. 4, 212-220.

Xu, B. 1996, "Identifying Fabric Structures with Fast Fourier Transform Techniques", *Textile Research Journal*, vol. 66, no. 8, pp. 496-506.

Xu, B. and Ting, Y. (1995), 'Measuring Structural Characteristics of Fiber Segments in nonwoven Fabrics', *Textile Research Journal*, vol. 65, no. 1, 41-48.]